

Universität
Rostock



Traditio et Innovatio



Dynamics of oxygen in coastal seas - the Baltic Sea example

Kumulative Dissertation zur
Erlangung des akademischen Grades
doctor rerum naturalium (Dr. rer. nat.)
der Mathematisch-Naturwissenschaftlichen Fakultät
der Universität Rostock
vorgelegt von

Lev Naumov

geboren am 06 August 1996 in Samara

Rostock, Oktober 2023



Dieses Werk ist lizenziert unter einer
Creative Commons Namensnennung 4.0 International Lizenz.

Gutachter*innen:

1. Gutachter

Prof. Dr. H.E. Markus Meier

Leibniz-Institut für Ostseeforschung Warnemünde

2. Gutachter

Dr. Bo Gustafsson

Stockholm University

Datum der Einreichung: 10.10.2023

Datum der Verteidigung: 16.02.2024

Dynamics of oxygen in coastal seas - the Baltic Sea example

ABSTRACT

In this thesis, oxygen dynamics in the coastal seas is investigated utilizing the Baltic Sea as a prominent example of a marine system severely affected by human impact, which led to the biggest hypoxic area worldwide. Since the oxygen sources and especially sinks are difficult to measure, a regional coupled circulation model (RCM) was applied to reconstruct oxygen sources and sinks in the central Baltic Sea on the climatological time scale and to run a few sensitivity studies with reduced nutrient forcing. In addition, the multidecadal variability in the Baltic Sea's salinity field is discussed. Conceptually, three different topics are discussed.

The first topic is oxygen dynamics in the central Baltic Sea during the 71-year period (1948-2018) and its ventilation by oxygen transported from the North Sea with the 29 biggest inflows during that time. The overall trend of deoxygenation during that time was observed. It is accompanied by a shift in oxygen consumption from the sediments to the water column. The effectiveness of the ventilation by inflows has reduced dramatically, especially in the remote sub-basins, due to elevated oxygen consumption. However, the processes triggered by inflowing oxygen did not change noticeably. It is mostly mineralization of detritus. Mineralization of detritus in the sediments and nitrification in the water column were found to be the biggest oxygen sinks.

The second topic deals with the question of how the Baltic Sea would react to a reduced nutrient forcing and whether it can be returned to the anthropogenically unperturbed state. Two sensitivity experiments with a reduced nutrient forcing (1st experiment with the Baltic Sea Action Plan Maximum Allowable Input - BSAP MAI, and 2nd with halved BSAP MAI). Both simulations encompassed a 70-year period. An overall improvement was observed in the case of both scenarios, especially in the remote sub-basin. The oxygen consumption shifted back to the sediments, and upward advection of hydrogen sulfide ceased in the remote sub-basins. It was found that the system could be returned to its unperturbed state (in this case, the year 1948), but it happened within the next 71 years only under the more rigorous halved BSAP MAI forcing.

The third topic is dedicated to the multidecadal salinity variations in the Baltic Sea. Conducting five sensitivity experiments, it was found that the multidecadal variability of the salinity field is mainly controlled by both the North Atlantic Oscillation (NAO) and the Atlantic Multidecadal Variability (AMV). In addition, the positive feedback connecting mean salinity and Major Baltic Inflows (MBIs) was observed. When the mean salinity is lower, the MBIs also transport less salt into the Baltic Sea (since the water transported out of the Baltic Sea is less saline), and vice versa.

In summary, the Baltic Sea has been rapidly deoxygenating since the 1970s. It is still possible to reverse those changes, but it will take a long time.

Dynamik des Sauerstoffs in Küstengewässern - das Beispiel der Ostsee

ZUSAMMENFASSUNG

In dieser Dissertation wird untersucht die Sauerstoffdynamik in den Küstengewässern unter Verwendung der Ostsee als prominentes Beispiel für ein marines System, das schwerwiegend vom menschlichen Einfluss betroffen ist und als Folge zur größten hypoxischen Zone weltweit wurde. Da die Sauerstoffquellen und insbesondere die Senken schwer zu messen sind, wurde ein regionales, gekoppeltes Ozeanmodell angewendet, um Sauerstoffquellen und -senken in der zentralen Ostsee im klimatologischen Zeitrahmen zu rekonstruieren und einige Sensitivitätsstudien mit reduzierter Nährstoffzufuhr durchzuführen. Darüber hinaus wird die multidekadische Variabilität des Salzgehalts der Ostsee diskutiert. Konzeptionell konzentriert sich die Dissertation auf drei verschiedene Themen.

Das erste Thema ist die Sauerstoffdynamik in der zentralen Ostsee während eines 71-jährigen Zeitraums (1948-2018) und die dortige Belüftung durch Sauerstoff, der durch die 29 größten Einströme aus der Nordsee in die Ostsee gelangt. Es wurde ein Trend der Sauerstoffabnahme beobachtet. Dies geht einher mit einer Verschiebung des Sauerstoffverbrauchs von den Sedimenten in die Wassersäule. Die Effektivität der Belüftung durch Einströme hat sich besonders in den entfernten Teilbecken aufgrund des erhöhten Sauerstoffverbrauchs drastisch reduziert, jedoch sind die Prozesse, die durch einströmenden Sauerstoff ausgelöst werden, größtenteils die gleichen (hauptsächlich Mineralisierung von Detritus). Es stellte sich heraus, dass die Mineralisierung von Detritus in den Sedimenten und die Nitrifikation in der Wassersäule die größten Sauerstoffsenken sind.

Das zweite Thema befasst sich mit der Frage, wie die Ostsee auf eine reduzierte Nährstoffzufuhr reagieren würde und ob sie in ihren "ursprünglichen Zustand" zurückversetzt werden kann. Es wurden zwei Sensitivitätsexperimente mit reduzierter Nährstoffzufuhr durchgeführt (erstes Experiment mit dem höchstzulässigen Eintrag nach dem Ostsee-Aktionsplan - BSAP und ein zweites mit halbiertem höchstzulässigen Eintrag). Beide Simulationen umfassten einen Zeitraum von 70 Jahren. Es wurde insgesamt eine Verbesserung beobachtet, insbesondere in entfernten Teilbecken. Der Sauerstoffverbrauch verlagerte sich zurück in die Sedimente und der nach oben gerichtete Transport von Wasserstoffsulfid in den entfernten Teilbecken hörte auf. Es wurde festgestellt, dass das System in seinen ursprünglichen Zustand zurückversetzt werden kann, aber dies wird nur im Falle eines rigorosen Szenarios mit halbiertem höchstzulässigen Nährstoffeintrag innerhalb des Simulationszeitraums geschehen.

Das dritte Thema widmet sich den multidekadischen Salzgehaltsvariationen in der Ostsee. Durch die Durchführung von fünf Sensitivitätsexperimenten wurde festgestellt, dass die multidekadische Variabilität des Salzgehalts hauptsächlich durch die Nordatlantische Oszillation (NAO) und die Atlantische Multidekadische-Variabilität (AMV) gesteuert wird. Darüber hinaus wurde eine positive Rückkopplung zwischen dem mittleren Salzgehalt und den Haupteinströmen in die Ostsee (Major Baltic Inflows - MBIs) beobachtet. Wenn der mittlere Salzgehalt niedriger ist, transportieren auch die MBIs weniger Salz in die Ostsee (da das aus der Ostsee transportierte Wasser weniger salzhaltig ist) und umgekehrt.

Zusammenfassend hat sich der Sauerstoffgehalt in der Ostsee seit den 1970er Jahren rapide verringert. Es ist immer noch möglich, diese Veränderungen umzukehren und in den "ursprünglichen Zustand" zurückzukehren, aber es wird lange dauern.

Contents

1	INTRODUCTION	1
2	THE BALTIC SEA	5
2.1	Physical properties	5
2.1.1	Climate	5
2.1.2	Circulation	7
2.1.3	Temperature, salinity, and ice cover	9
2.2	Biogeochemical properties	11
2.2.1	Oxygen and hydrogen sulfide	11
2.2.2	Biogens	14
3	DATA AND METHODS	17
3.1	Models	17
3.1.1	General information about models	17
3.1.2	Tracer experiment (ventilation paper)	19
3.1.3	Sensitivity studies (sensitivity paper)	21
3.2	Statistical methods	22
3.2.1	Linear regression framework (ventilation and sensitivity papers)	22
3.2.2	Cluster analysis (ventilation paper)	24
3.2.3	EOF analysis (ventilation and sensitivity papers)	24
3.2.4	GAMM framework (variability paper)	25
3.3	Observational datasets (ventilation and variability papers)	25
4	OXYGEN DYNAMICS OF THE BALTIC SEA	27
4.1	Validation summary	27
4.1.1	MOM-ERGOM (ventilation paper)	27
4.1.2	RCO (variability paper)	28
4.2	Oxygen sources and sinks during the last 71 years (ventilation paper)	30
4.2.1	The biggest oxygen sources and sinks	30
4.2.2	Different sources and sinks contributing to the variability of O ₂ and H ₂ S	30
4.2.3	Temporal variability of O ₂ and H ₂ S sources and sinks	31
4.3	Ventilation by the inflows (variability and ventilation papers)	32
4.3.1	Multidecadal variability in the salinity and inflows (variability paper)	32
4.3.2	Temporal trends in the central BS ventilation by the inflows (ventilation paper)	33
4.3.3	Changes in the ventilation patterns (ventilation paper)	33
4.4	Oxygen dynamics under reduced nutrient input (sensitivity paper)	36
4.4.1	Trends in oxygen sources and sinks	36

4.4.2	O ₂ and H ₂ S budgets' composition in different scenarios	37
4.4.3	O ₂ and H ₂ S sources and sinks' variability induced by the nutrient forcing	38
5	DISCUSSION AND CONCLUSIONS	41
5.1	Discussion	41
5.2	Conclusions	42
	REFERENCES	44
	APPENDIX A SUPPLEMENTARY MATERIAL	69
	APPENDIX B CURRICULUM VITAE	78
	APPENDIX C DECLARATION OF MY CONTRIBUTIONS TO THE PUBLICATIONS	83
C.1	Multidecadal climate variability dominated past trends in the water balance of the Baltic Sea watershed	83
C.2	Limited ventilation of the central Baltic Sea due to elevated oxygen consumption	83
C.3	Dynamics of oxygen sources and sinks in the Baltic Sea under different nutrient inputs	83
	APPENDIX D PUBLICATIONS	85

Publications

PUBLICATIONS FOR THE CUMULATIVE DISSERTATION

- A **Naumov, L.**, *Neumann, T., Radtke, H., and Meier, H. E. M.* (2023). Limited ventilation of the central Baltic Sea due to elevated oxygen consumption. *Frontiers in Marine Science*, 10.
<https://www.frontiersin.org/articles/10.3389/fmars.2023.1175643>
- B **Naumov, L.**, *Meier, H. E. M., and Neumann, T.* (2023). Dynamics of oxygen sources and sinks in the Baltic Sea under different nutrient inputs. *Frontiers in Marine Science*, 10.
<https://www.frontiersin.org/articles/10.3389/fmars.2023.1233324>
- C *Markus Meier, H. E., Barghorn, L., Börgel, F., Gröger, M., Naumov, L., and Radtke, H.* (2023). Multidecadal climate variability dominated past trends in the water balance of the Baltic Sea watershed. *Npj Climate and Atmospheric Science*, 6(1), Article 1.
<https://doi.org/10.1038/s41612-023-00380-9>

CONFERENCES

- Elevated oxygen consumption in the central Baltic Sea reduces ventilation
L. Naumov, *T. Neumann, H. Radtke, and H. E. M. Meier*
Poster | XXVIII General Assembly of the International Union of Geodesy and Geophysics (IUGG) | Berlin, Germany | 12.07.2023
- Oxygen dynamics in the Baltic Sea: A budget
L. Naumov, *T. Neumann, H. Radtke, and H. E. M. Meier*
Talk | 4th Baltic Earth Conference | Jastarnia, Poland | 30.05.2022

Abbreviations

DO	Dissolved Oxygen
OMZ	Oxygen Minimum Zone
IOP-UNESCO	Intergovernmental Oceanographic Commission of UNESCO
MCA	Medieval Climate Anomaly
OM	Organic Matter
LIA	Little Ice Age
GCM	Global Circulation Model
RCM	Regional Circulation Model
BS	Baltic Sea
SST	Sea Surface Temperature
EOF	Empirical Orthogonal Functions
NAO	North Atlantic Oscillation
AMV	Atlantic Multidecadal Variability
MBI	Major Baltic Inflow
SSS	Sea Surface Salinity
DOM	Dissolved Organic Matter
POM	Particulate Organic Matter
DOC	Dissolved Organic Carbon
DIC	Dissolved Inorganic Carbon
DIP	Dissolved Inorganic Phosphorus
DIN	Dissolved Inorganic Nitrogen
BSAP	Baltic Sea Action Plan
HELCOM	Baltic Marine Environment Protection Commission or Helsinki Commission
BALTSEM	BAltic sea Long-Term large Scale Eutrophication Model
MAI	Maximum Allowable Input
GAMM	Generalized Additive Mixed Models
MOM	Modular Ocean Model
ERGOM	Ecological Regional Ocean Model
RCO	Rosby Centre Ocean circulation model
NOAA GFDL	National Oceanic and Atmospheric Administration Geophysical Fluid Dynamics Laboratory
SIS	Sea Ice Simulator
KPP	K-profile parameterization
OBC	Ocean Boundary Conditions
BB	Bornholm Basin

eGB	eastern Gotland Basin
nGB	northern Gotland Basin
wGB	western Gotland Basin
OLS	Ordinary Least Squares
NN	Nearest Neighbor
ICES	International Council for the Exploration of the Sea
IOW	Leibniz Institute for Baltic Sea Research Warnemünde
NEMO	Nucleus for European Modelling of the Ocean
SCOB	Swedish Coastal and Ocean Biogeochemical model

O_2	Oxygen
H_2S	Hydrogen sulfide
NO_3^-	Nitrate
NO_2^-	Nitrite
NO^-	Oxoazanide
N_2	Dinitrogen Gas
NH_4^+	Ammonium
PO_4^{3-}	Phosphate
SO_4^{2-}	Sulfate
S	Elemental Sulfur
CH_4	Methane
H^+	Hydrogen
H_2O	Water
HCO_3^-	Bicarbonate
Mn^{2+}	Manganese
Fe^{2+}	Iron
FeS_2	Pyrite
CO_2	Carbon Dioxide
C	Carbon
N	Nitrogen
P	Phosphorus

DO. OR DO NOT. THERE IS NO TRY.
MASTER YODA

Acknowledgments

It seems that accomplishing PhD is not as straightforward as I imagined when I just started. I actually find it very exciting to have such an experience because, in the end, the thesis is just a bunch of paper, but the knowledge and experience I have gained during those 3 years, hopefully, will stay with me forever. I would like to thank everyone who has been shaping that for me since my arrival at IOW. In the beginning, I would like to thank my supervisor - Markus Meier, for his useful comments and assistance. I think now I know much more about how it feels to be a scientist. I would also like to say a big thank you to Thomas Neumann and Hagen Radtke. It seems you can explain any complicated matter in a super understandable way, and you always have some time to help. I think it is huge luck to have such senior colleagues. I am also very grateful to the rest of my PhD committee, Jerome Kaiser and Karol Kuliński. Thank you both for all the advice you gave to me. On a bigger scale, I think my working group is super nice, friendly, and supportive. I hope my future working groups will be like this one. In addition, I would like to thank in advance the reviewers of my thesis. Thank you for the time you spent reading and commenting on them.

I would also like to thank all the incredible people I spent my time at IOW with. Erika, Markus, Marvin, Leonie, Sven, and many others. It was very pleasant both to discuss scientific matters and to spend free time with you.

Auf Deutsch möchte ich mich insbesondere bei Mira und Anna bedanken. Vielen, vielen Dank! Ich habe von euch sehr viel über die Sprache und, generell, Deutschland gelernt. Ohne euch würde ich überhaupt super schlecht Deutsch sprechen und nicht so perfekt intergiert werden. Ich bin sehr sehr glücklich, dass ich euch kennengelernt habe.

Наконец, по-русски, я бы хотел поблагодарить Ксению. Большое спасибо за твою помощь и поддержку, которые очень сложно переоценить, в течении этих трех лет. Я очень рад, что этот этап был пройден вместе с тобой.

1

Introduction

Oxygen is fundamental for biodiversity and chemical processes in terrestrial and marine ecosystems on Earth (Limburg et al., 2020). While terrestrial organisms can efficiently take up oxygen from the atmosphere, most marine species use dissolved oxygen (DO) to support their metabolic activity. However, the amount of DO may be limited, promoting the development of oxygen minimum zones (OMZs) or hypoxic zones in the water. The terminology used in oceanography is drawn from medical sciences (Van Liere and Stickney, 1964; Barach, 1950). Hypoxia is defined as oxygen concentration below an arbitrary threshold (in oceanography, it is usually 2 ml O₂/l, which is used in this thesis, or 2 mg O₂/l), and anoxia – as the absence of oxygen (Roman et al., 2019; Conley et al., 2002b; Sarmiento et al., 1988). Both hypoxia and anoxia have been capturing oceanographers' attention for decades.

Many scientists are concerned about the expansion of OMZs. “The Ocean is Losing its Breath” is the title of the bulletin published by IOP-UNESCO (Intergovernmental Oceanographic Commission of UNESCO) in 2018 (Breitburg et al., 2018a). Indeed, numerous studies reported a decline in oxygen in the World Ocean (e.g., Diaz and Rosenberg, 2008; Breitburg et al., 2018b; Watson, 2016). More precisely, according to Schmidtko et al. (2017), the World Ocean's oxygen content has decreased by 4.8 ± 2.1 petamoles (10^{15} moles) since 1960. If the negative trend continues, the following expansion of the hypoxic and anoxic zones may significantly affect the nutrient cycle and World Ocean's productivity (Altieri et al., 2021; Falkowski et al., 2011; Limburg and Casini, 2018; Laffoley and Baxter, 2019). Figure 1.1 illustrates the problem of OMZs expansion.

Figure 1.1 shows two distinct types of marine systems affected by hypoxia. The first type is represented by open ocean areas where hypoxia occurs at the intermediate depths (from 100 to 500 m) (Paulmier and Ruiz-Pino, 2009). Those areas are bound to the highly productive upwelling systems (off the coast of Peru, California, Namibia, etc.) (Escribano et al., 2009; Mullins et al., 1985; Glessmer et al., 2009) and in the Indian Ocean, where they are connected to the seasonal monsoon circulation (McCreary et al., 2013). The second type consists of the coastal systems worldwide. These include the Chesapeake Bay, the Northern Gulf of Mexico, the Gulf of St. Lawrence in North America, the Black Sea, the Baltic Sea, the East China Sea in Eurasia, etc. They are strongly heterogeneous in physical and geographical properties, as summarized in Fennel and Testa (2019). In shallow systems with pronounced tidal dynamics (e.g., Chesapeake Bay), the hypoxic zone is spatially limited and not permanent in time (usually establishes in spring as a result of the enhanced pycnocline and disappears in autumn due to enhanced mixing) (Zhou et al.,

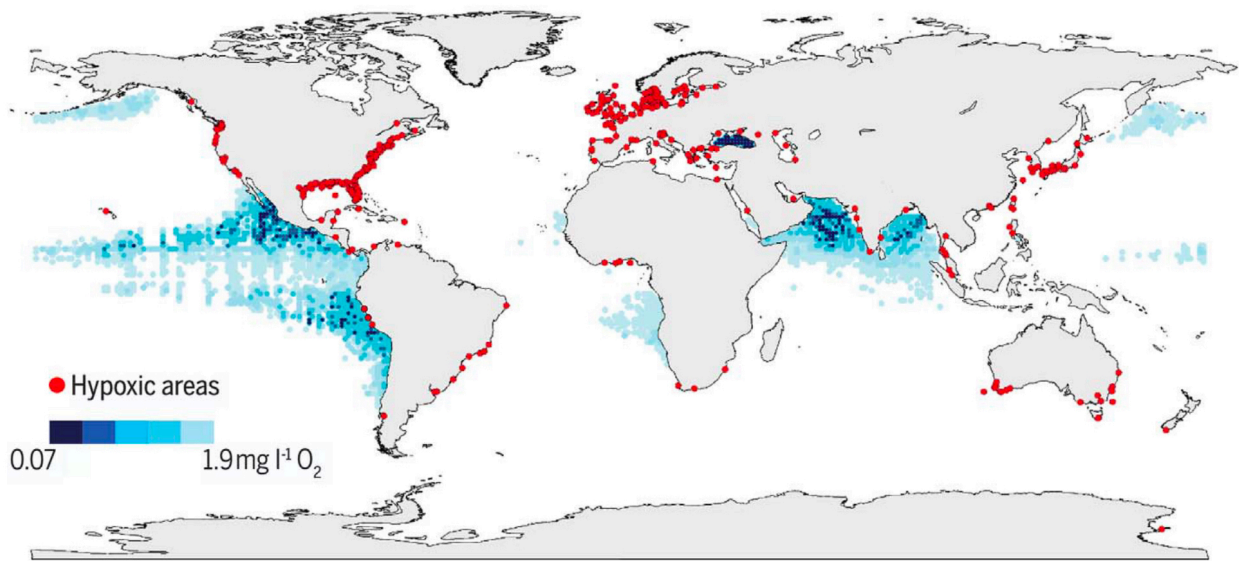


Figure 1.1: Global map of OMZs at 300 m of depth (blue-shaded areas) and the coastal sites where anthropogenic nutrient input has exacerbated or caused the oxygen decline down to less than 2 mg/l (red dots). Data downloaded from the World Ocean Atlas 2009. From Breitburg et al. (2018b). Reprinted with permission from the American Association for the Advancement of Science (AAAS).

2014; Testa and Kemp, 2014; Li et al., 2016). During summer, hypoxia can be interrupted by a strong storm but is quickly reestablished afterward (Testa et al., 2017). In the deeper highly stratified marine systems (e.g., the Baltic Sea), hypoxia is permanent in deep basins due to the lack of vertical exchange with the upper oxygenated layer (Carstensen et al., 2014) and intermittently occurs in shallow areas when the water column is stratified as a result of calm and warm weather (Conley et al., 2011).

Although all systems suffering from expanding hypoxia are usually naturally prone to it (Fennel and Testa, 2019; Conley et al., 2009), they all react to the same anthropogenic drivers, namely climate change and elevated nutrient loads from agriculture and sewage. Meier et al. (2011) proposed several critical mechanisms through which global warming impacts hypoxia. The first mechanism is bound with rising temperatures, causing a decrease in oxygen solubility. Many studies reported positive water temperature trends on regional and global scales (e.g., Levitus et al., 2000; Stramska and Białogrodzka, 2015; Amos et al., 2013; Shaltout and Omstedt, 2014). Belkin (2009) observed accelerated warming in European and East Asian seas between 1982 and 2006. Some studies are considering the impact of increasing water temperatures on hypoxia. For instance, Pezner et al. (2023) studied the response of coral reefs worldwide to the projected changes in water temperatures. They found a significant increase in both duration and intensity of hypoxia, threatening biodiversity and ecosystem functioning. Whitney (2022) demonstrated significant declines in oxygen uptake capacity due to climate change. The effect was particularly noticeable in temperate regions of the Northern Hemisphere, where many hypoxia-prone marine systems are situated. The second crucial mechanism, as outlined by Meier et al. (2011); Yindong et al. (2021) (investigated freshwater lake), Sanz-Lázaro et al. (2015), and Voss et al. (2013), involves a change in the intensity of biochemical processes occurring within ecosystems. Biological activity of living organisms, which includes mineralization and respiration, is roughly described by a Q_{10} function, which tells that the rates of biological processes would increase two times per every 10°C increase in temperature (Wu

et al., 2021). That means elevated mineralization of organic matter (OM) and respiration of marine organisms in warmer climate. Börgel et al. (2023) demonstrated that during the Medieval Climate Anomaly (MCA), higher rates of OM mineralization in the Baltic Sea's sediments led to a significant expansion of hypoxia in the Baltic Sea, compared to the Little Ice Age (LIA), where the temperatures were lower. Another climate change-related mechanism that might affect oxygen dynamics in the future climate is pycnocline strengthening due to a warmer upper layer (Li et al., 2020; Capotondi et al., 2012). It decouples the surface and deep ocean layers, limiting the vertical oxygen transport therefore contributing to hypoxia development (Couespel et al., 2019). All listed mechanisms collectively contribute to the spread of hypoxia under future climate projections.

Another factor in hypoxia formation is nutrient input from land, which has noticeably increased during the 20th century (Beusen et al., 2016). Despite the undeniable role of climate change in hypoxia expansion, the effects of elevated nutrient input from land may dominate, especially in the near future (e.g., Meier et al. (2019a) for the Baltic Sea). Nutrient supply promotes extensive phytoplankton growth. The dead organisms consequently sink in the water column as OM (or detritus), where they are mineralized by bacteria back to inorganic nutrients. Mineralization requires oxygen, so it forms an oxygen demand. Therefore, studying the effects of different nutrient reduction policies being applied to various marine systems worldwide (e.g., Artioli et al. (2008) for European seas) is as crucial as experiments involving climate change.

To be able to predict and, eventually, tackle the problem of hypoxia expansion in a certain marine system, its oxygen dynamics, i.e. a set of complex biochemical (e.g., mineralization, respiration, and photosynthesis) and physical (e.g., advection and diffusion) processes, have to be quantified. It requires numerical experiments with coupled hydrodynamical-biogeochemical models since many processes cannot be measured directly (e.g., mineralization of OM) (e.g., Williams and Askew, 1968), making the measurements both spatially and temporally scarce. The study of Jin et al. (2007) serves as an example of that approach applied to the entire World Ocean. However, the Global Circulation Models (GCMs) do not resolve some critical coastal marine systems correctly (for example, the Baltic Sea or the Chesapeake Bay) due to their complex coastline and bathymetry features and coarse resolution in atmospheric forcing (Ye et al., 2018; Jakobsson et al., 2019). Therefore, the Regional Circulation Models (RCMs) were developed to properly investigate the oxygen dynamics of the regional marine systems. Studies of the regional marine systems are very important since they are mostly affected by anthropogenic pressure (Korpinen et al., 2021), and, at the same time, coastal communities are highly dependent on them Lazarus et al. (2016).

This thesis is focused on the semi-enclosed Baltic Sea – a marginal sea located in Northern Europe with one of the largest man-made hypoxic areas in the world. Despite substantial progress in understanding its oxygen dynamics, it was recently set as one of the primary objectives for future research within the Baltic Sea community (Kuliński et al., 2022). One of the most prominent questions is how the composition of the oxygen sources and sinks altered during the major deoxygenation of the Baltic Sea and what would happen with oxygen sources and sinks when the nutrient forcing is reduced. Is there any way back to the past pre-anthropogenic state, or will the hysteresis effect make the required effort unbearable for the Baltic Sea nations? Another question is related to the Baltic Sea inflows – a natural mechanism ventilating its deep waters. Are they getting less effective? How is the O₂ that is introduced by an inflow, consumed in the Baltic Sea?

In the following, these questions are answered with these studies: Naumov et al. (2023b), referred to as the ventilation paper, Naumov et al. (2023a), referred to as the sensitivity paper, and Meier et al. (2023),

referred to as the variability paper. In the [ventilation paper](#), the dynamics of O₂ and H₂S sources and sinks in the central Baltic Sea below the halocline are investigated on a climatological timescale (from 1948 to 2018) utilizing a regional coupled model. In the [sensitivity paper](#), the two sensitivity experiments with reduced nutrient inputs were carried out to estimate the system's response to it. The Baltic Sea's ventilation by the inflows from 1948 to 2018 and their internal variability in general are also covered in the ventilation and variability papers. In addition, the model validation, i.e. comparing the model with observational and reanalysis data, is performed and discussed in the [ventilation](#) and [variability](#) papers.

The thesis is structured as follows. In [Section 2](#), the main physical and biogeochemical features of the Baltic Sea are discussed. [Section 3](#) presents material and methods applied in all three studies. In [Section 4](#), the main results of the three studies are demonstrated. In the last Section ([Section 5](#)), the results are discussed, and the main conclusions are formulated.

2

The Baltic Sea

The Baltic Sea (BS) is a semi-enclosed sea located in the temperate latitudes of the Northern Hemisphere. Its restricted connection to the open ocean makes it highly sensitive to external forcing (Pedersen, 1982) to such an extent that Stigebrandt and Gustafsson (2003) describe the BS's state as a result of external forcing. The BS's bathymetry, catchment area, and location of the main monitoring stations are shown in Figure 2.1. This Section provides an overview of the BS's physical (Section 2.1) and biogeochemical (Section 2.2) properties and features, making it a unique coastal marine system. Section 2.2 also describes the processes governing the O₂ and H₂S dynamics of the BS.

2.1 PHYSICAL PROPERTIES

2.1.1 CLIMATE

Since the BS and its catchment area are located in a temperate climate, meteorological parameters and sea surface temperature (SST) exhibit strong intra-annual variations. Based on the ERA5 reanalysis data (Hersbach et al., 2020, 2023) averaged from 1940 to 2022 over the BS and its catchment area (Klemeshev et al., 2017), surface air temperature varies from approximately -6 °C (January) to more than 16 °C (July). The negative temperatures persist during the 3 winter months (December, January, February) and March. Energy and water balances are defined as the right-hand sides of the energy (2.1) and water budgets (2.2) equations:

$$EB = R_{\text{net}} + SF + LF \quad (2.1)$$

$$WB = P - E \quad (2.2)$$

EB [Wt m⁻²] and WB [mm day⁻¹] stand for water and energy balances, respectively. When they are negative, the unit area is losing energy/water. R_{net}, SF, and LF are net radiation at the surface, and sensible and latent heat fluxes, respectively (positive fluxes are downward). P and E represent evaporation and total precipitation.

They also exhibit intra-annual variability governed by variations in radiation forcing. Figure 2.2 shows the spatial distribution (Panels C, D) and seasonal cycles (Panels A, B) of water and energy balances over

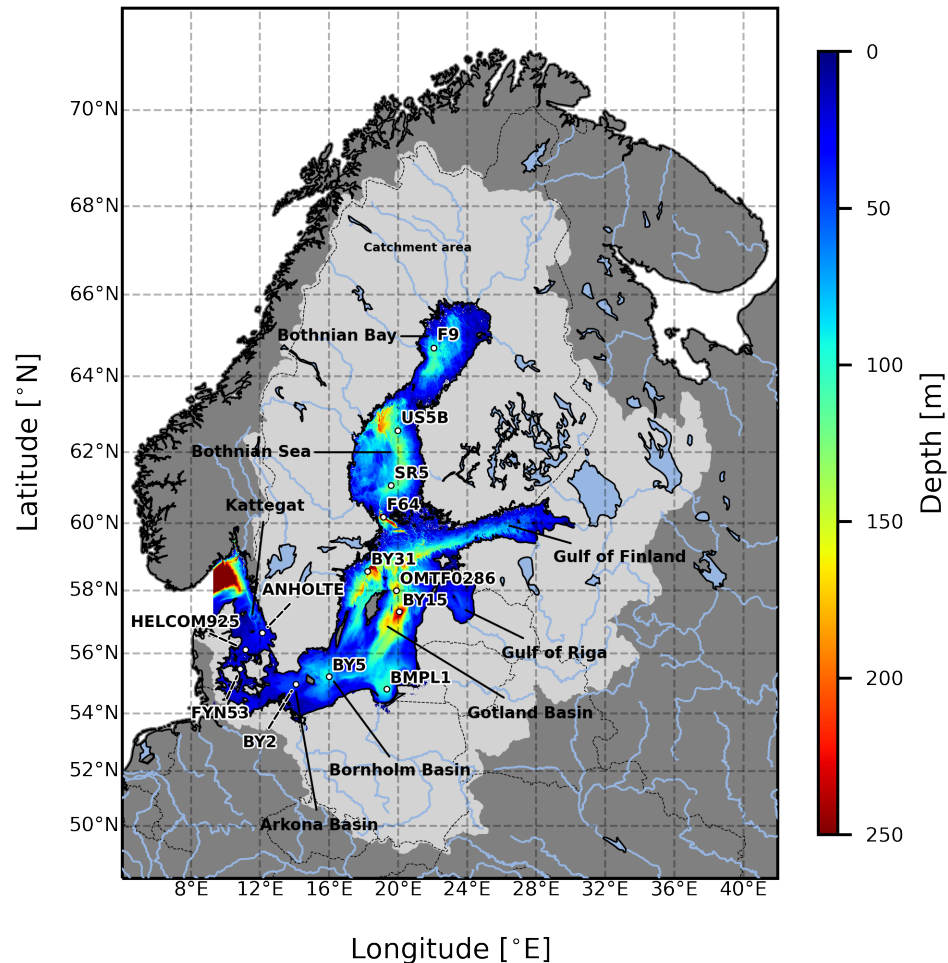


Figure 2.1: Bathymetry of the BS (color-shaded area), its catchment area (light grey area), and the location of selected monitoring stations (white dots). The color bar is limited to a depth of 250 meters (Meier et al., 2023).

the BS and its catchment area according to the ERA5 data. It is visible that the water balance is only positive, which indicates the deposition of precipitated water later discharging into the BS with rivers and ground waters. The smallest values are observed in the central part of the BS, where precipitation is almost balanced by evaporation. The lowest difference between mean E and P is observed from May to July due to the high values of E during the summer. The energy balance is evenly distributed over land with 2-3 Wt m^{-2} values. Over the sea, the gradients are much stronger due to the more variable latent and sensible fluxes identified by Kniebusch et al. (2019a) as the main drivers of SST changes across the main part of the BS. As for the variability within the year, the energy balance is positive from March to September following the increase of incoming shortwave solar radiation. The findings based on the ERA5 data are in good agreement with the observational-based study (Lindau, 2002).

The BS is characterized by strong natural variability (Markus Meier et al., 2021). A pronounced periodicity with a period of 30 years was observed in many parameters of the BS (Radtke et al., 2020; Medvedev and Kulikov, 2019; Kniebusch et al., 2019b). In many studies (e.g., Johansson et al., 2001; Rutgersson

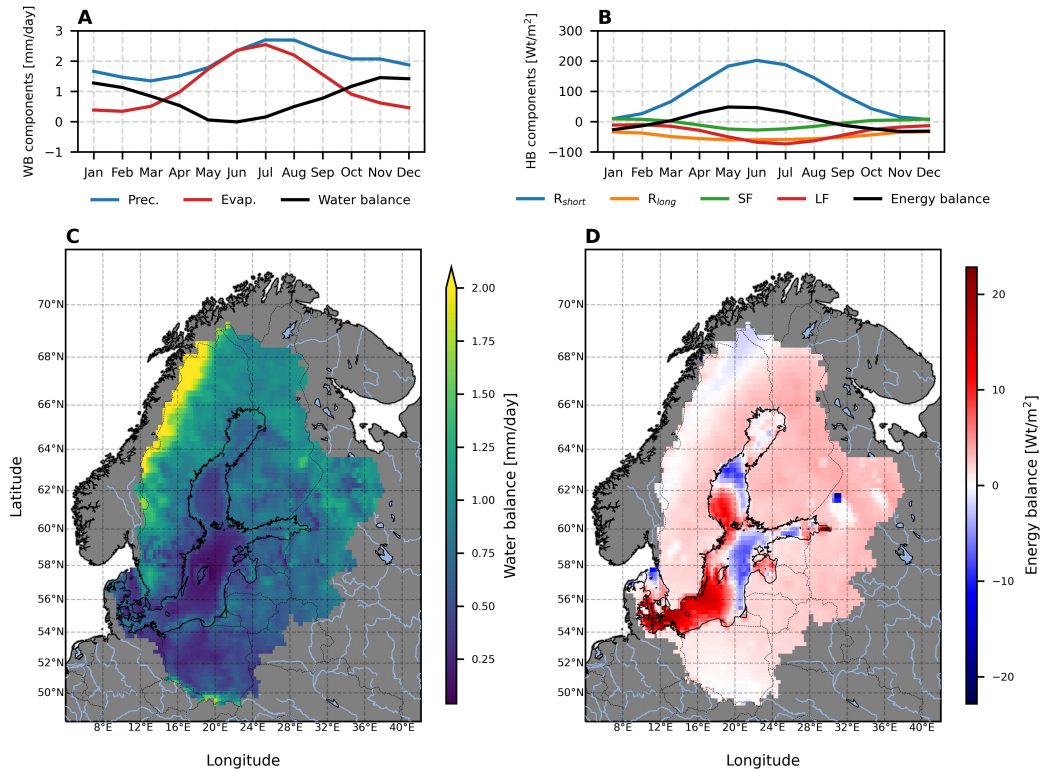


Figure 2.2: The seasonal cycle of water and energy balances and their components (A, B) and the spatial distribution of water and energy balances over the BS and its catchment area (C, D).

et al., 2014; Kniefbusch et al., 2019a), this internal variability was attributed to the North Atlantic Oscillation (NAO) - a climate pattern defined as either the difference between sea level pressure in certain stations in the Iceland and Azores regions or as the first empirical orthogonal function (EOF) of the sea-level pressure field in the North Atlantic (Pokorná and Huth, 2015). The NAO affects atmospheric circulation, determining climate at the interannual timescale on both sides of the North Atlantic (Trigo et al., 2002; Bonsal et al., 2001; Pociask-Karteczka, 2006). Börgel et al. (2020) found that the Atlantic Multidecadal Variability (AMV), defined as the SST anomaly in the North Atlantic, interacts with the NAO by shifting its centers of action and consequently altering the internal variability caused by the NAO. In conclusion, both NAO and AMV have pronounced signals in the internal variability over the BS region.

2.1.1.2 CIRCULATION

The BS is characterized by estuarine circulation (Placke et al., 2018). This type of circulation implies rather decoupled surface and bottom layers with different dynamics. Figure 2.3 outlines the main circulation of the BS. It shows two different types of circulation (in the upper and lower layers) driven by different mechanisms.

The circulation in the upper layer is driven by river runoff water entering the sea, mainly from the Gulf of Finland, Bothnian Sea, and Bothnian Bay to the north (Lehmann and Hinrichsen, 2000). This water flows toward the Danish straits due to barotropic differences in pressure forming a few cyclonic

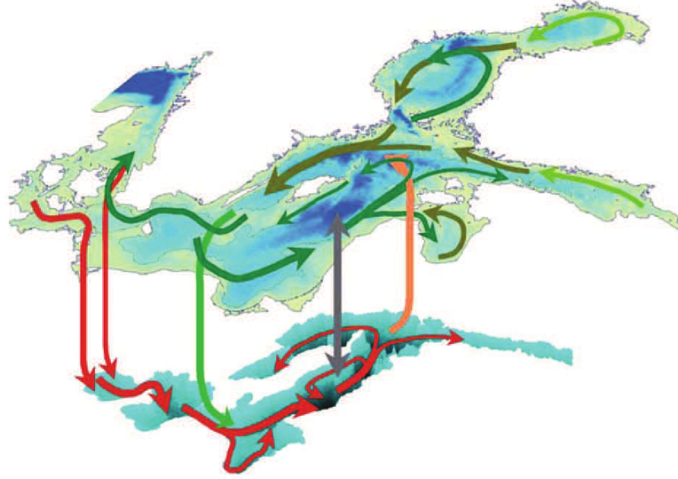


Figure 2.3: Mean circulation of the BS (Elken and Matthäus, 2008). Green lines represent the surface brackish waters, and red lines – the bottom salty waters. Vertical orange and green arrows indicate upwelling and downwelling, respectively. The gray arrow depicts mixing.

cells in geostrophic balance (Döös et al., 2004). The bottom circulation is mainly driven by the inflows from the North Sea propagating to the BS's deep basins along the bottom as gravity currents (Meier, 2007). The inflows do not bring the same amount of salt and O_2 to all BS sub-basins. Sub-basins closer to the North Sea (the Arkona and Bornholm basins) receive disproportionately more salt and O_2 than the Gotland Basin, as shown in many studies (e.g., Meier, 2007; Mohrholz et al., 2015; Matthäus and Lass, 1995). Not all inflows from the North Sea are driven by the same mechanism. There are baroclinic and barotropic inflows (Meier et al., 2006).

The non-homogeneous temperature and salinity fields along the horizontal transect induce baroclinic inflows. It causes pressure differences promoting the water movement (Stigebrandt, 2001). Since density gradients are essential for baroclinic inflows, calm, warm weather with reduced mixing promotes their development (Feistel et al., 2006). Those conditions are usually met during the summer. Baroclinic inflows are considered small or medium-scale, so they do not usually transport high amounts of oxygen or salt to the BS. A recent study by Barghorn et al. (2023) demonstrated that small inflows, but not necessarily baroclinic, are changing their seasonality, probably due to climate change.

Barotropic inflows are driven by wind and can transport a high amount of oxygen and salt to the BS. The Major Baltic Inflows (MBIs) are the strongest barotropic inflows, defined as inflows transporting more than 1Gt of salt to the BS. They occur intermittently, approximately every 10 years (Mohrholz, 2018; Matthäus et al., 2008). Those inflows require first easterly winds for approximately 20 days, creating a sea level difference between the North Sea and the BS, and then strong westerly winds with the same duration (Lass and Matthäus, 1996). Since wind is the main factor driving barotropic inflows, they occur more often in winter (Matthäus and Franck, 1992). Although some studies reported a decrease in MBIs frequency (e.g., Schinke and Matthäus, 1998), considering the recent long stagnation period (from 1983 to 1992), recent studies assumed this long stagnation period to be part of the natural variability (e.g., Schimanke and Meier, 2016; Mohrholz, 2018; Lehmann et al., 2022). Hence, a systematic long-term trend in MBIs was not detected.

Overall, the BS's circulation is a good example of an estuarine-like circulation where the motion of the upper layer is driven by the sea level gradients due to the runoff and Coriolis force. The bottom circulation is mainly driven by the gravity currents caused by inflows from the North Sea. The upper and lower layers of the BS are dynamically connected via upwellings and downwellings. There is also some exchange via mixing. Tidal waves do not affect the motion of the BS significantly, but the local wind, as well as low-pressure systems, produce standing waves (called seiches), usually with a period of 2 days or less (Wübber and Krauss, 1979; Samuelsson and Stigebrandt, 1996).

2.1.3 TEMPERATURE, SALINITY, AND ICE COVER

Temperature and salinity are two essential physical properties of the seawater. In addition to their sole effects on the physical and biological processes (e.g., sea ice formation and species distribution), together they form a density field, which also significantly affects physical and biogeochemical processes in the sea (Kahru and Nommann, 1990; Nielsen, 2005). To illustrate the mean state of the sea surface temperature (SST), sea surface salinity (SSS), and sea ice cover in the BS, the data from the Copernicus physical re-analysis for the BS (Copernicus, 2023b) were analyzed. For constructing the mean fields, the data were averaged between 1993 and 2021. The results are presented in Figure 2.4. It is visible that all three fields (SST, SSS, and sea ice) have very pronounced gradients.

SSS varies in the BS from 0 to 30 g kg^{-1} , which greatly exceeds the variability in the open ocean (Carton et al., 2019). The salinity gradient is mostly zonal – from the Danish straits with the highest salinity to the eastern Gulf of Finland, where water is very close to fresh. However, in the northern BS, there is also a negative meridional gradient (the water is less salty to the north), which is explained by the higher river discharge toward the north (Snoeijs-Leijonmalm and Andrén, 2017). So, the SSS in the BS is controlled mainly by the river discharge (Leppäranta and Myrberg, 2009). The bottom salinity is mainly controlled by the inflows from the North Sea. They bring high amounts of salt from the much saltier North Sea (Janssen et al., 1999), which accumulates in the deep BS's basins (e.g., Lehmann et al., 2004), setting the mean salinity of the deep waters (deeper than 70 meters) close to 11 g kg^{-1} (Copernicus, 2023b). The profound difference between surface and bottom salinities leads to the permanent halocline located at 60–80 meters depth (Väli et al., 2013), which decouples surface and bottom waters and plays an important role in oxygen dynamics (see the next Subsection). Changes in precipitation and runoff govern the large-scale temporal dynamics of the BS's salinity (which explains more than 50% of the variability according to Meier and Kauker (2003)), which themselves are influenced by the modes of natural climate variability (e.g., NAO or AMV) (e.g., Börgel et al., 2022; Hänninen et al., 2000). It leads to a 30-year periodicity in the precipitation, runoff, and salinity fields (Radtko et al., 2020). Some studies reported a significant negative trend in the BS's salinity (e.g., Hänninen et al., 2000). However, in the variability paper, it was shown that no trends in the BS salinity take place within a few hundred years (see Section 4).

Since the BS is located in temperate latitudes, its temperature and ice cover exhibit strong seasonal variability following the changes in the energy balance (see Section 2.1.1). The spatial gradients in SST and ice cover also reflect the spatial distribution of the energy balance. Thus, the highest mean SST (around $10 \text{ }^\circ\text{C}$) is observed in the southern part of the sea. To the north, SST is decreasing, with the lowest in the Bothnian Bay (around $5 \text{ }^\circ\text{C}$). However, the instantaneous distribution of the SST in the BS along the coast is influenced by upwelling, which may significantly lower the SST (Lehmann and Myrberg, 2008). Due to the features of local circulation, the typical upwelling region in the BS is the Swedish coast (Gidhagen,

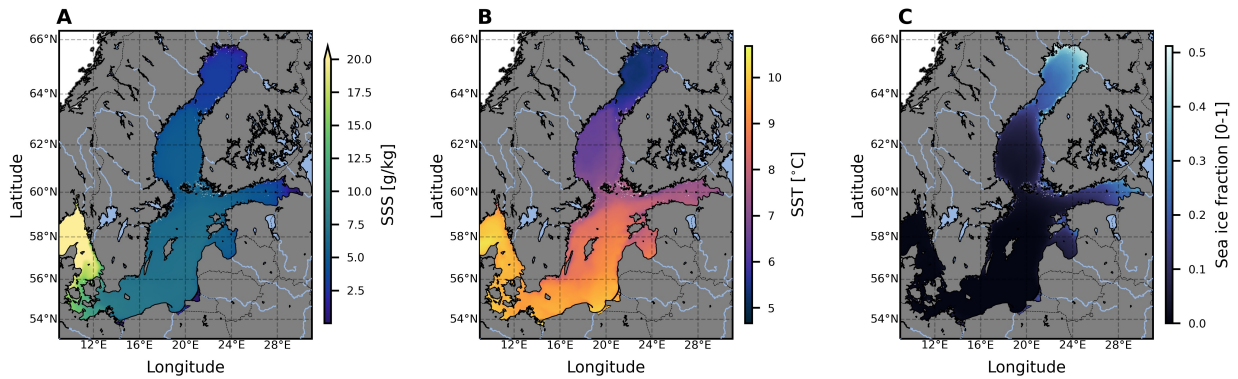


Figure 2.4: Mean SSS (Panel A), SST (Panel B), and sea ice cover (Panel C) based on the data from Copernicus physical BS reanalysis (Copernicus, 2023b).

1987; Zhang et al., 2022), but in the case of specific winds, upwelling could also be observed along the southern coast of the sea (Zhang et al., 2022). In the vertical BS temperature distribution, the one notable feature is the cold intermediate layer, which can be observed in the BS for almost the whole year and is a unique feature of the BS (Chubarenko and Stepanova, 2018). Climate variability of the BS temperature is characterized by a pronounced positive trend making the BS one of the fastest-warming seas in the world (Mackenzie and Schiedek, 2007). From 1982 to 2006, the BS's SST increased by 1.35°C , around seven times larger than the global rate (Belkin, 2009). Kniebusch et al. (2019a) conducted an in-depth analysis of the temperature trends in the BS for 1850-2008. They found that the BS is not warming at the same rate everywhere. The strongest trends were observed in the bottom temperature of the Bornholm Deep ($0.15^{\circ}\text{K/decade}$), which was connected by Barghorn et al. (2023) to the shift in the inflows' activity, and in the summer mean SST in Bothnian Bay ($0.09\text{-}0.12^{\circ}\text{K/decade}$). They also identified the possible drivers of observed SST trends, which are sensitive and latent heat fluxes, so the SST trend is driven by climate change, which is supported by other studies (e.g., Dutheil et al., 2022).

The mean sea ice fraction is only present in the northern region of the BS (mostly the Bothnian Bay) and in the enclosed gulfs (e.g., the Gulf of Finland and the Gulf of Riga). Omstedt and Nyberg (1996) investigated the sensitivity of the BS ice toward climate change utilizing a hydrodynamical model. They split winters into three categories (mild, normal, and severe). According to their results, on average, in a severe winter, almost the whole sea (except the central Gotland Basin) is covered by ice. In a normal winter, the ice cover is limited to the northern BS (the Bothnian Sea and Bay) and the coastal zone in the eastern BS, including the Gulf of Finland and the Gulf of Riga. Ice cover in a mild winter is only present in the Gulf of Finland and the Bothnian Bay. Omstedt and Nyberg (1996) also conducted sensitivity studies applying the warmer atmospheric forcing. They found that, in this case, the number of severe winters drastically decreased, forcing the climate toward more oceanic conditions. Thus, the BS's ice cover is projected to dwindle with climate change, and the ice season to shorten. The same is reported, e.g., by Vihma and Haapala (2009), Haapala et al. (2015), Meier et al. (2022), and Jevrejeva et al. (2004).

2.2 BIOGEOCHEMICAL PROPERTIES

The BS demonstrates complex biogeochemistry due to its location and unique features (e.g., MBIs) (Kuliński et al., 2022). MBIs induce strong salinity gradients and may even temporarily change the species distribution (Hinrichsen et al., 2022). But even in the absence of MBIs, the BS exhibits a strong mean salinity gradient, which restricts the habitat of some species making them more vulnerable to the changing environment (Vuorinen et al., 2015). One of the prominent examples is the eastern Baltic cod, whose abundance was greatly decreased during the last stagnation period (Nissling and Westin, 1997). Some problems of the BS have primarily anthropogenic origin. Those include the spreading of hypoxia and anoxia due to elevated primary production rates (e.g., Andersen et al., 2017), and climate change, which alters biogeochemical interactions in the BS (Andersson et al., 2015; Viitasalo and Bonsdorff, 2022) and promotes its deoxygenation.

2.2.1 OXYGEN AND HYDROGEN SULFIDE

A permanent halocline and a long residence time make the BS naturally inclined toward hypoxia in the deep basins (Leppäranta and Myrberg, 2009). Evidence of hypoxia presence manifested as laminated sediments and as the change in concentration of some trace metals was found since the established connection between the BS and the World Ocean (Lenz et al., 2015; van Helmond et al., 2018). Hypoxia and anoxia presence were also reported by the model studies covering the period from 1850-2006 (Meier et al., 2018) and the last millennium (Börgel et al., 2023). However, hypoxia in the BS has been spreading intensively since the second half of the 20th century, which was observed in both observations and reanalyses (e.g., Krapf et al., 2022; Kōuts et al., 2021; Almroth-Rosell et al., 2021), and model simulations (e.g., Meier et al., 2018). Carstensen et al. (2014) reported a more than 10-fold increase in hypoxia in the last 114 years. The hypoxic area in the late summer of 2018, calculated by Hansson et al. (2018), was 82 000 km² (32% of the Baltic Proper), and the hypoxic volume was 3 100 km³ (22% of the Baltic Proper’s water volume). The general decline in DO concentrations, although accompanied by peaks caused by MBIs, is visible in Figure 2.5 (especially in the Gotland Deep).

The oxygen concentration in a given volume is determined by its supply due to its advection and diffusion into the volume, as well as its uptake by photosynthesis, and its consumption by remineralization of OM, respiration by marine biota, and its advection and diffusion out of the volume (Fennel and Testa, 2019). It is described by equation (2.3), where the left-hand side represents the total change of the O₂ content within a certain box, and the right side represents the total flux across the box’s boundaries (the first term) and the total change of O₂ within the box due to biogeochemical processes. The rearrangement of equation (2.3) leads to equation (2.4) with zero on the right-hand side.

$$\frac{d}{dt} \iiint_V O_2 \, dx \, dy \, dz = \iint_S \vec{v} \vec{n} O_2 \, dx \, dy + \iiint_V \frac{\partial O_2}{\partial t} \, dx \, dy \, dz \quad (2.3)$$

$$\frac{d}{dt} \iiint_V O_2 \, dx \, dy \, dz - \iint_S \vec{v} \vec{n} O_2 \, dx \, dy - \iiint_V \frac{\partial O_2}{\partial t} \, dx \, dy \, dz = 0 \quad (2.4)$$

The first mechanism of the deep waters’ ventilation is the intermittent inflows from the North Sea. They advect the high amounts of oxygen to the deep basins, temporarily interrupting hypoxia and anoxia (e.g., Mohrholz, 2018; Lehmann and Post, 2015). This is visible in Figure 2.5, where the Gotland Deep

gets oxygenated after each MBI from 1975/76 to 2014. Neumann et al. (2017) concluded that the most important parameter of MBI for oxygenation is its acting time. They compared two MBIs – one from 2014 (the biggest MBI in terms of transported salt) and one from 2003 (an event composed of several smaller inflows, but longer in total). They found that the longer 2003 event brought more oxygen to the deep BS than the stronger 2014 event (Figure 2.5). Despite the temporal reduction of hypoxia and anoxia, MBIs cannot fully ventilate the deep BS. After the inflow ceases, hypoxia and anoxia quickly re-establish, sometimes even expanding (Liblik et al., 2018). Meier et al. (2018) explained the recent spread of hypoxia by elevated respiration of heterotrophic plankton and nitrification. In addition, they pointed out that MBIs themselves may contribute to the central BS' deoxygenation by importing OM alongside DO. MBIs also strengthen pycnocline limiting the oxygen exchange with the upper oxygenated layer, which further promotes hypoxia. This mechanism explains the overall recession of hypoxia during the last stagnation period reported, e.g., by Almroth-Rosell et al. (2021) and Conley et al. (2002a).

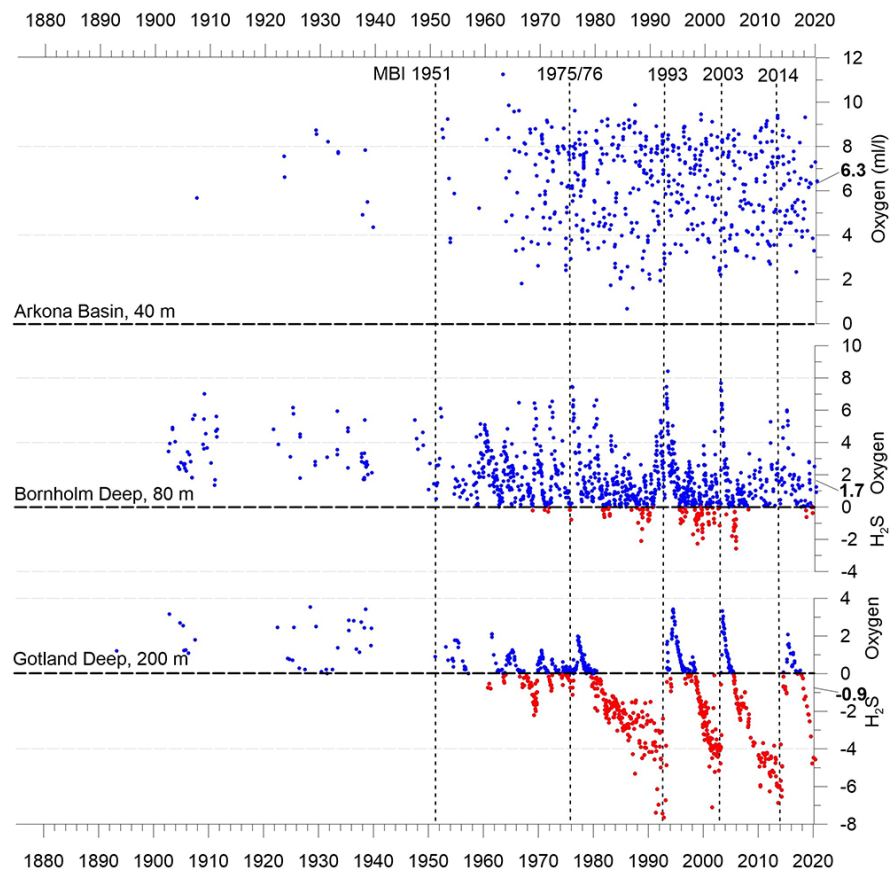
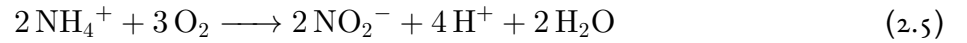


Figure 2.5: Long-term variations in dissolved oxygen concentrations (blue dots) and hydrogen sulfide (red dots) converted to negative oxygen equivalents in the near-bottom layer at the following stations: BY1 (Arkona Basin, 45m), BY5 (Bornholm Basin, 92m), and BY15 (Gotland Deep, 245m) based on the IOW and ICES observational data (Kuliński et al., 2022).

The oxygen supply across the pycnocline is another mechanism that influences hypoxia development in the deep BS. This mechanism is controlled by small- and mesoscale processes (Elken et al., 2006; Kuzmina et al., 2008; Conley et al., 2009; Väli et al., 2013). Increased halocline strength (the salt gradient between upper and lower layers) decouples the upper and lower layers limiting the vertical exchange between them,

which, in turn, facilitates hypoxia formation. The vertical exchange plays an important role on small to intermediate temporal scales, especially in the Gotland Basin. According to the measurements conducted by [Holtermann et al. \(2022\)](#), the annual oxygen flux across pycnocline is equal to 2.39-3.97 Mt O₂, which is more than would be transported by a typical MBI (around 1-2 Mt O₂).

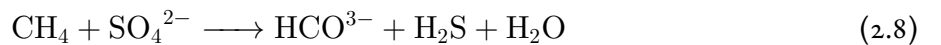
Oxygen is the electron acceptor with the highest energy yield. Therefore, remineralization of OM, nitrification, and oxidation of hydrogen sulfide (H₂S), each performed by a different group of bacteria, consume oxygen when it is available, making oxygen a key factor determining zonation of diagenetic reactions in the BS ([Lehtoranta et al., 2009](#)). Nitrification transforms ammonium (NH₄⁺) into nitrite (NO₂⁻) and eventually into nitrate (NO₃⁻). It is performed by nitrifying bacteria and is governed by the following reactions:



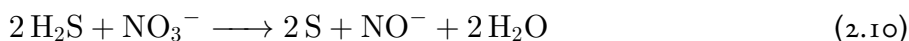
Nitrification mostly occurs at the redoxcline in the water column or in the sediments, where there is a constant supply of oxygen from one side and a constant supply of ammonium from the other side ([Jäntti et al., 2018](#)). High nitrification rates were also reported by [Myllykangas et al. \(2017\)](#) during the MBI that supplied O₂ to the environment containing NH₄⁺. Remineralization of OM transforms all dissolved and particulate organic matter (DOM and POM) into inorganic form (DIC, DIP, and DIN). The rate of the transformation is determined by the type of OM. Labile OM is quickly remineralized, semi-labile OM is remineralized slower, and refractory OM will be most likely buried since its mineralization rates are quite low ([Schneider et al., 2002](#)). When the rate of OM supply exceeds the remineralization rate, deposition of OM takes place. Unmineralized OM constitutes oxygen debt calculated as the amount of O₂ needed to remineralize all stored OM and oxidize all stored reduced compounds. This deposition has happened in the BS for a few decades ([Rolff et al., 2022](#)). In the BS, H₂S is produced and stored in the deep basins in the absence of oxygen and is oxidized when it enters the oxic environment. This might happen either by advection of O₂ by the MBI or via leaking to the upper oxic levels from below, indicating the upward shift of redoxcline, which is usually coupled with overall deoxygenation. The dynamics of H₂S are described in the same way as for O₂:

$$\frac{d}{dt} \iiint_V \text{H}_2\text{S} \, dx \, dy \, dz - \iint_S \vec{v}\vec{n}\text{H}_2\text{S} \, dx \, dy - \iiint_V \frac{\partial \text{H}_2\text{S}}{\partial t} \, dx \, dy \, dz = 0 \quad (2.7)$$

The first two terms in the equation (2.7) represent the same processes as in the equation (2.4), namely the total change of H₂S content in a given volume and the advection and diffusion of H₂S across the volume's boundaries. The third term consists of a different from O₂ set of processes. H₂S is produced via sulfate reduction, which takes place in anoxic environments. This means no oxygen and other electron acceptors, e.g., nitrogen, iron, or manganese oxides available. It is operated by the sulfate-reducing bacteria, see, e.g., [Korneeva et al. \(2015\)](#) for the Gdansk Deep. Via sulfate reduction, OM is remineralized, and SO₄²⁻ is reduced to H₂S ([Jørgensen et al., 2019](#)). Sulfate reduction is also a pathway in anaerobic CH₄ (methane) oxidation, described by equation (2.8).



Sulfate reduction occurs in the BS's deep basins (e.g., Gotland Deep and Landsort Deep) and in the anoxic sediments (Fonselius, 1963), which are considered to be the biggest H₂S source in the BS. H₂S can be oxidized to S (elemental sulfur) by O₂ or any oxide, e.g., NO₃⁻ (equations 2.9 and 2.10, respectively).



In addition, H₂S can be removed from the system via pyrite (FeS₂) formation and via Mn²⁺ and Fe²⁺ reduction. According to Henkel et al. (2019) and Schulz-Vogt et al. (2019), Mn²⁺ reduction contributes significantly to H₂S removal in the Black Sea. Reed et al. (2016) pointed out the iron shuttle mechanism (iron, precipitated as oxyhydroxides, transported from coastal waters to the deep basins and contributes to the H₂S budget) as an important term in the H₂S and indirectly O₂ budgets. Hydrogen sulfide has been deposited in the BS during the last few decades, expanding the euxinic (H₂S is present) area in the BS (Krapf et al., 2022).

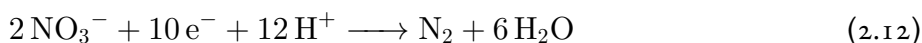
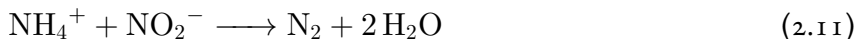
2.2.2 BIOGENS

As was reported in the previous Subsection, a substantial decline in the BS's O₂ content was observed during the last few decades. This was attributed to the significant anthropogenically-induced increase in N and P loads from land (mainly from agriculture and sewage) and from the atmosphere. Atmospheric loads are mainly applicable for N since its airborne input constitutes around 20% to 40% of the total input (Wulff et al., 1990), which were 4 times larger in the 1980s compared to the year 1900 (Gustafsson et al., 2012).

The response of the BS's ecosystem to the elevated nutrient input from land is outlined in Figure 2.6. Compared to the normal state of the BS' ecosystem (Figure 2.6, left Panel), increased nutrient input stimulates primary production (this phenomenon is called eutrophication) (Rönnberg and Bonsdorff, 2004), which in turn boosts the total DOM and POM pools as well as respiration of the biota from higher trophic levels. This situation leads to elevated oxygen consumption primarily due to aerobic remineralization of OM in the sediments (see Section 2.2.1 for more details). To mitigate the harmful effect of eutrophication, the BS Action Plan (BSAP) was developed by HELCOM (the Baltic Marine Environment Protection Commission, also known as the Helsinki Commission – an intergovernmental organization, that connects the BS countries in the field of the BS protection) in 2007 (HELCOM, 2007). It was adopted by all HELCOM member states. BSAP is based on the BALTSEM model (Savchuk et al., 2012) and limits nutrient input into the BS by implementing a fixed quota (maximum allowable input or MAI) of total nitrogen and phosphorus discharging into the sea. Initially, the BSAP's goal was to reach a “good environmental state of the BS” – a state with less hypoxic area and reduced eutrophication (Borja et al., 2015) by 2021. However, in the last update of the BSAP in 2021 (HELCOM, 2021), the initial goals were concluded to be not met. Indeed, the BS's environmental state has not improved during the last two decades despite significant nutrient loads reduction (Savchuk, 2018).

The most plausible reason for the absence of any improvement in the BS's environmental state during the last two decades is the strong inertia in removing nutrients from the biogeochemical cycles in the sea. Phosphorus is removed from the biogeochemical cycles only via burial in the sediments (Radtke et al., 2012), where, in the presence of oxygen, it binds with iron forming complex compounds. If the environ-

ment becomes anoxic, stored phosphorus is released back into the water column (Lehtoranta et al., 2009). Nitrogen is removed from water in the form of dinitrogen gas (N_2), which is produced via anammox 2.11 and denitrification 2.12 reactions:



In the anammox reaction, ammonium is oxidized by nitrite, producing dinitrogen. The anammox reaction is carried out by anammox bacteria. Anammox can be a significant pathway for nitrogen removal in the BS, according to Hylén et al. (2022) and Hannig et al. (2007). Denitrification is run by denitrifying bacteria in the absence of oxygen but in the presence of NO_3^- . Therefore, the highest rates of denitrification are observed in the redoxcline in the water column, which for the BS corresponds to the halocline depth of 60-80 meters (Väli et al., 2013), and in the sedimentary redoxcline, which is usually located within the first 10 millimeters of the sediments Bonaglia et al. (2013); Hietanen and Kuparinen (2008). Since denitrification mostly occurs at the redoxcline, it is coupled with nitrification, which is called coupled nitrification-denitrification (Conley et al., 1997).

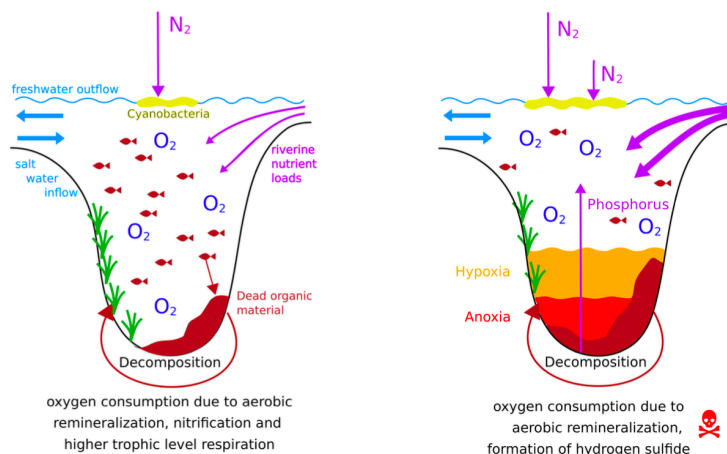


Figure 2.6: Simplified sketch demonstrating normal biogeochemical functioning of the BS (left) and the biogeochemical processes altered by the eutrophication. Adapted from Kniebusch (2019).

The pools of dissolved inorganic phosphorus (DIP), which is mainly made up of PO_4^{3-} , and dissolved inorganic nitrogen (DIN), which primarily consists of NO_3^- , NO_2^- , and NH_4^+ , depend on oxygen availability. When little or no oxygen is available, the DIP pool gets larger since phosphorus is released from the sediments, and the DIN pool shrinks due to elevated denitrification (Conley et al., 2002a; Savchuk, 2018). That pattern was also observed by Andersen et al. (2017), especially during the winter. These conditions might favor cyanobacteria development, which, unlike the other phytoplankton, takes up dinitrogen from the atmosphere, and therefore depends only on phosphorus availability in the water. Since the BS (except the northernmost part) is a nitrogen-limiting system Thomas et al. (2003), cyanobacteria sustain eutrophication, generating more nitrogen necessary for other phytoplankton to grow (e.g., Karlson et al., 2015). This builds the positive feedback that links the BS deoxygenation with further eutrophication.

cation via cyanobacteria's development. It was called "the vicious circle of the BS's eutrophication" by [Vahtera et al. \(2007\)](#) and depicted in [Figure 2.6](#), where the right panel features phosphorus release from the sediments under hypoxic and anoxic conditions and cyanobacteria's expansion. The "Vicious circle" was further studied, e.g., by [Savchuk \(2013\)](#), and [Rydin et al. \(2017\)](#). [Meier et al. \(2018\)](#) proposed an extension of the feedback loop driven by saltwater inflows, which, according to their results, bring additional OM to the system, further promoting oxygen consumption. Since calm and warm weather facilitates cyanobacteria growth ([Kaiser et al., 2020](#); [Kanoshina et al., 2003](#)), climate change may exacerbate the "vicious circle of the BS". However, a significant increase in cyanobacteria's biomass was found neither in future projections ([Meier et al., 2019b](#)) nor in past simulations, e.g., during the MCA ([Börgel et al., 2023](#)). Cyanobacteria's biomass might also change in response to a different nutrient forcing. For instance, [Neumann et al. \(2002\)](#) conducted a model experiment with reduced nutrient loads and found increased cyanobacteria's biomass. Due to all the presented uncertainties, it might be concluded that the BS's response, modulated by climate change or nutrient loads reduction, still needs to be studied more.

3

Data and methods

In this Section, the different models (Section 3.1), statistical methods applied for data postprocessing (Section 3.2), and observational datasets used for model validation (Section 3.3) are discussed. Three model simulations were conducted and analyzed. The reference simulation from 1948 to 2018 was analyzed in the [ventilation paper](#), and two sensitivity studies from 2019 to 2089 were performed in the [sensitivity paper](#). The reference simulation was validated against the observations in the [ventilation paper](#). In addition, another model setup was thoroughly validated in the [variability paper](#). Various statistical methods were used in the data post-processing. That includes iterative and agglomerative cluster analysis techniques (Jaeger and Banks, 2023), that were applied in the [ventilation paper](#), a linear regression framework, which allows ranking predictors based on their contribution to the total explained variability, linear trend analysis, Empirical Orthogonal Functions (EOF) analysis (Hannachi et al., 2007). Those methods were applied in both the [sensitivity](#) and [ventilation](#) papers. In addition, the Generalized Additive Mixed Models (GAMM) framework (Simpson, 2014) was applied in the [variability paper](#). In all statistical tests conducted in this thesis, the result was regarded as statistically significant if the confidence level was more than 95% ($p\text{-level} < 0.05$), which is the common standard for environmental sciences (see, e.g., Kwak, 2023).

3.1 MODELS

3.1.1 GENERAL INFORMATION ABOUT MODELS

Two different model systems were utilized in the thesis. The coupled 3-dimensional hydrodynamical-biogeochemical Modular Ocean Model (MOM) – Ecological Regional Ocean Model (ERGOM) (MOM-ERGOM) regional model setup for the BS (applied in the [sensitivity](#) and [ventilation](#) papers) and the Rossby Centre Ocean (RCO) circulation model (Meier et al., 1999) (applied in the [variability paper](#)).

MOM was developed in the NOAA’s Geophysical Fluid Dynamics Laboratory (NOAA GFDL) in 1990. Ever since, the model has been upgraded, and new versions have been released. This study employs the fifth version of the model (MOM₅), which was released in 2012 (Griffies, 2012). It simulates the ocean- and, by coupling with the SIS ice model (Hunke and Dukowicz, 1997), sea ice dynamics. MOM₅ employs a finite-difference numerical method to solve the complete set of primitive equations, namely the 3-dimensional Reynolds-averaged equation of motion under the Boussinesq and hydrostatic approxima-

tions, continuity equation, and two tracer equations for salinity and temperature, to calculate the motion of water, sea-level differences, and transports of salt and heat. The k-profile parameterization (KPP), described by Large et al. (1994), was applied as a turbulence closure scheme. The regional MOM setup utilized in this study has the regular orthogonal Arakawa B grid (Arakawa and Lamb, 1977) with 224 longitude and 242 latitude grid points corresponding to 3 nautical miles horizontal resolution. The vertical domain was discretized into 152 vertical levels by applying the z^* vertical coordinate (Griffies, 2012). It covers a depth range down to 264 meters with a vertical resolution of 0.5 at the surface to 2 meters near the bottom. This means the deepest BS basin (the Landsort Deep) is approximately 200 meters artificially shallower in the model, which does not introduce any big uncertainties since its area is very small. As a regional setup, it has a western open boundary in the Skagerrak, enabling exchange with the North Sea. For the barotropic open boundary conditions (OBC), the hourly sea level data (1948-2018) from a tide gauge station were used. Baroclinic OBC and biogeochemical tracers' OBC were set as climatology mean values for each month (12 timesteps) to represent the seasonal variability. Initial conditions were devised from the spin-up simulation to represent the system's state adequately. The CoastDat2 meteorological dataset (Geyer, 2014) was used to force the model.

The biogeochemical part of the coupled MOM-ERGOM model was performed by ERGOM (Neumann et al., 2022, 2021; Radtke et al., 2019). ERGOM reproduces the dynamics of the main nutrients, namely carbon (C), nitrogen (N), and phosphorus (P). Phosphorus in ERGOM is represented by its inorganic form (phosphates – PO_4^{3-}) and organic forms (particulate, defined in ERGOM as phosphorus in particulate organic carbon, and dissolved organic phosphorus – POCP and DOP, respectively). Inorganic forms of nitrogen in the model are ammonium (NH_4^+) and nitrates (NO_3^-). Organic forms of nitrogen include particulate nitrogen (also defined as nitrogen in particulate organic carbon) – POCN, and dissolved – DON. All forms of inorganic carbon are aggregated into dissolved inorganic carbon (DIC) state variable, which is treated in the model as carbon dioxide (CO_2). Organic carbon is represented in the model by particulate and dissolved organic carbon (POC and DOC) state variables. ERGOM splits the phytoplankton community into three functional groups: large phytoplankton (lpp), small phytoplankton (spp) (both assimilate inorganic nutrients), and cyanobacteria (cya), which take up dinitrogen from the atmosphere. The grazing pressure on phytoplankton is implemented via the zooplankton state variable (zoo). Phyto- and zooplankton transform into detritus, represented by a single state variable (det) in the model. Model detritus contains all main nutrients (C, N, and P) in the fixed ratio known as the Redfield ratio (C:N:P ratio is 106:16:1) (Redfield, 1934). However, in particulate and dissolved organic carbon (DOC and POC) state variables, the C:N:P ratio might be non-Redfield if a certain nutrient is limited (Neumann et al., 2022). ERGOM includes the closed O_2 and H_2S cycles, and both elements are included in the model as separate state variables. Their dynamics can be briefly described as follows: oxygen is produced via photosynthesis carried out by phytoplankton, air-sea exchange, and utilized in organic matter's mineralization, which includes both detritus and all OM state variables, both in sediments and in the water column. Nitrification also consumes oxygen in the model. Since ERGOM has no separate variable for NO_2^- , nitrification transforms NH_4^+ directly to NO_3^- . In the water column, it is represented by a separate process. At the same time, in the sediments, it is coupled with denitrification and therefore called coupled nitrification-denitrification in the sediments (see Section 2 for more information about that process). Oxygen is also consumed via the oxidation of H_2S to SO_4^{2-} , which is carried out in the model in two steps, first from H_2S to S (elemental sulfur) and later from S to SO_4^{2-} . Oxygen is also consumed by the aerobic metabolic activity of all forms of living organisms in the model (respiration). H_2S

is produced under anoxic conditions via mineralization of OM (sulfate reduction) in the water column and sediments and, being in contact with O_2 or NO_3^- , oxidized to elemental sulfur. A detailed description of all model equations can be found in [Neumann et al. \(2022\)](#). The BS setup of the MOM-ERGOM coupled model has already been applied in numerous studies in which it demonstrated good performance (e.g., [Neumann, 2010](#); [Voss et al., 2011](#); [Kuznetsov and Neumann, 2013](#); [Neumann et al., 2017](#)).

RCO is a physical model in which the ocean circulation model is coupled with a Hibler-type model simulating sea ice dynamics ([Meier et al., 2003](#); [Meier, 2007](#)). Mixing on the subgrid scale is parametrized via a state-of-the-art $k - \epsilon$ turbulence closure scheme applying flux boundary conditions ([Meier, 2001](#)). An FCT (flux-corrected, monotonicity-preserving transport) scheme is embedded in the model without explicit horizontal diffusion ([Meier, 2007](#)). The model domain encompasses the BS, excluding the Skagerrak, with an open horizontal boundary in northern Kattegat. In case of an inflow, the model results at the open boundary are perturbed toward the climatological profiles. If there is an outflow, a modified Orlanski radiation condition is applied ([Meier et al., 2003](#)). Heat, radiation, momentum, and matter fluxes between ocean, atmosphere, and sea ice are parametrized via the bulk formulae adjusted for the BS region ([Meier, 2002](#)). The model's horizontal resolution was 3.7 km (around 2 nautical miles), and the vertical resolution was 3 m. The vertical domain covers the depth range down to 248 m (83 depth levels in total). The horizontal domain has 320 longitude and 362 latitude points. Model simulation spanned the period from 1850 to 2008 with every-other-day output frequency. The RCO setup used in this study has already been applied successfully to the BS region in many studies (e.g., [Meier, 2007](#); [Meier et al., 2003](#); [Eilola et al., 2011](#)).

3.1.2 TRACER EXPERIMENT (VENTILATION PAPER)

In the [ventilation paper](#), a tracer experiment made up of two parts was performed. The first part investigated the dynamics of the O_2 and H_2S budget terms on the climatological time scale (from 1948 to 2018 – 71 years). This analysis utilized the monthly mean output of the MOM-ERGOM model. To investigate the budget of any tracer, a certain volume of water has to be chosen. The vertical domain was restricted by the depth of 70 meters, which roughly separates well-oxygenated upper waters from hypoxic lower waters ([Holtermann et al., 2020](#)). In the horizontal plane, the central BS was divided into four separate sub-basins listed from the closest to the BS's entrance to the most distant: the Bornholm Basin (BB) – the shallowest sub-basin with only the upper boundary active, the eastern Gotland Basin (eGB) with three active boundaries (two lateral – Slupsk Furrow in the West, and the nGB in the North, and one upper boundary), the northern Gotland Basin (nGB), which borders eGB in the South and wGB in the North, therefore having two lateral boundaries and one vertical upper boundary, and the most distant western Gotland Basin (wGB), which has one lateral boundary (borders nGB in the East) and one vertical boundary (upper). Graphically it is depicted in [Figure 3.1](#).

The second part of the experiment is dedicated to the central BS's deep water ventilation by the North Sea inflows and its changes from 1948 to 2018. Daily zonal O_2 transport data from the Arkona transect (see [Figure 3.1](#)) from the MOM-ERGOM model were used to detect the inflows. First, a 5-day running mean filter was applied to the transport data to remove the high-frequency variability. Positive values of O_2 transport for more than five consecutive days were considered an inflow event, following [Mohrholz \(2018\)](#). Two following inflow events with a time interval of less than five days were considered a single event. An example of the algorithm's performance is shown in [Figure 3.2](#) (only the year 1948 is depicted).

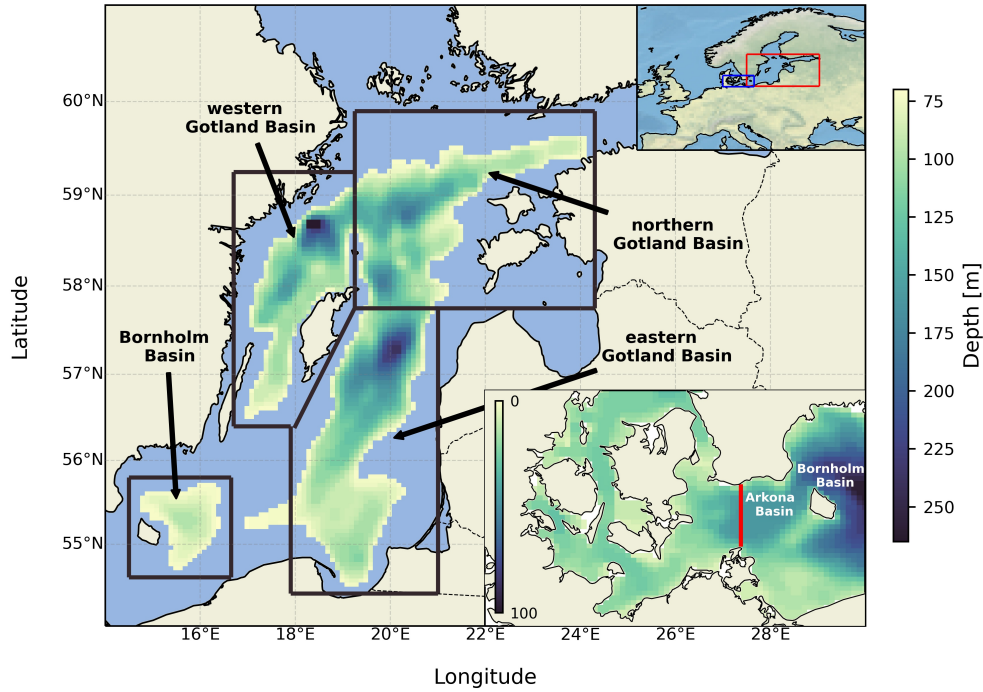


Figure 3.1: MOM-ERGOM bathymetry at 70 meters depth and four defined sub-basins. The Arkona transect is marked in the lower right panel via the vertical red line. The central and western BS (main and lower right panels, respectively) are designated on the upper right panel as red and blue rectangles, respectively (Naumov et al., 2023b).

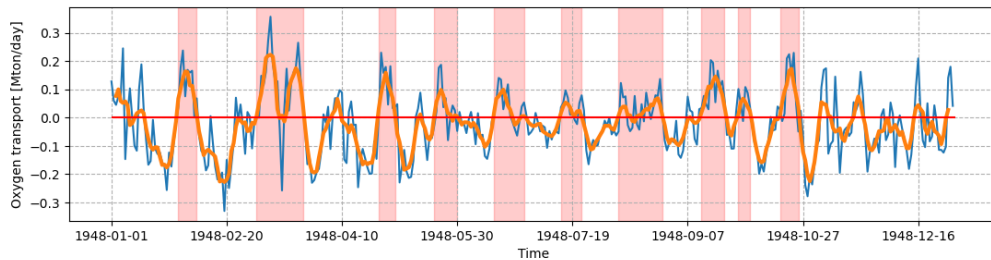


Figure 3.2: Oxygen zonal transport across Arkona transect (see Figure 3.1). The orange curve denotes 5-day rolling averaged data, and the red curve marks zero. Identified inflows are colored red (Naumov et al., 2023b).

For each identified inflow, the following statistics were collected: inflow start and end dates, duration, and the total amount of oxygen transported during the event. In the next step, an agglomerative cluster analysis method with Euclidean distance metric (Dokmanic et al., 2015) and Ward’s clusterization algorithm (Ward, 1963) was applied to clusterize the result into four distinct groups of inflows based on the amount of oxygen transported to the central BS (strong, moderate, small, and very small inflows). Following Figure 3.3, 29 strong, 147 moderate, 313 small, and 306 very small inflows were identified. In the absence of strong inflows, moderate and small inflows usually carry the most oxygen. Strong inflows, if they occur, transport up to 50% of the total oxygen transported to the central BS. Strong inflows occur irregularly with no long-term trend. The ventilation paper is focused on the 29 strongest inflows (1st class). Although they may not carry the most oxygen in a particular year, they are essential to the ventilation of

remote sub-basins (particularly the wGB) since they are accompanied by salt inflows and therefore are less buoyant.

To study the distribution of oxygen transported to the central BS by the 29 biggest inflows, an additional MOM-ERGOM model run was carried out with 29 new oxygen tracers included, following the approach proposed by Ménesguen et al. (2006). Each tracer initiates as zero and represents oxygen brought to the central BS by a specific oxygen inflow. During a certain inflow's action time, all oxygen crossing the Arkona transect is attributed to the corresponding tracer. Since all additional inflows' tracers have their transport equations and participate in their own biogeochemical cycles, it is possible to estimate how fast oxygen imported by a specific inflow is consumed and which processes are responsible for that. This so-called element tagging method has already been applied to the MOM-ERGOM model, e.g., by Neumann et al. (2017).

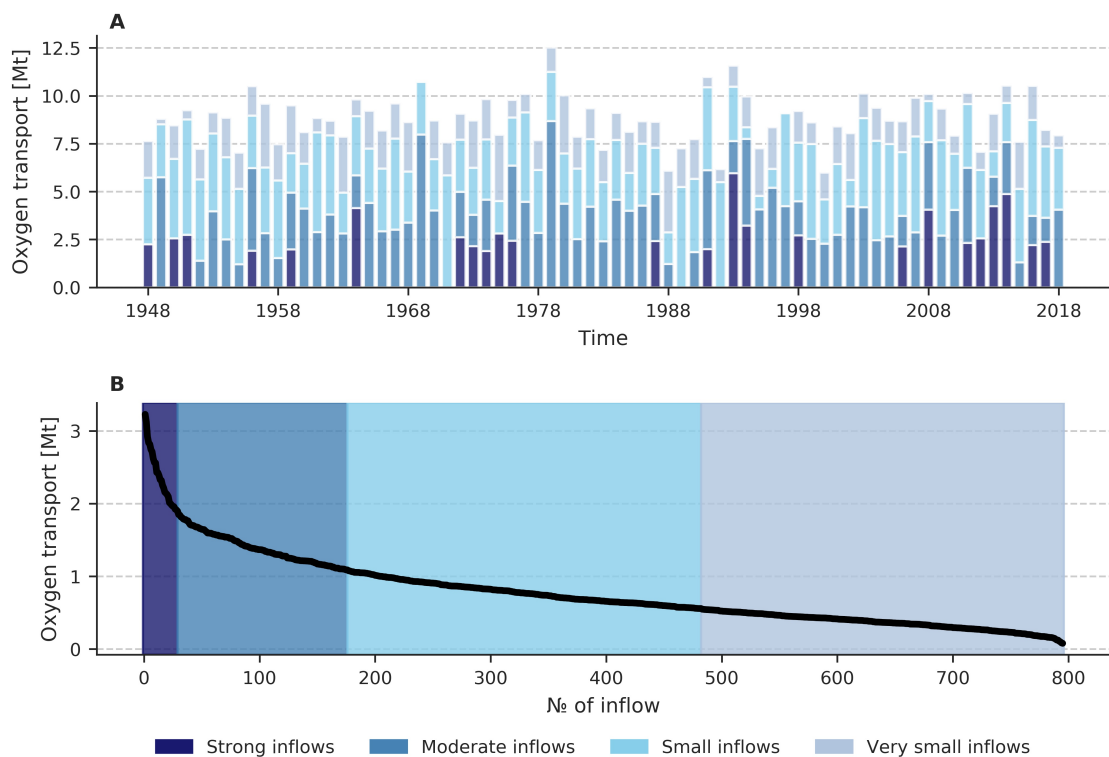


Figure 3.3: Annual oxygen transport across the Arkona transect (see Figure 3.1) by each inflow class (A). Total oxygen transport per individual inflow in descending order (B). Colors show inflow classes. The following classes were found: strong inflows (carry more than 1.8 Mt O₂), moderate inflows (carry from 1.8 Mt O₂ to 1 Mt O₂), small inflows (carry from 1 Mt O₂ to 0.5 Mt O₂), and very small inflows (carry less than 0.5 Mt O₂). Mt stands for 10⁹ kg (Naumov et al., 2023b).

3.1.3 SENSITIVITY STUDIES (SENSITIVITY PAPER)

Sensitivity studies were performed in the [sensitivity paper](#) and were dedicated to investigating the BS's response to the reduced nutrient inputs into the sea. In total, three different nutrient loads scenarios were analyzed. The reference scenario (short Ref.) utilized the data from the MOM-ERGOM setup, which

has already been analyzed in the [ventilation paper](#). It employs a realistic nutrient forcing based on the HELCOM’s nutrient loads data from 1948 to 2018 ([Svendsen and Gustafsson, 2020](#)). Data gaps were filled with linear interpolation. The BSAP scenario applies constant nutrient input, which follows the BSAP’s 2021 MAI ([HELCOM, 2021](#)). The BSAP scenario prescribes only the total nutrient input into the BS without separation between land and atmospheric loads. The mean atmospheric loads’ seasonal cycle was applied to calculate the atmospheric loads. It was adjusted in a way that matched the BSAP’s MAI. The more rigorous 0.5 BSAP scenario assumes a constant nutrient forcing matching halved BSAP’s 2021 MAI (airborne and waterborne input). Both reduction scenarios encompass the period from 2019 to 2089 (71 years) and were initiated utilizing the data from the reference scenario’s last time step. Total N and P loads were set to 792.2 and 21.7 Kton/a in the BSAP scenario, respectively. It constitutes 97% of the N loads averaged for the last 10 years (815.4 Kton N/a) and 82% of P loads (21.7 Kton P/a). The 0.5 BSAP scenario implies that the numbers presented above are halved. So the total N and P inputs equal 396.1 Kton N/a and 10.85 Kton P/a, respectively. This constitutes 48 and 41% of the loads averaged over the last 10 years, respectively. [Figure 3.4](#) and [Figure 3.5](#) show total nitrogen and phosphorus loads per BS’s sub-basins under all three scenarios, respectively. All sensitivity experiments were run with the same atmospheric forcing from the reference simulation (CoastDat2). This assumption excludes any possible impact of climate change on the BS state.

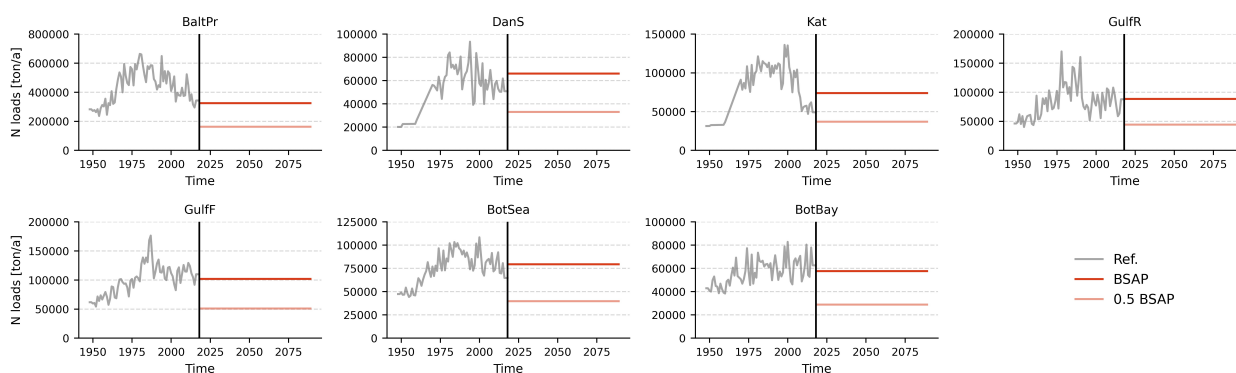


Figure 3.4: Total nitrogen loads to the HELCOM sub-basins of the BS. Reference data are HELCOM data and constant loads are BSAP and 0.5 BSAP Maximum Allowable Input and half of it, respectively. The following abbreviations are used: BaltPr – Baltic Proper, DanS – Danish Straights, Kat – Kattegat, GulfR – Gulf of Riga, GulfF – Gulf of Finland, BotSea – Bothnian Sea, and BotBay – Bothnian Bay ([Naumov et al., 2023a](#)).

3.2 STATISTICAL METHODS

3.2.1 LINEAR REGRESSION FRAMEWORK (VENTILATION AND SENSITIVITY PAPERS)

The linear regression framework was applied to the MOM-ERGOM data (both in [sensitivity](#) and [ventilation](#) papers) to evaluate each budget term’s relative contribution to the total O_2 or H_2S variability, which was done in two separate analyses. In this case, the dependent variable (\bar{y}) is represented by the sum of the independent variables (\bar{x}):

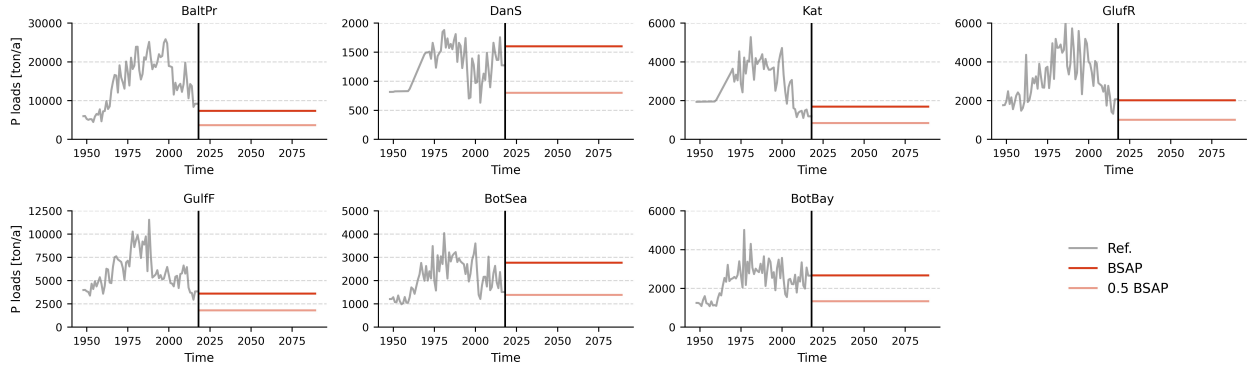


Figure 3.5: Same as Figure 3.4, but for phosphorus (Naumov et al., 2023a).

$$\bar{y} = \sum_{i=1}^N \bar{x}_i \quad (3.1)$$

The regression problem, in this case, is formulated as follows:

$$\tilde{y}_k = \sum_{j=1}^k \alpha_j \tilde{x}_j + \beta_k \quad (3.2)$$

Where k is the iteration (varies from 1 to N), alpha and beta are regression coefficients (fitted by the ordinary least square, or OLS, method), and \tilde{x} is the set of dependent variables selected as follows:

$$k = 1 \rightarrow \tilde{x}_1 = \max_{i \in \{1, 2, \dots, N\}} (\text{corr}[\bar{y}; \bar{x}_i]) \quad (3.3)$$

$$k \neq 1 \rightarrow \tilde{x}_i = \max_{i \in \{1, 2, \dots, N\} \setminus \rho} (\text{corr}[\varepsilon_i; \bar{x}_i]) \quad (3.4)$$

Where the operator corr represents a correlation between the given vectors and is defined in the following way (for standardized data):

$$\text{corr}[Y; X] = \frac{1}{N} \langle Y, X \rangle \quad (3.5)$$

And ε represents the residuals (a part of the variability that the current set of independent variables has not explained) obtained at a certain iteration:

$$\varepsilon_{k-1} = \bar{y} - \tilde{y}_k \quad (3.6)$$

Set ρ is an empty set at the first iteration. It gets a new element after each iteration, which is the serial number of the independent variable selected using either equation (3.3) or equation (3.4), ensuring that no variable is used twice in regression. As comes from the equations, the regression model expands with iterations starting with only one independent variable and finishing with all of them, which, by definition, will give $R^2 = 1$. Each independent variable's relative contribution to the variability can be estimated as

R^2 growth after each iteration. [Kniebusch et al. \(2019a\)](#) applied the analysis with similar logic to the SST data.

3.2.2 CLUSTER ANALYSIS (VENTILATION PAPER)

Cluster analysis is a statistical tool that categorizes data based on a certain feature. The goal of cluster analysis is to maximize the different clusters' variance between each other and, at the same time, minimize the variance within each cluster. In this thesis, two cluster analysis techniques were utilized: hierarchical agglomerative and iterative techniques.

Agglomerative methods treat all data points as distinct clusters and compute a distance matrix at the first iteration. The two closest clusters are merged in the next step, and the distance matrix is recomputed. The algorithm stops when there is only one single cluster left. This agglomeration is summarized in a so-called dendrogram plot. The final step is to decide which number of clusters fits the best based on the dendrogram plot. In the [ventilation paper](#), the distance matrix was computed utilizing the Euclidean distance metric ([Dokmanic et al., 2015](#)) and Ward's algorithm for splitting the clusters ([Ward, 1963](#)).

From iterative methods, the k-means cluster analysis ([Hartigan and Wong, 1979](#)) was used in the [ventilation paper](#). This analysis is much faster than agglomerative methods and consists of the following steps. At first, the predefined number of centroids (equals the number of clusters) is randomly displaced across the vector space. Next, using the distance matrix, each data point is attributed to a specific cluster. After that step, the centroids' coordinates are recomputed using the data points' mean values. The algorithm is repeated until no data point has changed its cluster. In the [ventilation paper](#), the k-means analysis was performed with the Euclidean distance metric to detect periods when an inflow transported a significant amount of oxygen to a certain sub-basin.

3.2.3 EOF ANALYSIS (VENTILATION AND SENSITIVITY PAPERS)

Empirical Orthogonal Functions (EOF) analysis is primarily used as a dimensionality reduction tool. It projects the data to a new EOF space, where the first coordinate axis points in the direction of maximum variability. Each next one always explains less and less variability. Finally, the contributions to the variability become negligible. Hence, the number of dimensions is reduced. Mathematically, the EOF analysis applies the data's covariation (or correlation if the data is standardized) matrix decomposition into eigenvalues and eigenvectors:

$$R = QAQ^{-1} \quad (3.7)$$

Where R is a covariation matrix, A , and Q are matrices containing eigenvalues and eigenvectors of R , respectively. In this formulation, eigenvalues describe the variability explained by each EOF (constantly decreasing), and eigenvectors describe the connection between the original variables and calculated EOFs (can be interpreted as weights of each variable). EOFs' scores themselves are calculated as follows:

$$S = DQ \quad (3.8)$$

Where D is the original data matrix. An EOF analysis was both applied in the [sensitivity](#) and [ventilation](#) papers. In the [ventilation paper](#), it was used to estimate the response of the different O_2 and H_2S budgets terms to inflowing oxygen, and in the [sensitivity paper](#) to separate the nutrient loads reduction effect on O_2 and H_2S budgets from other variability. In the [sensitivity paper](#), the EOFs' scores for the reference

scenario were calculated first:

$$S_{\text{ref}} = D_{\text{ref}} Q_{\text{ref}} \quad (3.9)$$

After that, the obtained Q_{ref} matrix was used to calculate EOFs' scores for the rest two scenarios (BSAP and 0.5 BSAP):

$$S_{\text{BSAP}} = D_{\text{BSAP}} Q_{\text{ref}} \quad (3.10)$$

$$S_{0.5\text{BSAP}} = D_{0.5\text{BSAP}} Q_{\text{ref}} \quad (3.11)$$

This approach guarantees that all three sets of EOFs will describe the same patterns as in the reference scenario. Earth science applications of EOF analysis are described in numerous studies (e.g., [Hannachi et al., 2007](#); [Roundy, 2015](#); [Bi et al., 2021](#)).

3.2.4 GAMM FRAMEWORK (VARIABILITY PAPER)

A generalized additive mixed model (GAMM) framework helps in decomposing the irregular timeseries into long-term and seasonal signals so that:

$$T_i = T_{\text{long}}(t_i) + T_{\text{season}}(\tau_i) + T_0 + \varepsilon_i \quad (3.12)$$

Where the first term represents a smooth decadal variation, the second is a seasonal signal (τ_i denotes intra-annual sampling time ranging from 0 (1st of January) to 1 (31st of December)), the third is an offset (constant), and the fourth is residuals, those temporal autocorrelation is assumed to follow a continuous first-order autoregression model (AR(1)) ([Radtke et al., 2020](#)). The GAMM setup applied in the [variability paper](#) is the same as in [Radtke et al. \(2020\)](#), which means the model was fitted using a restricted maximum likelihood approach, and the functions T_{long} and T_{season} are defined as penalized and cyclic cubic regression splines with 1 degree of freedom per month and decade, respectively. In the [variability paper](#), GAMM was applied to remove seasonal bias in the irregular observational data, therefore, correcting its long-term averages:

$$T_i^{\text{corr}} = T_i - T_{\text{season}}(\tau_i) \quad (3.13)$$

More information on GAMM and its application to observational timeseries might be found in, e.g., [Simpson \(2014\)](#).

3.3 OBSERVATIONAL DATASETS (VENTILATION AND VARIABILITY PAPERS)

Both RCO (applied in the [variability paper](#)) and MOM-ERGOM (applied in both [ventilation](#) and [sensitivity](#) papers, validated in the [ventilation paper](#)) were thoroughly validated. For that purpose, both observational and reanalysis data were used. All datasets utilized in this study are summarized in [Table 3.1](#).

For the MOM-ERGOM validation, which was performed in the [ventilation paper](#), the observational data were made up of two data sources – the ICES (International Council of the Exploration of the Sea) dataset ([ICES, 2023](#)) and the IOW (Leibniz Institute for Baltic Sea Research Warnemünde) observations' database ([IOW, 2023](#)). All observations were acquired as instantaneous point measurements from 1993 to 2018. The following postprocessing algorithm was applied: at the first step, each measurement was associated with a certain region in the central BS (BB, eGB, nGB, or wGB). Next, the observations were attributed to a certain model depth level utilizing the Nearest Neighbor (NN) interpolation method. In

Table 3.1: Description of observational and reanalysis datasets employed in the papers.

Paper	Model	Data	Time frame	Averaging	
				Spatial	Temporal
Variability paper	RCO	ICES	1850-2008	Station-wide	Annual
Ventilation paper	MOM ₅ - ERGOM	ICES, IOW, Copernicus reanalyses	1993-2018	Basin-wide	Monthly
Sensitivity paper					

the third step, all observations were spatially averaged within the domain they were attributed to. Lastly, the observations were temporally averaged to both monthly and climatology means. The Copernicus regional BS biological and physical reanalyses were chosen as model-based continuous references for the model validation (Copernicus, 2023b,a). Both reanalyses utilize a single regional setup of the coupled NEMO-SCOBI model system (Almroth-Rosell et al., 2014; Hordoir et al., 2019). Both reanalyses employ a data assimilation technique, which includes the assimilation of satellite-based SST and Chlorophyll-a measurements and ship and station-based profiles of temperature, salinity, nutrients, and oxygen (T, S, O₂, N, and P). The reanalysis data have a spatial resolution of 2 nautical miles and 56 depth levels. They were obtained as monthly mean fields from 1993 to 2018. The data were remapped to both vertical and horizontal MOM-ERGOM grids by applying combined linear-NN interpolation techniques. In the next step, the result was attributed to a specific region in the central BS and spatially averaged within it. Since the SCOBI model represents H₂S as O₂ equivalents, but ERGOM has a separate H₂S tracer variable, another postprocessing step has to be done. Negative O₂ concentrations were recalculated as H₂S adhering to the following rule: 1 mole of H₂S equals -2 moles of O₂ (Fonselius, 1981). The MOM-ERGOM data were spatially averaged for each studying sub-basin in the central BS for validation. To avoid an undersampling bias in the long-term averaging, in both MOM-ERGOM and Copernicus reanalysis datasets, only months with at least one observation available were included in the long-term average. Variability within a month was considered to be insignificant and was neglected. For the validation results, see Section 4.

In the variability paper, the RCO model was validated against ICES observational data at specific stations (see Figure 2.1 for the stations' names) from 1850 to 2008. The model grid cell nearest to the station was regarded as the station data. For the same station, all observations within a 1° x 0.5° rectangle were considered to belong to that station, i.e., they were spatially averaged. All observations within a single day were averaged. The seasonal signal, calculated by applying the GAMM framework, was subtracted from the observational data to eliminate the undersampling bias when computing the long-term averages. This RCO setup was also validated in, e.g., Meier et al. (2019a, 2022) against various reanalysis and observational data. For the validation results, see Section 4.

4

Oxygen dynamics of the Baltic Sea

In this section, the results of the three papers, namely, [ventilation](#), [variability](#), and [sensitivity](#) papers, are summarized. In [Section 4.2](#), the results of the [ventilation paper](#) are described. There, oxygen dynamics in the central BS on a climatological time scale are discussed. [Section 4.3](#) continues with the results of the [ventilation paper](#), focusing on trends in the BS ventilation by the inflows. In addition, the inflows' variability is discussed in that Section ([variability paper](#)). The results of the [sensitivity paper](#), namely, the sensitivity simulations with the reduction of nutrient loads and the system's response to it, are discussed in [Section 4.4](#). In addition, the summary of the RCO ([variability paper](#)) and MOM-ERGOM ([ventilation paper](#)) validations is given ([Section 4.1](#)).

4.1 VALIDATION SUMMARY

4.1.1 MOM-ERGOM (VENTILATION PAPER)

In the [ventilation paper](#), the MOM-ERGOM model was thoroughly validated against combined ICES and IOW observational datasets and Copernicus regional reanalysis data. Here, only climatological oxygen profiles' and hypoxic and anoxic areas' validation is shown ([Figure 4.1](#) and [Figure A.1](#), respectively). Based on the validation results, it can be concluded that the MOM-ERGOM model adequately reproduces the temporal variability and the mean state of all investigated variables (only O₂ is shown) in all considered sub-basins (BB, eGB, nGB, and wGB).

In [Figure 4.1](#), it is visible that the modeled mean climatology profiles are within the variability range of Copernicus reanalyses' data and observational data, highlighting their overall agreement. However, some uncertainty was also observed. The MOM-ERGOM underestimates the oxygen concentrations in the remote nGB and wGB, which is manifested in [Figure 4.1](#) as stronger, compared to the observations and Copernicus data, oxycline and reduced (or non-existent) variability (translucent area) after approximately 100 meters depth. This indicates the total absence of oxygen in the model, which is not fully consistent with observations and reanalysis, both exhibiting some variability below that depth. At the same time, in the Bornholm Basin, the modeled oxygen profile positively deviates from the observational and reanalysis profiles, starting from approximately 50 meters depth and exhibiting a less pronounced redoxcline. The same pattern can be observed in [Figure A.1](#), manifested there as positive anomalies of bottom oxygen

concentration in the BB and, as a result, a smaller hypoxic and anoxic area. At the same time, the overall hypoxic and anoxic area is overestimated by MOM-ERGOM, but mainly in the Gulf of Finland and the Bothnian Sea (the latter demonstrates neither hypoxic nor anoxic area in reality). However, the agreement is better in the central BS, especially in the eGB, with some overestimation of hypoxic and anoxic areas in the model.

To find a reason behind the observed mismatch between the model and observational/reanalysis data, the halocline depth and strength were calculated for each sub-basin in the BS employing the approach proposed by Väli et al. (2013). A bigger halocline strength was observed across the whole Gotland Basin, where oxygen concentrations were underestimated, and a lower halocline strength was observed in the BB, where the model overestimated the oxygen concentration (see Figure A.2). A possible explanation is an elevated transport from the North Sea caused by the relatively coarse model resolution, which resulted in better oxygenation of the BB – the closest region to the Danish straits, and, simultaneously, in limited oxygen exchange in the Gotland Basin due to the stronger stratification.

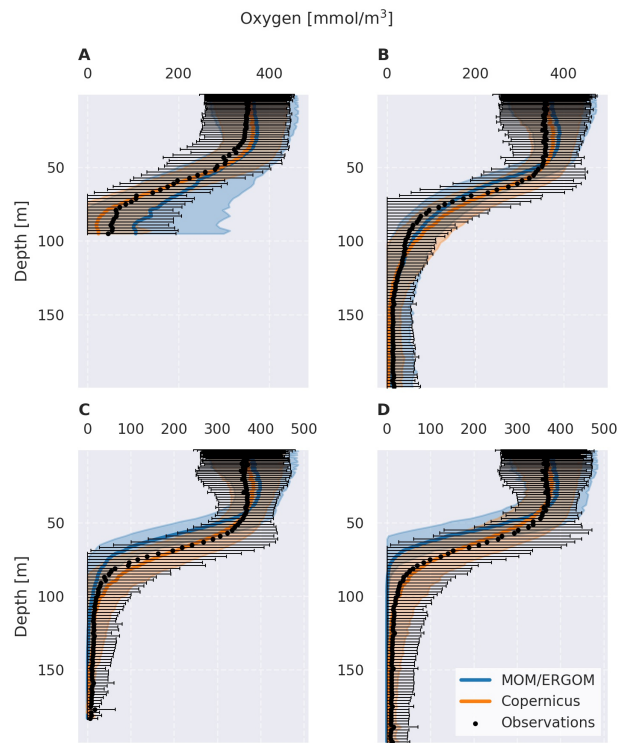


Figure 4.1: Mean climatology DO profiles for all sub-basins (BB (A), eGB (B), nGB (C), and wGB (D)). Colored translucent and black whiskers for model data and observations, respectively, depict the variability ($\pm 2\sigma$). (Naumov et al., 2023b).

4.1.2 RCO (VARIABILITY PAPER)

Figure 4.2 provides some information on the comparison between the time series of simulated and observed (taken from the ICES database) bottom and surface salinities at the selected monitoring stations (see Figure 2.1 for stations' locations) conducted in the variability paper. For most of the stations, the model reproduces the observed multidecadal variability with 30-year periodicity, both in surface and bottom salinity. However, the stations located close to the BS entrance demonstrated less good agreement with the model results. It can be explained by both the undersampling in this area and complex dynamical processes in the transition region between the brackish BS and the salty North Sea. In addition, a lesser agreement between observational and model data is observed at the central BS's stations (e.g., BY15, OMTFo286, BY31) in 1950-1970. This might be related to the models' underestimation of the large MBI in 1951 (Mohrholz, 2018). This was attributed to the coarse atmospheric forcing since the RCO reproduces inflows' activity well with better forcing (Meier et al., 2004).

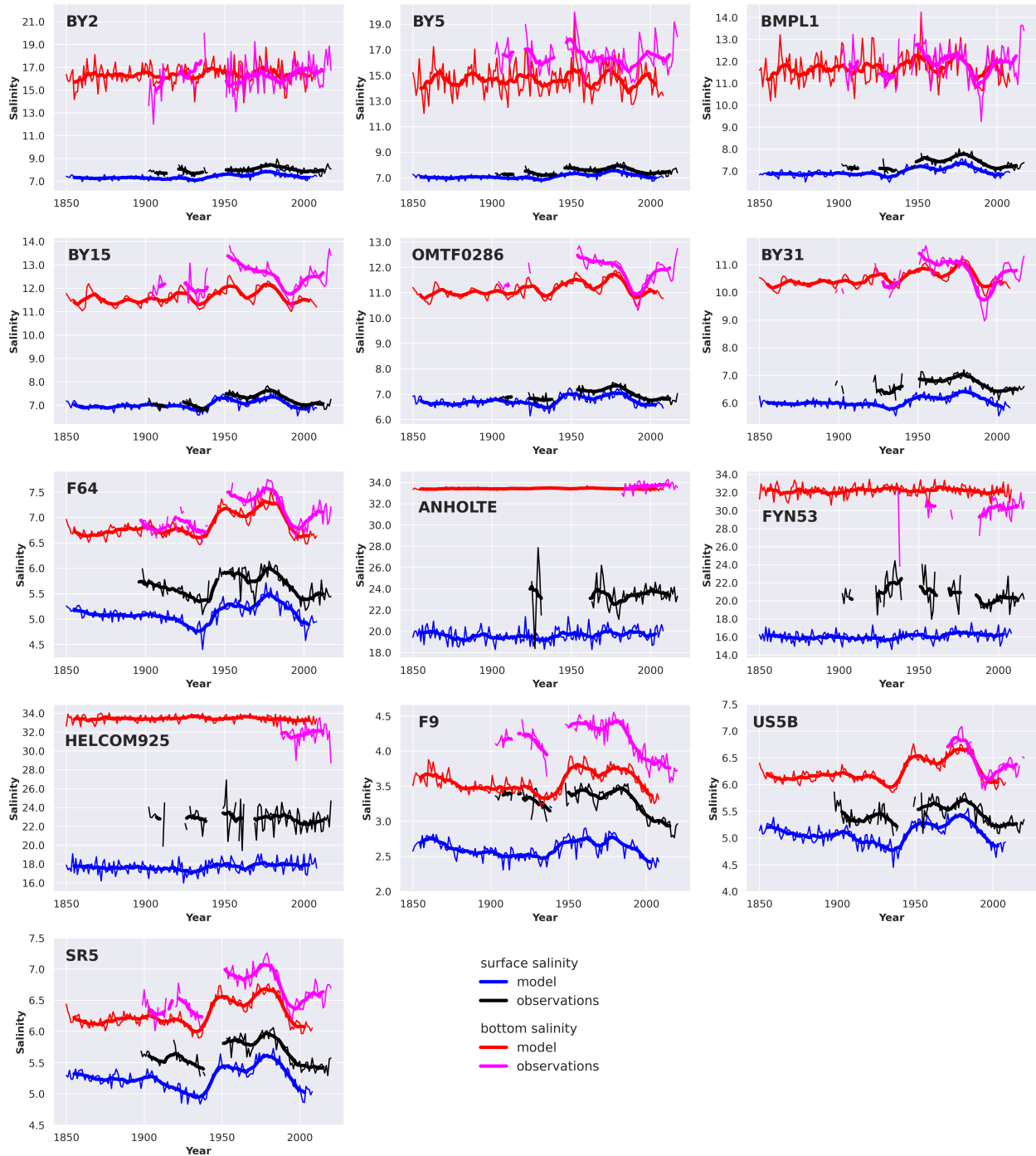


Figure 4.2: Simulated and observed surface and bottom salinities [g kg^{-1}] at various stations across the BS. Thick lines represent the 11-year running mean. Observational data are processed to exclude the seasonal cycle following Radtke et al. (2020) (Meier et al., 2023).

4.2 OXYGEN SOURCES AND SINKS DURING THE LAST 71 YEARS (VENTILATION PAPER)

This Section provides an overview of the results from the [ventilation paper](#). Those include a description of processes governing the oxygen variability in the central BS, namely their differentiation based on their mean values and their contribution to the oxygen variability. The temporal variability is also shown in [Section 4.2.3](#).

4.2.1 THE BIGGEST OXYGEN SOURCES AND SINKS

The annual mean values of the O_2 and H_2S sources and sinks across the central BS were compared to differentiate them based on their absolute values. [Table A.1](#) presents the five biggest processes consuming/supplying oxygen in each of the central BS sub-basins. It highlights the upper advection as the largest oxygen supplier and the biggest term of the oxygen budget as well in the BB, eGB, and wGB. In the nGB, the lateral advection from the southern boundary is the biggest term in the oxygen budget. This pattern highlights the importance of the inflows from the North Sea in the interannual O_2 dynamics in the central BS. It also differentiates sub-basins in terms of their geographical location. The BB and eGB, which are closer to the North Sea, receive more oxygen via the inflows compared to the remote nGB and wGB, which significantly affects their dynamics. For instance, oxidation of H_2S is more pronounced in the nGB and wGB compared to the BB and eGB. Nitrification is the largest oxygen sink in the water column for all sub-basins except the wGB, where oxidation of S to SO_4^{2-} exceeds it. However, nitrification is still among the biggest oxygen sinks in the wGB. Sulfur oxidation consumes a significant amount of oxygen in the nGB as well. Contradictory to [Meier et al. \(2018\)](#), respiration of living organisms was found negligible in all sub-basins of the central BS. Detritus mineralization in the sediments is the biggest biological sink of oxygen in all sub-basins except the wGB, where sulfur oxidation exceeds it.

The distribution of sources and sinks of H_2S differs significantly from O_2 . Vertical advection of H_2S is directed out of the domain and is the biggest advective term in the nGB and wGB. In the eGB, lateral advection of H_2S to the more remote basins exceeds the vertical one, which indicates a positive feedback mechanism that leads to even less oxygen in the remote sub-basins. The water column acts mainly as a sink for H_2S and the sediments as a source. Oxidation of H_2S by NO_3^- and O_2 contributes significantly to H_2S removal. Mineralization of detritus is the biggest H_2S production term in the sediments and the water column. Numbers for H_2S are presented in [Table A.2](#).

4.2.2 DIFFERENT SOURCES AND SINKS CONTRIBUTING TO THE VARIABILITY OF O_2 AND H_2S

To investigate how the variability of annual O_2 and H_2S is distributed across their sources and sinks within a certain sub-basin, a regression analysis (see [Section 3.2.1](#) for description) was applied, where the total change of O_2 or H_2S within a sub-basin was taken as a dependent variable and the three groups of processes (physical fluxes, water column, and sediments) as the independent variables. The physical fluxes group contains all processes related to the physical transport of oxygen or H_2S (advection, diffusion, etc.). The water column group is made up of all biochemical processes consuming and supplying oxygen and H_2S (e.g., mineralization of OM, either by O_2 or SO_4^{2-} , nitrification, photosynthesis, and respiration, etc.), and the sediments group includes processes situated in the sediments (e.g., mineralization of detritus). The results are presented in [Figure 4.3](#).

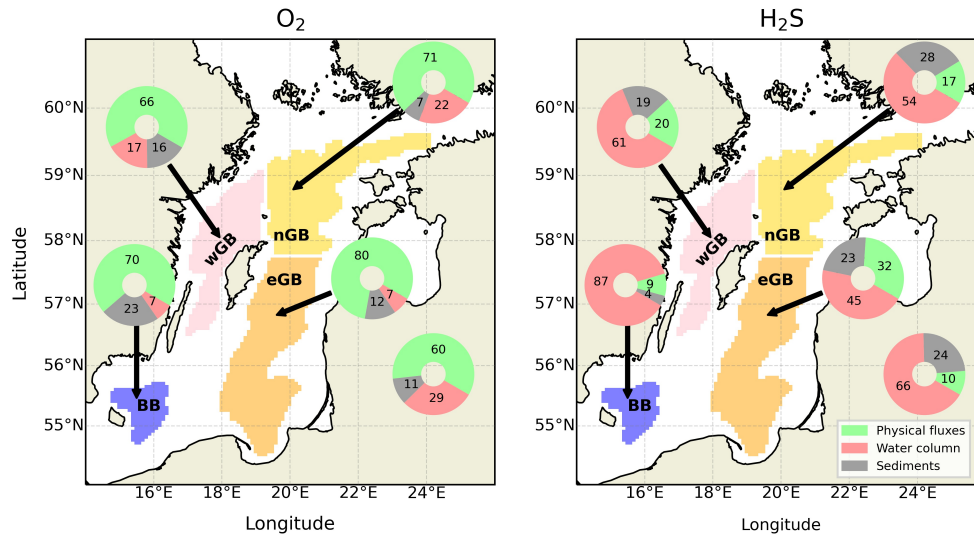


Figure 4.3: Fraction of interannual O₂ (left panel) and H₂S (right panel) variability (in %) explained by a certain group of processes (physical fluxes, water column, and sediments) (pie charts). Colored areas mark different sub-basins. The lower right pie chart shows the whole central BS. (Naumov et al., 2023b).

Figure 4.3 highlights a profound difference in the O₂ and H₂S dynamics. For oxygen, most variability is explained by physical processes (mainly advection) in all central BS sub-basins. In contrast, the dynamics of H₂S is governed by processes situated in the water column (explain 45% to 87% of the variability). The contributions of the remaining groups differ regionally. For oxygen, water column processes in the wGB and nGB explain slightly more variability compared to the BB and eGB. At the same time, 17% of the variability in the nGB is explained by sedimentary consumption, the second largest number after the BB (22%), which stresses the influence of the sedimentary O₂ consumption on the O₂ dynamics in the wGB. The analysis of H₂S sources and sinks showed the increasing role of advection toward the remote sub-basins, which again highlights their vulnerable positions as both producers and dynamical sinks of H₂S.

4.2.3 TEMPORAL VARIABILITY OF O₂ AND H₂S SOURCES AND SINKS

To detect any shifts in O₂ and H₂S consumption, a linear trend analysis was carried out for the same three groups of processes as in the previous Section (see Figure 4.3 for groups' names). The results are presented in Figure 4.7 (O₂, see reference curve) and in Figure A.6 (H₂S, see reference curve). Apart from the BB (Figure 4.7, Panel A), no significant linear trends in oxygen supply by physical fluxes were identified. This trend could be explained either by internal changes within the BB, e.g., changes in stratification, or by unidentified small inflows from the North Sea. Trends in sedimentary and water column consumption vary regionally. In the BB, both of them exhibit significant negative trends (i.e., an increase in O₂ consumption). Other basins show a significant negative trend in the water column O₂ consumption and a significant positive trend in the sedimentary O₂ consumption (Figure 4.7, Panels B, C). This pattern is mostly pronounced in the nGB, where most O₂ was initially consumed in the sediments. But, since the 1980s, more O₂ has been consumed in the water column than the sediments, indicating a pronounced shift

in O_2 consumption from the sediments to the water column. The same applies to the wGB (Figure 4.7, Panel D). This indicates less O_2 in the remote basins, which started in the 1970s and is still happening. Trends in H_2S production and consumption mainly highlight the H_2S deposition in the remote nGB and wGB. It is manifested as significant trends in the sedimentary H_2S production and water column H_2S consumption, with the latter exceeding the former. Since more H_2S is being produced than consumed, the positive trends in the H_2S advection mainly directed upwards are observed. The same is true for the eGB but to a lesser extent. No significant trends were observed in the BB, indicating the balance between produced and oxidized H_2S .

4.3 VENTILATION BY THE INFLOWS (VARIABILITY AND VENTILATION PAPERS)

As has already been pointed out, advection plays a crucial role in deep central BS ventilation. This Section is split between the [hyperlinkvarpapervariability](#) and [hyperlinkventpaperventilation](#) papers. Sections 4.3.2 and 4.3.3 are based on the [ventilation paper](#). There, an element tagging technique (see Section 3.1.2) was employed to estimate the change in ventilation based on the 29 biggest inflows from 1948 to 2018 (Section 4.3.2) and the processes that are triggered by a sudden rise in oxygen concentration in the deep BS sub-basins during an inflow (Section 4.3.3). Section 4.3.1 is based on the [variability paper](#) and briefly discusses the inflows' multidecadal variability.

4.3.1 MULTIDECADAL VARIABILITY IN THE SALINITY AND INFLOWS (VARIABILITY PAPER)

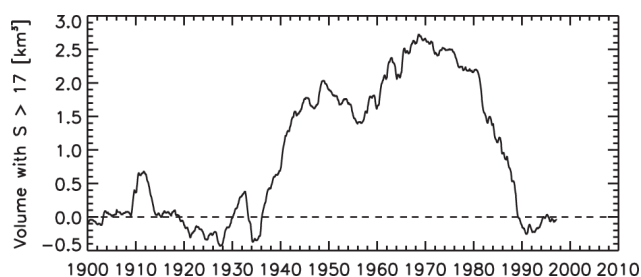


Figure 4.4: Inflowing volume (salinity $> 17 \text{ g kg}^{-1}$) differences between the sensitivity experiments REF+ and RUNOFF+. Inflowing volume was low-pass filtered with a cut-off period of 12 years. The dashed line indicates zero (Meier et al., 2023).

[et al., 2020](#)). The multidecadal variability in the salinity field was found to be amplified by the positive feedback related to the saltwater inflows. The inflows' intensity was approximated in the model as an inflowing volume with salinity of more than 17 g kg^{-1} (V_{17}). After this metric was calculated for each sensitivity experiment, the difference between the REF+ (reference scenario with sea level rise) and RUNOFF+ (scenario with the climatological mean runoff and constant net precipitation with sea level rise) scenarios was calculated. The result is presented in Figure 4.4. It can be concluded that when salinity in the BS decreases due to elevated runoff, the V_{17} difference tends to be negative. The opposite is true when salinity is increased. This mechanism can be explained as follows: when the BS salinity is lower, the outflowing low saline water is mixed with the North Sea's saline water, leading to less salty inflows. When the salinity

In the [variability paper](#), the multidecadal variability of the BS salinity field was analyzed using 5 sensitivity experiments performed with the RCO model. It was found, that the pronounced 30-year period in BS salinity is caused by both NAO and AMV (and their interactions). The NAO affects the precipitation over the BS catchment area, influencing salinity via the direct dilution effect (Radtke et al., 2020). The AMV affects the NAO's centers of action, causing their spatial shift (Börgel

is higher, the opposite is true.

4.3.2 TEMPORAL TRENDS IN THE CENTRAL BS VENTILATION BY THE INFLOWS (VENTILATION PAPER)

In the [ventilation paper](#), an analysis of inflowing O₂ content and inflows' lifetimes was carried out to study the temporal variability of the ventilation by inflows. The total content of O₂ transported by an inflow (or multiple inflows) to a certain sub-basin is a simple measure of the ventilation by inflows. It is integrated over a sub-basin volume. Inflow's lifetime measures how fast O₂ brought by a certain inflow is consumed. It is presented by time, after which a certain fraction of inflowed O₂ (e.g., 95% or 50%) is utilized. The inflows were also ranked from strongest to weakest based on the amount of O₂ they transported to the BS to detect the trends in their variability. The results are shown in [Figure 4.5](#).

[Figure 4.5](#) (Panel A) demonstrates no significant trend in the inflows' strength, which indicates that all stagnation periods are simply part of the natural variability, as also found by other studies (e.g., [Schimanke and Meier, 2016](#); [Mohrholz, 2018](#); [Fonselius and Valderrama, 2003](#)). At the same time, strong negative trends in the inflows' lifetimes were observed across the whole central BS (Panels C, E, G, and I). Those trends explain from around 30% of the variability in the BB up to over 80% in the wGB. This sub-basin also shows the most rapid decline in the inflows' lifetime and the inflowed O₂ content. All inflows after 1965-66 (even the largest in 1993-94 and 2014-15) brought almost no oxygen here. The nGB exhibits the same pattern as the wGB, but the changes are less pronounced. That pattern suggests an elevated O₂ consumption everywhere across the central BS, more manifested in the remote nGB and wGB. BB and eGB are less affected by the elevated O₂ consumption and still ventilated by the inflows. The biggest peaks in inflowed O₂ content were observed here during the strongest 1993-94 and 2014-15 inflows. However, even here, the inflowed O₂ was utilized significantly faster at the end of the study period compared to the beginning. It can be concluded that all sub-basins across the central BS are now less well-oxygenated by the inflows than in 1948. Since no significant trend in inflows' strength was observed, the only driver of those changes is the elevated O₂ consumption.

4.3.3 CHANGES IN THE VENTILATION PATTERNS (VENTILATION PAPER)

To answer the question which processes are mostly triggered by the inflowed O₂ and whether they have changed during the investigated 71 years, an EOF analysis (see [Section 3.2.3](#)) was applied in the [ventilation paper](#) to the spatio-temporal matrices of temporally integrated consumption or production by O₂/H₂S budgets terms (or aggregated groups of terms) during each inflow from 29 studied inflows. The results ([Figure 4.6](#)) portray the two leading EOFs that describe more than 90% of the produced/consumed O₂ during the inflow events. From those two, the first explains about 90% and the second about 5% ([Figure 4.6](#), Panel A).

The first EOF's loadings ([Figure 4.6](#), Panel C) are negatively connected to the mineralization of detritus in the eGB and, to a certain extent, in the nGB. They show no spatial variability in signs, and the first EOF has no trend ([Figure 4.6](#), Panel B), which makes the response uniform and constant in time. This suggests that the first EOF mainly describes the default reaction to the inflowed O₂, which includes elevated rates of detritus mineralization in the eGB. It only correlates with the inflow's duration and strength.

The second EOF demonstrates more complex dynamics. It becomes positive in the 1970s, which might serve as a proxy for changed oxygen dynamics. The second EOF's loadings are not spatially uniform, with

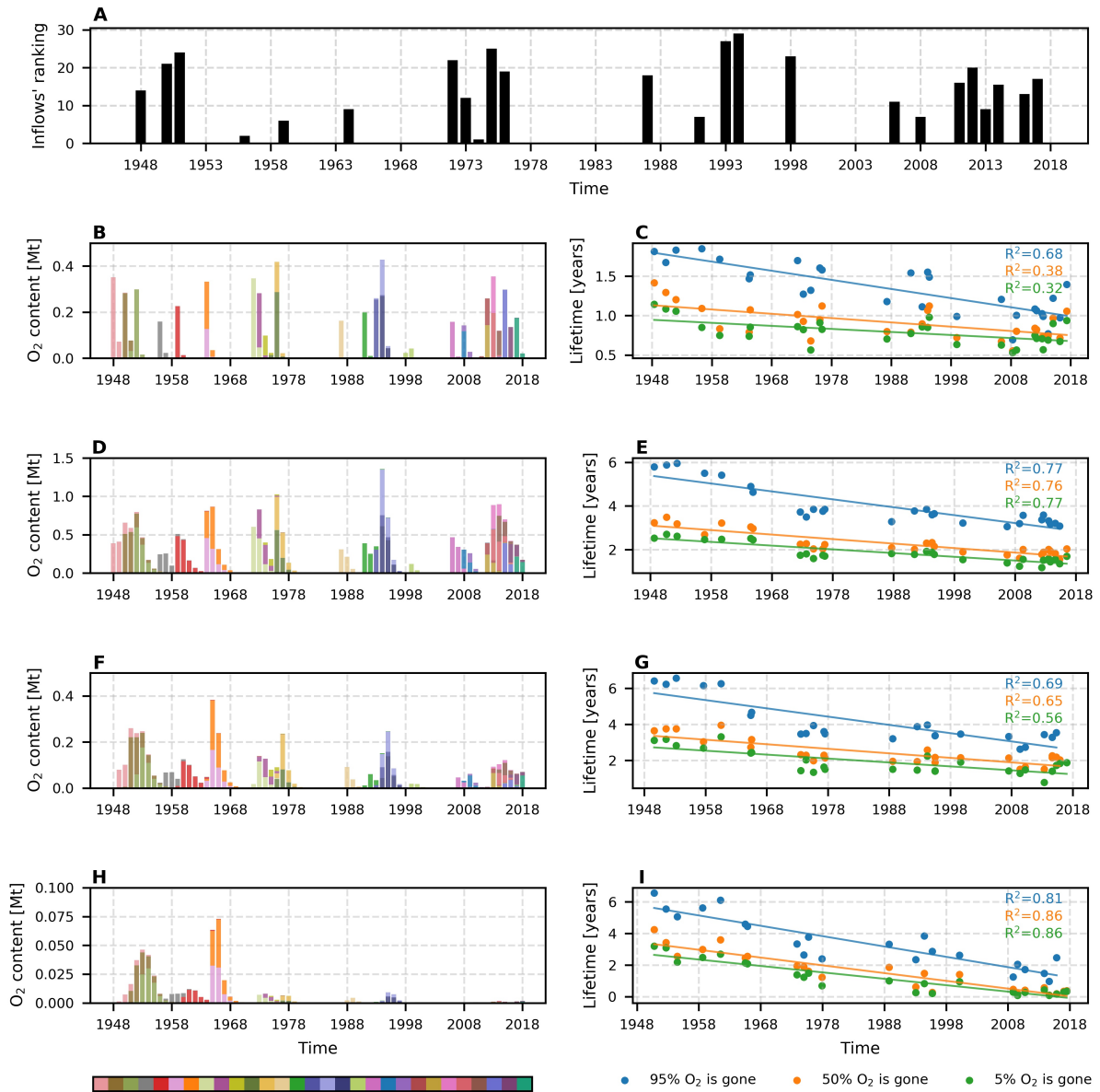


Figure 4.5: Panel A shows the ranked inflows' temporal distribution. The ranking is based on the total amount of O₂ transported across the Arkona transect by an individual inflow. Number 29 stands for the most transported O₂, and number 1 for the least. The total yearly inflowed O₂ content in each sub-basin is depicted in panels B, D, F, and H. Different inflows are displayed in different colors in the histogram. Bar heights indicate the total inflowed O₂ content. The color bar shows the inflows chronologically (i.e., the earliest inflow is pink, the next one is brown, etc.). Panels C, E, G, and I depict the lifetime of inflowed O₂ per sub-basin (dots). It is defined as the time when inflowed O₂ reaches a certain fraction of its maximal value. In total, three fractions are shown: green dots mark the time when 5% of inflowed O₂ is consumed (95% remains), orange dots mark the time when 50% of inflowed O₂ is consumed (50% remains), and blue dots mark the time when 95% of inflowed O₂ is consumed (5% remains). Linear trends are shown for each scatter plot. They demonstrate the decay of the inflowed O₂ lifetime. Determination coefficients (R^2) for each linear trend are presented in the upper-left section of the panels. Their colors indicate the trends they belong to. Panels B and C stand for the Bornholm Basin, D, and E for the eastern Gotland Basin, F and G for the northern Gotland Basin, and H and I for the western Gotland Basin. Mt corresponds to 10^9 kg. (Naumov et al., 2023b).

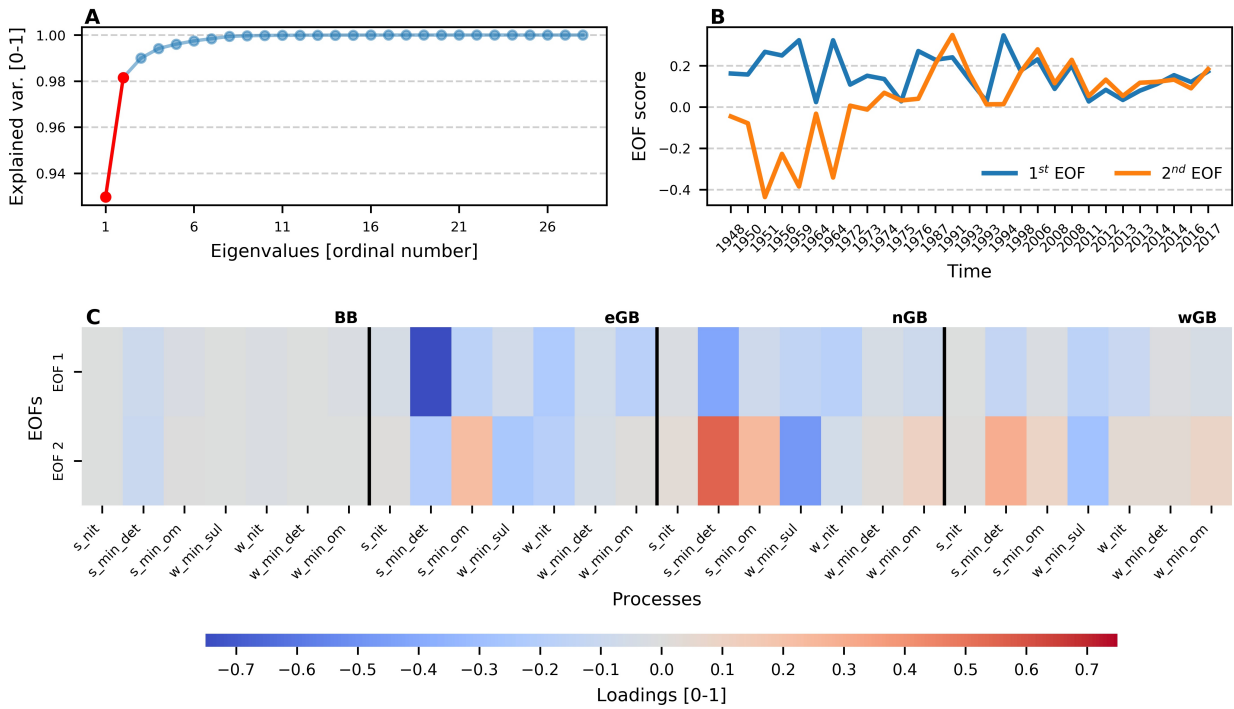


Figure 4.6: EOF analysis for O₂ consumption during inflow events. Panel A shows the fraction of variance explained by each EOF. The first two EOFs (explain more than 95% of the variance) are highlighted. Panel B shows the first two EOFs' timeseries. Panel C demonstrates the EOF loadings, indicating how strong a certain EOF is connected to a certain process. Positive values (red) mean a direct relationship between EOF and a process, and negative values (blue) a reverse relationship. The processes' names in Panel C are read in the following way: {domain}_{process}. A domain can be w (water column) or s (sediments). Processes can be nit (nitrification) or min_om/det/sul (mineralization of OM without detritus, detritus, or H₂S) (Naumov et al., 2023b).

a distinct response in the eGB and other parts of the Gotland Basin. What is depicted by the second EOF is a transformation of oxygen consumption during the 1970s. The changes are opposite between eGB and nGB, wGB. An inflow during the first period differs from an inflow during the second period by a greater second EOF's value. This, based on the second EOF's loads, means a shift in detritus mineralization to the eGB, while in the nGB and wGB, the main oxygen consumption is moved from detritus mineralization to oxidation of H₂S and S. This is most visible in the nGB.

The same H₂S sources and sinks analysis revealed a similar pattern (Figure A.5). It is a fluctuating first EOF without any significant temporal trend and a second EOF that switches its sign during the 1970s. Its spatial pattern can be interpreted similarly as a changed response to the inflowed O₂. Sedimentary H₂S production moves from the remote wGB and nGB closer to the North Sea in the eGB. Its consumption is shifted upstream as well but to a lesser extent. It indicates an increase in H₂S downstream transport.

The conducted analysis fully confirms the previous conclusions. There are only two patterns affecting the O₂ and H₂S dynamics during inflow events. The first pattern is related to the amount of O₂ brought into the BS by an inflow. The second pattern is related to the change in the main O₂ sinks due to the deoxygenation of the central BS. Together they explain more than 95% of the variability. Thus, it can be concluded that O₂ consumption mostly depends on the inflow's duration and strength, with some small shifts in processes due to the overall deoxygenation of the central BS during 1948-2018.

4.4 OXYGEN DYNAMICS UNDER REDUCED NUTRIENT INPUT (SENSITIVITY PAPER)

The results presented in the previous Section demonstrated that despite the nutrient reduction since the 1980s, the central BS has not demonstrated any significant improvement in oxygen conditions yet. Contrarily, O_2 consumption has only amplified in recent years resulting in weakened ventilation of the remote sub-basins, which facilitates the reduced compounds' deposition. This section is fully based on the results presented in the [sensitivity paper](#) and answers whether the central BS can be returned to its initial state (or the good environmental state as defined in the BSAP) and on which timescales it is feasible. For that purpose, the two sensitivity experiments with the MOM-ERGOM model were carried out. They both assume a reduced (compared to the current HELCOM values) constant nutrient input. The BSAP scenario assumes an input following the BSAP 2021 MAI, and the more rigorous 0.5 BSAP scenario assumes a halved BSAP MAI input (for more information, see [Section 3.1.3](#)).

4.4.1 TRENDS IN OXYGEN SOURCES AND SINKS

As in [Section 4.2](#), all O_2 and H_2S sources and sinks in the ERGOM model were aggregated into three groups: phy (or physical fluxes), bio (or water column processes), and sed (or sedimentary processes). For those three groups, the temporal variability over 71 years was investigated by applying linear trend analysis. The results for O_2 are presented in [Figure 4.7](#) and [Figure A.3](#). For H_2S , see [Figure A.4](#).

[Figure 4.7](#) and [Figure A.3](#) demonstrate substantial changes in the composition of O_2 consumption under both the BSAP and 0.5 BSAP scenarios. The main pattern is a shift of oxygen consumption back to the sediments. The showcase of those changes is the nGB, where sedimentary consumption was at the end of the study period the main sink of oxygen in both scenarios, with the 0.5 BSAP further amplifying sedimentary consumption and reducing consumption in the water column. The same is true for the wGB, but only under the 0.5 BSAP. Under the BSAP scenario, only sedimentary consumption demonstrates a significant negative trend and does not reach the water column consumption at the end of the study period. Elevated sedimentary consumption, most visible in the nGB, indicates reoxygenation of the sediments, which is accompanied by oxidation of the deposited reduced material there. This is more pronounced under the 0.5 BSAP scenario indicating more O_2 in the system. A significant positive trend in the physical fluxes of O_2 was observed in the wGB, which means more O_2 supply, primarily via advection. It was attributed to better ventilation by the inflows following the oxygenation of the neighboring nGB. Both the eGB and BB do not demonstrate striking further oxygenation. In eGB, only a significant positive trend in the O_2 consumption in the water column (less O_2 consumption with time) was observed under both scenarios. This indicates more O_2 in the water column since less consumption means less reduced material stored there. BB only demonstrated a positive significant trend in oxygen consumption under the 0.5 BSAP scenario, which points out its well-oxygenated state in the model.

H_2S sources and sinks ([Figure A.6](#)) also demonstrated significant changes. The eGB returned to the dynamic balance between H_2S production and consumption by the end of the study period, suggesting that H_2S is no longer deposited here. The same is observed in the nGB under the more rigorous 0.5 BSAP scenario, but the BSAP scenario also highlights a significant reduction of H_2S content in the nGB, which, however, stabilizes in the 2070s. Nevertheless, the H_2S advection across the upper boundary terminates in both scenarios. The wGB shows the most pronounced difference between the two scenarios. Under the BSAP, the wGB is still supplying the upper levels with H_2S by the end of the study period, but to a

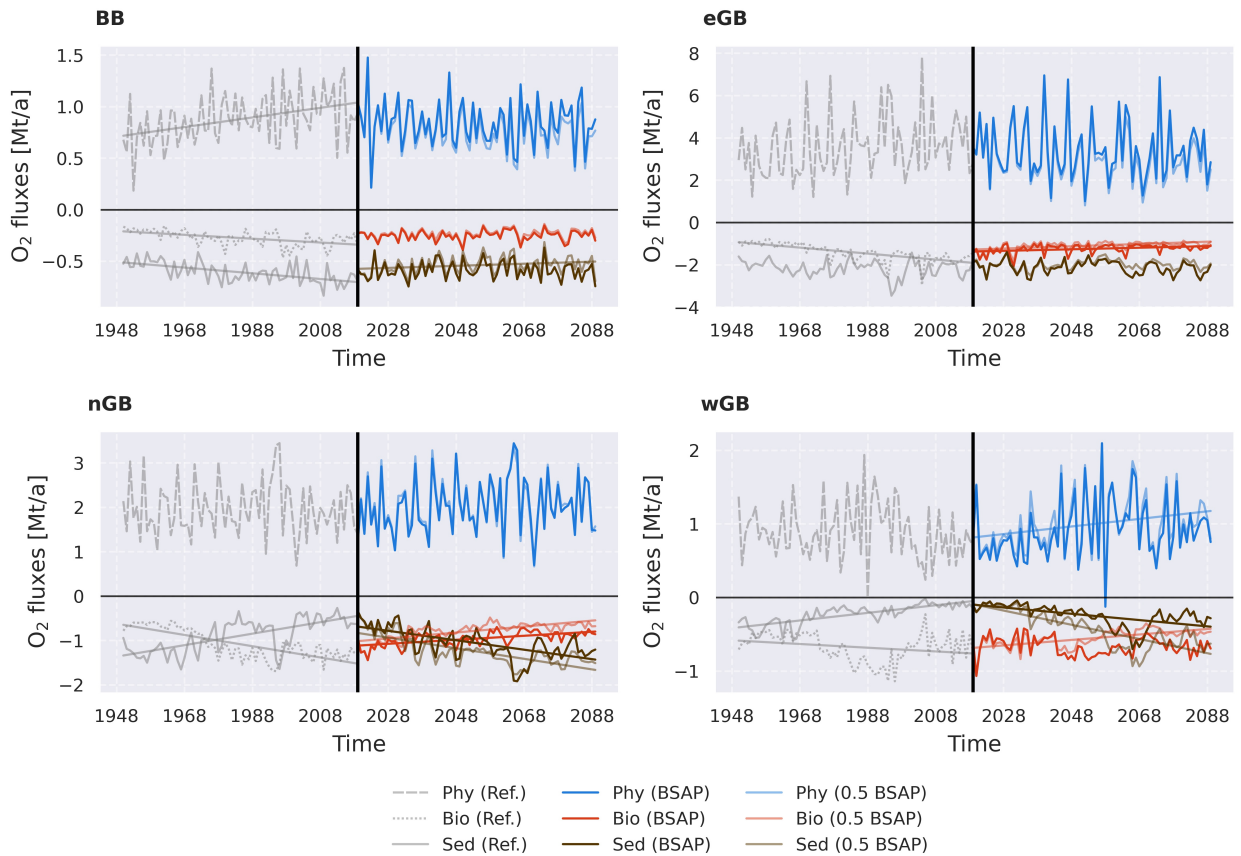


Figure 4.7: Temporal dynamics of the total annual O₂ fluxes by the three categories (physical fluxes – Phy (blue line), water column consumption – Bio (red line), and sedimentary consumption – Sed (dark brown line)). The horizontal black translucent line indicates zero. Positive fluxes mean O₂ supply, and negative fluxes mean O₂ consumption. Grey lines represent the reference scenario (see Section 3.1.3). Only significant linear trends ($p < 0.05$) are shown. Mt/a stands for 10^9 kg per year (Naumov et al., 2023a).

much lower extent. Despite having a significant negative trend, the sedimentary production stabilizes in the 2070s, and the water column consumption demonstrates no trend. Under the 0.5 BSAP, the export ceased by the end of the study period, and the sedimentary production continued to decrease. The water column consumption shows a significant positive trend under the 0.5 BSAP.

4.4.2 O₂ AND H₂S BUDGETS' COMPOSITION IN DIFFERENT SCENARIOS

The linear regression analysis (see Sections 4.2.2 and 3.2.1) was applied to the same groups of O₂ and H₂S sources and sinks (phy, bio, and sed) to determine their contribution to O₂ and H₂S variability. The results are shown in Figure 4.8. The general pattern of oxygen variability is the same as in Section 4.2.2: advection dominates in both scenarios. In addition, the water column processes in Figure 4.8 explain less and less variability moving from the reference scenario to the 0.5 BSAP. It complements conclusions made in the previous Section about less variability in the O₂ consumption in the water column going from the reference scenario to the 0.5 BSAP. The H₂S processes' composition patterns are generally more complex (both regionally and in different scenarios). It suggests a strong connection between nutrient forcing and

H₂S dynamics (see Figure A.6 for more details). Overall, it can be concluded that the H₂S dynamics are more affected by nutrient input than O₂, with some regional differences existing in both.

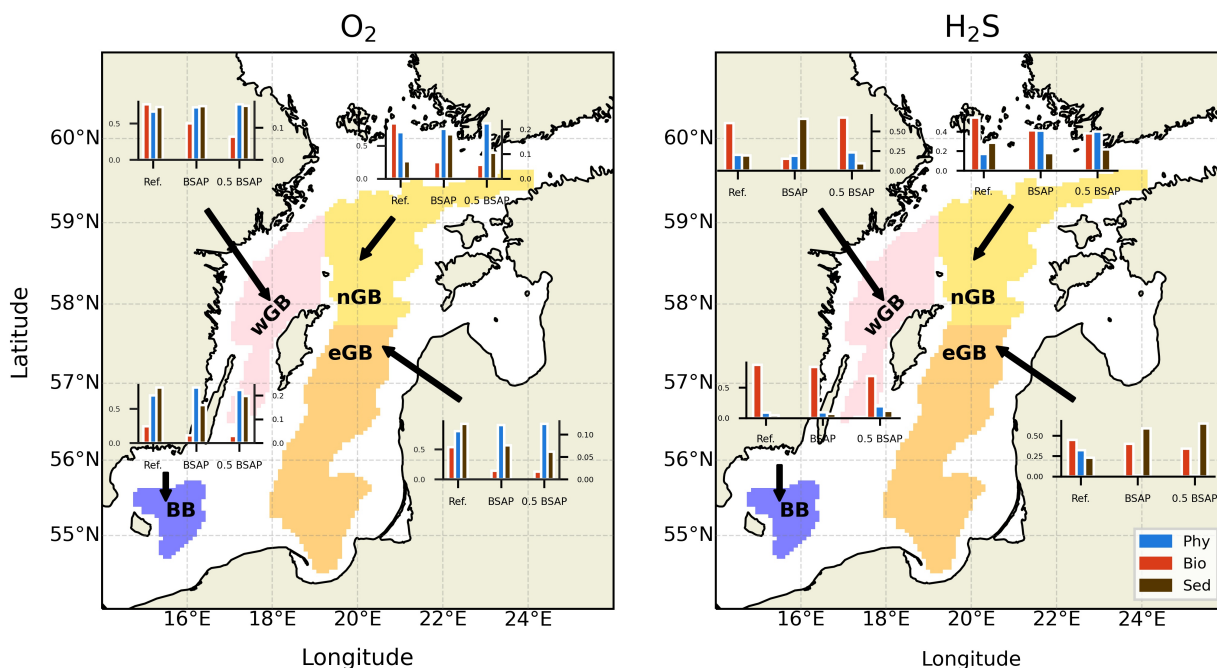


Figure 4.8: Maps showing different processes' contributions to the O₂ (left) and H₂S (right) variability. Processes are aggregated into the same three groups (phy, bio, and sed) as in Figure 4.7. In bar plots, the y-axis represents a fraction of the total variability explained by a certain group of processes, and the x-axis represents scenarios. Note that O₂ charts have two y-axes with different scales. The left and right axes represent the fraction of variability explained by the group phy, and the groups bio and sed, respectively (Naumov et al., 2023a).

4.4.3 O₂ AND H₂S SOURCES AND SINKS' VARIABILITY INDUCED BY THE NUTRIENT FORCING

Nutrient loads determine a substantial fraction of the variability in O₂ concentration in the deep central BS, as shown, e.g., by Meier et al. (2019a); Friedland et al. (2012); Saraiva et al. (2019). This Section presents the results of the analysis dedicated to quantifying the nutrient loads' influence on the O₂ and H₂S variability, separating it from the natural variability, but not from the future climate change signal since it is not included in the model forcing. To do so, the EOF analysis was applied to the matrices of annual O₂ and H₂S production/consumption anomalies for the reference period. The resulting loadings were applied to both sensitivity experiments' data to get the same patterns (see Section 3.2.3 for more information). The results are outlined in Figure 4.9 (for O₂) and Figure A.7 (for H₂S).

Judging upon eigenvalues, the first three EOFs were considered significant for O₂ and H₂S. In the case of O₂, the first EOF explains around 60% of variability, the second EOF explains around 20%, and the third explains around 10%. H₂S eigenvalues converge faster. The first EOF already explains approximately 85% of the variability, and the two remaining leading EOFs explain 5% each. Based on the loadings' scores (Panel E in Figure 4.9 and Figure A.7), both leading EOFs seem to represent the same O₂ and H₂S variability pattern. For O₂ and H₂S data, the first EOF shows a bold, positive bond with sedimentary

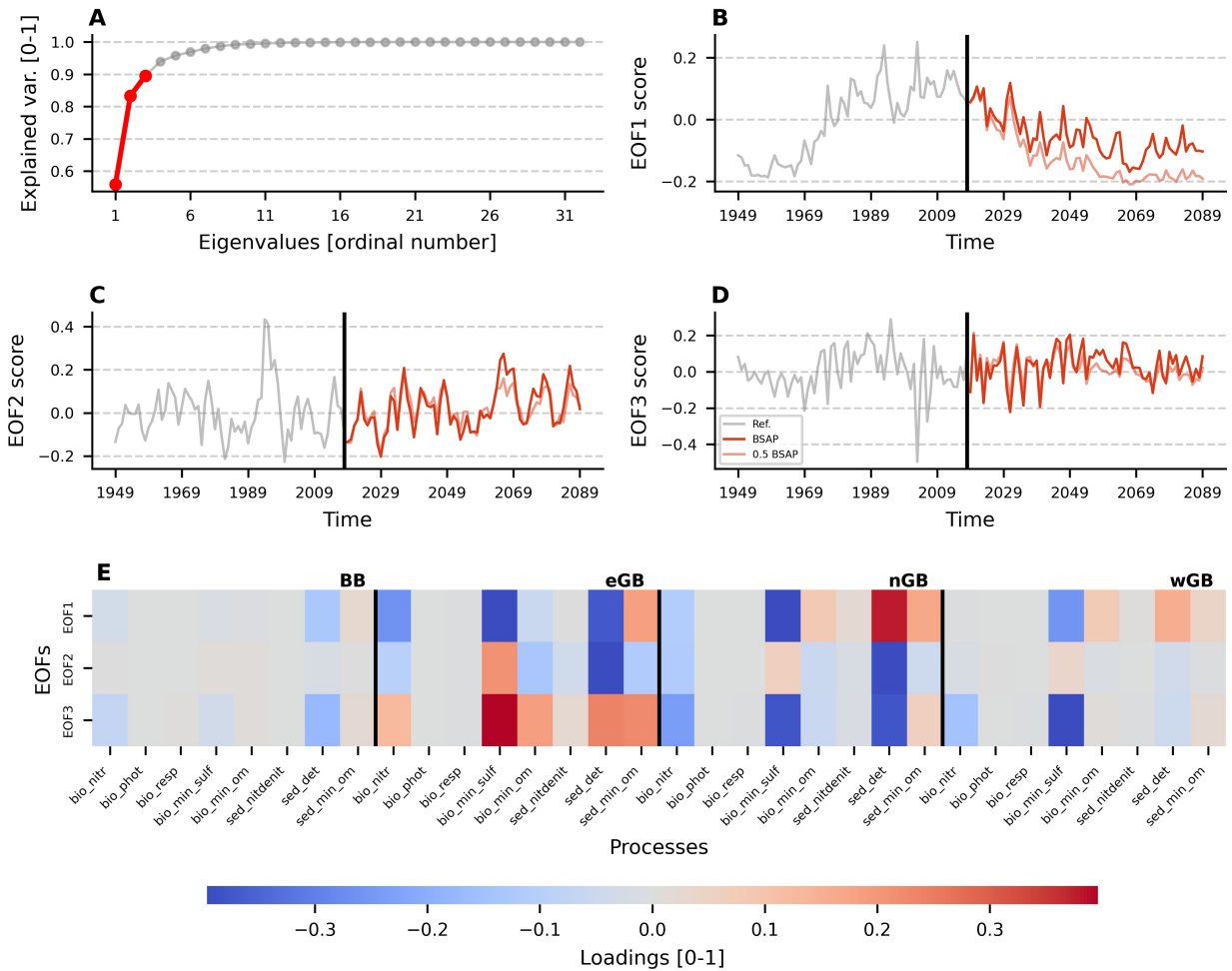


Figure 4.9: EOF decomposition of the spatial-temporal matrix of O_2 consumption terms aggregated into specific groups. Group names (x-axis labels in Panel E) are read as follows: {domain}_{name of processes}. There are two possible domains: bio – water column, and sed – sediments; and six processes: nitr/nitdenit – nitrification, phot – photosynthesis, resp – respiration of biota, min_sulf – mineralization of sulfur, min_om – mineralization of organic matter, and det – mineralization of detritus only. Panel A shows the fraction of variability explained by all EOFs. Only the first three EOFs were considered significant and highlighted. Panels B-D depict their temporal variability. Here, the black vertical line demarcates the reference scenario (grey curve) and sensitivity studies (BSAP and 0.5 BSAP scenarios), which are shown by vivid and translucent red lines, correspondingly. Panel E demonstrates their loadings. Loadings vary from minus one to one and show the direction and magnitude of the connection between an EOF and a variable. Black lines highlight the spatial structure of the matrix by separating the sub-basins (Naumov et al., 2023a).

detritus’ oxidation anomalies (either by O_2 or SO_4^{2-} reduction). The first EOF for oxygen functions as follows: when its score is positive (the period from the 1970s to the 2030s, following Panel B in both discussed Figures), H_2S is produced in the nGB via sulfate reduction to mineralize sedimentary detritus, which indicates the limited supply of oxygen into the deep layers of nGB. The same dynamics apply, but to a lesser extent, to the two other sub-basins within the Gotland Basin (eGB and wGB). Simultaneously, the mineralization of detritus with O_2 as an electron acceptor amplifies in the eGB but diminishes in both the nGB and wGB, which also points out the elevated oxygen debt (deposition of H_2S and NH_4^+)

in those two remote basins. The negative first EOF scores describe the opposite situation. H_2S is not actively produced in the eGB, wGB, and especially nGB but is oxidized by O_2 or NO_3^- . The detritus' oxidation via O_2 increases in the nGB and wGB (which means oxygen debt's depletion) but decreases in eGB (which highlights a better state without any long-standing oxygen debt). This indicates the overall oxygenation of the deep central BS. The first EOF for oxygen is negative during the first few decades of the reference period (before the 1980s), starting from the 2030s and 2040s under the 0.5 BSAP and BSAP, respectively. These dynamics highlight the connection between the first oxygen EOF and the nutrient loads (since they were peaking in the 1980s and since then are being reduced). The same reasoning can be applied to the first EOF in the H_2S data (see [Figure A.7](#)), making it possible to attribute it to the nutrient forcing. This means nutrients are responsible for approximately 60% and 85% of interannual O_2 and H_2S dynamics, respectively. Interannual oxygen variability is also partially governed by inflow events. They were attributed to the second EOF. The third EOF might depict some sort of natural variability. The second and the third EOFs do not show any trends in all scenarios. The first EOFs for BSAP and 0.5 BSAP scenarios exhibit a very high correlation (>0.9), which means the system responds to different degrees of nutrient loads reduction in the same way. However, the EOF's scores are more negative in the 0.5 BSAP scenario, which indicates the more resilient state of the central BS. The last two EOFs in H_2S data are difficult to interpret, but since they do not demonstrate any trends, they are less important for the analysis.

5

Discussion and conclusions

5.1 DISCUSSION

In this thesis, the composition of O_2 and H_2S sources and sinks and their long-term trends, as well as variability, were calculated for the first time. It complements the work of, e.g., [Gustafsson and Stigebrandt \(2007\)](#); [Schneider and Otto \(2019\)](#), who estimated some O_2 sources and sinks based on the observational data but only for a short time period and for a limited area. As any model study, this thesis has some degree of uncertainty introduced by model simplifications. To validate the results of the thesis against the observational data, the paper by [Rolff et al. \(2022\)](#) can be used. Their results are well-aligned with this thesis. Namely, they found a rapid increase in NH_4^+ concentrations based on the observational data. They also identified the upward advection of NH_4^+ from the deep BS layers, which was also observed in the thesis (both shown for NH_4^+ , but discussed for H_2S). In addition, estimates of O_2 vertical fluxes across the pycnocline in the eGB by [Holtermann et al. \(2022\)](#) are in the same order of magnitude as in the MOM-ERGOM model.

The reason for still deteriorating O_2 conditions in the deep central BS seems to be related to the "vicious circle" of the BS ([Vahtera et al., 2007](#)). The hypothesis of an extended "vicious circle" proposed by [Meier et al. \(2018\)](#) seems to be trustworthy, despite our slightly different results (they have identified respiration of higher trophic levels as one of the primary sinks of O_2 , but this thesis found it to be negligible). At the same time, they identified nitrification as one of the primary O_2 sinks as in this thesis. However, to fully certify or falsify it, additional studies need to be done (e.g., estimating the transport of detritus).

[Mohrholz \(2018\)](#) mentioned studying BS inflows from the O_2 perspective as one of the scientific problems. This thesis presents for the first time the long-term estimates of oxygen brought into the deep BS by the 29 biggest O_2 inflows from 1948 to 2018. The 1993 inflow ([Jakobsen, 1995](#)) was found to bring the most O_2 into the BS. No temporal trend in the amount of O_2 brought by inflows was observed. Despite this, the ventilation of the central BS has significantly decreased during the last few decades, which only can be attributed to elevated oxygen consumption. There are still knowledge gaps related to the BS inflows and ventilation caused by them. First of all, the oxygen inflows statistics have to be elaborated based on the observational data, which is an ambitious problem since the oxygen measurements are less common than the salinity measurements. In addition, the importance of the oxygen inflows can be evaluated in, e.g., a sensitivity study employing an inflows-favorable forcing.

The results of the sensitivity studies support the findings of, e.g., Saraiva et al. (2019), Markus Meier et al. (2021), Bartosova et al. (2019), and Friedland et al. (2012), stating that the nutrient input explains the biggest part of the variability in O₂ sources and sinks in the deep central BS. The new results of this thesis are that the system is able to reverse negative changes in oxygen content happening during the last two decades and return to the initial state without any hysteresis effect. The next step in this research would be constructing proper multimodel climate projections, disentangling oxygen sources and sinks. The latter allows for the building of more robust estimates and tracking of the impact of climate change on O₂ sources and sinks, as proposed by Börgel et al. (2023), for example. In addition, some quantification of the multidecadal variability of the BS O₂ content and its attribution to the local modes of climate variability (e.g., NAO and AMV) can be done. In the end, there is still ample room for new studies.

5.2 CONCLUSIONS

The following conclusions were drafted based on the [variability paper](#):

- As validation results suggested, the RCO model demonstrated a good performance in the BS region.
- The positive feedback between mean BS salinity and inflowing salt content was identified.

The following conclusions were drafted based on the [ventilation paper](#):

- The MOM-ERGOM model was validated against reanalysis and observational data and showed acceptable results. However, the bottom DO concentrations were underestimated.
- Interannual O₂ dynamics in all scenarios is mainly governed by advection. At the same time, H₂S dynamics is governed either by the water column or sedimentary processes indicating its local origin.
- Mineralization of sedimentary detritus was identified as the biggest sink of O₂ and, simultaneously, the biggest source of H₂S (via SO₄²⁻ reduction).
- During the study period (1948-2018), an overall deoxygenation of the deep central BS was observed. It manifested as a shift from predominant sedimentary O₂ consumption to predominant O₂ consumption in the water column. This was attributed to the total absence of O₂ in the sediments and an upward shift of the redoxcline. The most notable shift occurred in the nGB, but the same pattern, to a lesser extent, was also visible in the eGB, where it is less pronounced, and in the wGB, where the absence of O₂ limits its manifestation. The nGB and wGB were identified as especially vulnerable sub-basins since they are both remote and, therefore, less ventilated by the saltwater inflows and serve as sinks for H₂S advected from neighboring sub-basins. The BB exhibited much less deoxygenation because of its location.
- A drastic decrease in the deep central BS ventilation was found. This is especially visible in the nGB and wGB, which both received only small amounts of O₂ from the strongest 1993-94 and 2014-15 inflows. Since no trend in inflows' strength was identified, the observed changes can only be attributed to elevated O₂ consumption in all considered sub-basins.

- Two EOFs of O₂ consumption during the inflow events are significant. The first EOF explains more than 90% of the variability, and the second explains around 5%. The first EOF was attributed to the inflows' duration and strength, and the second describes the response to the central BS's overall deoxygenation, which shifts the inflowing O₂ consumption from detritus mineralization to H₂S oxidation in the nGB and wGB. Since the first EOF explains more than 90% of the variability, the inflows' duration and strength are the key parameters determining their effectiveness.

The following conclusions were drafted based on the [sensitivity paper](#):

- The adherence to the BSAP MAI and to the even more rigorous halved BSAP MAI will improve the deep central BS and transit it to a more oxic state after 2018 within the simulated 71 years. In the nGB, a shift back to predominant sedimentary O₂ consumption occurred in both the BSAP and 0.5 BSAP scenarios (in the wGB, only in the 0.5 BSAP scenario). The water column O₂ consumption reduces primarily due to the diminished oxidation of H₂S and nitrification toward the end of the study (the year 2089), and the O₂ consumption in the sediments increases primarily due to more OM mineralization. The faster improvement of the wGB and nGB is explained by the positive feedback related to the improvement in the eGB and, therefore, less advection of reduced materials to the remote sub-basins and better ventilation due to less O₂ consumption.
- Three EOFs were considered significant for O₂ and H₂S sources and sinks variability. The first EOFs explain around 60% of the O₂ budget terms anomalies variability and 80% of the H₂S budget terms anomalies variability. The leading EOFs were attributed to nutrient forcing, with positive scores indicating a deposition phase of reduced material and organic matter and deoxygenation. Contrary, the negative scores indicate a phase of oxidation of the reduced material and oxygenation. The first EOF for O₂ budget terms went into a constant negative phase, which means no deposition of reduced material and oxidation of already existing one, in the 2050s under the BSAP nutrient forcing, and in the 2030s under the 0.5 BSAP nutrient forcing. For H₂S budget terms, under both the BSAP and 0.5 BSAP nutrient forcing scenarios, this state was reached in the 2030s. It indicates a transformation to the oxic regime, which is more resilient under the 0.5 BSAP nutrient forcing.
- The conducted sensitivity studies suggest that a return to the BS initial state (the year 1948) is possible within 71 years under the forcing from the rigorous 0.5 BSAP scenario. In the case of the BSAP scenario's forcing, the BS did not reach its initial state within 71 years, but since no hysteresis effect was observed, it seems to be feasible in the future.

References

Elin Almroth-Rosell, Kari Eilola, Ivan Kuznetsov, Per Hall, and Markus Meier. A new approach to model oxygen dependent benthic phosphate fluxes in the Baltic Sea. *Journal of Marine Systems*, 144, November 2014. doi: 10.1016/j.jmarsys.2014.11.007.

Elin Almroth-Rosell, Iréne Wahlström, Martin Hansson, Germo Väli, Kari Eilola, Pia Andersson, Lena Viktorsson, Magnus Hieronymus, and Lars Arneborg. A Regime Shift Toward a More Anoxic Environment in a Eutrophic Sea in Northern Europe. *Frontiers in Marine Science*, 8:799936, December 2021. ISSN 2296-7745. doi: 10.3389/fmars.2021.799936. URL <https://www.frontiersin.org/articles/10.3389/fmars.2021.799936/full>.

Andrew H. Altieri, Maggie D. Johnson, Sara D. Swaminathan, Hannah R. Nelson, and Keryn B. Gedan. Resilience of Tropical Ecosystems to Ocean Deoxygenation. *Trends in Ecology & Evolution*, 36(3):227–238, March 2021. ISSN 0169-5347. doi: 10.1016/j.tree.2020.11.003. URL [https://www.cell.com/trends/ecology-evolution/abstract/S0169-5347\(20\)30336-0](https://www.cell.com/trends/ecology-evolution/abstract/S0169-5347(20)30336-0). Publisher: Elsevier.

C. L. Amos, Thamer B. Al-Rashidi, Karim Rakha, Hamdy El-Gamily, and R. J. Nicholls. Sea surface temperature trends in the coastal ocean. *Current Development in Oceanography*, 6(1):1–13, March 2013. ISSN 0976-6960. URL <https://eprints.soton.ac.uk/351005/>. Number: 1.

Jesper H. Andersen, Jacob Carstensen, Daniel J. Conley, Karsten Dromph, Vivi Fleming-Lehtinen, Bo G. Gustafsson, Alf B. Josefson, Alf Norkko, Anna Villnäs, and Ciarán Murray. Long-term temporal and spatial trends in eutrophication status of the Baltic Sea. *Biological Reviews*, 92(1):135–149, 2017. ISSN 1469-185X. doi: 10.1111/brv.12221. URL <https://onlinelibrary.wiley.com/doi/abs/10.1111/brv.12221>. _eprint: <https://onlinelibrary.wiley.com/doi/pdf/10.1111/brv.12221>.

Agneta Andersson, H. E. Markus Meier, Matyas Ripszam, Owen Rowe, Johan Wikner, Peter Haglund, Kari Eilola, Catherine Legrand, Daniela Figueroa, Joanna Paczkowska, Elin Lindehoff, Mats Tysklind, and Ragnar Elmgren. Projected future climate change and Baltic Sea ecosystem management. *AMBIO*, 44(3):345–356, June 2015. ISSN 1654-7209. doi: 10.1007/s13280-015-0654-8. URL <https://doi.org/10.1007/s13280-015-0654-8>.

AKIO Arakawa and VIVIAN R. Lamb. Computational Design of the Basic Dynamical Processes of the UCLA General Circulation Model. In JULIUS Chang, editor, *Methods in Computational Physics: Advances in Research and Applications*, volume 17 of *General Circulation Models of the Atmosphere*, pages 173–265. Elsevier, January 1977. doi: 10.1016/B978-0-12-460817-7.50009-4. URL <https://www.sciencedirect.com/science/article/pii/B9780124608177500094>.

Yuri Artioli, Jana Friedrich, Alison J. Gilbert, Abigail McQuatters-Gollop, Laurence D. Mee, Jan E. Vermaat, Fred Wulff, Christoph Humborg, Luca Palmeri, and Falk Pollehne. Nutrient budgets for European seas: A measure of the effectiveness of nutrient reduction policies. *Marine Pollution Bulletin*,

56(9):1609–1617, September 2008. ISSN 0025-326X. doi: 10.1016/j.marpolbul.2008.05.027. URL <https://www.sciencedirect.com/science/article/pii/S0025326X08003172>.

A.L. Barach. The treatment of anoxia in clinical medicine. *Bulletin of the New York Academy of Medicine*, 26(6):370–383, June 1950.

L. Barghorn, H. E. M. Meier, and H. Radtke. Changes in Seasonality of Saltwater Inflows Caused Exceptional Warming Trends in the Western Baltic Sea. *Geophysical Research Letters*, 50(12):e2023GL103853, 2023. ISSN 1944-8007. doi: 10.1029/2023GL103853. URL <https://onlinelibrary.wiley.com/doi/abs/10.1029/2023GL103853>. _eprint: <https://onlinelibrary.wiley.com/doi/pdf/10.1029/2023GL103853>.

Alena Bartosova, René Capell, Jørgen E. Olesen, Mohamed Jabloun, Jens Christian Refsgaard, Chantal Donnelly, Kari Hyytiäinen, Sampo Pihlainen, Marianne Zandersen, and Berit Arheimer. Future socioeconomic conditions may have a larger impact than climate change on nutrient loads to the Baltic Sea. *Ambio*, 48(11):1325–1336, November 2019. ISSN 1654-7209. doi: 10.1007/s13280-019-01243-5. URL <https://doi.org/10.1007/s13280-019-01243-5>.

Igor M. Belkin. Rapid warming of Large Marine Ecosystems. *Progress in Oceanography*, 81(1-4):207–213, April 2009. ISSN 00796611. doi: 10.1016/j.pocean.2009.04.011. URL <https://linkinghub.elsevier.com/retrieve/pii/S0079661109000317>.

Arthur H. W. Beusen, Alexander F. Bouwman, Ludovicus P. H. Van Beek, José M. Mogollón, and Jack J. Middelburg. Global riverine N and P transport to ocean increased during the 20th century despite increased retention along the aquatic continuum. *Biogeosciences*, 13(8):2441–2451, April 2016. ISSN 1726-4170. doi: 10.5194/bg-13-2441-2016. URL <https://bg.copernicus.org/articles/13/2441/2016/>. Publisher: Copernicus GmbH.

Shuoben Bi, Xiangkai Qiu, Guojie Wang, Yucheng Gong, Luye Wang, and Mengya Xu. Spatial distribution characteristics of drought disasters in Hunan Province of China from 1644 to 1911 based on EOF and REOF methods. *Environmental Earth Sciences*, 80(16):533, August 2021. ISSN 1866-6299. doi: 10.1007/s12665-021-09867-1. URL <https://doi.org/10.1007/s12665-021-09867-1>.

S. Bonaglia, M. Bartoli, J. S. Gunnarsson, L. Rahm, C. Raymond, O. Svensson, S. Shakeri Yekta, and V. Brüchert. Effect of reoxygenation and *Marenzelleria* spp. bioturbation on Baltic Sea sediment metabolism. *Marine Ecology Progress Series*, 482:43–55, May 2013. ISSN 0171-8630, 1616-1599. doi: 10.3354/meps10232. URL <https://www.int-res.com/abstracts/meps/v482/p43-55/>.

Barrie R. Bonsal, Amir Shabbar, and Kaz Higuchi. Impacts of low frequency variability modes on Canadian winter temperature. *International Journal of Climatology*, 21(1):95–108, 2001. ISSN 1097-0088. doi: 10.1002/joc.590. URL <https://onlinelibrary.wiley.com/doi/abs/10.1002/joc.590>. _eprint: <https://onlinelibrary.wiley.com/doi/pdf/10.1002/joc.590>.

A Borja, M Elliott, JH. Andersen, AC Cardoso, J Carstensen, JG Ferreira, A-S Heiskanen, JC. Marques, JM Neto, H Teixeira, L Uusitalo, MC Uyarra, N Zampoukas, T Prins, N Simboura, T Berg, N Papadopoulou, J Reker, and I Menchaca. Report on potential definition of good environmental status. *Deliverable 6.2, DEVOTES Project*, page ”62”, 2015.

D. Breitburg, G. Marilaure, and I. Kirsten. The ocean is losing its breath: declining oxygen in the world's ocean and coastal waters; summary for policy makers. *Intergovernmental Oceanographic Commission*, 2018a.

Denise Breitburg, Lisa A. Levin, Andreas Oschlies, Marilaure Grégoire, Francisco P. Chavez, Daniel J. Conley, Véronique Garçon, Denis Gilbert, Dimitri Gutiérrez, Kirsten Isensee, Gil S. Jacinto, Karin E. Limburg, Ivonne Montes, S. W. A. Naqvi, Grant C. Pitcher, Nancy N. Rabalais, Michael R. Roman, Kenneth A. Rose, Brad A. Seibel, Maciej Telszewski, Moriaki Yasuhara, and Jing Zhang. Declining oxygen in the global ocean and coastal waters. *Science*, 359(6371):eaam7240, January 2018b. doi: 10.1126/science.aam7240. URL <https://www.science.org/doi/10.1126/science.aam7240>. Publisher: American Association for the Advancement of Science.

Florian Börgel, Claudia Frauen, Thomas Neumann, and H. E. Markus Meier. The Atlantic Multidecadal Oscillation controls the impact of the North Atlantic Oscillation on North European climate. *Environmental Research Letters*, 15(10):104025, September 2020. ISSN 1748-9326. doi: 10.1088/1748-9326/aba925. URL <https://dx.doi.org/10.1088/1748-9326/aba925>. Publisher: IOP Publishing.

Florian Börgel, H. E. Markus Meier, Matthias Gröger, Monika Rhein, Cyril Dutheil, and Jan Moritz Kaiser. Atlantic multidecadal variability and the implications for North European precipitation. *Environmental Research Letters*, 17(4):044040, March 2022. ISSN 1748-9326. doi: 10.1088/1748-9326/ac5ca1. URL <https://dx.doi.org/10.1088/1748-9326/ac5ca1>. Publisher: IOP Publishing.

Florian Börgel, Thomas Neumann, Jurjen Rooze, Hagen Radtke, Leonie Barghorn, and H. E. Markus Meier. Deoxygenation of the Baltic Sea during the last millennium. *Frontiers in Marine Science*, 10, 2023. ISSN 2296-7745. URL <https://www.frontiersin.org/articles/10.3389/fmars.2023.1174039>.

Antonietta Capotondi, Michael A. Alexander, Nicholas A. Bond, Enrique N. Curchitser, and James D. Scott. Enhanced upper ocean stratification with climate change in the CMIP3 models. *Journal of Geophysical Research: Oceans*, 117(C4), 2012. ISSN 2156-2202. doi: 10.1029/2011JC007409. URL <https://onlinelibrary.wiley.com/doi/abs/10.1029/2011JC007409>. _eprint: <https://onlinelibrary.wiley.com/doi/pdf/10.1029/2011JC007409>.

Jacob Carstensen, Jesper H. Andersen, Bo G. Gustafsson, and Daniel J. Conley. Deoxygenation of the Baltic Sea during the last century. *Proceedings of the National Academy of Sciences of the United States of America*, 111(15):5628–5633, April 2014. ISSN 1091-6490. doi: 10.1073/pnas.1323156111.

James A. Carton, Stephen G. Penny, and Eugenia Kalnay. Temperature and Salinity Variability in the SODA₃, ECCO_{4r3}, and ORAS₅ Ocean Reanalyses, 1993–2015. *Journal of Climate*, 32(8):2277–2293, April 2019. ISSN 0894-8755, 1520-0442. doi: 10.1175/JCLI-D-18-0605.1. URL <https://journals.ametsoc.org/view/journals/clim/32/8/jcli-d-18-0605.1.xml>. Publisher: American Meteorological Society Section: Journal of Climate.

Irina Chubarenko and Natalia Stepanova. Cold intermediate layer of the Baltic Sea: Hypothesis of the formation of its core. *Progress in Oceanography*, 167:1–10, October 2018. ISSN

00796611. doi: 10.1016/j.pocean.2018.06.012. URL <https://linkinghub.elsevier.com/retrieve/pii/S0079661117301179>.

D. J. Conley, A. Stockenberg, R. Carman, R. W. Johnstone, L. Rahm, and F. Wulff. Sediment-water Nutrient Fluxes in the Gulf of Finland, Baltic Sea. *Estuarine, Coastal and Shelf Science*, 45(5):591–598, November 1997. ISSN 0272-7714. doi: 10.1006/ecss.1997.0246. URL <https://www.sciencedirect.com/science/article/pii/S0272771497902468>.

Daniel J. Conley, Christoph Humborg, Lars Rahm, Oleg P. Savchuk, and Fredrik Wulff. Hypoxia in the Baltic Sea and Basin-Scale Changes in Phosphorus Biogeochemistry. *Environmental Science & Technology*, 36(24):5315–5320, December 2002a. ISSN 0013-936X. doi: 10.1021/es025763w. URL <https://doi.org/10.1021/es025763w>. Publisher: American Chemical Society.

Daniel J. Conley, Christoph Humborg, Lars Rahm, Oleg P. Savchuk, and Fredrik Wulff. Hypoxia in the Baltic Sea and Basin-Scale Changes in Phosphorus Biogeochemistry. *Environmental Science & Technology*, 36(24):5315–5320, December 2002b. ISSN 0013-936X, 1520-5851. doi: 10.1021/es025763w. URL <https://pubs.acs.org/doi/10.1021/es025763w>.

Daniel J. Conley, Svante Björck, Erik Bonsdorff, Jacob Carstensen, Georgia Destouni, Bo G. Gustafsson, Susanna Hietanen, Marloes Kortekaas, Harri Kuosa, H. E. Markus Meier, Baerbel Müller-Karulis, Kjell Nordberg, Alf Norkko, Gertrud Nürnberg, Heikki Pitkänen, Nancy N. Rabalais, Rutger Rosenberg, Oleg P. Savchuk, Caroline P. Slomp, Maren Voss, Fredrik Wulff, and Lovisa Zillén. Hypoxia-Related Processes in the Baltic Sea. *Environmental Science & Technology*, 43(10):3412–3420, May 2009. ISSN 0013-936X. doi: 10.1021/es802762a. URL <https://doi.org/10.1021/es802762a>. Publisher: American Chemical Society.

Daniel J. Conley, Jacob Carstensen, Juris Aigars, Philip Axe, Erik Bonsdorff, Tatjana Eremina, Britt-Marie Haahti, Christoph Humborg, Per Jonsson, Jonne Kotta, Christer Lännegren, Ulf Larsson, Alexey Maximov, Miguel Rodriguez Medina, Elzbieta Lysiak-Pastuszek, Nijolė Remeikaitė-Nikienė, Jakob Walve, Sunhild Wilhelms, and Lovisa Zillén. Hypoxia Is Increasing in the Coastal Zone of the Baltic Sea. *Environmental Science & Technology*, 45(16):6777–6783, August 2011. ISSN 0013-936X. doi: 10.1021/es201212r. URL <https://doi.org/10.1021/es201212r>. Publisher: American Chemical Society.

Copernicus. Baltic sea biogeochemistry reanalysis. https://data.marine.copernicus.eu/product/BALTICSEA_REANALYSIS_BIO_003_012, 2023a. Accessed August 28, 2023.

Copernicus. Baltic sea physics reanalysis. https://data.marine.copernicus.eu/product/BALTICSEA_REANALYSIS_PHY_003_011, 2023b. Accessed: 2023-08-28.

Damien Couespel, Marina Lévy, and Laurent Bopp. Major Contribution of Reduced Upper Ocean Oxygen Mixing to Global Ocean Deoxygenation in an Earth System Model. *Geophysical Research Letters*, 46(21):12239–12249, 2019. ISSN 1944-8007. doi: 10.1029/2019GL084162. URL <https://onlinelibrary.wiley.com/doi/abs/10.1029/2019GL084162>. eprint: <https://onlinelibrary.wiley.com/doi/pdf/10.1029/2019GL084162>.

Robert J. Diaz and Rutger Rosenberg. Spreading Dead Zones and Consequences for Marine Ecosystems. *Science*, 321(5891):926–929, August 2008. doi: 10.1126/science.1156401. URL <https://www.science.org/doi/10.1126/science.1156401>. Publisher: American Association for the Advancement of Science.

Ivan Dokmanic, Reza Parhizkar, Juri Ranieri, and Martin Vetterli. Euclidean Distance Matrices: Essential Theory, Algorithms and Applications. *IEEE Signal Processing Magazine*, 32(6):12–30, November 2015. ISSN 1053-5888. doi: 10.1109/MSP.2015.2398954. URL <http://arxiv.org/abs/1502.07541>. arXiv:1502.07541 [cs].

Kristofer Döös, H. E Markus Meier, and Ralf Döscher. The Baltic Haline Conveyor Belt or The Overturning Circulation and Mixing in the Baltic. *AMBIO: A Journal of the Human Environment*, 33(4):261–266, 2004. doi: 10.1579/0044-7447-33.4.261. URL <https://doi.org/10.1579/0044-7447-33.4.261>.

C. Dutheil, H. E. M. Meier, M. Gröger, and F. Börgel. Understanding past and future sea surface temperature trends in the Baltic Sea. *Climate Dynamics*, 58(11):3021–3039, June 2022. ISSN 1432-0894. doi: 10.1007/s00382-021-06084-1. URL <https://doi.org/10.1007/s00382-021-06084-1>.

K. Eilola, B. G. Gustafsson, I. Kuznetsov, H. E. M. Meier, T. Neumann, and O. P. Savchuk. Evaluation of biogeochemical cycles in an ensemble of three state-of-the-art numerical models of the Baltic Sea. *Journal of Marine Systems*, 88(2):267–284, November 2011. ISSN 0924-7963. doi: 10.1016/j.jmarsys.2011.05.004. URL <https://www.sciencedirect.com/science/article/pii/S0924796311001230>.

J. Elken and W. Matthäus. Baltic sea oceanography. assessment of climate change for the baltic sea basin. *BALTEX Publication*, 2008.

Jüri Elken, Mälkki Pentti, Pekka Alenius, and Tapani Stipa. Large halocline variations in the Northern Baltic Proper and associated meso- and basin-scale processes. *Oceanologia*, 48, June 2006.

Ruben Escribano, Pamela Hidalgo, and Cristina Krautz. Zooplankton associated with the oxygen minimum zone system in the northern upwelling region of Chile during March 2000. *Deep Sea Research Part II: Topical Studies in Oceanography*, 56(16):1083–1094, July 2009. ISSN 0967-0645. doi: 10.1016/j.dsr2.2008.09.009. URL <https://www.sciencedirect.com/science/article/pii/S0967064508003287>.

Paul G. Falkowski, Thomas Algeo, Lou Codispoti, Curtis Deutsch, Steven Emerson, Burke Hales, Raymond B. Huey, William J. Jenkins, Lee R. Kump, Lisa A. Levin, Timothy W. Lyons, Norman B. Nelson, Oscar S. Schofield, Roger Summons, Lynne D. Talley, Ellen Thomas, Frank Whitney, and Carl B. Pilcher. Ocean deoxygenation: Past, present, and future. *Eos, Transactions American Geophysical Union*, 92(46):409–410, 2011. ISSN 2324-9250. doi: 10.1029/2011EO460001. URL <https://onlinelibrary.wiley.com/doi/abs/10.1029/2011EO460001>. _eprint: <https://onlinelibrary.wiley.com/doi/pdf/10.1029/2011EO460001>.

R. Feistel, G. Nausch, and E. Hagen. Unusual Baltic inflow activity in 2002-2003 and varying deep-water properties. *Oceanologia*, 48(S), 2006. ISSN 0078-3234. URL <http://agro.icm.edu.pl/agro/>

element/bwmetal.element.agro-article-809a7615-1f79-42da-b7fe-83721d50e5df. Publisher: -.

Katja Fennel and Jeremy M. Testa. Biogeochemical Controls on Coastal Hypoxia. *Annual Review of Marine Science*, 11(1):105–130, January 2019. ISSN 1941-1405, 1941-0611. doi: 10.1146/annurev-marine-010318-095138. URL <https://www.annualreviews.org/doi/10.1146/annurev-marine-010318-095138>.

S. Fonselius. Oxygen and hydrogen sulphide conditions in the Baltic Sea. *Marine Pollution Bulletin*, 12(6):187–194, June 1981. ISSN 0025-326X. doi: 10.1016/0025-326X(81)90169-7. URL <https://www.sciencedirect.com/science/article/pii/0025326X81901697>.

Stig Fonselius and Jorge Valderrama. One hundred years of hydrographic measurements in the Baltic Sea. *Journal of Sea Research*, 49(4):229–241, June 2003. ISSN 1385-1101. doi: 10.1016/S1385-1101(03)00035-2. URL <https://www.sciencedirect.com/science/article/pii/S1385110103000352>.

Stig H. Fonselius. Hydrogen sulfide basins and a stagnant period in the Baltic Sea. *Journal of Geophysical Research (1896-1977)*, 68(13):4009–4016, 1963. ISSN 2156-2202. doi: 10.1029/JZ068i013p04009. URL <https://onlinelibrary.wiley.com/doi/abs/10.1029/JZ068i013p04009>. _eprint: <https://onlinelibrary.wiley.com/doi/pdf/10.1029/JZ068i013p04009>.

René Friedland, Thomas Neumann, and Gerald Schernewski. Climate change and the Baltic Sea action plan: Model simulations on the future of the western Baltic Sea. *Journal of Marine Systems*, 105-108: 175–186, December 2012. ISSN 0924-7963. doi: 10.1016/j.jmarsys.2012.08.002. URL <https://www.sciencedirect.com/science/article/pii/S0924796312001625>.

B. Geyer. High-resolution atmospheric reconstruction for Europe 1948–2012: coastDat2. *Earth System Science Data*, 6(1):147–164, April 2014. ISSN 1866-3508. doi: 10.5194/essd-6-147-2014. URL <https://essd.copernicus.org/articles/6/147/2014/>. Publisher: Copernicus GmbH.

Lars Gidhagen. Coastal upwelling in the Baltic Sea—Satellite and in situ measurements of sea-surface temperatures indicating coastal upwelling. *Estuarine, Coastal and Shelf Science*, 24(4):449–462, April 1987. ISSN 0272-7714. doi: 10.1016/0272-7714(87)90127-2. URL <https://www.sciencedirect.com/science/article/pii/0272771487901272>.

Mirjam S. Glessmer, Carsten Eden, and Andreas Oschlies. Contribution of oxygen minimum zone waters to the coastal upwelling off Mauritania. *Progress in Oceanography*, 83(1):143–150, December 2009. ISSN 0079-6611. doi: 10.1016/j.pocan.2009.07.015. URL <https://www.sciencedirect.com/science/article/pii/S0079661109001050>.

S. M. Griffies. Elements of the modular ocean model. gfdl ocean group technical report no. 7. *Princeton: NOAA/Geophysical Fluid Dynamics Laboratory*, page 632, 2012.

Bo G. Gustafsson and Anders Stigebrandt. Dynamics of nutrients and oxygen/hydrogen sulfide in the Baltic Sea deep water. *Journal of Geophysical Research: Biogeosciences*, 112(G2), 2007. ISSN 2156-2202. doi: 10.1029/2006JG000304. URL <https://onlinelibrary.wiley.com/doi/abs/10.1029/2006JG000304>. _eprint: <https://onlinelibrary.wiley.com/doi/pdf/10.1029/2006JG000304>.

Bo G. Gustafsson, Frederik Schenk, Thorsten Blenckner, Kari Eilola, H. E. Markus Meier, Bärbel Müller-Karulis, Thomas Neumann, Tuija Ruoho-Airola, Oleg P. Savchuk, and Eduardo Zorita. Reconstructing the Development of Baltic Sea Eutrophication 1850–2006. *AMBIO*, 41(6):534–548, September 2012. ISSN 1654-7209. doi: 10.1007/s13280-012-0318-x. URL <https://doi.org/10.1007/s13280-012-0318-x>.

Jari J. Haapala, Iina Ronkainen, Natalija Schmelzer, and Marzenna Sztobryn. Recent Change—Sea Ice. In The BACC II Author Team, editor, *Second Assessment of Climate Change for the Baltic Sea Basin*, Regional Climate Studies, pages 145–153. Springer International Publishing, Cham, 2015. ISBN 978-3-319-16006-1. doi: 10.1007/978-3-319-16006-1_8. URL https://doi.org/10.1007/978-3-319-16006-1_8.

A. Hannachi, I. T. Jolliffe, and D. B. Stephenson. Empirical orthogonal functions and related techniques in atmospheric science: A review. *International Journal of Climatology*, 27(9):1119–1152, 2007. ISSN 1097-0088. doi: 10.1002/joc.1499. URL <https://onlinelibrary.wiley.com/doi/abs/10.1002/joc.1499>. _eprint: <https://onlinelibrary.wiley.com/doi/pdf/10.1002/joc.1499>.

M. Hannig, G. Lavik, M. M. M. Kuypers, D. Woebken, W. Martens-Habbena, and K. Jürgens. Shift from denitrification to anammox after inflow events in the central Baltic Sea. *Limnology and Oceanography*, 52(4):1336–1345, 2007. ISSN 1939-5590. doi: 10.4319/lo.2007.52.4.1336. URL <https://onlinelibrary.wiley.com/doi/abs/10.4319/lo.2007.52.4.1336>. _eprint: <https://onlinelibrary.wiley.com/doi/pdf/10.4319/lo.2007.52.4.1336>.

Martin Hansson, Lena Viktorsson, and Lars Andersson. *Oxygen Survey in the Baltic Sea 2017 - Extent of Anoxia and Hypoxia, 1960-2017*. 2018. URL <https://urn.kb.se/resolve?urn=urn:nbn:se:smhi:diva-4675>.

J. A. Hartigan and M. A. Wong. Algorithm as 136: A k-means clustering algorithm. *Journal of the Royal Statistical Society. Series C (Applied Statistics)*, 28(1):100–108, 1979.

HELCOM. The helcom baltic sea action plan. helsinki commission. www.helcom.fi, 2007. Accessed: 2023-08-28.

HELCOM. Helcom baltic sea action plan – 2021 update. helsinki commission. www.helcom.fi, 2021. Accessed: 2023-08-28.

Jan V. Henkel, Olaf Dellwig, Falk Pollehne, Daniel P. R. Herlemann, Thomas Leipe, and Heide N. Schulz-Vogt. A bacterial isolate from the Black Sea oxidizes sulfide with manganese(IV) oxide. *Proceedings of the National Academy of Sciences*, 116(25):12153–12155, June 2019. ISSN 0027-8424, 1091-6490. doi: 10.1073/pnas.1906000116. URL <https://pnas.org/doi/full/10.1073/pnas.1906000116>.

H. Hersbach, B. Bell, P. Berrisford, G. Biavati, A. Horányi, J. Muñoz Sabater, J. Nicolas, C. Peubey, R. Radu, I. Rozum, D. Schepers, A. Simmons, C. Soci, D. Dee, and J-N. Thépaut. Era5 monthly averaged data on single levels from 1940 to present. *Copernicus Climate Change Service (C3S) Climate Data Store (CDS)*, 2023. doi: 10.24381/cds.f17050d7. Accessed on 2023-09-13.

Hans Hersbach, Bill Bell, Paul Berrisford, Shoji Hirahara, András Horányi, Joaquín Muñoz-Sabater, Julien Nicolas, Carole Peubey, Raluca Radu, Dinand Schepers, Adrian Simmons, Cornel Soci, Saleh Abdalla, Xavier Abellan, Gianpaolo Balsamo, Peter Bechtold, Gionata Biavati, Jean Bidlot, Massimo Bonavita, Giovanna De Chiara, Per Dahlgren, Dick Dee, Michail Diamantakis, Rossana Dragani, Johannes Flemming, Richard Forbes, Manuel Fuentes, Alan Geer, Leo Haimberger, Sean Healy, Robin J. Hogan, Elías Hólm, Marta Janisková, Sarah Keeley, Patrick Laloyaux, Philippe Lopez, Cristina Lupu, Gabor Radnoti, Patricia de Rosnay, Iryna Rozum, Freja Vamborg, Sebastien Villaume, and Jean-Noël Thépaut. The ERA5 global reanalysis. *Quarterly Journal of the Royal Meteorological Society*, 146(730): 1999–2049, 2020. ISSN 1477-870X. doi: 10.1002/qj.3803. URL <https://onlinelibrary.wiley.com/doi/abs/10.1002/qj.3803>. _eprint: <https://onlinelibrary.wiley.com/doi/pdf/10.1002/qj.3803>.

Susanna Hietanen and Jorma Kuparinen. Seasonal and short-term variation in denitrification and anammox at a coastal station on the Gulf of Finland, Baltic Sea. *Hydrobiologia*, 596(1):67–77, January 2008. ISSN 1573-5117. doi: 10.1007/s10750-007-9058-5. URL <https://doi.org/10.1007/s10750-007-9058-5>.

Hans-Harald Hinrichsen, Uwe Piatkowski, and Cornelia Jaspers. Sightings of extraordinary marine species in the SW Baltic Sea linked to saline water inflows. *Journal of Sea Research*, 181:102175, March 2022. ISSN 1385-1101. doi: 10.1016/j.seares.2022.102175. URL <https://www.sciencedirect.com/science/article/pii/S1385110122000132>.

P. Holtermann, O. Pinner, R. Schwefel, and L. Umlauf. The Role of Boundary Mixing for Diapycnal Oxygen Fluxes in a Stratified Marine System. *Geophysical Research Letters*, 49(20):e2022GL098917, 2022. ISSN 1944-8007. doi: 10.1029/2022GL098917. URL <https://onlinelibrary.wiley.com/doi/abs/10.1029/2022GL098917>. _eprint: <https://onlinelibrary.wiley.com/doi/pdf/10.1029/2022GL098917>.

Peter Holtermann, Ralf Prien, Michael Naumann, and Lars Umlauf. Interleaving of oxygenized intrusions into the Baltic Sea redoxcline. *Limnology and Oceanography*, 65(3):482–503, 2020. ISSN 1939-5590. doi: 10.1002/lno.11317. URL <https://onlinelibrary.wiley.com/doi/abs/10.1002/lno.11317>. _eprint: <https://onlinelibrary.wiley.com/doi/pdf/10.1002/lno.11317>.

Robinson Hordoir, Lars Axell, Anders Höglund, Christian Dieterich, Filippa Fransner, Matthias Gröger, Ye Liu, Per Pemberton, Semjon Schimanke, Helen Andersson, Patrik Ljungemyr, Petter Nygren, Saeed Falahat, Adam Nord, Anette Jönsson, Iréne Lake, Kristofer Döös, Magnus Hieronymus, Heiner Dietze, Ulrike Löptien, Ivan Kuznetsov, Antti Westerlund, Laura Tuomi, and Jari Haapala. Nemo-Nordic 1.0: a NEMO-based ocean model for the Baltic and North seas – research and operational applications. *Geoscientific Model Development*, 12(1):363–386, January 2019. ISSN 1991-959X. doi: 10.5194/gmd-12-363-2019. URL <https://gmd.copernicus.org/articles/12/363/2019/>. Publisher: Copernicus GmbH.

E. C. Hunke and J. K. Dukowicz. An Elastic–Viscous–Plastic Model for Sea Ice Dynamics. *Journal of Physical Oceanography*, 27(9):1849–1867, September 1997. ISSN 0022-3670, 1520-0485. doi: 10.1175/1520-0485(1997)027<1849:AEVPMF>2.0.CO;2. URL <https://journals.ametsoc.org/>

view/journals/phoc/27/9/1520-0485_1997_027_1849_aevpmf_2.0.co_2.xml. Publisher: American Meteorological Society Section: Journal of Physical Oceanography.

Astrid Hylén, Stefano Bonaglia, Elizabeth Robertson, Ugo Marzocchi, Mikhail Kononets, and Per O. J. Hall. Enhanced benthic nitrous oxide and ammonium production after natural oxygenation of long-term anoxic sediments. *Limnology and Oceanography*, 67(2):419–433, 2022. ISSN 1939-5590. doi: 10.1002/lno.12001. URL <https://onlinelibrary.wiley.com/doi/abs/10.1002/lno.12001>. _eprint: <https://onlinelibrary.wiley.com/doi/pdf/10.1002/lno.12001>.

Jari Hänninen, Ilppo Vuorinen, and Pekka Hjelt. Climatic factors in the Atlantic control the oceanographic and ecological changes in the Baltic Sea. *Limnology and Oceanography*, 45(3):703–710, 2000. ISSN 1939-5590. doi: 10.4319/lno.2000.45.3.0703. URL <https://onlinelibrary.wiley.com/doi/abs/10.4319/lno.2000.45.3.0703>. _eprint: <https://onlinelibrary.wiley.com/doi/pdf/10.4319/lno.2000.45.3.0703>.

ICES. Dataset collections. <https://www.ices.dk/data/dataset-collections>, 2023. Accessed August 28, 2023.

IOW. Odin 2. <https://odin2.io-warnemuende.de>, 2023. Accessed August 28, 2023.

Adam Jaeger and David Banks. Cluster analysis: A modern statistical review. *WIREs Computational Statistics*, 15(3):e1597, 2023. ISSN 1939-0068. doi: 10.1002/wics.1597. URL <https://onlinelibrary.wiley.com/doi/abs/10.1002/wics.1597>. _eprint: <https://onlinelibrary.wiley.com/doi/pdf/10.1002/wics.1597>.

F. Jakobsen. The major inflow to the baltic sea during january 1993. *Journal of Marine Systems*, 6(3):227–240, 1995. ISSN 0924-7963. doi: [https://doi.org/10.1016/0924-7963\(94\)00025-7](https://doi.org/10.1016/0924-7963(94)00025-7). URL <https://www.sciencedirect.com/science/article/pii/0924796394000257>.

Martin Jakobsson, Christian Stranne, Matt O’Regan, Sarah L. Greenwood, Bo Gustafsson, Christoph Humborg, and Elizabeth Weidner. Bathymetric properties of the Baltic Sea. *Ocean Science*, 15(4):905–924, July 2019. ISSN 1812-0784. doi: 10.5194/os-15-905-2019. URL <https://os.copernicus.org/articles/15/905/2019/>. Publisher: Copernicus GmbH.

F. Janssen, C. Schrum, and J. O. Backhaus. A climatological data set of temperature and salinity for the Baltic Sea and the North Sea. *Deutsche Hydrographische Zeitschrift*, 51:5–245, November 1999. doi: 10.1007/BF02933676. URL <https://ui.adsabs.harvard.edu/abs/1999DeHyZ..51....5J>. ADS Bibcode: 1999DeHyZ..51....5J.

S. Jevrejeva, V. V. Drabkin, J. Kostjukov, A. A. Lebedev, M. Leppäranta, Ye U. Mironov, N. Schmelzer, and M. Sztobryn. Baltic Sea ice seasons in the twentieth century. *Climate Research*, 25(3):217–227, January 2004. ISSN 0936-577X, 1616-1572. doi: 10.3354/cr025217. URL <https://www.int-res.com/abstracts/cr/v25/n3/p217-227/>.

X. Jin, R. G. Najjar, F. Louanchi, and Scott C. Doney. A modeling study of the seasonal oxygen budget of the global ocean. *Journal of Geophysical Research: Oceans*, 112(C5), 2007. ISSN 2156-2202. doi: 10.

1029/2006JC003731. URL <https://onlinelibrary.wiley.com/doi/abs/10.1029/2006JC003731>.
_eprint: <https://onlinelibrary.wiley.com/doi/pdf/10.1029/2006JC003731>.

Milla Johansson, Hanna Boman, Kimmo K Kahma, and Jouko Launiainen. Trends in sea level variability in the Baltic Sea. *Boreal Environment Research*, 6:159–179, September 2001. ISSN 1239-6095.

Helena Jäntti, Bess B. Ward, Joachim W. Dippner, and Susanna Hietanen. Nitrification and the ammonia-oxidizing communities in the central Baltic Sea water column. *Estuarine, Coastal and Shelf Science*, 202:280–289, March 2018. ISSN 0272-7714. doi: 10.1016/j.ecss.2018.01.019. URL <https://www.sciencedirect.com/science/article/pii/S0272771417307035>.

Bo Barker Jørgensen, Alyssa J. Findlay, and André Pellerin. The Biogeochemical Sulfur Cycle of Marine Sediments. *Frontiers in Microbiology*, 10, 2019. ISSN 1664-302X. URL <https://www.frontiersin.org/articles/10.3389/fmicb.2019.00849>.

M. Kahru and S. Nommann. The phytoplankton spring bloom in the Baltic Sea in 1985, 1986: multitude of spatio-temporal scales. *Continental Shelf Research*, 10(4):329–354, April 1990. ISSN 0278-4343. doi: 10.1016/0278-4343(90)90055-Q. URL <https://www.sciencedirect.com/science/article/pii/027843439090055Q>.

Jérôme Kaiser, Norbert Wasmund, Mati Kahru, Anna K. Wittenborn, Regina Hansen, Katharina Häusler, Matthias Moros, Detlef Schulz-Bull, and Helge W. Arz. Reconstructing N₂-fixing cyanobacterial blooms in the Baltic Sea beyond observations using 6- and 7-methylheptadecane in sediments as specific biomarkers. *Biogeosciences*, 17(9):2579–2591, May 2020. ISSN 1726-4170. doi: 10.5194/bg-17-2579-2020. URL <https://bg.copernicus.org/articles/17/2579/2020/>. Publisher: Copernicus GmbH.

Inga Kanoshina, Urmas Lips, and Juha-Markku Leppänen. The influence of weather conditions (temperature and wind) on cyanobacterial bloom development in the Gulf of Finland (Baltic Sea). *Harmful Algae*, 2(1):29–41, March 2003. ISSN 1568-9883. doi: 10.1016/S1568-9883(02)00085-9. URL <https://www.sciencedirect.com/science/article/pii/S1568988302000859>.

Agnes M. L. Karlson, Jon Duberg, Nisha H. Motwani, Hedvig Hogfors, Isabell Klawonn, Helle Ploug, Jennie Barthel Svedén, Andrius Garbaras, Brita Sundelin, Susanna Hajdu, Ulf Larsson, Ragnar Elmgren, and Elena Gorokhova. Nitrogen fixation by cyanobacteria stimulates production in Baltic food webs. *AMBIO*, 44(3):413–426, June 2015. ISSN 1654-7209. doi: 10.1007/s13280-015-0660-x. URL <https://doi.org/10.1007/s13280-015-0660-x>.

A. P. Klemeshev, V. S. Korneevets, T. Palmowski, T. Studzieniecki, and G. M. Fedorov. Approaches to the Definition of the Baltic Sea Region. *Baltic Region*, 9(4):4–20, 2017. ISSN 20798555, 23100524. doi: 10.5922/2079-8555-2017-4-1. URL https://journals.kantiana.ru/upload/iblock/70a/klemeshev_4-20.pdf.

M. Kniebusch. *Detection and attribution studies of climate related changes in the Baltic Sea since 1850*. dissertation, Universität Rostock, 2019. URL https://doi.org/10.18453/rosdok_id00002664.

Madline Kniebusch, H.E. Markus Meier, Thomas Neumann, and Florian Börgel. Temperature Variability of the Baltic Sea Since 1850 and Attribution to Atmospheric Forcing Variables. *Journal of Geophysical Research: Oceans*, 124(6):4168–4187, 2019a. ISSN 2169-9291. doi: 10.1029/2018JC013948. URL <https://onlinelibrary.wiley.com/doi/abs/10.1029/2018JC013948>. _eprint: <https://onlinelibrary.wiley.com/doi/pdf/10.1029/2018JC013948>.

Madline Kniebusch, H.E. Markus Meier, and Hagen Radtke. Changing Salinity Gradients in the Baltic Sea As a Consequence of Altered Freshwater Budgets. *Geophysical Research Letters*, 46(16):9739–9747, 2019b. ISSN 1944-8007. doi: 10.1029/2019GL083902. URL <https://onlinelibrary.wiley.com/doi/abs/10.1029/2019GL083902>. _eprint: <https://onlinelibrary.wiley.com/doi/pdf/10.1029/2019GL083902>.

V. A. Korneeva, N. V. Pimenov, A. V. Krek, T. P. Tourova, and A. L. Bryukhanov. Sulfate-reducing bacterial communities in the water column of the Gdansk Deep (Baltic Sea). *Microbiology*, 84(2):268–277, March 2015. ISSN 1608-3237. doi: 10.1134/S002626171502006X. URL <https://doi.org/10.1134/S002626171502006X>.

Samuli Korpinen, Leena Laamanen, Lena Bergström, Marco Nurmi, Jesper H. Andersen, Juuso Haapaniemi, E. Therese Harvey, Ciaran J. Murray, Monika Peterlin, Emilie Kallenbach, Katja Klančnik, Ulf Stein, Leonardo Tunesi, David Vaughan, and Johnny Reker. Combined effects of human pressures on Europe’s marine ecosystems. *Ambio*, 50(7):1325–1336, July 2021. ISSN 1654-7209. doi: 10.1007/s13280-020-01482-x. URL <https://doi.org/10.1007/s13280-020-01482-x>.

Karina Krapf, Michael Naumann, Cyril Dutheil, and H. E. Markus Meier. Investigating Hypoxic and Euxinic Area Changes Based on Various Datasets From the Baltic Sea. *Frontiers in Marine Science*, 9, 2022. ISSN 2296-7745. URL <https://www.frontiersin.org/articles/10.3389/fmars.2022.823476>.

Karol Kuliński, Gregor Rehder, Eero Asmala, Alena Bartosova, Jacob Carstensen, Bo Gustafsson, Per O. J. Hall, Christoph Humborg, Tom Jilbert, Klaus Jürgens, H. E. Markus Meier, Bärbel Müller-Karulis, Michael Naumann, Jørgen E. Olesen, Oleg Savchuk, Andreas Schramm, Caroline P. Slomp, Mikhail Sofiev, Anna Sobek, Beata Szymczycha, and Emma Undeman. Biogeochemical functioning of the Baltic Sea. *Earth System Dynamics*, 13(1):633–685, March 2022. ISSN 2190-4979. doi: 10.5194/esd-13-633-2022. URL <https://esd.copernicus.org/articles/13/633/2022/>. Publisher: Copernicus GmbH.

N. P. Kuzmina, V. M. Zhurbas, B. Rudels, T. Stipa, V. T. Paka, and S. S. Muraviev. Role of eddies and intrusions in the exchange processes in the Baltic halocline. *Oceanology*, 48(2):149–158, April 2008. ISSN 1531-8508. doi: 10.1134/S000143700802001X. URL <https://doi.org/10.1134/S000143700802001X>.

Ivan Kuznetsov and Thomas Neumann. Simulation of carbon dynamics in the Baltic Sea with a 3D model. *Journal of Marine Systems*, 111-112:167–174, February 2013. ISSN 0924-7963. doi: 10.1016/j.jmarsys.2012.10.011. URL <https://www.sciencedirect.com/science/article/pii/S0924796312002072>.

Sanggyu Kwak. Are Only p-Values Less Than 0.05 Significant? A p-Value Greater Than 0.05 Is Also Significant! *Journal of Lipid and Atherosclerosis*, 12(2):89–95, May 2023. ISSN 2287-2892. doi: 10.12997/jla.2023.12.2.89. URL <https://www.ncbi.nlm.nih.gov/pmc/articles/PMC10232224/>.

Mariliis Kõuts, Ilja Maljutenko, Jüri Elken, Ye Liu, Martin Hansson, Lena Viktorsson, and Urmas Raudsepp. Recent regime of persistent hypoxia in the Baltic Sea. *Environmental Research Communications*, 3(7):075004, July 2021. ISSN 2515-7620. doi: 10.1088/2515-7620/ac0cc4. URL <https://dx.doi.org/10.1088/2515-7620/ac0cc4>. Publisher: IOP Publishing.

D. Laffoley and J. M. Baxter. Ocean deoxygenation : everyone’s problem. *Gland, Switzerland : IUCN*, page 562, 2019. ISSN 978-2-8317-2014-2. doi: 10.2305/IUCN.CH.2019.13.en.

W. G. Large, J. C. McWilliams, and S. C. Doney. Oceanic vertical mixing: A review and a model with a nonlocal boundary layer parameterization. *Reviews of Geophysics*, 32(4):363–403, 1994. doi: <https://doi.org/10.1029/94RG01872>. URL <https://agupubs.onlinelibrary.wiley.com/doi/abs/10.1029/94RG01872>.

H. U. Lass and W. Matthäus. On temporal wind variations forcing salt water inflows into the Baltic Sea. *Tellus A*, 48(5):663–671, 1996. ISSN 1600-0870. doi: 10.1034/j.1600-0870.1996.t01-4-00005.x. URL <https://onlinelibrary.wiley.com/doi/abs/10.1034/j.1600-0870.1996.t01-4-00005.x>.
_eprint: <https://onlinelibrary.wiley.com/doi/pdf/10.1034/j.1600-0870.1996.t01-4-00005.x>.

Eli D. Lazarus, Michael A. Ellis, A. Brad Murray, and Damon M. Hall. An evolving research agenda for human–coastal systems. *Geomorphology*, 256:81–90, March 2016. ISSN 0169-555X. doi: 10.1016/j.geomorph.2015.07.043. URL <https://www.sciencedirect.com/science/article/pii/S0169555X15301082>.

A Lehmann and H. H Hinrichsen. On the wind driven and thermohaline circulation of the Baltic Sea. *Physics and Chemistry of the Earth, Part B: Hydrology, Oceans and Atmosphere*, 25(2):183–189, January 2000. ISSN 1464-1909. doi: 10.1016/S1464-1909(99)00140-9. URL <https://www.sciencedirect.com/science/article/pii/S1464190999001409>.

A. Lehmann and P. Post. Variability of atmospheric circulation patterns associated with large volume changes of the Baltic Sea. *Advances in Science and Research*, 12(1):219–225, October 2015. ISSN 1992-0628. doi: 10.5194/asr-12-219-2015. URL <https://asr.copernicus.org/articles/12/219/2015/>.
Conference Name: 14th EMS Annual Meeting & 10th European Conference on Applied Climatology (ECAC) - Publisher: Copernicus GmbH.

Andreas Lehmann and Kai Myrberg. Upwelling in the Baltic Sea — A review. *Journal of Marine Systems*, 74:S3–S12, December 2008. ISSN 0924-7963. doi: 10.1016/j.jmarsys.2008.02.010. URL <https://www.sciencedirect.com/science/article/pii/S0924796308002492>.

Andreas Lehmann, Philip Lorenz, and Daniela Jacob. Modelling the exceptional Baltic Sea inflow events in 2002–2003. *Geophysical Research Letters*, 31(21), 2004. ISSN 1944-8007. doi: 10.1029/2004GL020830. URL <https://onlinelibrary.wiley.com/doi/abs/10.1029/2004GL020830>.
_eprint: <https://onlinelibrary.wiley.com/doi/pdf/10.1029/2004GL020830>.

Andreas Lehmann, Kai Myrberg, Piia Post, Irina Chubarenko, Inga Dailidienė, Hans-Harald Hinrichsen, Karin Hüssy, Taavi Liblik, H. E. Markus Meier, Urmas Lips, and Tatiana Bukanova. Salinity dynamics of the Baltic Sea. *Earth System Dynamics*, 13(1):373–392, February 2022. ISSN 2190-4979. doi: 10.5194/esd-13-373-2022. URL <https://esd.copernicus.org/articles/13/373/2022/>. Publisher: Copernicus GmbH.

Jouni Lehtoranta, Petri Ekholm, and Heikki Pitkänen. Coastal Eutrophication Thresholds: A Matter of Sediment Microbial Processes. *AMBIO: A Journal of the Human Environment*, 38(6):303–308, September 2009. ISSN 0044-7447, 1654-7209. doi: 10.1579/09-A-656.1. URL <https://bioone.org/journals/ambio-a-journal-of-the-human-environment/volume-38/issue-6/09-A-656.1/Coastal-Eutrophication-Thresholds-A-Matter-of-Sediment-Microbial-Processes/10.1579/09-A-656.1.full>. Publisher: Royal Swedish Academy of Sciences.

Conny Lenz, Tom Jilbert, Daniel J. Conley, and Caroline P. Slomp. Hypoxia-driven variations in iron and manganese shuttling in the Baltic Sea over the past 8 kyr. *Geochemistry, Geophysics, Geosystems*, 16(10):3754–3766, 2015. ISSN 1525-2027. doi: 10.1002/2015GC005960. URL <https://onlinelibrary.wiley.com/doi/abs/10.1002/2015GC005960>. _eprint: <https://onlinelibrary.wiley.com/doi/pdf/10.1002/2015GC005960>.

Matti Leppäranta and Kai Myrberg. *Physical Oceanography of the Baltic Sea*. Springer, Berlin, Heidelberg, 2009. ISBN 978-3-540-79702-9 978-3-540-79703-6. doi: 10.1007/978-3-540-79703-6. URL <http://link.springer.com/10.1007/978-3-540-79703-6>.

Sydney Levitus, John I. Antonov, Timothy P. Boyer, and Cathy Stephens. Warming of the World Ocean. *Science*, 287(5461):2225–2229, March 2000. doi: 10.1126/science.287.5461.2225. URL <https://www.science.org/doi/full/10.1126/science.287.5461.2225>. Publisher: American Association for the Advancement of Science.

Guancheng Li, Lijing Cheng, Jiang Zhu, Kevin E. Trenberth, Michael E. Mann, and John P. Abraham. Increasing ocean stratification over the past half-century. *Nature Climate Change*, 10(12):1116–1123, December 2020. ISSN 1758-6798. doi: 10.1038/s41558-020-00918-2. URL <https://www.nature.com/articles/s41558-020-00918-2>. Number: 12 Publisher: Nature Publishing Group.

Ming Li, Younjoo J. Lee, Jeremy M. Testa, Yun Li, Wenfei Ni, W. Michael Kemp, and Dominic M. Di Toro. What drives interannual variability of hypoxia in Chesapeake Bay: Climate forcing versus nutrient loading? *Geophysical Research Letters*, 43(5):2127–2134, March 2016. ISSN 0094-8276, 1944-8007. doi: 10.1002/2015GL067334. URL <https://onlinelibrary.wiley.com/doi/10.1002/2015GL067334>.

Taavi Liblik, Michael Naumann, Pekka Alenius, Martin Hansson, Urmas Lips, Günther Nausch, Laura Tuomi, Karin Wesslander, Jaan Laanemets, and Lena Viktorsson. Propagation of Impact of the Recent Major Baltic Inflows From the Eastern Gotland Basin to the Gulf of Finland. *Frontiers in Marine Science*, 5, 2018. ISSN 2296-7745. URL <https://www.frontiersin.org/articles/10.3389/fmars.2018.00222>.

Karin E. Limburg and Michele Casini. Effect of Marine Hypoxia on Baltic Sea Cod *Gadus morhua*: Evidence From Otolith Chemical Proxies. *Frontiers in Marine Science*, 5, 2018. ISSN 2296-7745. URL <https://www.frontiersin.org/articles/10.3389/fmars.2018.00482>.

Karin E. Limburg, Denise Breitburg, Dennis P. Swaney, and Gil Jacinto. Ocean Deoxygenation: A Primer. *One Earth*, 2(1):24–29, January 2020. ISSN 2590-3322. doi: 10.1016/j.oneear.2020.01.001. URL <https://www.sciencedirect.com/science/article/pii/S2590332220300014>.

Ralf Lindau. Energy and water balance of the Baltic Sea derived from merchant ship observations. *Boreal Environment Research*, 7:417–424, December 2002. ISSN 1239-6095.

Brian R. Mackenzie and Doris Schiedek. Daily ocean monitoring since the 1860s shows record warming of northern European seas. *Global Change Biology*, 13(7):1335–1347, 2007. ISSN 1365-2486. doi: 10.1111/j.1365-2486.2007.01360.x. URL <https://onlinelibrary.wiley.com/doi/abs/10.1111/j.1365-2486.2007.01360.x>. _eprint: <https://onlinelibrary.wiley.com/doi/pdf/10.1111/j.1365-2486.2007.01360.x>.

H. E. Markus Meier, Christian Dieterich, and Matthias Gröger. Natural variability is a large source of uncertainty in future projections of hypoxia in the Baltic Sea. *Communications Earth & Environment*, 2(1):1–13, February 2021. ISSN 2662-4435. doi: 10.1038/s43247-021-00115-9. URL <https://www.nature.com/articles/s43247-021-00115-9>. Number: 1 Publisher: Nature Publishing Group.

W. Matthäus, D. Nehring, R. Feistel, G. Nausch, V. Mohrholz, and H.-U. Lass. The Inflow of Highly Saline Water into the Baltic Sea. In *State and Evolution of the Baltic Sea, 1952-2005: A Detailed 50-Year Survey of Meteorology and Climate, Physics, Chemistry, Biology, and Marine Environment*, pages 265–309. 2008. ISBN 978-0-471-97968-5. doi: 10.1002/9780470283134.ch10.

Wolfgang Matthäus and Herbert Franck. Characteristics of major Baltic inflows—a statistical analysis. *Continental Shelf Research*, 12(12):1375–1400, December 1992. ISSN 0278-4343. doi: 10.1016/0278-4343(92)90060-W. URL <https://www.sciencedirect.com/science/article/pii/027843439290060w>.

Wolfgang Matthäus and Hans Ulrich Lass. The Recent Salt Inflow into the Baltic Sea. *Journal of Physical Oceanography*, 25(2):280–286, February 1995. ISSN 0022-3670, 1520-0485. doi: 10.1175/1520-0485(1995)025<0280:TRSIT>2.0.CO;2. URL https://journals.ametsoc.org/view/journals/phoc/25/2/1520-0485_1995_025_0280_trsiit_2_0_co_2.xml. Publisher: American Meteorological Society Section: Journal of Physical Oceanography.

Julian P. McCreary, Zuojun Yu, Raleigh R. Hood, P. N. Vinayachandran, Ryo Furue, Akio Ishida, and Kelvin J. Richards. Dynamics of the Indian-Ocean oxygen minimum zones. *Progress in Oceanography*, 112-113:15–37, May 2013. ISSN 0079-6611. doi: 10.1016/j.pocean.2013.03.002. URL <https://www.sciencedirect.com/science/article/pii/S007966111300027x>.

Igor Medvedev and Evgueni Kulikov. Low-Frequency Baltic Sea Level Spectrum. *Frontiers in Earth Science*, 7, 2019. ISSN 2296-6463. URL <https://www.frontiersin.org/articles/10.3389/feart.2019.00284>.

H. Meier. Regional ocean climate simulations with a 3D ice-ocean model for the Baltic Sea. Part 1: model experiments and results for temperature and salinity. *Climate Dynamics*, 19(3):237–253, July 2002. ISSN 1432-0894. doi: 10.1007/s00382-001-0224-6. URL <https://doi.org/10.1007/s00382-001-0224-6>.

H. E. M. Meier, R. Doscher, B. Broman, and J. Piechura. The major Baltic inflow in January 2003 and preconditioning by smaller inflows in summer-autumn 2002: a model study. *Oceanologia*, 46(4), 2004. ISSN 0078-3234. URL <http://agro.icm.edu.pl/agro/element/bwmeta1.element/agro-article-321fc259-88fa-497f-982b-79e210c8db9e>. Publisher: -.

H. E. M. Meier, H. C. Andersson, K. Eilola, B. G. Gustafsson, I. Kuznetsov, B. Müller-Karulis, T. Neumann, and O. P. Savchuk. Hypoxia in future climates: A model ensemble study for the Baltic Sea: HYPOXIA IN FUTURE CLIMATES. *Geophysical Research Letters*, 38(24):n/a–n/a, December 2011. ISSN 00948276. doi: 10.1029/2011GL049929. URL <http://doi.wiley.com/10.1029/2011GL049929>.

H. E. M. Meier, K. Eilola, E. Almroth-Rosell, S. Schimanke, M. Kniebusch, A. Höglund, P. Pember-ton, Y. Liu, G. Väli, and S. Saraiva. Disentangling the impact of nutrient load and climate changes on Baltic Sea hypoxia and eutrophication since 1850. *Climate Dynamics*, 53(1):1145–1166, July 2019a. ISSN 1432-0894. doi: 10.1007/s00382-018-4296-y. URL <https://doi.org/10.1007/s00382-018-4296-y>.

H. E. Markus Meier. On the parameterization of mixing in three-dimensional Baltic Sea models. *Journal of Geophysical Research: Oceans*, 106(C12):30997–31016, 2001. ISSN 2156-2202. doi: 10.1029/2000JC000631. URL <https://onlinelibrary.wiley.com/doi/abs/10.1029/2000JC000631>. _eprint: <https://onlinelibrary.wiley.com/doi/pdf/10.1029/2000JC000631>.

H. E. Markus Meier and Frank Kauker. Modeling decadal variability of the Baltic Sea: 2. Role of freshwater inflow and large-scale atmospheric circulation for salinity. *Journal of Geophysical Research: Oceans*, 108(C11), 2003. ISSN 2156-2202. doi: 10.1029/2003JC001799. URL <https://onlinelibrary.wiley.com/doi/abs/10.1029/2003JC001799>. _eprint: <https://onlinelibrary.wiley.com/doi/pdf/10.1029/2003JC001799>.

H. E. Markus Meier, Ralf Döscher, and Torgny Faxén. A multiprocessor coupled ice-ocean model for the Baltic Sea: Application to salt inflow. *Journal of Geophysical Research: Oceans*, 108(C8), 2003. ISSN 2156-2202. doi: 10.1029/2000JC000521. URL <https://onlinelibrary.wiley.com/doi/abs/10.1029/2000JC000521>. _eprint: <https://onlinelibrary.wiley.com/doi/pdf/10.1029/2000JC000521>.

H. E. Markus Meier, Germo Väli, Michael Naumann, Kari Eilola, and Claudia Frauen. Recently Accelerated Oxygen Consumption Rates Amplify Deoxygenation in the Baltic Sea. *Journal of Geophysical Research: Oceans*, 123(5):3227–3240, 2018. ISSN 2169-9291. doi: 10.1029/2017JC013686. URL <https://onlinelibrary.wiley.com/doi/abs/10.1029/2017JC013686>. _eprint: <https://onlinelibrary.wiley.com/doi/pdf/10.1029/2017JC013686>.

H. E. Markus Meier, Christian Dieterich, Kari Eilola, Matthias Gröger, Anders Höglund, Hagen Radtke, Sofia Saraiva, and Iréne Wahlström. Future projections of record-breaking sea surface temperature and cyanobacteria bloom events in the Baltic Sea. *Ambio*, 48(11):1362–1376, November 2019b. ISSN 0044-7447, 1654-7209. doi: 10.1007/s13280-019-01235-5. URL <http://link.springer.com/10.1007/s13280-019-01235-5>.

Markus Meier, Ralf Doescher, Andrew C. Coward, Jonas Nycander, and Kristofer Döös. *RCO – Rossby Centre regional Ocean climate model: model description (version 1.0) and first results from the hindcast period 1992/93*. SMHI, 1999. URL <https://urn.kb.se/resolve?urn=urn:nbn:se:smhi:diva-2664>.

Markus Meier, Christian Dieterich, Matthias Gröger, Cyril Dutheil, Florian Börgel, Kseniia Safonova, Ole Christensen, and Erik Kjellström. Oceanographic regional climate projections for the Baltic Sea until 2100. *Earth System Dynamics*, 13, January 2022. doi: 10.5194/esd-13-159-2022.

Markus H. E. Meier. Modeling the pathways and ages of inflowing salt- and freshwater in the Baltic Sea. *Estuarine, Coastal and Shelf Science*, 74(4):610–627, September 2007. ISSN 0272-7714. doi: 10.1016/j.ecss.2007.05.019. URL <https://www.sciencedirect.com/science/article/pii/S0272771407001631>.

Markus H. E. Meier, R. Feistel, J. Piechura, L. Arneborg, H. Burchard, V. Fiekas, N. Golenko, N. Kuzmina, V. Mohrholz, C. Nohr, V. T. Paka, J. Sellschopp, A. Stips, and V. Zhurbas. Ventilation of the Baltic Sea deep water: A brief review of present knowledge from observations and models. *Oceanologia*, 48(S), 2006. ISSN 0078-3234. URL <http://agro.icm.edu.pl/agro/element/bwmeta1.element/agro-article-f768b204-36f3-4a43-8f84-4d65f64a1f5c>. Publisher: -.

Markus H. E. Meier, Leonie Barghorn, Florian Börgel, Matthias Gröger, Lev Naumov, and Hagen Radtke. Multidecadal climate variability dominated past trends in the water balance of the Baltic Sea watershed. *npj Climate and Atmospheric Science*, 6(1):1–9, June 2023. ISSN 2397-3722. doi: 10.1038/s41612-023-00380-9. URL <https://www.nature.com/articles/s41612-023-00380-9>. Number: 1 Publisher: Nature Publishing Group.

V. Mohrholz, M. Naumann, G. Nausch, S. Krüger, and U. Gräwe. Fresh oxygen for the Baltic Sea — An exceptional saline inflow after a decade of stagnation. *Journal of Marine Systems*, 148:152–166, August 2015. ISSN 0924-7963. doi: 10.1016/j.jmarsys.2015.03.005. URL <https://www.sciencedirect.com/science/article/pii/S0924796315000457>.

Volker Mohrholz. Major Baltic Inflow Statistics – Revised. *Frontiers in Marine Science*, 5, 2018. ISSN 2296-7745. URL <https://www.frontiersin.org/articles/10.3389/fmars.2018.00384>.

Henry T. Mullins, Joel B. Thompson, Kristin McDougall, and Thomas L. Vercoutere. Oxygen-minimum zone edge effects: Evidence from the central California coastal upwelling system. *Geology*, 13(7):491–494, July 1985. ISSN 0091-7613. doi: 10.1130/0091-7613(1985)13<491:OZEEEF>2.0.CO;2. URL [https://doi.org/10.1130/0091-7613\(1985\)13<491:OZEEEF>2.0.CO;2](https://doi.org/10.1130/0091-7613(1985)13<491:OZEEEF>2.0.CO;2).

Jukka-Pekka Myllykangas, Tom Jilbert, Gunnar Jakobs, Gregor Rehder, Jan Werner, and Susanna Hietanen. Effects of the 2014 major Baltic inflow on methane and nitrous oxide dynamics in the water

column of the central Baltic Sea. *Earth System Dynamics*, 8(3):817–826, September 2017. ISSN 2190-4979. doi: 10.5194/esd-8-817-2017. URL <https://esd.copernicus.org/articles/8/817/2017/>. Publisher: Copernicus GmbH.

Alain Ménesguen, Philippe Cugier, and Isabelle Leblond. A new numerical technique for tracking chemical species in a multi-source, coastal ecosystem, applied to nitrogen causing *Ulva* blooms in the Bay of Brest (France). *Limnology and Oceanography*, 51(1part2): 591–601, 2006. ISSN 1939-5590. doi: 10.4319/lo.2006.51.1_part_2.0591. URL https://onlinelibrary.wiley.com/doi/abs/10.4319/lo.2006.51.1_part_2.0591. _eprint: https://onlinelibrary.wiley.com/doi/pdf/10.4319/lo.2006.51.1_part_2.0591.

Lev Naumov, H. E. Markus Meier, and Thomas Neumann. Dynamics of oxygen sources and sinks in the Baltic Sea under different nutrient inputs. *Frontiers in Marine Science*, 10, 2023a. ISSN 2296-7745. URL <https://www.frontiersin.org/articles/10.3389/fmars.2023.1233324>.

Lev Naumov, Thomas Neumann, Hagen Radtke, and H. E. Markus Meier. Limited ventilation of the central Baltic Sea due to elevated oxygen consumption. *Frontiers in Marine Science*, 10, 2023b. ISSN 2296-7745. URL <https://www.frontiersin.org/articles/10.3389/fmars.2023.1175643>.

Thomas Neumann. Climate-change effects on the Baltic Sea ecosystem: A model study. *Journal of Marine Systems*, 81(3):213–224, May 2010. ISSN 0924-7963. doi: 10.1016/j.jmarsys.2009.12.001. URL <https://www.sciencedirect.com/science/article/pii/S092479630900339x>.

Thomas Neumann, Wolfgang Fennel, and Christine Kremp. Experimental simulations with an ecosystem model of the Baltic Sea: A nutrient load reduction experiment. *Global Biogeochemical Cycles*, 16(3):7–1–7–19, 2002. ISSN 1944-9224. doi: 10.1029/2001GB001450. URL <https://onlinelibrary.wiley.com/doi/abs/10.1029/2001GB001450>. _eprint: <https://onlinelibrary.wiley.com/doi/pdf/10.1029/2001GB001450>.

Thomas Neumann, Hagen Radtke, and Torsten Seifert. On the importance of Major Baltic Inflows for oxygenation of the central Baltic Sea: IMPORTANCE OF MAJOR BALTIC INFLOWS. *Journal of Geophysical Research: Oceans*, 122(2):1090–1101, February 2017. ISSN 21699275. doi: 10.1002/2016JC012525. URL <http://doi.wiley.com/10.1002/2016JC012525>.

Thomas Neumann, Sampsa Koponen, Jenni Attila, Carsten Brockmann, Kari Kallio, Mikko Kervinen, Constant Mazeran, Dagmar Müller, Petra Philipson, Susanne Thulin, Sakari Väkevä, and Pasi Ylöstalo. Optical model for the Baltic Sea with an explicit CDOM state variable: a case study with Model ER-GOM (version 1.2). *Geoscientific Model Development*, 14(8):5049–5062, August 2021. ISSN 1991-959X. doi: 10.5194/gmd-14-5049-2021. URL <https://gmd.copernicus.org/articles/14/5049/2021/>. Publisher: Copernicus GmbH.

Thomas Neumann, Hagen Radtke, Bronwyn Cahill, Martin Schmidt, and Gregor Rehder. Non-Redfieldian carbon model for the Baltic Sea (ERGOM version 1.2) – implementation and budget estimates. *Geoscientific Model Development*, 15(22):8473–8540, November 2022. ISSN 1991-959X. doi: 10.5194/gmd-15-8473-2022. URL <https://gmd.copernicus.org/articles/15/8473/2022/>. Publisher: Copernicus GmbH.

Morten Holtegaard Nielsen. The baroclinic surface currents in the Kattegat. *Journal of Marine Systems*, 55(3):97–121, April 2005. ISSN 0924-7963. doi: 10.1016/j.jmarsys.2004.08.004. URL <https://www.sciencedirect.com/science/article/pii/S0924796304002921>.

A Nissling and L Westin. Salinity requirements for successful spawning of Baltic and Belt Sea cod and the potential for cod stock interactions in the Baltic Sea. *Marine Ecology Progress Series*, 152:261–271, June 1997. ISSN 0171-8630, 1616-1599. doi: 10.3354/meps152261. URL <https://www.int-res.com/abstracts/meps/v152/p261-271/>.

Anders Omstedt and Leif Nyberg. Response of Baltic Sea ice to seasonal, interannual forcing and climate change. *Tellus A*, 48(5):644–662, 1996. ISSN 1600-0870. doi: 10.1034/j.1600-0870.1996.t01-4-00004.x. URL <https://onlinelibrary.wiley.com/doi/abs/10.1034/j.1600-0870.1996.t01-4-00004.x>. _eprint: <https://onlinelibrary.wiley.com/doi/pdf/10.1034/j.1600-0870.1996.t01-4-00004.x>.

A. Paulmier and D. Ruiz-Pino. Oxygen minimum zones (OMZs) in the modern ocean. *Progress in Oceanography*, 80(3):113–128, March 2009. ISSN 0079-6611. doi: 10.1016/j.pocean.2008.08.001. URL <https://www.sciencedirect.com/science/article/pii/S0079661108001468>.

Fl. Bo Pedersen. The Sensitivity of the Baltic Sea to Natural and Man-Made Impact. In Jacques C. J. Nihoul, editor, *Elsevier Oceanography Series*, volume 34 of *Hydrodynamics of Semi-Enclosed Seas*, pages 385–397. Elsevier, January 1982. doi: 10.1016/S0422-9894(08)71251-0. URL <https://www.sciencedirect.com/science/article/pii/S0422989408712510>.

Ariel K. Pezner, Travis A. Courtney, Hannah C. Barkley, Wen-Chen Chou, Hui-Chuan Chu, Samantha M. Clements, Tyler Cyronak, Michael D. DeGrandpre, Samuel A. H. Kekuewa, David I. Kline, Yi-Bei Liang, Todd R. Martz, Satoshi Mitarai, Heather N. Page, Max S. Rintoul, Jennifer E. Smith, Keryea Soong, Yuichiro Takeshita, Martin Tresguerres, Yi Wei, Kimberly K. Yates, and Andreas J. Andersson. Increasing hypoxia on global coral reefs under ocean warming. *Nature Climate Change*, 13(4):403–409, April 2023. ISSN 1758-6798. doi: 10.1038/s41558-023-01619-2. URL <https://www.nature.com/articles/s41558-023-01619-2>. Number: 4 Publisher: Nature Publishing Group.

Manja Placke, H. E. Markus Meier, Ulf Gräwe, Thomas Neumann, Claudia Frauen, and Ye Liu. Long-Term Mean Circulation of the Baltic Sea as Represented by Various Ocean Circulation Models. *Frontiers in Marine Science*, 5, 2018. ISSN 2296-7745. URL <https://www.frontiersin.org/articles/10.3389/fmars.2018.00287>.

Joanna Pociask-Karteczka. River Hydrology and the North Atlantic Oscillation: A General Review. *Ambio*, 35(6):312–314, 2006. ISSN 0044-7447. URL <https://www.jstor.org/stable/4315743>. Publisher: [Springer, Royal Swedish Academy of Sciences].

Lucie Pokorná and Radan Huth. Climate impacts of the NAO are sensitive to how the NAO is defined. *Theoretical and Applied Climatology*, 119(3):639–652, February 2015. ISSN 1434-4483. doi: 10.1007/s00704-014-1116-0. URL <https://doi.org/10.1007/s00704-014-1116-0>.

H. Radtke, T. Neumann, M. Voss, and W. Fennel. Modeling pathways of riverine nitrogen and phosphorus in the Baltic Sea. *Journal of Geophysical Research: Oceans*, 117(C9), 2012. ISSN 2156-2202. doi: 10.1029/2012JC008119. URL <https://onlinelibrary.wiley.com/doi/abs/10.1029/2012JC008119>. _eprint: <https://onlinelibrary.wiley.com/doi/pdf/10.1029/2012JC008119>.

Hagen Radtke, Marko Lipka, Dennis Bunke, Claudia Morys, Jana Woelfel, Bronwyn Cahill, Michael Böttcher, Stefan Forster, Thomas Leipe, Gregor Rehder, and Thomas Neumann. Ecological Regional Ocean Model with vertically resolved sediments (ERGOM SED 1.0): Coupling benthic and pelagic biogeochemistry of the south-western Baltic Sea. *Geoscientific Model Development*, 12:275–320, January 2019. doi: 10.5194/gmd-12-275-2019.

Hagen Radtke, Sandra-Esther Brunnabend, Ulf Gräwe, and H. E. Markus Meier. Investigating interdecadal salinity changes in the Baltic Sea in a 1850–2008 hindcast simulation. *Climate of the Past*, 16(4):1617–1642, August 2020. ISSN 1814-9324. doi: 10.5194/cp-16-1617-2020. URL <https://cp.copernicus.org/articles/16/1617/2020/>. Publisher: Copernicus GmbH.

A. C. Redfield. On the proportions of organic derivatives in sea water and their relation to the composition of plankton. *James Johnstone Memorial*, 176, 1934. URL https://hahana.soest.hawaii.edu/cmoreserver/summercourse/2012/documents/bronk_05-30-12/Redfield_1934.pdf.

Daniel C. Reed, Bo G. Gustafsson, and Caroline P. Slomp. Shelf-to-basin iron shuttling enhances vivianite formation in deep Baltic Sea sediments. *Earth and Planetary Science Letters*, 434:241–251, January 2016. ISSN 0012-821X. doi: 10.1016/j.epsl.2015.11.033. URL <https://www.sciencedirect.com/science/article/pii/S0012821X15007372>.

Carl Rolff, Jakob Walve, Ulf Larsson, and Ragnar Elmgren. How oxygen deficiency in the Baltic Sea proper has spread and worsened: The role of ammonium and hydrogen sulphide. *Ambio*, 51(11):2308–2324, November 2022. ISSN 1654-7209. doi: 10.1007/s13280-022-01738-8. URL <https://doi.org/10.1007/s13280-022-01738-8>.

Michael R. Roman, Stephen B. Brandt, Edward D. Houde, and James J. Pierson. Interactive Effects of Hypoxia and Temperature on Coastal Pelagic Zooplankton and Fish. *Frontiers in Marine Science*, 6, 2019. ISSN 2296-7745. URL <https://www.frontiersin.org/articles/10.3389/fmars.2019.00139>.

Paul E. Roundy. On the Interpretation of EOF Analysis of ENSO, Atmospheric Kelvin Waves, and the MJO. *Journal of Climate*, 28(3):1148–1165, February 2015. ISSN 0894-8755, 1520-0442. doi: 10.1175/JCLI-D-14-00398.1. URL <https://journals.ametsoc.org/view/journals/clim/28/3/jcli-d-14-00398.1.xml>. Publisher: American Meteorological Society Section: Journal of Climate.

A. Rutgersson, J. Jaagus, F. Schenk, and M. Stendel. Observed changes and variability of atmospheric parameters in the Baltic Sea region during the last 200 years. *Climate Research*, 61(2):177–190, September 2014. ISSN 0936-577X, 1616-1572. doi: 10.3354/cr01244. URL <https://www.int-res.com/abstracts/cr/v61/n2/p177-190/>.

Emil Rydin, Linda Kumblad, Fredrik Wulff, and Per Larsson. Remediation of a Eutrophic Bay in the Baltic Sea. *Environmental Science & Technology*, 51(8):4559–4566, April 2017. ISSN 0013-936X. doi: 10.1021/acs.est.6b06187. URL <https://doi.org/10.1021/acs.est.6b06187>. Publisher: American Chemical Society.

Cecilia Rönnerberg and Erik Bonsdorff. Baltic Sea eutrophication: area-specific ecological consequences. *Hydrobiologia*, 514(1):227–241, February 2004. ISSN 1573-5117. doi: 10.1023/B:HYDR.0000019238.84989.7f. URL <https://doi.org/10.1023/B:HYDR.0000019238.84989.7f>.

Madleine Samuelsson and Anders Stigebrandt. Main characteristics of the long-term sea level variability in the Baltic sea. *Tellus A*, 48(5):672–683, 1996. ISSN 1600-0870. doi: 10.1034/j.1600-0870.1996.t01-4-00006.x. URL <https://onlinelibrary.wiley.com/doi/abs/10.1034/j.1600-0870.1996.t01-4-00006.x>. _eprint: <https://onlinelibrary.wiley.com/doi/pdf/10.1034/j.1600-0870.1996.t01-4-00006.x>.

C. Sanz-Lázaro, T. Valdemarsen, and M. Holmer. Effects of temperature and organic pollution on nutrient cycling in marine sediments. *Biogeosciences*, 12(15):4565–4575, August 2015. ISSN 1726-4170. doi: 10.5194/bg-12-4565-2015. URL <https://bg.copernicus.org/articles/12/4565/2015/>. Publisher: Copernicus GmbH.

Sofia Saraiva, H. E. Markus Meier, Helén Andersson, Anders Höglund, Christian Dieterich, Matthias Gröger, Robinson Hordoir, and Kari Eilola. Baltic Sea ecosystem response to various nutrient load scenarios in present and future climates. *Climate Dynamics*, 52(5):3369–3387, March 2019. ISSN 1432-0894. doi: 10.1007/s00382-018-4330-0. URL <https://doi.org/10.1007/s00382-018-4330-0>.

Jorge L. Sarmiento, Timothy D. Herbert, and J. R. Toggweiler. Causes of anoxia in the world ocean. *Global Biogeochemical Cycles*, 2(2):115–128, 1988. ISSN 1944-9224. doi: 10.1029/GB002i002p00115. URL <https://onlinelibrary.wiley.com/doi/abs/10.1029/GB002i002p00115>. _eprint: <https://onlinelibrary.wiley.com/doi/pdf/10.1029/GB002i002p00115>.

O. P. Savchuk, B. G. Gustafsson, and B. Müller-Karulis. Baltsem - a marine model for decision support within the baltic sea region. Retrieved from *Stockholm University website*, 2012. URL <https://urn.kb.se/resolve?urn=urn:nbn:se:su:diva-197187>.

Oleg P. Savchuk. Large-Scale Dynamics of Hypoxia in the Baltic Sea. In Evgeniy V. Yakushev, editor, *Chemical Structure of Pelagic Redox Interfaces: Observation and Modeling*, The Handbook of Environmental Chemistry, pages 137–160. Springer, Berlin, Heidelberg, 2013. ISBN 978-3-642-32125-2. doi: 10.1007/698_2010_53. URL https://doi.org/10.1007/698_2010_53.

Oleg P. Savchuk. Large-Scale Nutrient Dynamics in the Baltic Sea, 1970–2016. *Frontiers in Marine Science*, 5, 2018. ISSN 2296-7745. URL <https://www.frontiersin.org/articles/10.3389/fmars.2018.00095>.

Semjon Schimanke and H. E. Markus Meier. Decadal-to-centennial variability of salinity in the baltic sea. *Journal of Climate*, 29(20):7173 – 7188, 2016. doi: <https://doi.org/10.1175/JCLI-D-15-0443.1>. URL <https://journals.ametsoc.org/view/journals/clim/29/20/jcli-d-15-0443.1.xml>.

Holger Schinke and Wolfgang Matthäus. On the causes of major Baltic inflows —an analysis of long time series. *Continental Shelf Research*, 18(1):67–97, April 1998. ISSN 0278-4343. doi: 10.1016/S0278-4343(97)00071-X. URL <https://www.sciencedirect.com/science/article/pii/S027843439700071X>.

Sunke Schmidt, Lothar Stramma, and Martin Visbeck. Decline in global oceanic oxygen content during the past five decades. *Nature*, 542(7641):335–339, February 2017. ISSN 1476-4687. doi: 10.1038/nature21399. URL <https://www.nature.com/articles/nature21399>. Number: 7641 Publisher: Nature Publishing Group.

B. Schneider and S. Otto. Organic matter mineralization in the deep water of the Gotland Basin (Baltic Sea): Rates and oxidant demand. *Journal of Marine Systems*, 195:20–29, July 2019. ISSN 0924-7963. doi: 10.1016/j.jmarsys.2019.03.006. URL <https://www.sciencedirect.com/science/article/pii/S092479631830318X>.

B Schneider, G Nausch, H Kubsch, and I Petersohn. Accumulation of total CO₂ during stagnation in the Baltic Sea deep water and its relationship to nutrient and oxygen concentrations. *Marine Chemistry*, 77(4):277–291, March 2002. ISSN 0304-4203. doi: 10.1016/S0304-4203(02)00008-7. URL <https://www.sciencedirect.com/science/article/pii/S0304420302000087>.

Heide N. Schulz-Vogt, Falk Pollehne, Klaus Jürgens, Helge W. Arz, Sara Beier, Rainer Bahlo, Olaf Dellwig, Jan V. Henkel, Daniel P. R. Herlemann, Siegfried Krüger, Thomas Leipe, and Thomas Schott. Effect of large magnetotactic bacteria with polyphosphate inclusions on the phosphate profile of the suboxic zone in the Black Sea. *The ISME Journal*, 13(5):1198–1208, May 2019. ISSN 1751-7362, 1751-7370. doi: 10.1038/s41396-018-0315-6. URL <http://www.nature.com/articles/s41396-018-0315-6>.

Mohamed Shaltout and Anders Omstedt. Recent sea surface temperature trends and future scenarios for the Mediterranean Sea. *Oceanologia*, 56(3):411–443, June 2014. ISSN 0078-3234. doi: 10.5697/oc.56-3.411. URL <https://www.sciencedirect.com/science/article/pii/S0078323414500243>.

G. Simpson. Modelling seasonal data with gams. 2014. URL "<https://www.fromthebottomoftheheap.net/2014/05/09/modelling-seasonal-data-with-gam/>". last access: 28 August 2023.

Pauline Snoeijs-Leijonmalm and Elinor Andrén. Why is the Baltic Sea so special to live in? In Pauline Snoeijs-Leijonmalm, Hendrik Schubert, and Teresa Radziejewska, editors, *Biological Oceanography of the Baltic Sea*, pages 23–84. Springer Netherlands, Dordrecht, 2017. ISBN 978-94-007-0668-2. doi: 10.1007/978-94-007-0668-2_2. URL https://doi.org/10.1007/978-94-007-0668-2_2.

A. Stigebrandt. Physical Oceanography of the Baltic Sea. In Fredrik V. Wulff, Lars A. Rahm, and Per Larsson, editors, *A Systems Analysis of the Baltic Sea*, Ecological Studies, pages 19–74. Springer, Berlin, Heidelberg, 2001. ISBN 978-3-662-04453-7. doi: 10.1007/978-3-662-04453-7_2. URL https://doi.org/10.1007/978-3-662-04453-7_2.

Anders Stigebrandt and Bo G Gustafsson. Response of the Baltic Sea to climate change—theory and observations. *Journal of Sea Research*, 49(4):243–256, June 2003. ISSN 1385-1101. doi:

10.1016/S1385-1101(03)00021-2. URL <https://www.sciencedirect.com/science/article/pii/S1385110103000212>.

Malgorzata Stramska and Jagoda Białogrodzka. Spatial and temporal variability of sea surface temperature in the Baltic Sea based on 32-years (1982–2013) of satellite data. *Oceanologia*, 57(3):223–235, July 2015. ISSN 0078-3234. doi: 10.1016/j.oceano.2015.04.004. URL <https://www.sciencedirect.com/science/article/pii/S0078323415000718>.

L. M. Svendsen and B. Gustafsson. Waterborne nitrogen and phosphorus inputs and water flow to the baltic sea 1995-2018. *HELCOM Baltic Sea Environmental Fact Sheet*, 2020. URL <https://helcom.fi/media/documents/BSEFS-Waterborne-nitrogen-and-phosphorus-inputs-and-water-flow-to-the-Baltic-Sea.pdf>. Accessed 28 August 2023.

Jeremy M. Testa and W. Michael Kemp. Spatial and Temporal Patterns of Winter-Spring Oxygen Depletion in Chesapeake Bay Bottom Water. *Estuaries and Coasts*, 37(6):1432–1448, 2014. ISSN 1559-2723. URL <https://www.jstor.org/stable/44851217>. Publisher: [Coastal and Estuarine Research Federation, Springer].

Jeremy M. Testa, J. Blake Clark, William C. Dennison, E. Caroline Donovan, Alexander W. Fisher, Wenfei Ni, Matthew Parker, Donald Scavia, Suzanne E. Spitzer, Anthony M. Waldrop, Vanessa M.D. Vargas, and Gregory Ziegler. Ecological Forecasting and the Science of Hypoxia in Chesapeake Bay. *BioScience*, 67(7):614–626, July 2017. ISSN 0006-3568. doi: 10.1093/biosci/bix048. URL <https://doi.org/10.1093/biosci/bix048>.

Helmuth Thomas, Janusz Pempkowiak, Fred Wulff, and Klaus Nagel. Autotrophy, nitrogen accumulation and nitrogen limitation in the Baltic Sea: A paradox or a buffer for eutrophication? *Geophysical Research Letters*, 30(21), 2003. ISSN 1944-8007. doi: 10.1029/2003GL017937. URL <https://onlinelibrary.wiley.com/doi/abs/10.1029/2003GL017937>. _eprint: <https://onlinelibrary.wiley.com/doi/pdf/10.1029/2003GL017937>.

Ricardo M. Trigo, Timothy J. Osborn, and João M. Corte-Real. The North Atlantic Oscillation influence on Europe: climate impacts and associated physical mechanisms. *Climate Research*, 20(1):9–17, February 2002. ISSN 0936-577X, 1616-1572. doi: 10.3354/cr020009. URL <https://www.int-res.com/abstracts/cr/v20/n1/p9-17/>.

Emil Vahtera, Daniel J. Conley, Bo G. Gustafsson, Harri Kuosa, Heikki Pitkänen, Oleg P. Savchuk, Timo Tamminen, Markku Viitasalo, Maren Voss, Norbert Wasmund, and Fredrik Wulff. Internal Ecosystem Feedbacks Enhance Nitrogen-fixing Cyanobacteria Blooms and Complicate Management in the Baltic Sea. *AMBIO: A Journal of the Human Environment*, 36(2):186–194, April 2007. ISSN 0044-7447, 1654-7209. doi: 10.1579/0044-7447(2007)36[186:IEFENC]2.0.CO;2. URL [https://bioone.org/journals/ambio-a-journal-of-the-human-environment/volume-36/issue-2/0044-7447_2007_36_186_IEFENC_2.0.CO_2/Internal-Ecosystem-Feedbacks-Enhance-Nitrogen-fixing-Cyanobacteria-Blooms-and-Complicate/10.1579/0044-7447\(2007\)36\[186:IEFENC\]2.0.CO;2.full](https://bioone.org/journals/ambio-a-journal-of-the-human-environment/volume-36/issue-2/0044-7447_2007_36_186_IEFENC_2.0.CO_2/Internal-Ecosystem-Feedbacks-Enhance-Nitrogen-fixing-Cyanobacteria-Blooms-and-Complicate/). Publisher: Royal Swedish Academy of Sciences.

- Niels A. G. M. van Helmond, Tom Jilbert, and Caroline P. Slomp. Hypoxia in the Holocene Baltic Sea: Comparing modern versus past intervals using sedimentary trace metals. *Chemical Geology*, 493: 478–490, August 2018. ISSN 0009-2541. doi: 10.1016/j.chemgeo.2018.06.028. URL <https://www.sciencedirect.com/science/article/pii/S0009254118303309>.
- Edward J. Van Liere and J. Clifford Stickney. Hypoxia. *Academic Medicine*, 39(5):526, May 1964. ISSN 1040-2446. URL <https://journals.lww.com/academicmedicine/citation/1964/05000/hypoxia.27.aspx>.
- Timo Vihma and Jari Haapala. Geophysics of sea ice in the Baltic Sea: A review. *Progress in Oceanography*, 80(3-4):129–148, March 2009. ISSN 0079-6611. doi: 10.1016/j.pocean.2009.02.002. URL <https://www.sciencedirect.com/science/article/pii/S0079661109000123>. Publisher: Pergamon.
- Markku Viitasalo and Erik Bonsdorff. Global climate change and the Baltic Sea ecosystem: direct and indirect effects on species, communities and ecosystem functioning. *Earth System Dynamics*, 13(2):711–747, April 2022. ISSN 2190-4979. doi: 10.5194/esd-13-711-2022. URL <https://esd.copernicus.org/articles/13/711/2022/>. Publisher: Copernicus GmbH.
- Maren Voss, Joachim W. Dippner, Christoph Humborg, Jens Hürdler, Frederike Korth, T. Neumann, Gerald Schernewski, and Markus Venohr. History and scenarios of future development of Baltic Sea eutrophication. *Estuarine, Coastal and Shelf Science*, 92(3):307–322, May 2011. ISSN 0272-7714. doi: 10.1016/j.ecss.2010.12.037. URL <https://www.sciencedirect.com/science/article/pii/S0272771411000023>.
- Maren Voss, Hermann W. Bange, Joachim W. Dippner, Jack J. Middelburg, Joseph P. Montoya, and Bess Ward. The marine nitrogen cycle: recent discoveries, uncertainties and the potential relevance of climate change. *Philosophical Transactions of the Royal Society B: Biological Sciences*, 368(1621):20130121, July 2013. doi: 10.1098/rstb.2013.0121. URL <https://royalsocietypublishing.org/doi/10.1098/rstb.2013.0121>. Publisher: Royal Society.
- Ippo Vuorinen, Jari Hänninen, Marjut Rajasilta, Päivi Laine, Jan Eklund, Federico Montesino-Pouzols, Francesco Corona, Karin Junker, H. E. Markus Meier, and Joachim W. Dippner. Scenario simulations of future salinity and ecological consequences in the Baltic Sea and adjacent North Sea areas-implications for environmental monitoring. *Ecological Indicators*, 50:196–205, March 2015. ISSN 1470-160X. doi: 10.1016/j.ecolind.2014.10.019.
- Germo Väli, H. E. Markus Meier, and Jüri Elken. Simulated halocline variability in the Baltic Sea and its impact on hypoxia during 1961-2007: SIMULATED HALOCLINE VARIABILITY IN THE BALTIC SEA. *Journal of Geophysical Research: Oceans*, 118(12):6982–7000, December 2013. ISSN 21699275. doi: 10.1002/2013JC009192. URL <http://doi.wiley.com/10.1002/2013JC009192>.
- Joe H. Ward. Hierarchical Grouping to Optimize an Objective Function. *Journal of the American Statistical Association*, 58(301):236–244, 1963. ISSN 0162-1459. doi: 10.2307/2282967. URL <https://www.jstor.org/stable/2282967>. Publisher: [American Statistical Association, Taylor & Francis, Ltd.].

Andrew J. Watson. Oceans on the edge of anoxia. *Science*, 354(6319):1529–1530, December 2016. doi: 10.1126/science.aaj2321. URL <https://www.science.org/doi/full/10.1126/science.aaj2321>. Publisher: American Association for the Advancement of Science.

Michael M. Whitney. Observed and projected global warming pressure on coastal hypoxia. *Biogeosciences*, 19(18):4479–4497, September 2022. ISSN 1726-4170. doi: 10.5194/bg-19-4479-2022. URL <https://bg.copernicus.org/articles/19/4479/2022/>.

P. J. le B. Williams and C. Askew. A method of measuring the mineralization by micro-organisms of organic compounds in sea-water. *Deep Sea Research and Oceanographic Abstracts*, 15(3):365–375, June 1968. ISSN 0011-7471. doi: 10.1016/0011-7471(68)90012-0. URL <https://www.sciencedirect.com/science/article/pii/0011747168900120>.

Qiong Wu, Rongzhong Ye, Scott D. Bridgham, and Qusheng Jin. Limitations of the q_{10} coefficient for quantifying temperature sensitivity of anaerobic organic matter decomposition: A modeling based assessment. *Journal of Geophysical Research: Biogeosciences*, 126(8):e2021JG006264, 2021. doi: <https://doi.org/10.1029/2021JG006264>. URL <https://agupubs.onlinelibrary.wiley.com/doi/abs/10.1029/2021JG006264>. e2021JG006264 2021JG006264.

Fredrik Wulff, Anders Stigebrandt, and Lars Rahm. Nutrient Dynamics of the Baltic Sea. *Ambio*, 19(3):126–133, 1990. ISSN 0044-7447. URL <https://www.jstor.org/stable/4313678>. Publisher: [Springer, Royal Swedish Academy of Sciences].

Ch. Wübber and W. Krauss. The two-dimensional seiches of the baltic sea. *Oceanologia Acta*, 2(4):435–446, 1979.

Fei Ye, Yinglong J. Zhang, Harry V. Wang, Marjorie A. M. Friedrichs, Isaac D. Irby, Eli Alteljevich, Arnaldo Valle-Levinson, Zhengui Wang, Hai Huang, Jian Shen, and Jiabi Du. A 3D unstructured-grid model for Chesapeake Bay: Importance of bathymetry. *Ocean Modelling*, 127:16–39, July 2018. ISSN 1463-5003. doi: 10.1016/j.ocemod.2018.05.002. URL <https://www.sciencedirect.com/science/article/pii/S1463500318301562>.

Tong Yindong, Xu Xiwen, Qi Miao, Sun Jingjing, Zhang Yiyan, Zhang Wei, Wang Mengzhu, Wang Xuejun, and Zhang Yang. Lake warming intensifies the seasonal pattern of internal nutrient cycling in the eutrophic lake and potential impacts on algal blooms. *Water Research*, 188:116570, January 2021. ISSN 0043-1354. doi: 10.1016/j.watres.2020.116570. URL <https://www.sciencedirect.com/science/article/pii/S0043135420311052>.

Shuping Zhang, Lichuan Wu, Johan Arnqvist, Christoffer Hallgren, and Anna Rutgersson. Mapping coastal upwelling in the Baltic Sea from 2002 to 2020 using remote sensing data. *International Journal of Applied Earth Observation and Geoinformation*, 114:103061, November 2022. ISSN 1569-8432. doi: 10.1016/j.jag.2022.103061. URL <https://www.sciencedirect.com/science/article/pii/S1569843222002497>.

Yuntao Zhou, Donald Scavia, and Anna M. Michalak. Nutrient loading and meteorological conditions explain interannual variability of hypoxia in Chesapeake Bay. *Limnology and Oceanography*, 59(2):373–384, March 2014. ISSN 00243590. doi: 10.4319/lo.2014.59.2.0373. URL <http://doi.wiley.com/10.4319/lo.2014.59.2.0373>.

A

Supplementary material

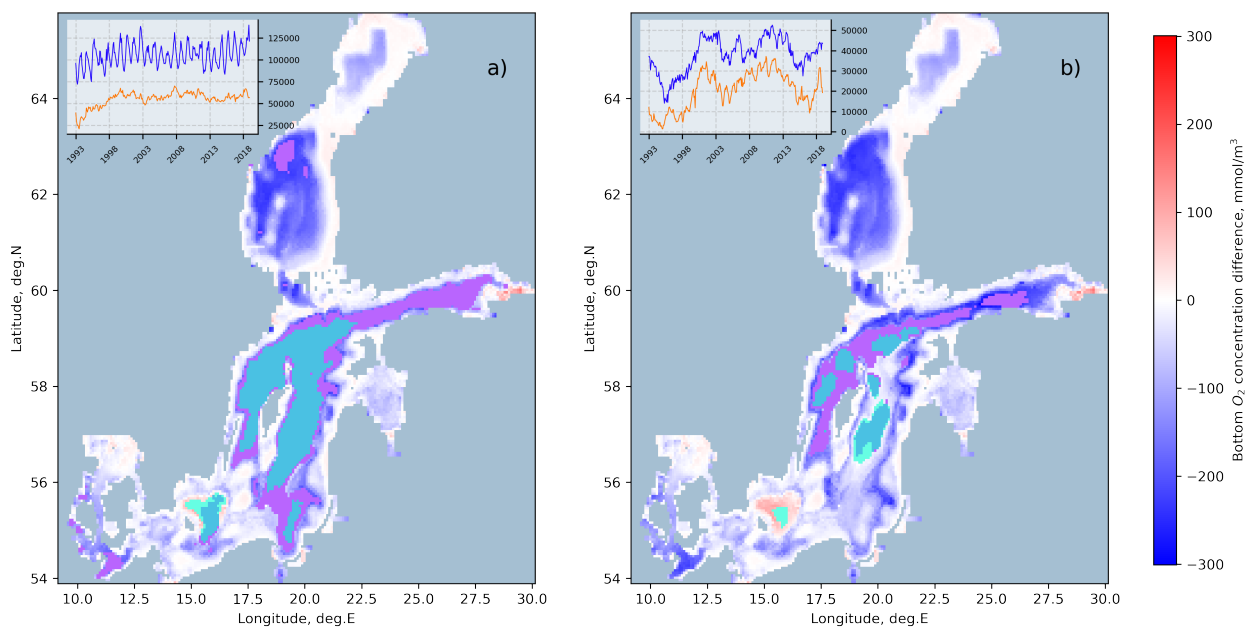


Figure A.1: Mean hypoxic (A) and anoxic (B) zones in the BS based on MOM-ERGOM (violet area), reanalysis (light turquoise area) data, and both of them (dark turquoise area). A grid cell is considered to be mean hypoxic/anoxic if it was hypoxic/anoxic for more than half of the considered period (1993-2018). Upper left plots depict total hypoxic (A) and anoxic (B) areas in km^2 according to reanalysis (orange) and MOM-ERGOM (blue) data (Naumov et al., 2023b).



Figure A.2: Estimated halocline depth (left panel) and halocline strength (right panel). The following abbreviations are used: BB – Bornholm Basin, BS – Bothnian Sea, wGB – western Gotland Basin, eGB – eastern Gotland Basin, nGB – northern Gotland Basin, GF – Gulf of Finland. The notable differences are observed between halocline strength in the Bornholm Basin (less strength in the model), Bothnian Sea (more strength in the model), and Gulf of Finland (more strength in the model) (Naumov et al., 2023b).

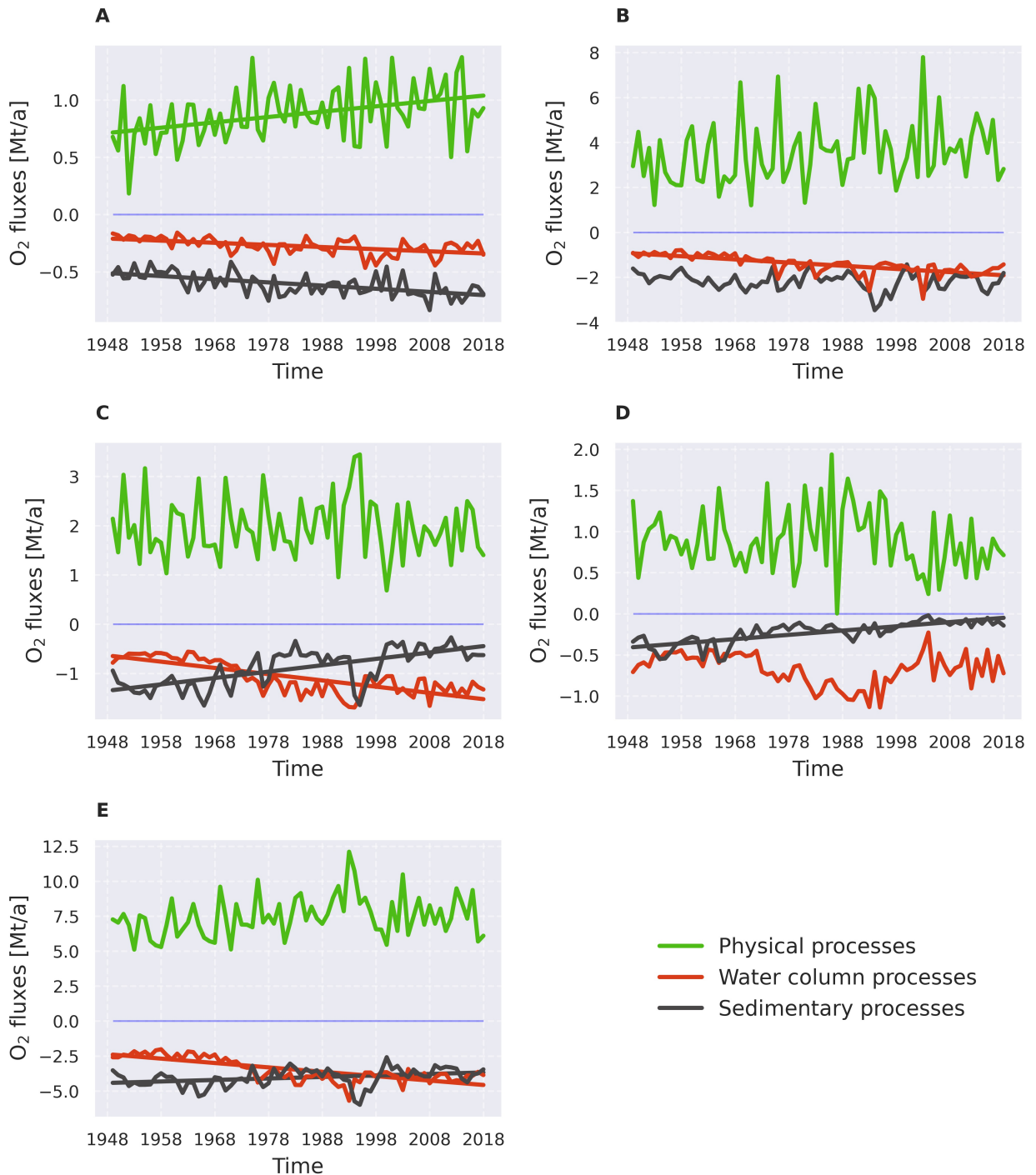


Figure A.3: Linear trends of groups of processes governing oxygen dynamics in the central BS (the Bornholm Basin (A), the eastern Gotland Basin (B), the northern Gotland Basin (C), the western Gotland Basin (D), and the whole central BS (E)). Groups of processes are identical to those in Figure 4.7. Trend lines are only shown if they are significant ($p < 0.05$). Mt/a stands for 10^9 kg per year (Naumov et al., 2023b).

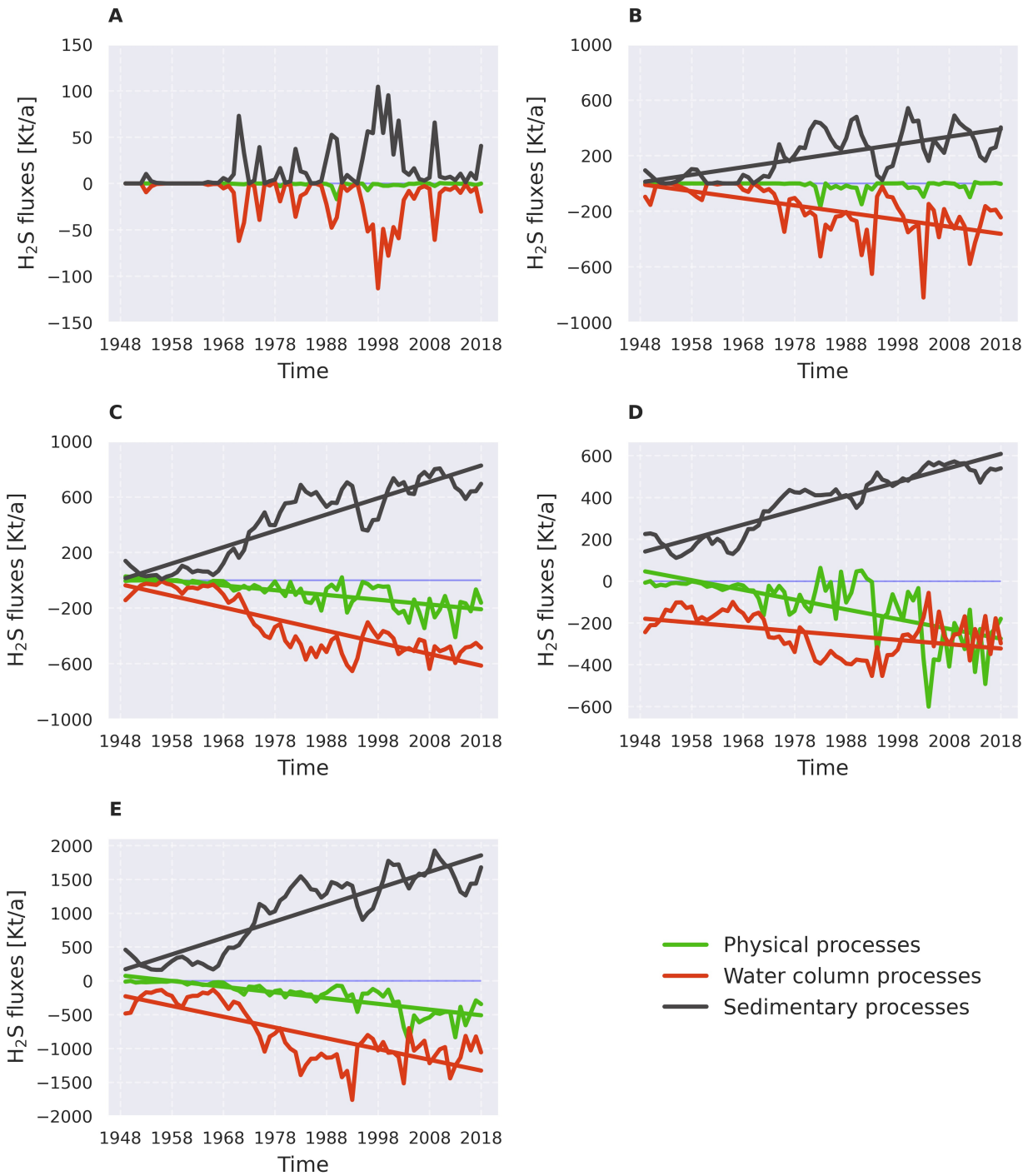


Figure A.4: As Figure A.2 but for H₂S. Kt/a stands for 10⁶ kg per year (Naumov et al., 2023b).

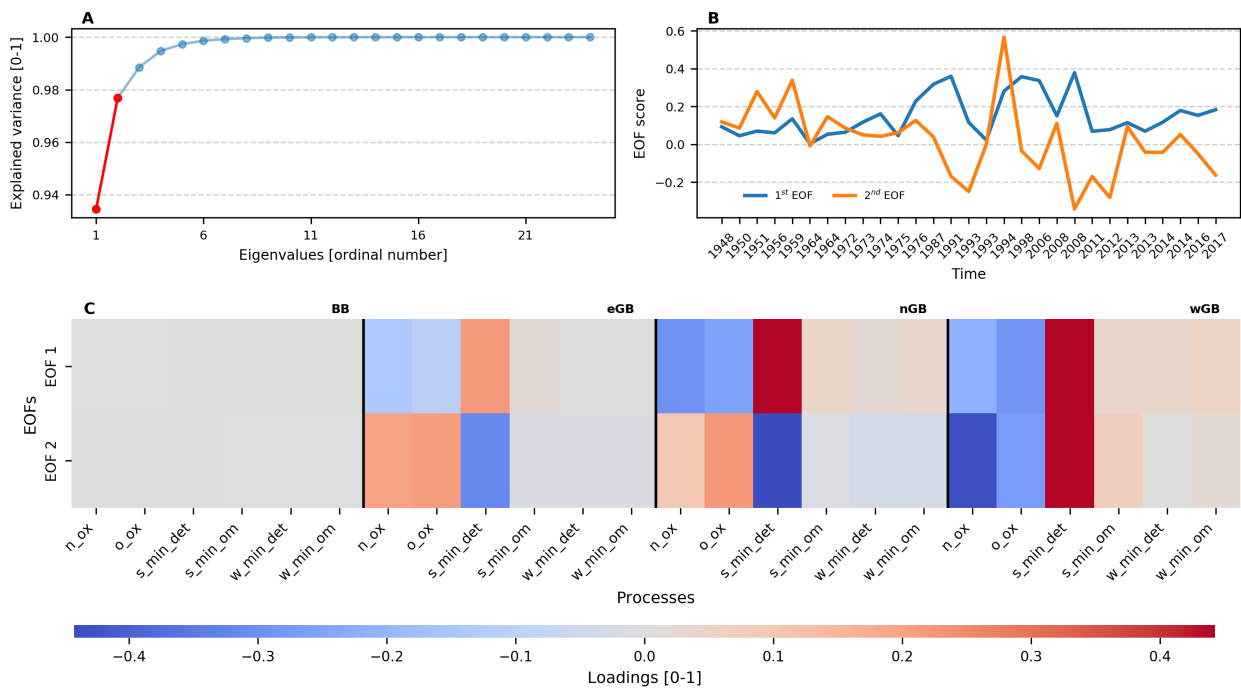


Figure A.5: Same as Figure 4.6 but for H₂S. Processes' names in Panel C are read the following way: {domain}_{process}. A domain can be w (water column) or s (sediments). Processes can be nit (nitrification) or min_om/det/sul (mineralization of OM without detritus, detritus, or H₂S). Processes n_ox and o_ox represent H₂S oxidation by NO₃⁻ and O₂, respectively (Naumov et al., 2023b).

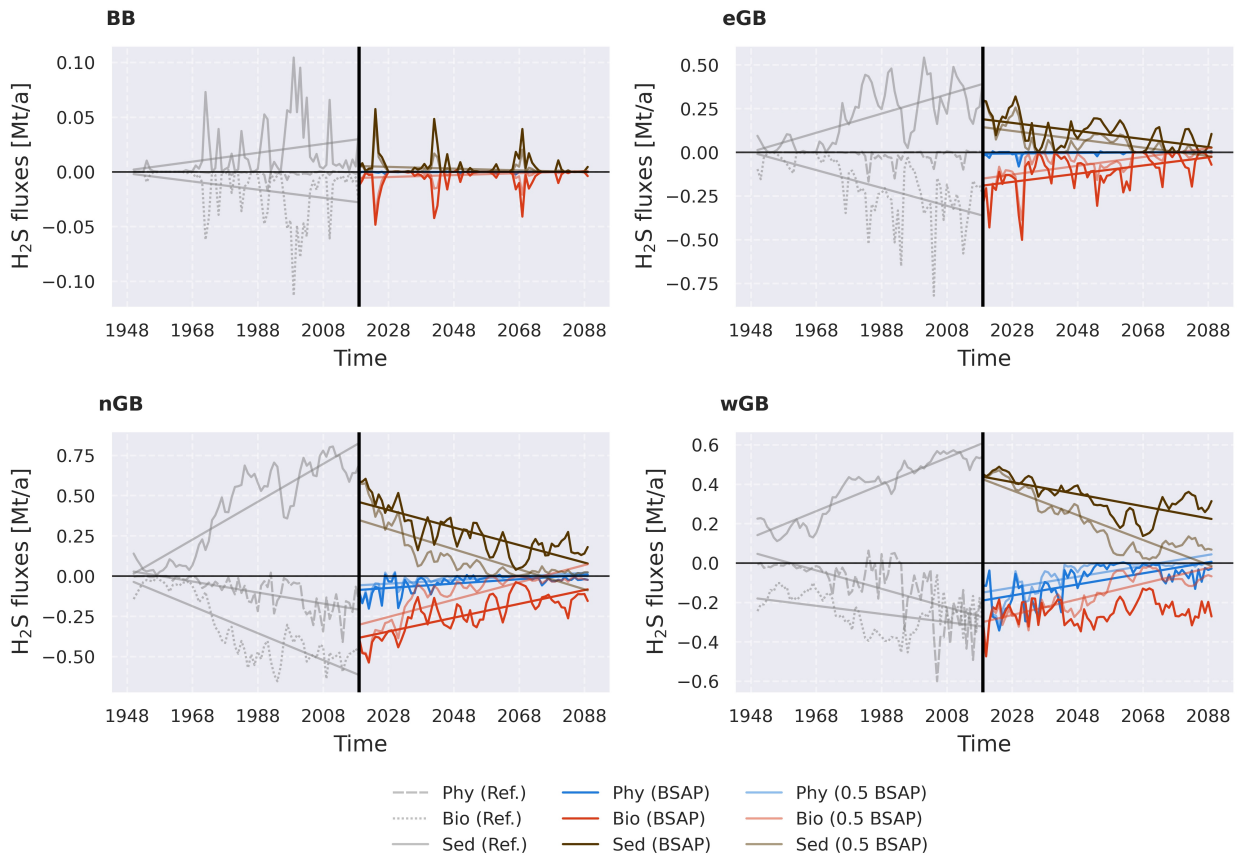


Figure A.6: Temporal variability of H₂S sources and sinks. Processes are aggregated into three groups: phy, bio, and sed. Each panel represents a specific sub-basin indicated in the upper left corner. Only significant trends (p-value < 0.05) are shown. Mt/a stands for 10⁹ kg per year (Naumov et al., 2023a).

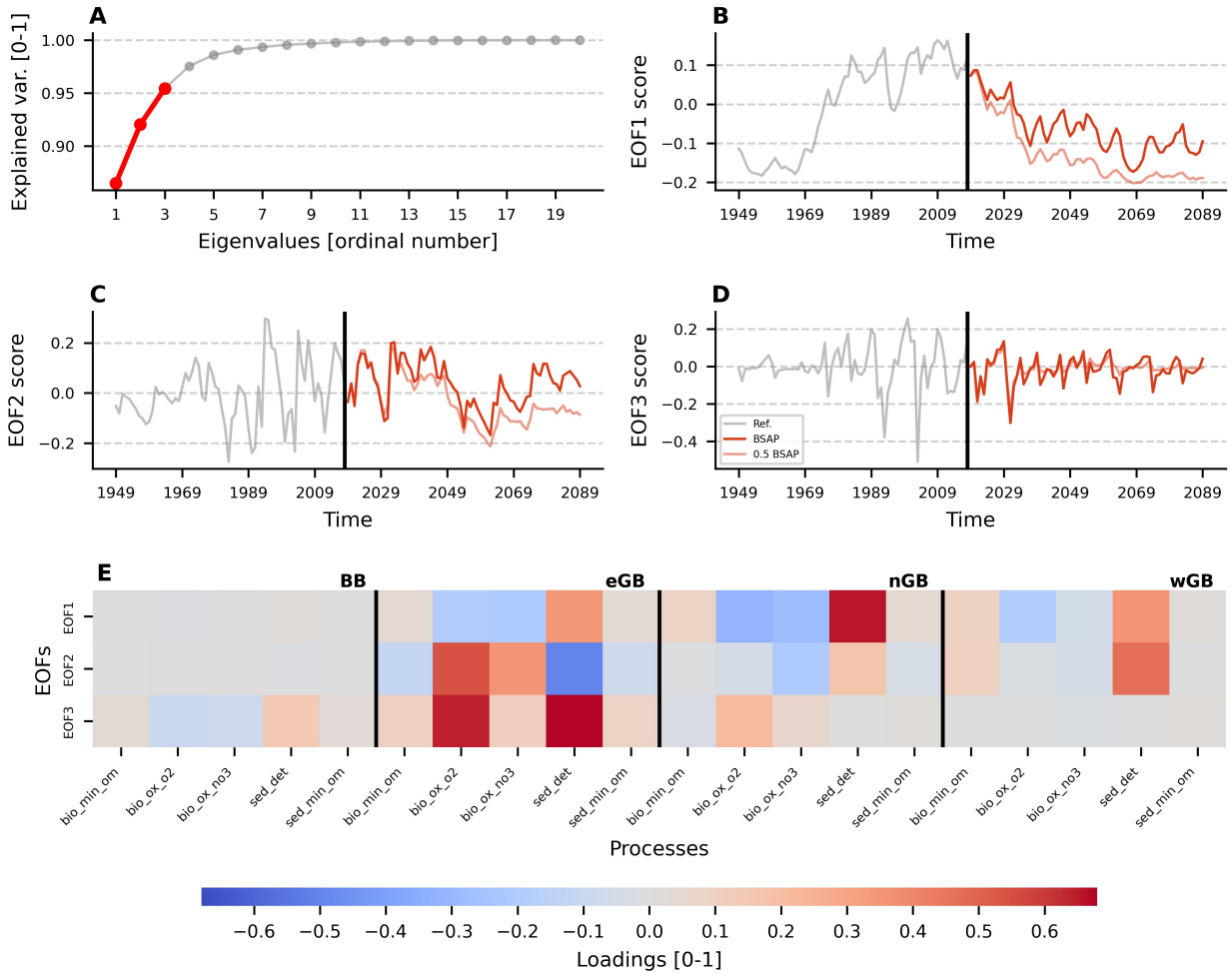


Figure A.7: EOF decomposition of the spatial-temporal matrix of H_2S consumption terms aggregated into specific groups. Panel A shows the explained variability by all calculated EOFs. Only the first three EOFs were considered significant and highlighted. Panels B-D display the temporal variability of three significant EOFs. Here, the black vertical line demarcates the reference scenario (grey curve) and sensitivity experiments (vivid and translucent red lines for BSAP and 0.5 BSAP scenarios, correspondingly). Panel E shows loadings of the significant EOFs. Loadings show the direction and magnitude of the connection between an EOF and a certain variable. Black lines highlight the spatial structure of the matrix, marking the sub-basins (Naumov et al., 2023a).

Table A.1: Processes supplying/consuming the most O₂ across the central Baltic Sea. Annual values are given in 10⁹ kg of O₂ (Mt). In some processes' names, information inside the parenthesis stands for a domain, i.e., sed. means sediments and w.col. means water column (Naumov et al., 2023b).

Bornholm Basin	
Advection, upper boundary	0.81 Mt O ₂
Mineralization of detritus (sed.)	-0.46 Mt O ₂
Nitrification (NH ₄ ⁺ to NO ₃ ⁻) (w.col.)	-0.11 Mt O ₂
Mineralization of POC (w.col.)	-0.08 Mt O ₂
Diffusion, upper boundary	0.08 Mt O ₂
Eastern Gotland Basin	
Advection, upper boundary	3.06 Mt O ₂
Advection, western boundary	2.14 Mt O ₂
Advection, northern boundary	-1.91 Mt O ₂
Mineralization of detritus (sed.)	-1.75 Mt O ₂
Nitrification (NH ₄ ⁺ to NO ₃ ⁻) (w.col.)	-0.57 Mt O ₂
Northern Gotland Basin	
Advection, southern boundary	1.91 Mt O ₂
Mineralization of detritus (sed.)	-0.74 Mt O ₂
Nitrification (NH ₄ ⁺ to NO ₃ ⁻) (w.col.)	-0.41 Mt O ₂
Oxidation of S to SO ₄ ²⁻ (w.col.)	-0.35 Mt O ₂
Advection, western boundary	-0.32 Mt O ₂
Western Gotland Basin	
Advection, upper boundary	0.46 Mt O ₂
Advection, eastern boundary	0.32 Mt O ₂
Oxidation of S to SO ₄ ²⁻ (w.col.)	-0.3 Mt O ₂
Nitrification (NH ₄ ⁺ to NO ₃ ⁻) (w.col.)	-0.21 Mt O ₂
Mineralization of detritus (sed.)	-0.19 Mt O ₂

Table A.2: Processes supplying/consuming the most H₂S across the central BS. Annual values are given in 10⁶ kg of H₂S (Kt). In some processes' names, information inside the parenthesis stands for a domain, i.e., sed. means sediments and w.col. means water column (Naumov et al., 2023b).

Bornholm Basin	
Mineralization of detritus (sed.)	13.4 Kt H ₂ S
Oxidation by O ₂ (w.col.)	-9.5 Kt H ₂ S
Oxidation by NO ₃ ⁻ (w.col.)	-8.57 Kt H ₂ S
Mineralization of POC (w.col.)	2.63 Kt H ₂ S
Mineralization of POC (sed.)	1.52 Kt H ₂ S
Eastern Gotland Basin	
Mineralization of detritus (sed.)	181 Kt H ₂ S
Oxidation by NO ₃ ⁻ (w.col.)	-113.26 Kt H ₂ S
Oxidation by O ₂ (w.col.)	-93.5 Kt H ₂ S
Advection, northern boundary	-13.1 Kt H ₂ S
Mineralization of POCN (sed.)	11 Kt H ₂ S
Northern Gotland Basin	
Mineralization of detritus (sed.)	387 Kt H ₂ S
Oxidation by NO ₃ ⁻ (w.col.)	-196 Kt H ₂ S
Oxidation by O ₂ (w.col.)	-175 Kt H ₂ S
Advection, upper boundary	-73.06 Kt H ₂ S
Advection, western boundary	-28.68 Kt H ₂ S
Western Gotland Basin	
Mineralization of detritus (sed.)	345 Kt H ₂ S
Oxidation by O ₂ (w.col.)	-175 Kt H ₂ S
Oxidation by NO ₃ ⁻ (w.col.)	-139 Kt H ₂ S
Advection, upper boundary	-132 Kt H ₂ S
Mineralization of POC (w.col.)	32 Kt H ₂ S

B

Curriculum Vitae

Lev Naumov, M.Sc.

✉ levnaumov96@gmail.com

🆔 0000-0002-2891-4766

📄 Lev Naumov

Citizenship: Russia

Location: Rostock, Germany

Employment

- 2018 – 2019 • **Engineer-Researcher** Russian State Hydrometeorological University.
As an engineer-researcher at RSHU, I carried out coupled 1D GOTM-ERSEM model simulations to reveal the influence of some benthic fauna on the benthic-pelagic fluxes of nutrients in the Gulf of Finland. I also carried out model validation and statistical analysis of the model output.
- 2018 – 2020 • **Engineer-Researcher** St. Petersburg State University.
As an engineer-researcher at SPBU, I estimated the quality of DT2018 satellite altimetry product by comparing it to the previous DT2014 product and observations. In addition, I studied thermohaline fluxes and mesoscale dynamics in the Lofoten Basin located in the Norwegian Sea.
- 2019 – 2020 • **Engineer-Researcher** St. Petersburg branch of the Shirshov Institute of Oceanology of Russian Academy of Sciences.
As an engineer-researcher at the St. Petersburg branch of the IO RAS, I conducted the statistical analysis of the regional climate model's output (more than 1 TB of data).
- 2020 – Present • **Research Scientist** Leibniz Institute for Baltic Sea Research Warnemünde.
As a research scientist at the IOW, I studied the oxygen dynamics in the Baltic Sea employing the coupled MOM-ERGOM model. I ran the model simulations, validated the model, conducted a statistical analysis of the model output, and modified the model.

Education

- 2014 – 2018 • **B.Sc. Applied Hydrometeorology with a focus on Applied Oceanography** in Russian State Hydrometeorological University.
Thesis title: Sea ice variability in the Kara Sea and its forecast (in Russian).
- 2018 – 2020 • **M.Sc. Operational Oceanography** in Russian State Hydrometeorological University.
Thesis title: Thermohaline advection in the Norwegian Sea and its influence on the mesoscale eddies dynamics in the Lofoten Basin region (in Russian).
- 2020 – Present • **Ph.D. Physical Oceanography** in Leibniz Institute for Baltic Sea Research Warnemünde; University of Rostock.
Thesis title: Dynamics of oxygen in coastal seas - the Baltic Sea example.

Research Publications

Journal Articles

- 1 H. E. M. Meier, L. Barghorn, F. Börgel, M. Gröger, **L. Naumov**, and H. Radtke, "Multidecadal climate variability dominated past trends in the water balance of the baltic sea watershed," *npj Climate and Atmospheric Science*, vol. 6, pp. 1–9, 2023. [DOI: 10.1038/s41612-023-00380-9](#).
- 2 **L. Naumov**, H. E. M. Meier, and T. Neumann, "Dynamics of oxygen sources and sinks in the baltic sea under different nutrient inputs," *Frontiers in Marine Science*, vol. 10, 2023, ISSN: 2296-7745. [DOI: 10.3389/fmars.2023.1233324](#).

- 3 **L. Naumov**, T. Neumann, H. Radtke, and H. E. M. Meier, "Limited ventilation of the central baltic sea due to elevated oxygen consumption," *Frontiers in Marine Science*, vol. 10, 2023, ISSN: 2296-7745. [DOI: 10.3389/fmars.2023.1175643](https://doi.org/10.3389/fmars.2023.1175643).
- 4 **L. Naumov**, S. Gordeeva, and T. Belonenko, "Quality assessment of a satellite altimetry data product DT18 in the norwegian sea: A comparison to tide gauge records and drifters data," *Advances in Space Research*, vol. 68, no. 2, 2021, ISSN: 0273-1177. [DOI: 10.1016/j.asr.2019.09.029](https://doi.org/10.1016/j.asr.2019.09.029).
- 5 **L. M. Naumov** and S. M. Gordeeva, "Lateral heat and salt transports in the lofoten basin: Comparison based on three databases (in Russian)," *Fundamental and Applied Hydrophysics*, vol. 13, no. 3, 2020, ISSN: 20736673. [DOI: 10.7868/S207366732003003X](https://doi.org/10.7868/S207366732003003X).
- 6 V. N. Malinin, S. M. Gordeeva, and **L. M. Naumov**, "Total precipitable water of the atmosphere as a climate forcing factor (in Russian)," *Sovremennye Problemy Distantionnogo Zondirovaniya Zemli iz Kosmosa*, vol. 15, no. 3, pp. 243–251, 2018, ISSN: 24110280 20707401. [DOI: 10.21046/2070-7401-2018-15-3-243-251](https://doi.org/10.21046/2070-7401-2018-15-3-243-251).
- 7 V. N. Malinin, S. M. Gordeeva, **L. M. Naumov**, A. A. Ershova, and A. S. Averkiev, "To the evaluation of trends in the components of ocean-atmosphere moisture exchange," *Fundamental and Applied Hydrophysics*, vol. 11, no. 4, 2018, ISSN: 20736673. [DOI: 10.7868/S2073667318040044](https://doi.org/10.7868/S2073667318040044).

Conference Proceedings

- 1 **L. Naumov**, T. Neumann, H. Radtke, and H. E. M. Meier, "Elevated oxygen consumption in the central baltic sea reduces ventilation," in *XXVIII General Assembly of the International Union of Geodesy and Geophysics (IUGG)*, Berlin, Germany, 2023. [DOI: 10.57757/iugg23-3478](https://doi.org/10.57757/iugg23-3478).
- 2 **L. Naumov**, T. Neumann, H. Radtke, and H. E. M. Meier, "Oxygen dynamics in the baltic sea: A budget," in *Proceedings of the 4th Baltic Earth Conference: Assessing the Baltic Sea Earth System*, Jastarnia, Poland, 2022, pp. 56–57.
- 3 **L. M. Naumov** and S. M. Gordeeva, "Advective fluxes of heat, mass, and salt in the lofoten vortex area based on the reanalyses data (in Russian)," in *Proceedings of the 5th Young Scientists Conference Complex Research of the World Ocean*, Kaliningrad, Russia, 2020, pp. 139–140.
- 4 **L. M. Naumov** and S. M. Gordeeva, "Statistical estimates of the vorticity at the lofoten basin borders (in Russian)," in *Proceedings of the 18th All-Russian Conference Current Problems in Remote Sensing of the Earth from Space*, Moscow, Russia, 2020, p. 168.
- 5 T. R. Eremina, **L. M. Naumov**, and A. V. Isaev, "Modeling of biogeochemical processes in the gulf of finland sediments using benthos module of the ersem model (in Russian)," in *Hydrometeorology and Ecology: Scientific Achievements and Perspectives of Development. Proceedings of the 3rd All-Russian Conference*, St. Petersburg, Russia, 2019, pp. 329–332.
- 6 **L. M. Naumov** and S. M. Gordeeva, "Fluxes of mass, salt, and heat through the lofoten basin (in Russian)," in *Proceedings of the 17th All-Russian Conference Current Problems in Remote Sensing of the Earth from Space*, Moscow, Russia, 2019, p. 313.
- 7 **L. M. Naumov** and S. M. Gordeeva, "Thermohaline advection in the lofoten vortex region (in Russian)," in *Hydrometeorology and Ecology: Scientific Achievements and Perspectives of Development. Proceedings of the 3rd All-Russian Conference*, St. Petersburg, Russia, 2019, pp. 642–646.
- 8 **L. M. Naumov**, S. M. Gordeeva, and T. V. Belonenko, "Statistical analysis of DT18 satellite altimetry product in the open ocean and coastal waters (in Russian)," in *Proceedings of the 17th All-Russian Conference Current Problems in Remote Sensing of the Earth from Space*, Moscow, Russia, 2019, p. 312.
- 9 **L. M. Naumov**, "External factors governing sea ice concentration in the Kara Sea (in Russian)," in *Proceedings of the 4th Young Scientists Conference Complex Research of the World Ocean*, St. Petersburg, Russia, 2018, pp. 287–288.

- 10 **L. M. Naumov**, S. M. Gordeeva, and T. V. Belonenko, "Verification of the DT18 satellite altimetry product in the polar region (in Russian)," in *Hydrometeorology and Ecology: Scientific Achievements and Perspectives of Development. Proceedings of the 2nd All-Russian Conference*, St. Petersburg, Russia, 2018, pp. 473–476.
- 11 V. N. Malinin, S. M. Gordeeva, and **L. M. Naumov**, "To the evaluation of trends in the components of ocean-atmosphere moisture exchange based on the satellite data (in Russian)," in *Proceedings of the 15th All-Russian Conference Current Problems in Remote Sensing of the Earth from Space*, Moscow, Russia, 2017, p. 186.
- 12 **L. M. Naumov** and S. M. Gordeeva, "Variability of sea ice concentration and sea ice forms in the Kara Sea in modern climate," in *Proceedings of the 3rd PICES-ICES Early Career Scientist Conference*, Busan, Republic of Korea, 2017, p. 21.
- 13 **L. M. Naumov**, "Polynjas area dynamics in the Kara Sea (in Russian)," in *Proceedings of the 2nd Young Scientists Conference Complex Research of the World Ocean*, Moscow, Russia, 2016, pp. 200–203.
- 14 **L. M. Naumov** and S. M. Gordeeva, "Sea ice in the Kara Sea in modern climate (in Russian)," in *Proceedings of the 14th All-Russian Conference Current Problems in Remote Sensing of the Earth from Space*, Moscow, Russia, 2016, p. 275.

Books and Chapters

- 1 S. M. Gordeeva and **L. M. Naumov**, *Handling of Hydrometeorological Databases in the Internet Network (in Russian)*. St.Petersburg, Russia: Russian State Hydrometeorological University, 2020.

Skills

Coding	<ul style="list-style-type: none"> • Python - advanced level (numpy, scipy, pandas, xarray, matplotlib, and scikit-learn libraries). • Fortran - intermediate level. • Git - intermediate level. • Bash - intermediate level. • R - beginner level. • Matlab - beginner level. • LaTeX - beginner level. • HTML - beginner level. • CSS - beginner level. • JavaScript - beginner level. • Work on the computational clusters (supercomputers).
Scientific programs	<ul style="list-style-type: none"> • Various programs for netCDF files pre- and postprocessing (Panoply, CDO, NCO, Ferret, ncview). • Program for statistical analysis (Past4).
Numerical models	<ul style="list-style-type: none"> • A set of numerical models of physical and biogeochemical processes in the ocean (GOTM, MITgcm, MOM5, ERGOM, ERSEM).
Basic programs	<ul style="list-style-type: none"> • MS Office programs (Word, Excel, Power Point).
Statistical analysis	<ul style="list-style-type: none"> • Single- and multivariate statistical technics (Hypothesis testing, linear regression, correlation analysis, PCA decomposition, cluster analysis).
Misc.	<ul style="list-style-type: none"> • Academic research, scientific writing.
Hobbys	<ul style="list-style-type: none"> • Outdoor activity, board games, cycling.

Languages

- Russian • **Mother tongue** (C2 CEFR).
English • **Advanced level** (C1 CEFR).
German • **Intermediate level** (B1 CEFR).

Awards and Achievements

- 2016 • **2nd place in the young scientists research competition.** St. Petersburg branch of Shirshov Institute of Oceanology of Russian Academy of Sciences, St. Petersburg.
2018 • **1st place in the young scientists research competition.** St. Petersburg branch of Shirshov Institute of Oceanology of Russian Academy of Sciences, St. Petersburg.
2019 • **Laureate of The Best Student of St. Petersburg award.** Government of St. Petersburg, St. Petersburg.
2016 • **2nd place in the students research competition.** Russian State Hydrometeorological University, St. Petersburg.
2017 • **2nd place in the students research competition.** Russian State Hydrometeorological University, St. Petersburg.
2018 • **1st place in the students research competition.** Russian State Hydrometeorological University, St. Petersburg.

Teaching

- 2022 • **Summer School “Climate of the Baltic Sea Region”.** Baltic Earth, Askö, Sweden.
Exercises dedicated to introduction to Python and statistical analysis of the oceanographic data.
2021 • **Code Generation Tool (CGT) seminar.** IOW, Rostock, Germany.
Biogeochemical modeling exercises with CGT.

Grants and Scholarships

- 2016 • **St.Petersburg Government Scholarship.** Was given by the government of St.Petersburg.
2017 • **St.Petersburg Government Grant for young scientists.** Was given by the government of St.Petersburg.
2018 • **St.Petersburg Government Grant for young scientists.** Was given by the government of St.Petersburg.

Schools and Workshops

- 2018 • **Summer School “Climate of the Baltic Sea Region”.** Baltic Earth, Askö, Sweden.
2019 • **Winter School “Analysis of Climate Variability”.** IOW, Rostock, Germany.
2023 • **Winter School for young scientists.** IOW, Rostock, Germany.



Declaration of my contributions to the publications

C.1 MULTIDECADAL CLIMATE VARIABILITY DOMINATED PAST TRENDS IN THE WATER BALANCE OF THE BALTIC SEA WATERSHED

As a co-author, I worked on this paper during my first year as an IOW PhD student. I was responsible for the model validation. I applied the GAMM framework to the observational data, following Radtke et al. (2020). In addition, I worked with bathymetry and produced Figure 1 in the paper. I was also involved in the editing of the first draft of the manuscript and helped with paper revision.

C.2 LIMITED VENTILATION OF THE CENTRAL BALTIC SEA DUE TO ELEVATED OXYGEN CONSUMPTION

I started to work on this rather long paper at the beginning of the second year of my PhD at IOW and had been working on it for a year. The topic of the paper was elaborated by me together with my supervisor (Prof. Dr. H.E. Markus Meier). For the first part of the paper (disentangling O_2 and H_2S sources and sinks etc.), I used already prepared model data by Dr. Thomas Neumann. All statistical analysis was performed by me. For the second part of the paper (ventilation by inflows), all necessary model simulations, as well as statistical analysis, were performed by me (for EOF analysis, I consulted Dr. Hagen Radtke). I presented the first draft of the paper and, following the comments by all co-authors, edited it. I also presented the first draft of the response to the reviewers and, considering all comments resubmitted the paper.

C.3 DYNAMICS OF OXYGEN SOURCES AND SINKS IN THE BALTIC SEA UNDER DIFFERENT NUTRIENT INPUTS

I worked on this short paper during my third year as a PhD student at IOW. I designed this research together with my supervisor (Prof. Dr. H.E. Markus Meier). I performed all sensitivity simulations with necessary manipulations with the model forcing and analyzed all model outputs. I wrote the first draft of the publication and, implementing all the comments of my co-authors, submitted the paper. I also

presented the first draft of the responses to the reviewers and, after consulting my co-authors, resubmitted the paper.

D

Publications

The following publications are included in the appendix in the order of appearance:

- A **Naumov, L., Neumann, T., Radtke, H., and Meier, H. E. M.** (2023). Limited ventilation of the central Baltic Sea due to elevated oxygen consumption. *Frontiers in Marine Science*, 10. <https://www.frontiersin.org/articles/10.3389/fmars.2023.1175643>
- B *Markus Meier, H. E., Barghorn, L., Börgel, F., Gröger, M., Naumov, L., and Radtke, H.* (2023). Multidecadal climate variability dominated past trends in the water balance of the Baltic Sea watershed. *Npj Climate and Atmospheric Science*, 6(1), Article 1. <https://doi.org/10.1038/s41612-023-00380-9>
- C **Naumov, L., Meier, H. E. M., and Neumann, T.** (2023). Dynamics of oxygen sources and sinks in the Baltic Sea under different nutrient inputs. *Frontiers in Marine Science*, 10. <https://www.frontiersin.org/articles/10.3389/fmars.2023.1233324>



OPEN ACCESS

EDITED BY
Wei-Bo Chen,
National Science and Technology Center
for Disaster Reduction (NCDR), Taiwan

REVIEWED BY
Beata Szymczycha,
Polish Academy of Sciences, Poland
Ricardo Torres,
Plymouth Marine Laboratory,
United Kingdom

*CORRESPONDENCE
Lev Naumov
✉ lev.naumov@io-warnemuende.de

SPECIALTY SECTION
This article was submitted to
Coastal Ocean Processes,
a section of the journal
Frontiers in Marine Science

RECEIVED 27 February 2023
ACCEPTED 05 April 2023
PUBLISHED 24 April 2023

CITATION
Naumov L, Neumann T, Radtke H and
Meier HEM (2023) Limited ventilation
of the central Baltic Sea due to
elevated oxygen consumption.
Front. Mar. Sci. 10:1175643.
doi: 10.3389/fmars.2023.1175643

COPYRIGHT
© 2023 Naumov, Neumann, Radtke and
Meier. This is an open-access article
distributed under the terms of the [Creative
Commons Attribution License \(CC BY\)](#). The
use, distribution or reproduction in other
forums is permitted, provided the original
author(s) and the copyright owner(s) are
credited and that the original publication in
this journal is cited, in accordance with
accepted academic practice. No use,
distribution or reproduction is permitted
which does not comply with these terms.

Limited ventilation of the central Baltic Sea due to elevated oxygen consumption

Lev Naumov*, Thomas Neumann, Hagen Radtke
and H. E. Markus Meier

Department of Physical Oceanography and Instrumentation, Leibniz Institute for Baltic Sea Research
Warnemünde, Rostock, Germany

The Baltic Sea is known as the world's largest marine system suffering from accelerating, man-made hypoxia. Notably, despite the nutrient load reduction policy adopted in the 1980s, the oxygen conditions of the Baltic Sea's deep waters are still worsening. This study disentangles oxygen and hydrogen sulfide sources and sinks using the results from the 3-dimensional coupled MOM-ERGOM numerical model and investigates ventilation of the deep central Baltic Sea by the 29 biggest oxygen inflows from 1948 to 2018 utilizing the element tagging technic. Everywhere across the central Baltic Sea, except in the Bornholm Basin, a shift in oxygen consumption from sediments to water column and a significant positive trend in hydrogen sulfide content were observed. The most notable changes happened in the northern and western Gotland basins. Mineralization of organic matter, both in the water column and sediments, was identified as the primary driver of the observed changes. A significant negative trend in the lifetime of inflowing oxygen was found everywhere in the central Baltic Sea. It leads to the reduced efficiency of natural ventilation of the central Baltic Sea via the saltwater inflows, especially in the northern and western Gotland basins.

KEYWORDS

Baltic Sea, hypoxia, O₂ and H₂S budgets, ventilation, saltwater inflows

1 Introduction

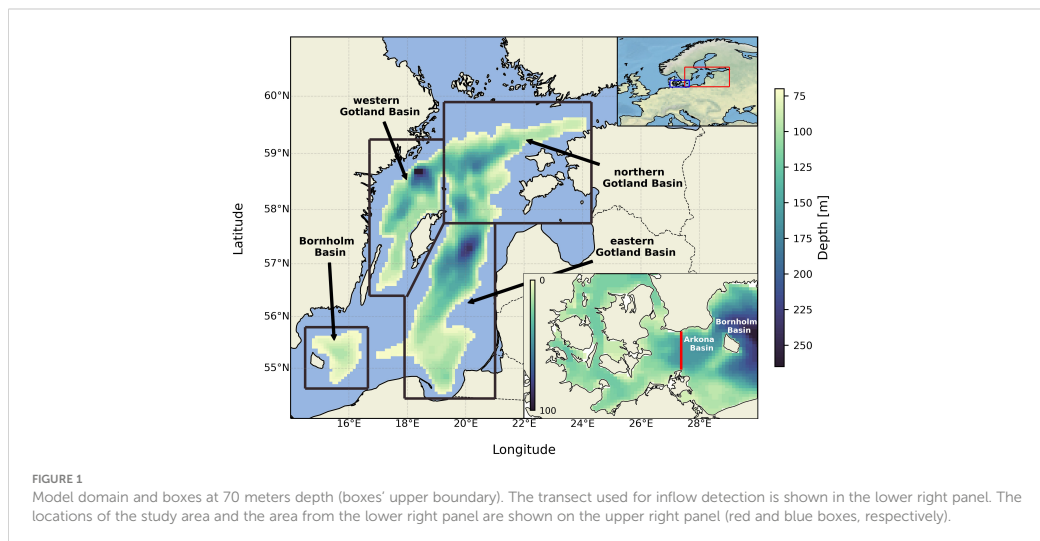
The phenomenon of hypoxia, usually defined as dissolved oxygen concentrations in seawater less than 2 ml/l (Conley et al., 2002) or 2 mg/l (Roman et al., 2019), has been capturing the attention of the marine researchers' community for decades. Hypoxic conditions can provoke substantial changes to marine ecosystems altering the trophic webs and disrupting the fluxes of material and energy through the trophic levels (Ekau et al., 2010; Breitburg et al., 2018; Limburg and Casini, 2018). Life in permanent hypoxic zones or even more extreme anoxic zones (total absence of oxygen), so-called dead zones, is usually limited to anaerobic chemotrophic bacteria (Vaquer-Sunyer and Duarte, 2008; Hale et al., 2016). Thus, hypoxic conditions in the sea harm marine communities and,

eventually, the human economy by changing the fish standing stocks (Pollock et al., 2007; Huang et al., 2010). Many marine systems are affected by hypoxia in the modern world. These include the Chesapeake Bay, the Northern Gulf of Mexico, and the Gulf of St. Lawrence in North America, the Black Sea, the Baltic Sea, and the East China Sea in Eurasia (Rabalais et al., 2007; Diaz and Rosenberg, 2008; Su et al., 2017; Breitburg et al., 2018; Fennel and Testa, 2019). Although local physical and biochemical conditions might vary depending on the specific marine system, one factor that might affect all of them is climate change. Meier et al. (2011) suggest a few critical mechanisms by which global warming affects hypoxia. Firstly, the solubility of gases decreases with increasing temperature. Whitney (2022) showed that this effect is accountable for significant negative trends in oxygen uptake capacity, especially in temperate latitudes in the Northern Hemisphere, where many marine systems prone to hypoxia are located. Belkin (2009) found accelerated warming of European and East Asian seas during 1982–2006. The second important mechanism, described by Meier et al. (2011); Yindong et al. (2021) (investigated freshwater lake case), Sanz-Lázaro et al. (2015), and Voss et al. (2013), is related to the processes happening within ecosystems, namely accelerated rates of internal nutrient cycling, which can stimulate mineralization and respiration of marine organisms. Those mechanisms reinforce hypoxia development under future climate projections. To detect and quantify these anticipated changes in the future, the current state of a hypoxic environment and its recent trends need to be assessed on a regional scale. In this paper, the oxygen dynamics and budgets of the Baltic Sea are studied in detail.

The Baltic Sea is a semi-enclosed sea located in Northern Europe (Figure 1). This aquatic system is widely known to suffer from severe hypoxic and anoxic conditions (Conley et al., 2009; Carstensen et al., 2014). It experiences the largest anthropogenically induced hypoxic area among all estuaries worldwide (Fennel and Testa, 2019). The Baltic Sea is connected with the North Sea via the

shallow and narrow Danish straits, which limit the water exchange significantly and consequently increase the residence time (Leppäranta and Myrberg, 2009). This and an estuarine-like circulation, characterized by the permanent halocline, make the sea naturally prone to hypoxia. However, Hansson and Viktorsson (2020); Almroth-Rosell et al. (2021); Kouts et al. (2021), and Krapf et al. (2022) found a significant increase in hypoxic area in the 20th century. Those changes are attributed to the elevated anthropogenic nutrient loads peaking in the second half of the 20th century (Savchuk, 2018; Capell et al., 2021). Since the peak of the nutrient loads to the Baltic Sea in the 1980s, the Baltic Sea countries have been reducing their nutrient emissions. In 2007, the Baltic Sea Action Plan (BSAP) was implemented by HELCOM (Baltic Marine Environment Protection Commission or Helsinki Commission) and adopted by Baltic Sea states to mitigate the Baltic Sea eutrophication. It was updated in 2021 (Jetoo, 2019; HELCOM, 2021). But despite the implemented nutrient reductions, it is still unknown yet how the marine system will respond (Neumann et al., 2002; Funkey et al., 2014; Meier et al., 2018a; Meier et al., 2019).

A natural ventilation mechanism for the central part of the Baltic Sea is provided by sporadic inflows of saline water through the Danish straits, so-called Major Baltic Inflow events (MBIs) (Matthäus and Franck, 1992; Matthäus et al., 2008; Hansson and Andersson, 2015; Lehmann et al., 2022). They occur under specific meteorological conditions and transport saline, oxygen-rich water from the North Sea into the Baltic Sea (Lehmann and Post, 2015; Mohrholz, 2018). Due to the high density, North Sea water flows along the bottom slope and fills the deep Baltic Sea basins (Bornholm Basin, Eastern, Northern, and Western Gotland basins) (see Figure 1), where the oxygen content is usually low. Neumann et al. (2017) compared two inflow events in 2003 and 2014, the latter being one of the strongest MBIs in the history of the observations. They concluded that the less intense 2003 event supplied more oxygen to the central Baltic Sea than the stronger



2014 event due to the longer overall duration of the consecutive inflow events which made out the 2003 event. However, this paper did not consider the possibly different biochemical responses to those two inflows. Another source of uncertainty is related to the biochemical response to the inflow's oxygen-rich water. The study by Meier et al. (2018b) showed that oxygen consumption in the water column and the sediments has increased during recent decades, which can exceed the oxygen supply and even contribute to elevated hypoxia and anoxia.

Another mechanism controlling hypoxic area development in the Baltic Sea is the halocline depth and strength. This mechanism, which affects hypoxia *via* modulation of the vertical oxygen supply across the pycnocline, is controlled by small and mesoscale processes (Elken et al., 2006; Kuzmina et al., 2008; Conley et al., 2009; Väli et al., 2013). Increasing halocline strength (the salt gradient between upper and lower layers) limits the vertical exchange with the upper layer, which alleviates hypoxia. Strengthening of the halocline is known to accompany the Major Baltic Inflows (MBIs), potentially limiting their aeration effectiveness (Conley et al., 2002).

This study aims to address the oxygenation mechanisms of the central Baltic Sea by MBIs and its uncertainties with the help of a numerical model. This is done by investigating the 29 most significant oxygen inflows from 1948 to 2018 and their influence on oxygen and hydrogen sulfide sources and sinks in the deep water and sediments. Another goal is to disentangle oxygen and hydrogen sulfide sources and sinks in the central Baltic Sea to sort them for their contribution to the total oxygen variability on the interannual timescale, and to study their long-term trends.

2 Materials and methods

2.1 Model description

This study utilized a coupled hydrodynamical/biogeochemical 3-dimensional regional ocean model. A regional three nautical miles Baltic Sea setup of the Modular Ocean Model (MOM) (Pacanowski and Griffies, 2000; Griffies, 2004) served as a hydrodynamical model. This model uses a finite-difference method to solve the full set of primitive equations to calculate the motion of the water and the transport of heat and salt. K-profile parameterization (KPP, Large et al., 1994) was used as a turbulence closure scheme. The western open boundary was placed in the Skagerrak, enabling exchange with the North Sea. Model depths in the Baltic Sea setup, used in this study, were limited to 264 meters due to computational reasons related to the vertical grid representation. Hence, the Landsort Deep region was artificially shallowed. Potential uncertainties this approach entails are discussed in the Section 4. Biogeochemical cycles were simulated by the ERGOM model (Radtke et al., 2019; Neumann et al., 2021; Neumann et al., 2022). This model simulates the dynamics of the main nutrient elements, namely carbon (C), nitrogen (N), and phosphorus (P). Nitrogen and phosphorus are characterized by their organic and inorganic forms. ERGOM separates the phytoplankton community into three separate groups: large

phytoplankton (lpp), small phytoplankton (spp), and cyanobacteria (cya). The zooplankton state variable (zoo) implements the grazing pressure on phytoplankton. There is a separate state variable representing detritus. Carbon is contained in these state variables in the fixed Redfield ratio and is additionally represented as particulate and dissolved organic carbon (DOC and POC), where the C:N:P ratio might be non-Redfield (Neumann et al., 2022), and dissolved inorganic carbon (DIC). ERGOM includes the closed O₂ and H₂S cycles, which can be briefly described as follows: oxygen is produced *via* the photosynthesis carried out by the phytoplankton and utilized in mineralization of organic matter and nitrification both in the sediments and in the water column. Hydrogen sulfide is represented as a separate state variable. It is produced under anoxic conditions *via* sulfate reduction and can be oxidized to sulfur, and subsequently to sulfate, either by oxygen or nitrates. The detailed description of all model equations can be found in Neumann et al. (2022). The model was forced by CoastDat2 meteorological forcing (Geyer, 2014) and time-dependent river runoff. The model setup used in this study has already been applied to the Baltic Sea and demonstrated a good performance in the study area (e.g. Neumann et al., 2017). The study's time frame spanned the period from 1948 to 2018 (71 years). Two series of model results were produced. The first one was averaged monthly and the second one – daily. Monthly mean data were used in the budget analysis (Section 3.2) and daily mean – in the inflows' ventilation analysis (Section 3.3).

2.2 Budget approach

Both physical and biochemical processes contribute to O₂ budget in a particular volume in the sea. Physical terms of the oxygen budget include lateral and vertical advection and diffusion of oxygen into and out of the volume. Biochemical terms include mineralization of organic matter, photosynthesis, respiration of marine organisms, oxidation of reduced material (elemental sulfur, hydrogen sulfide, and ammonium), and denitrification. If the oxygen budget is positive, oxygen concentration increases within the considered volume, e.g., a selected box of a sub-domain, and vice versa. The same reasoning is applicable to H₂S.

To perform the budget analysis, the central Baltic Sea was split into four boxes (see Figure 1). In the vertical, each box spans from 70 meters depth to the bottom. These boxes represent four different basins, namely the Bornholm Basin (BB) – the shallowest among all selected sub-basins with only the upper boundary active; the eastern Gotland Basin (eGB), which has two lateral boundaries: the Slupsk Furrow in the West, and the northern Gotland Basin in the North; and correspondingly the northern (nGB) and western (wGB) Gotland basins with two and one lateral boundaries, respectively. The fifth box, for which the analysis was conducted, represents the whole central Baltic Sea (the total area depicted in Figure 1) comprising all four boxes and the small Slupsk Furrow, westerly adjacent to the eGB. Mass conservation was checked for all boxes, both for oxygen and hydrogen sulfide. The errors are a few orders of magnitude less than all budget terms (see Supplementary Figures 1

and 2), which suggests that the coupled MOM-ERGOM model obeys the mass conservation law and can be utilized for this type of analysis.

2.3 Validation against the observations

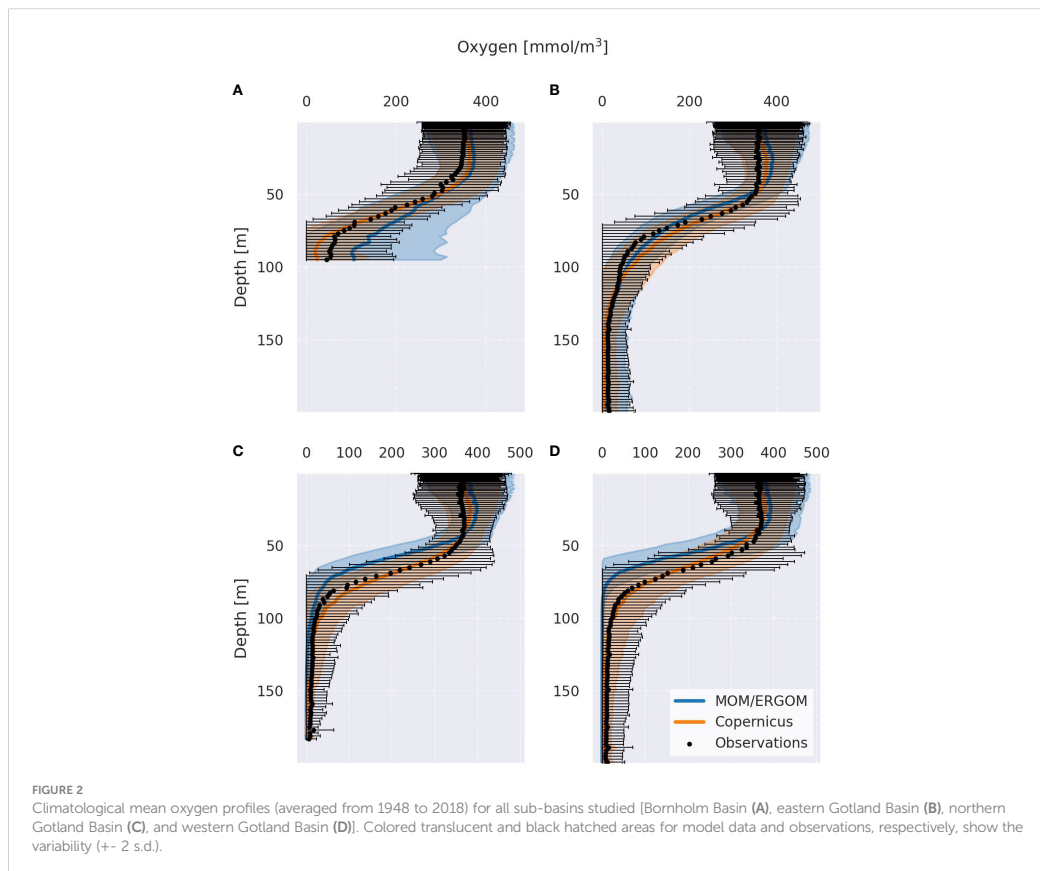
The model setup was thoroughly validated against the observational and reanalysis datasets. Observational data are combined data sampled from the ICES (International Council of the Exploration of the Sea) web archive (ICES, 2023) and the IOW (Leibniz Institute for Baltic Sea Research Warnemuende) observational database (IOW, 2023). As another, continuous dataset for validation, the Copernicus regional Baltic Sea reanalysis (BALTICSEA_REANALYSIS_BIO_003_012) was chosen (Copernicus, 2023a). This product is based on the coupled NEMO/SCOB1 model system (Almroth-Rosell et al., 2014; Hordoir et al., 2019) and includes data assimilation of oxygen concentration and nutrients observations (O_2 , P, N). It has two nautical miles horizontal resolution and 56 depth levels. Temperature and salinity fields were taken from the Copernicus regional physical reanalysis

for the Baltic Sea (BALTICSEA_REANALYSIS_PHY_003_011) (Copernicus, 2023b). This reanalysis product is identical to the biological reanalysis. For simplification, later in the text and the figures, all fields from those products will be presented under the “Copernicus” label.

The evaluation was performed for several model variables (temperature, salinity, PO_4^{3-} , NO_3^- , NH_4^+ , O_2 (dissolved oxygen), and H_2S (dissolved hydrogen sulfide). Hypoxic area and volume, as the key indicators of redox conditions, were also validated against the Copernicus data. Only the climatological (1993-2018) oxygen profiles are shown in the paper (Figure 2). More validation results are presented in Supplementary Figures 5-17.

2.4 Statistical methods used for sources and sinks processing

For the model data postprocessing, a few statistical methods were utilized. A simple linear regression model was applied to calculate the trends. Trend significance was checked by testing the statistical hypothesis about the equality of the trend slope coefficient



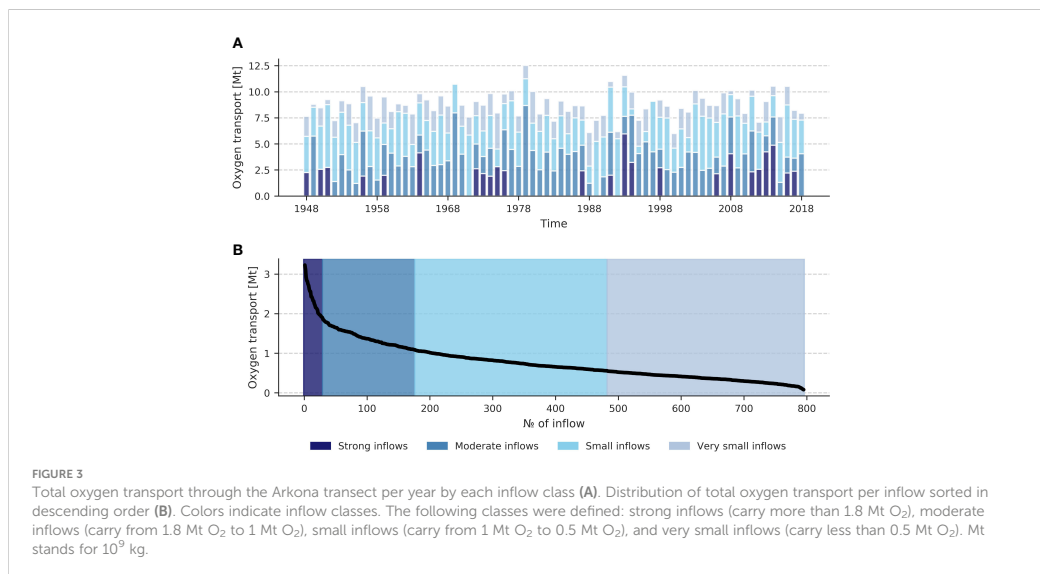
to zero with $\alpha=0.05$ employing the Wald test (Wald, 1943; Murtagh and Legendre, 2014). The linear regression framework has been adopted to rank the processes by the explained proportion of oxygen variance. Starting from a simple linear regression to the process that explains most of the variance, we then use a series of multilinear regressions, every time adding a single next process that increases the explained variance most. Relative contributions were calculated by comparing the two determination coefficients (R^2) of neighboring fits.

A hierarchical agglomerative cluster analysis technique (Ward's method) was chosen to classify the identified oxygen and saltwater inflows according to the import of oxygen/salt into the Baltic Sea (Ward, 1963). A distance matrix was computed using the Euclidean distance measure (Dokmanic et al., 2015) to get a classification based on the differences in the mean value. The cluster analysis aims to maximize the variance between the different clusters and minimize the variance within a single cluster. In agglomerative algorithms, all data points are attributed to the distinctive clusters at the first iteration, so the number of clusters equals the number of data points. In the next step, the closest clusters are merged, forming a bigger cluster. In the end, there is only one cluster encompassing all data points. The algorithm produces a diagram, so-called dendrogram, showing at which distance the specific clusters were merged. Dendrograms for total oxygen and salt transported into the Baltic Sea by inflows are shown in Supplementary Figures 18 and 19.

2.5 Inflows detection algorithm

Daily model total oxygen/salt transport across the vertical transect in the Arkona Basin (Arkona transect) (see Figure 1) was

analyzed to detect the inflow events. The resulting time series was preprocessed with a 5-day running mean to remove the high-frequency variability. In the filtered time series, consecutive positive transport values for more than 5 days were considered to be an inflow event (Mohrholz, 2018). Supplementary Figure 20 shows the identified inflows for the year 1948. The statistics for oxygen and salinity inflows were collected from 1948 to 2018. They include the inflow's start date, end date, duration, and the total amount of salt/oxygen transported during the event. Tables containing the 10 largest inflow events for oxygen and salt can be found in Supplementary Tables 3, 4. The hierarchical clusterization algorithm (described in the previous subsection) was applied to the total transport per inflow time series to classify the inflows by their strength. The oxygen transport time-series was split into four classes, while the salt transport time series was divided into two classes only (see Supplementary Figures 18, 19). Figure 3 demonstrates the main properties of identified O_2 inflows clustered into four distinct clusters. The number of inflows per class varies significantly. There are 29 strong inflows, 147 moderate, 313 small, and 306 very small. Moderate and small inflows usually carry the most oxygen in years without strong inflows. In a year with strong inflows, these can constitute up to around 50% of the total oxygen transport by the inflows. Strong oxygen inflows are distributed unevenly on the time axis. There are periods with enhanced transport (the 1950s, 1972-1976, 1993-1994, and the 2010s) and periods with no transport (the 1960s, 1977-1992, 1999-2005). Overall, no trend was found, neither in the oxygen transport by the inflows, nor in the salt transport (for the salt inflows, see Supplementary Figure 21). Later we will only focus on the 29 strong oxygen inflow events. Although they might not constitute the largest oxygen source in a particular year, they all are accompanied by large salt inflows (according to the provided



classification). This choice is essential because only inflows that reach the remote central Baltic Sea basins (eGB, nGB, and possibly wGB) shall be studied. To analyze all 29 strong inflows separately, the tagging method was applied following Ménesguen et al. (2006). That method allows having a separate tracer variable for oxygen brought to the Baltic Sea by a specific inflow event. The results are discussed in Section 3.3.

3 Results

3.1 Validation summary

Validation showed that the coupled MOM/ERGOM model was able to reproduce the mean state and temporal variability of all investigated variables within each selected sub-basin (BB, eGB, nGB, and wGB). In Figure 2, model oxygen profiles are predominantly located within two standard deviations from Copernicus and observations. Validation also highlights some sources of uncertainty in the model estimates. Model overestimates hypoxic conditions in the whole Gotland Basin (especially in the wGB and nGB). At the same time, it underestimates hypoxia in the Bornholm Basin (see Supplementary Figure 5). This pattern can be seen in Figure 2 as well. Starting at 50 meters depth, the model oxygen profile in the BB positively deviates from both Copernicus reanalysis and observations. It also shows a weaker oxycline. Both in the wGB and nGB, model oxygen profiles demonstrate a stronger oxycline and an absence of variability below a certain depth (see Supplementary Figures 12, 14). The mechanisms that likely cause these oxygen misrepresentations are deviations in the halocline depth and strength in the MOM model (Supplementary Figure 17). Since there are no other significant deviations caused by ERGOM, the model results can be trusted, but the uncertainties should be considered.

3.2 Processes governing O₂ and H₂S dynamics in the central Baltic Sea

Understanding oxygen and hydrogen sulfide dynamics requires knowledge of the main processes governing their variability. In this Section, all processes contributing to the O₂ and H₂S budgets were analyzed in terms of average values and their temporal variability for each sub-basin.

3.2.1 The biggest O₂ and H₂S sources and sinks

First, we analyzed the time-averaged contributions to the oxygen and hydrogen sulfide budgets for each sub-basin. The processes were grouped into physical fluxes, water column processes, and sedimentary processes (see Supplementary Tables 1, 2).

For the oxygen budget, vertical advection dominates in the physical processes group in the BB, eGB, and wGB. In the nGB, lateral advection across the southern boundary brings the most oxygen into the domain. The other advection terms comparably

contribute to oxygen supply to the eGB and wGB. However, this is less true for the nGB sub-basin, where both vertical and western advection terms are at least one order of magnitude less than the advective transport from the south. This pattern in oxygen advection indicates the importance of oxygen inflows for deep sea ventilation and separates sub-basins in terms of oxygen supply. BB and eGB are relatively close to the Danish straits and therefore receive more oxygen *via* the inflows. Conversely, wGB is a remote sub-basin with limited oxygen supply. Among the water column processes, nitrification was found to be the largest oxygen sink in all sub-basins except wGB, where oxidation of elemental sulfur turned out to be the biggest sink of oxygen. However, in the wGB, oxygen consumption by water column nitrification cannot be neglected. Elemental sulfur oxidation is one of the largest water column oxygen consumption terms in the eGB and nGB. Oxygen supply by photosynthesis and consumption by living organisms' respiration is negligible in the whole study area. Oxygen consumption in the sediments is dominated by detritus mineralization, which is the biggest oxygen sink everywhere except wGB, where oxidation of elemental sulfur in the water column exceeds it. The contributions change over time, though. The biggest oxygen sink in the wGB changes from nitrification to sulfur mineralization. This, together with a decreased oxygen consumption in the sediments, could indicate a deterioration of oxygen conditions, where redoxcline movement to shallower depths facilitates the accumulation of reduced material in the sediments.

Sources and sinks of hydrogen sulfide differ from those of oxygen, their hierarchy is also different. Advection of hydrogen sulfide across the upper boundary out of the basin dominates among the advective and diffusive fluxes in the remote sub-basins (the nGB and wGB). In the eGB, the biggest advection term is the transport across the northern boundary, which brings H₂S out of the domain towards the more remote basins, activating a positive feedback mechanism further worsening the oxygen conditions there. The water column serves mainly as a sink of hydrogen sulfide. Both H₂S sink terms (oxidation by O₂ and NO₃-) contribute significantly to the hydrogen sulfide removal, having the same order of magnitude. Oxidation by O₂ dominates in the BB and wGB, and oxidation by NO₃- in the eGB and nGB. The biggest H₂S production term in the water column is the mineralization of detritus. In the sediments, mineralization of detritus is also the biggest source of H₂S across all sub-basins. Numbers are presented in Supplementary Tables 5-10.

3.2.2 Contribution of the different processes to the O₂ and H₂S variability

To study the dynamic aspect of O₂ and H₂S sources and sinks in the sub-basins, regression analysis (for the method description, see Section 2) was performed for both aggregated process categories (Figure 4) and individual processes (Supplementary Figures 22, 23). There are significant differences in oxygen and hydrogen sulfide dynamics. More than half of the oxygen's variance is explained by physical processes. In contrast, hydrogen sulfide dynamics is governed by the water column processes, which explain 45% to 87% of its variability. The remaining groups do not have the same contributions from sub-basin to sub-basin. For oxygen, there is a

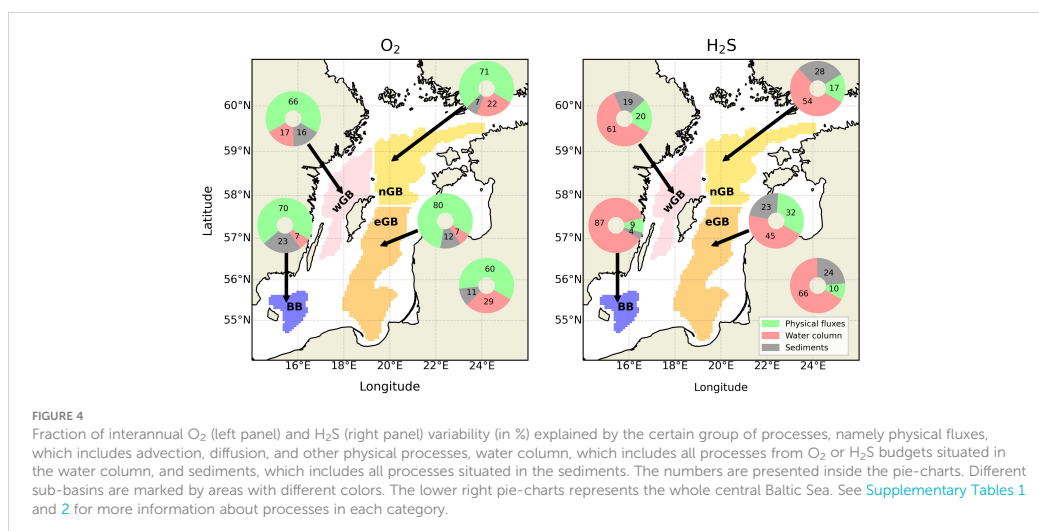


FIGURE 4

Fraction of interannual O_2 (left panel) and H_2S (right panel) variability (in %) explained by the certain group of processes, namely physical fluxes, which includes advection, diffusion, and other physical processes, water column, which includes all processes from O_2 or H_2S budgets situated in the water column, and sediments, which includes all processes situated in the sediments. The numbers are presented inside the pie-charts. Different sub-basins are marked by areas with different colors. The lower right pie-charts represents the whole central Baltic Sea. See [Supplementary Tables 1 and 2](#) for more information about processes in each category.

slight increase in the explained variance by the water column processes in the remote sub-basins. At the same time, 17% of the variability in the wGB is explained by sedimentary consumption, which is the second largest fraction after 22% in BB. Analysis of the more specific processes' contribution to the oxygen and hydrogen sulfide dynamics reinforces the conclusions about advection-driven oxygen dynamics. In all sub-basins, advective terms explain the largest fraction of variability. Coupled nitrification-denitrification processes in oxic sediments significantly contribute to the oxygen variability in the BB and eGB. However, in the nGB and wGB, those processes are not included in the list of significant processes, giving their place to nitrification in the water column. In the nGB, the only considerable process related to the oxygen consumption in the sediments is mineralization of the particulate organic matter (POM) (including both detritus mineralization and mineralization of non-Redfield particulate organic carbon (POC)). In the wGB, no critical processes related to sedimentary consumption are detected.

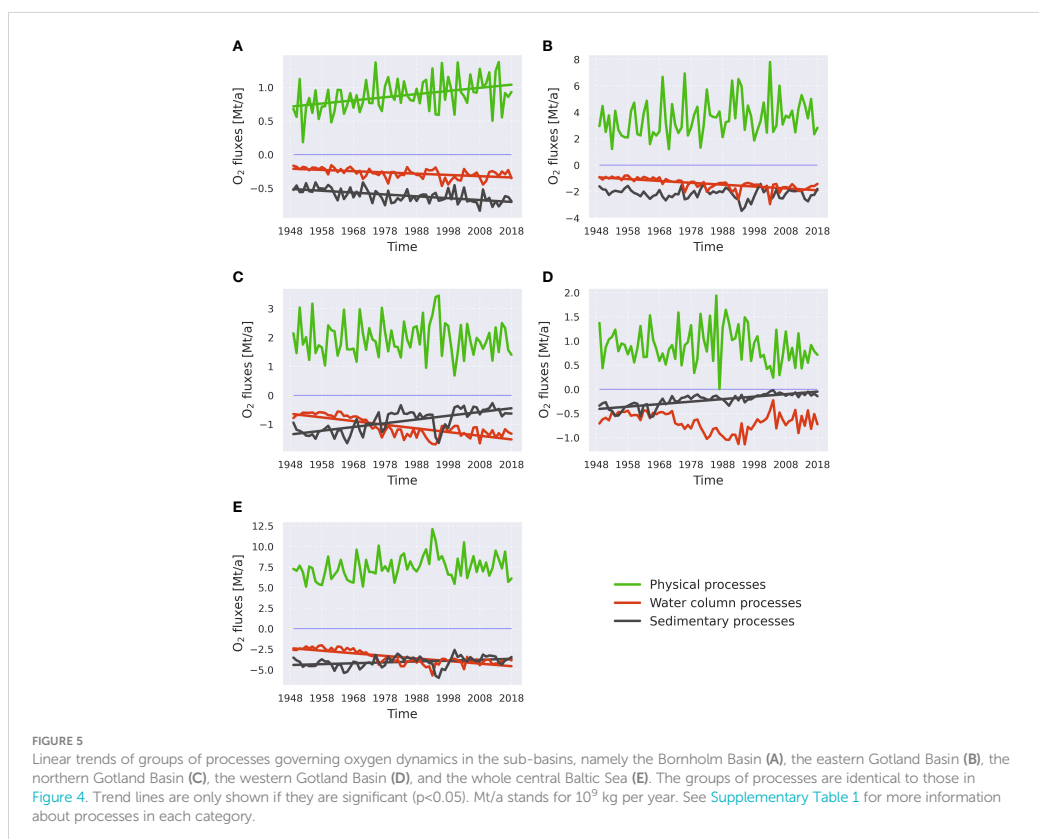
Analysis of terms contributing to hydrogen sulfide dynamics featured some notable patterns. Oxidation, either by O_2 or NO_3^- , explains the significant fraction of H_2S variability everywhere in the central Baltic Sea. Among the sedimentary processes, the mineralization of detritus is the universal significant term in all sub-basins. This clearly distinguishes water column and sediments, making former the sink of H_2S and latter - the source. Both lateral and vertical advection terms play an important role in the hydrogen sulfide dynamics only in the two remote basins. This again stresses their vulnerable position as H_2S producers and, in addition, sinks of hydrogen sulfide from the neighboring basins.

3.2.3 Temporal variability of O_2 and H_2S sources and sinks

A linear trend analysis has been conducted to detect shifts in oxygen and hydrogen sulfide budget terms (Figures 5, 6). No significant change in oxygen supply by the physical fluxes was

found anywhere except in the BB (Figure 5A). That trend might be attributed to internal changes within the basin, e.g., stratification or unidentified small inflows. Trends in the oxygen consumption in the water column and sediments are not identical from region to region. In the BB, both water column and sedimentary consumption exhibit a significant negative trend (i.e., an increase in their magnitude, since consumption is counted negative). Other sub-basins show the common pattern of temporal variability in the water column and sedimentary oxygen consumption. It is a significant negative trend in water column consumption [found in the eGB (Figure 5B) and nGB (Figure 5C)], and a significant positive trend in the sedimentary consumption [found in the nGB and wGB (Figure 5D)], which represents a shift in oxygen consumption from sediments to the water column. The most pronounced example of that pattern is the nGB, where initially consumption in the sediments dominated over consumption in the water column but, starting from the 1980s, the latter exceeds the former, highlighting the shift of oxygen consumption from the sediments to the water column. No significant trend in the water column consumption was observed in the wGB, but there is a significant, positive trend in the sedimentary consumption. This could indicate that the worsening of oxygen conditions across the remote basins in the central Baltic Sea is started in the 1970s and is still happening. It is especially visible in the wGB, where the absence of a negative trend in the water column consumption indicates elevated import of reduced material, including H_2S .

Trends of the H_2S production/consumption exhibit some spatial variability. In the BB diagram (Figure 6A), the curve, indicating H_2S consumption in the water column, is mirrored by the H_2S sedimentary production curve without any significant linear trend. This pattern reflects the fact that there is no long-term accumulation of hydrogen sulfide happening in the BB. All H_2S produced here is oxidized within a short time. H_2S terms across the different regions of the Gotland Basin exhibit the significant



linear trends in water column consumption and sedimentary production with the opposite signs. No significant trend in physical fluxes was found in the eGB (Figure 6B), whereas in both nGB (Figure 6C) and wGB (Figure 6D), a significant negative trend in physical processes was observed, meaning the export of H_2S out of the sub-basin. The magnitude of the trend in physical fluxes follows the difference between magnitudes of the water column H_2S consumption and sedimentary H_2S production trends. See Supplementary Tables 11, 12 for information about the trends of individual processes.

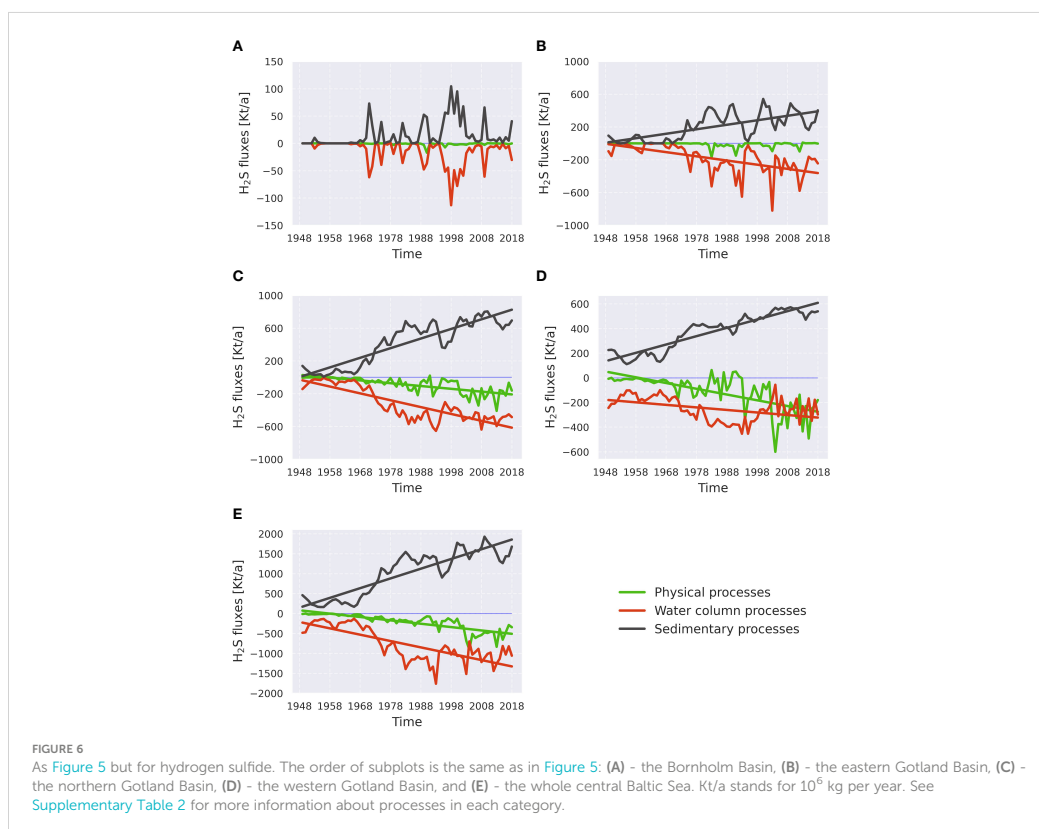
3.3 Ventilation by inflows

As shown in the previous section, advection governs the oxygen dynamics in the deep basins of the central Baltic Sea. The sole mechanism of oxygen advection into the deep waters is the Baltic Sea inflows, transporting oxygen and salt from the North Sea through the shallow and narrow Danish straits. In this section, the dynamics of oxygen inflows have been rigorously assessed. Despite the constant exchange between the Baltic Sea and the North Sea *via* small and medium-sized inflows, the biggest inflows are of

primary importance for the ventilation of the deepest parts of the central Baltic Sea. We utilized the approach proposed by Ménesguen et al. (2006) to tag the oxygen that enters the Baltic Sea with the 29 biggest inflows that happened from 1948 to 2018 and were identified in advance (see Figure 3 and Section 2.5 for more details). The tagging was activated in total 29 times (each time when inflow water arrives at the Arkona transect depicted in Figure 1). We tagged all dissolved oxygen below 70 meters depth west of the Arkona transect. The tagging was stopped at the end of the inflow event (this means no new tagged oxygen is generated, however, the old one remains). This approach allowed us to track oxygen brought to the Baltic Sea by a specific inflow event. The tagged oxygen is modeled as an additional active biogeochemical tracer, which participates in its own set of reactions and undergoes separate advection and mixing. In total, 29 additional tracers were added to the model, each one representing a certain inflow event. The described tagging approach was also employed in Neumann (2007); Radtke et al. (2012), and Neumann et al. (2017).

3.3.1 Temporal trends in inflows' ventilation

To study the temporal patterns of the ventilation by saltwater inflows, analysis of the regional inflowed oxygen content and

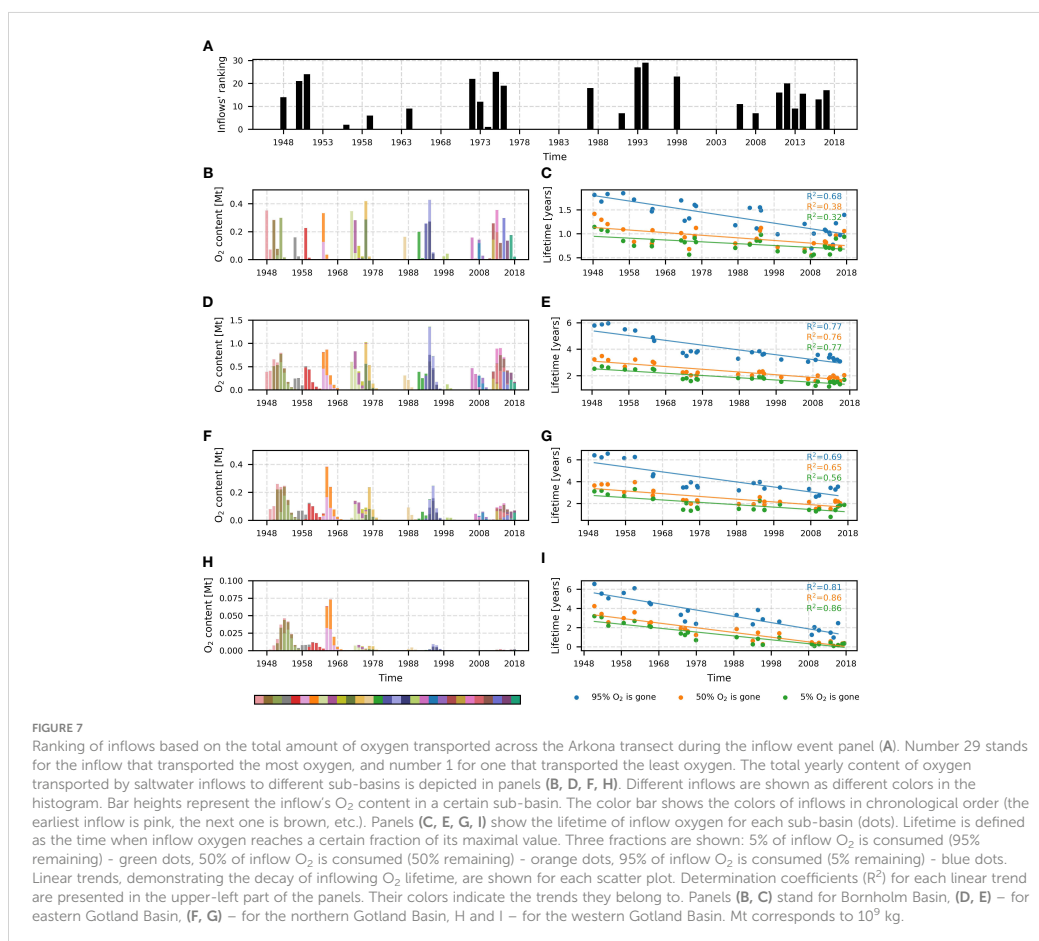


inflows' lifetime was conducted. (Figure 7A) revealed no presence of a significant trend in the inflows' strength, this statement is supported by Figure 3. At the same time, a clear negative trend is visible in the inflows' lifetimes across all sub-basins (Figure 7, right panels). All linear trends explain more than 30% of the variability, with the lowest numbers in the BB and the highest in the wGB. This sub-basin also demonstrates the steepest trend across all four sub-basins. The inflow-derived oxygen content in the wGB (Figure 8H), which is generally very limited in the wGB, also shows a rapid decline. The inflows after 1965-66 brought almost no oxygen. Even the largest inflows, which happened in 1993-94 and 2014-15, brought nearly no oxygen to the wGB. The nGB exhibits, in general, the same behavior as the wGB. The largest inflows, which took place in the 1990s and the 2000s, brought less oxygen to the sub-basin than inflows from the 1960s. This might be attributed to the elevated oxygen consumption in the nGB and in other sub-basins. In the BB and eGB, no significant decrease in the inflow-derived oxygen content was found. In the BB, the large fraction of oxygen is usually originating from the inflows. In the eGB, this number drops two times. The most considerable amount of oxygen was brought to the BB and eGB during the 1993-94 inflows. Considering the results presented in Figure 7, it can be concluded that currently all four sub-basins are less well oxygenated by

saltwater inflows than 70 years ago. This is especially visible in the remote nGB and wGB, where the total content of inflowing O_2 dramatically dropped compared to the first half of the 20th century. Assuming no significant trend in the inflows' strength (amount of O_2 transported across the Arkona transect), the only reason for those changes is accelerated oxygen consumption provoked by the overall deoxygenation of the central Baltic Sea.

3.3.2 Changes in ventilation pattern

It has been shown that there is a significant decline in inflowing oxygen lifetime in the deep waters (below 70 m) across the central Baltic Sea, especially the nGB and wGB. However, we did not yet investigate which processes contributed most to the enhanced inflowing oxygen consumption and whether the pattern of inflowed O_2 consumption is changing with time. To answer that question, temporally integrated oxygen consumption and hydrogen sulfide production/consumption per process (or per group of processes) was calculated for each of the inflows (for more details, see Figure 9). The integration for a specific inflow is stopped when (a) another inflow event occurs or (b) the oxygenation by the inflow has ended. From the analysis of Figure 9, it can be noted that mineralization of detritus is the process consuming most oxygen in all sub-basins. However, in the remote nGB and wGB, water

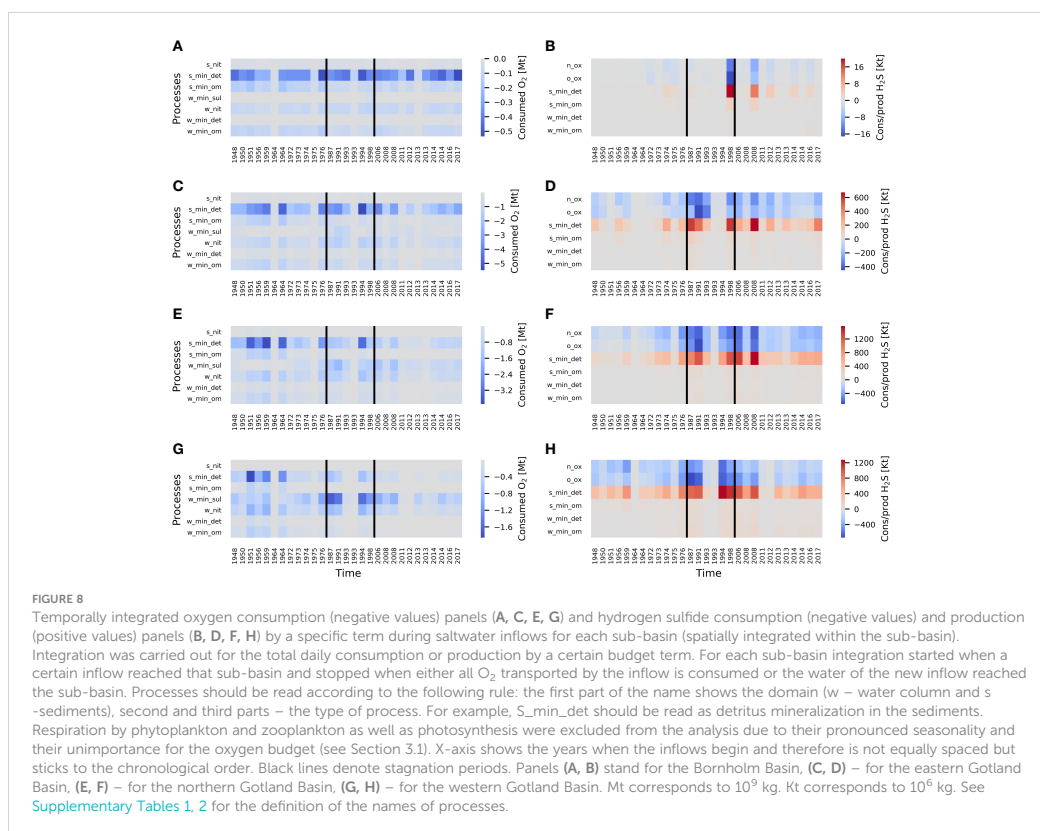


column processes play a larger role, namely the oxidation of sulfur and H₂S (the sum of two processes, namely, oxidation of H₂S to elemental S and oxidation of elemental S to SO₄²⁻) and nitrification. It fits the conclusions about shifting the main oxygen sink from sediments to the water column demonstrated in the previous sections.

For the hydrogen sulfide budget, the most important source during the inflow events is the mineralization of detritus in the sediments. Sinks of H₂S are oxidation by O₂ and NO₃, which similarly contribute to the H₂S consumption. No time-dependent pattern of H₂S consumption and production is observed in the wGB. In the nGB and eGB, the slight increase in both production and consumption of H₂S starting from the 1970s is visible.

To identify and understand the dominating patterns in the O₂ and H₂S dynamics during the inflow events, EOF analysis (Hannachi et al., 2007) was conducted for these spatiotemporal matrices. The results (see Figure 8) suggest that there are two EOFs describing more than 95% of the variance in O₂ data. The first EOF explains approximately 90% of the variability, and the second

explains about 5% (Figure 8A). Loadings of the first EOF demonstrate no spatial dependency, having the same sign across all sub-basins. The first spatial pattern thus describes a default reaction of all basins to an inflow that brings oxygen, while the first EOF varies with the amount of oxygen input and is positively correlated with the duration of the inflow effect (Figure 8C). The first EOF might be attributed to the inflow's strength and duration because those patterns are spatially independent and should affect especially eGB since it is the first deep basin on the way of the inflowing water. The second EOF shows more sophisticated dynamics. It changes in the sign during the 1970s indicating the shift in contributing processes (Figure 8B). Loadings of the second EOF show opposite patterns between the sub-basins, which indicates the spatial non-uniformness of the pattern behind the second EOF. What the second EOF reveals is a change in the oxygen-consuming processes between the two periods before and after the 1970s. This change in the processes is opposite between the basins. A strong inflow in the later period differs from a strong inflow in the earlier period by a larger value of the second EOF. That



means that the corresponding loads (lower panel of [Figure 8](#)) directly show the change in the reaction of the basins to an oxygen input. Since all processes in the figure are consuming oxygen, the negative values (shown in blue) mean an amplification. Oxygen consumption for the mineralization of sedimentary detritus is shifted spatially. It is enhanced in the eastern Gotland Basin and reduced in the northern and western Gotland Basin. An increase in all subbasins is seen for the consumption related to sulfur oxidation (w_min_sul), but it is most pronounced in the nGB.

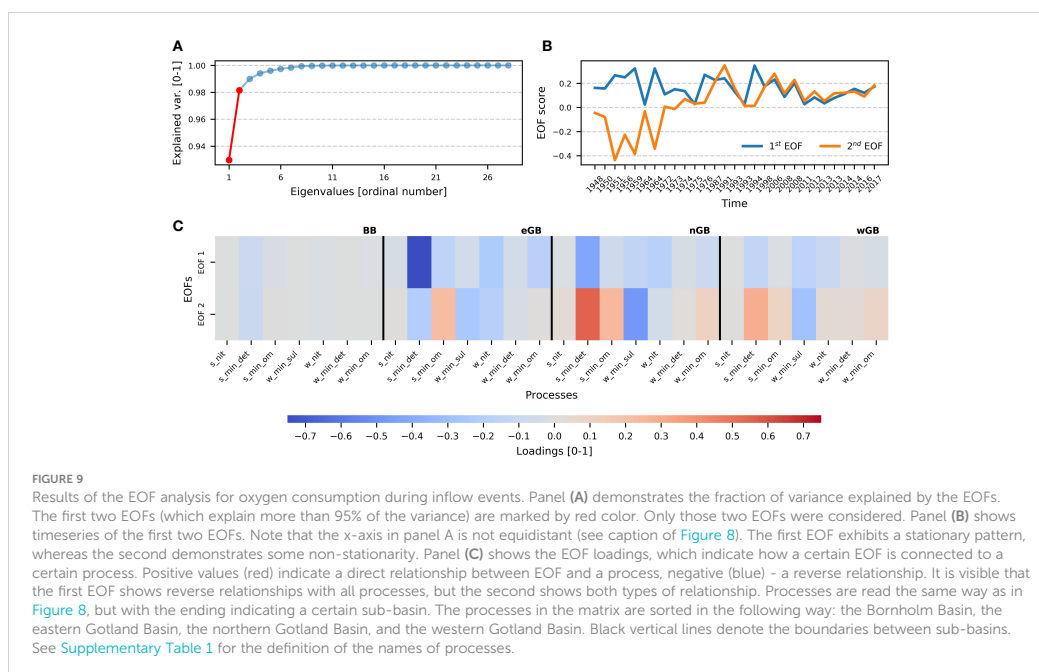
The EOFs for the H₂S budget ([Supplementary Figure 27](#)) show approximately the same pattern, a positive but fluctuating EOF1 and an EOF2 that is slightly increasing. So, we can interpret the spatial pattern of the second EOF in the same way, as a change in the reaction of the Baltic Sea to inflowing oxygen. The production of H₂S in the sediments shifts from the remote wGB to the nGB and the eGB located upstream of the inflow plume. Also, its consumption by oxidation is shifted upstream, but to a lesser extent, which means that the downstream transport of H₂S increases.

The EOF analysis thus essentially confirms the previous findings showing that just these two patterns, (a) a constant spatial signal that varies with the amount of imported oxygen and (b) the change in processes explain more than 95% of the variance. The spatial

redistribution described by the second EOF can almost completely explain the spatiotemporal variability seen in the model, with the first EOF explaining the overwhelming part of the variability. So, it could be stated that inflows' duration and strength govern the oxygen consumption with some little variability explained by the shifted consumption due to the overall deoxygenation.

4 Discussion

The Baltic Sea is experiencing deteriorating oxygen conditions in the deep waters despite the adopted nutrient loads reduction policy ([Carstensen and Conley, 2019](#); [HELCOM, 2021](#); [Krapf et al., 2022](#)). The reason for that might be related to the slow system response to the changing forcing ([Gustafsson et al., 2012](#)) and the "vicious circle" of eutrophication ([Vahtera et al., 2007](#)). This research indicates, based on a model experiment, significant deterioration of oxygen conditions across the central Baltic Sea, which includes significant negative long-term trends of oxygen concentration and positive long-term trends of the concentration of the reduced material (ammonium and hydrogen sulfide). This is clearly shown in [Figure 10](#) (right panels). [Rolf et al. \(2022\)](#) studied the oxygen debt (the amount of oxygen required to oxidize all reduced material) and



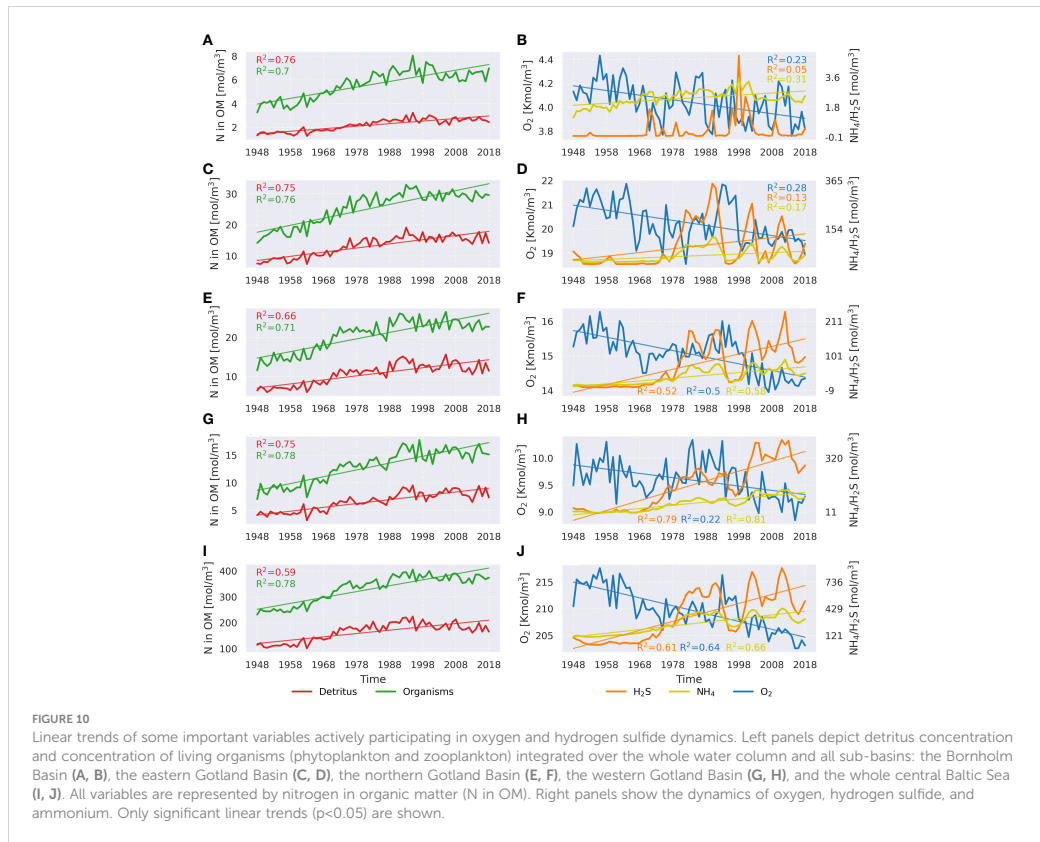
its dynamics based on observational data. They found a significant contribution by NH_4^+ to the oxygen debt, as well as the oxygen debt's increase, especially in the remote basins. Our results are well-aligned with the results by Rolff et al. (2022). As was shown, the mineralization of detritus in the sediments acts as the biggest oxygen sink across all sub-basins. Ammonium is produced as a product of detritus mineralization. Since detritus mineralization is increasing, so is ammonium release. This process explains positive trends in NH_4^+ in the deep waters of the central Baltic Sea and accelerates further oxygen consumption (which is supported by the high oxygen consumption by nitrification observed in the model).

The observed trends in oxygen consumption in the model were attributed to the worsening of oxygen conditions across the central Baltic Sea and uplifting of the redoxcline. The bacterial communities living in the suboxic and sulfidic waters are quite different (Hannig et al., 2006; Anderson et al., 2012). Discussed changes in the central Baltic Sea, especially in the Gotland Basin, should be visible in the long-term observational data related to the bacterial communities. A trend analysis in bacterial abundances, like Hoppe et al. (2013) did for the near-coastal site of Boknis Eck, could be used to verify (or falsify) the modelled trends.

The reason behind elevated trends in phytoplankton and detritus concentrations is not completely clear. The hypothesis about an extended vicious circle proposed by Meier et al. (2018b) is credible. However, we propose an additional positive feedback mechanism: NH_4^+ emerging after detritus mineralization might be advected to the upper layer and thereafter might accelerate further phytoplankton growth. Meier et al. (2018b) conducted a model experiment studying oxygen sinks from 1850 to 2015. They found a

shift toward the water column oxygen consumption. Our study supports this result. In addition, our method allowed the detailed analysis of various sub-basins. It was shown that the most notable change happened in the nGB, where initially, the sediments consumed more oxygen, but today, the water column took the role of the dominant oxygen sink. The same pattern, but not as pronounced, was observed in the eGB and wGB. Meier et al. (2018b) also observed drastically increased water column respiration by phytoplankton and higher trophic levels as well as nitrification, making them the dominant oxygen sinks during the last decade of their simulation. In our study, an increase in phytoplankton and zooplankton biomasses was also found (see Figure 10, left panels) as well as the increasing nitrification. However, no significant role of biota respiration was found. The possible source of disagreement might be related to different process formulations in the different models (RCO-SCOB1 and MOM-ERGOM), specifically the zooplankton respiration, which can be used as a closure term representing the effect of higher trophic levels that are not represented in the model.

The 29 biggest oxygen inflows from 1948 to 2018 were studied separately, using the element marking approach proposed by Ménesguen et al. (2006). Most oxygen was brought to the deep central Baltic Sea during the 1993-1994 inflow events. Although, in accordance with Mohrholz (2018), no trend in the inflow activity was found, and the change of ventilation pattern related to the oxic state of the deep waters shows little variability, significant negative trends of inflow oxygen lifetime were observed everywhere, especially in the nGB and wGB. Therefore, the strongest inflow 2014-2015 did not ventilate deep waters so well not only due to the shorter duration



compared to the 1993-1994 event, but also because of more elevated reducing conditions, especially in the nGB and wGB.

The model uncertainties, presented in Section 2, are likely related to the overestimation of halocline strength, which in turn is related to the overestimated salt transport from the North Sea due to the model resolution. The biggest misrepresentation was observed in the Gulf of Finland and the Bothnian Sea, both of them were excluded from the analysis. However, their effect on the closest nGB was not quantified. Considering the circulation of the deep water in the Baltic Sea, the transport is mainly directed towards the Gulf of Finland and the Bothnian Sea (Elken and Matthäus, 2008). The reversed transport is mainly carried out in the upper layer, so the overestimation of the Gulf of Finland's and the Bothnian Sea's hypoxia should not affect the nGB significantly. Another possible uncertainty, related to the artificially shallowed Landsort Deep, is negligible due to the very small affected area (0.19 km², which corresponds to roughly 1% of the total wGB area, which is 17.62 km²). Deepening the Landsort Deep won't change the composition of the processes either since even the shallowed Landsort Deep is constantly anoxic in our model. The more considerable uncertainties are related to representation of the biological community by ERGOM. In ERGOM, the full spectrum

of phytoplankton species is divided into three functional groups. This assumption does not represent the changing Baltic Sea phytoplankton community (Olli et al., 2011). However, Wasmund et al. (2011) and Suikkanen et al. (2007) found long-term trends in some phytoplankton species based on observational data, proving at least the tendency of increasing phytoplankton concentrations in ERGOM. In addition, in other model studies the increase in phytoplankton biomass, primarily related to the availability of nutrients, is shown (Hieronymus et al., 2018). Also, the absence of refractory detritus in the ERGOM model may lead to exaggeration of the detritus mineralization, which might possibly contribute to the results. In addition to the refractory matter that is completely preserved, organic matter in the sediments can be remineralized at very different rates depending on its composition, which will strongly influence the time scales on which the sedimentary carbon pool influences the oxygen budgets. What is also missing in the model is a representation of iron and manganese, which take part in the redox cycle (Henkel et al., 2019; Schulz-Vogt et al., 2019). In reality, oxidation of H₂S or organic matter may happen implicitly, by reducing iron or manganese oxides and later on oxidizing the reduced metals again by oxygen. Uncertainty is introduced here

since these metals also have sources (e.g. from riverine input) and sinks (e.g. for iron in the form of pyrite).

All the discussed uncertainties make it very difficult to build a robust comparison between modeled processes and the actual ones. Here, we only present qualitative estimates. Hietanen et al. (2012) studied nitrogen-related processes situated at the oxic-anoxic interface in the Baltic proper. They found an increased rate of nitrification at the oxic-anoxic interface, which was also in general observed in our model results. Schneider and Otto (2019) calculated mineralization rates in the deep layer. Although we could not directly compare our results, we also observed some similar patterns, e.g., acceleration after the inflow. However, we were able to validate the vertical oxygen transport in the eGB with the observational data from Holtermann et al. (2022). According to their measurements, the mean annual vertical oxygen flux in the eGB equals to 2.39–3.97 Mt O₂ year⁻¹. Our results suggest a mean flux of 3.75 Mt O₂ year⁻¹, which aligns with their results. However, this comparison might be misleading due to the different definition of the eGB's areas, different depths (our fluxes are calculated across the 70 meters depth layer, not across the pycnocline), and different study periods.

The obtained results shed light on long-term dynamics of processes related to the O₂ and H₂S budgets in the central Baltic Sea, which is not possible to capture *via* the observations due to irregular measurement campaigns and the complexity of the data postprocessing. Although model (Eilola et al., 2011; Meier et al., 2018b; Savchuk, 2018) and observational (Schneider et al., 2002; Gustafsson and Stigebrandt, 2007; Schneider et al., 2010; Schneider and Otto, 2019) studies, as well as studies related to the inflows' propagation (Liblik et al., 2018), have already been conducted, this study covers wide spatial and temporal scales and decomposes O₂ and H₂S budget terms based on their contribution to their variability. The results suggested that a better trophic state for the future Baltic Sea is still beyond the grasp.

5 Conclusions

The employed analysis allowed us to sort the processes, contributing to the O₂ and H₂S budgets, according to their importance for the overall dynamics of those elements. It was found that the inter-annual oxygen dynamics is mainly governed by advection in all sub-basins, whereas hydrogen sulfide is mainly driven by local production and consumption. Mineralization of detritus in the sediments and nitrification are found to be the biggest oxygen sinks. These processes are coupled with each other because ammonium is the result of the oxidation of detritus, so the oxygen debt generated by detritus is resolved in two steps: mineralization of detritus itself and nitrification later. Mineralization of detritus is also the biggest producer of hydrogen sulfide in the sediments in the whole central Baltic Sea. The water column acts as the sink of H₂S, where the oxidation both by NO₃ and O₂ contribute equally to the H₂S consumption.

Analysis of the linear trends in the three categories of processes contributing to the O₂ and H₂S budgets (water column processes, physical fluxes, and sedimentary processes) revealed different regional dynamics. Amplified oxygen consumption in the water column and the sediment was observed in the Bornholm Basin with

the latter dominating. A different pattern was observed in the three Gotland basins that showed a shift to dominating water column consumption. The overall transition from sedimentary to water column oxygen consumption was connected to the shortage of oxygen in the sediments which resulted in the upward movement of the redoxcline. An amplified upward spread of H₂S in the wGB and nGB was found as a result of its deposition there.

We found a dramatic decrease in the content of O₂ from inflows in the nGB and wGB that started in the second half of the 20th century. As no significant trend in inflow strength was found, the decreased lifetime is attributed to the amplified oxygen consumption, which was also observed.

Two significant EOFs of oxygen consumption after inflows per sub-basin were identified with the first EOF explaining more than 90% of the variability and the second explaining approximately 5%. The first EOF showed no spatial dependence and was attributed to the inflow duration and strength. The second EOF describes the response to the deoxygenation of the central Baltic Sea. It leads to the shift of the inflowing O₂ consumption from the mineralization of detritus to the oxidation of H₂S and elemental sulfur in the nGB and wGB. However, since the overwhelming fraction of variability is explained by the first EOF, we conclude that the duration and strength of inflows are the key parameters determining ventilation regardless of the trophic state of the sea.

Data availability statement

Reanalysis and observational data used in this study can be found under Copernicus, ICES, and IOW webpages (<https://data.marine.copernicus.eu/products>, <https://www.ices.dk/data/dataset-collections>, and <https://odin2.io-warnemuende.de>, respectively). The data, which are needed to reproduce the analysis shown in the study, are stored on Zenodo (<https://doi.org/10.5281/zenodo.7661035>). The full monthly-mean generated model data are stored on the IOW server (<http://doi.io-warnemuende.de/10.12754/data-2023-0003>).

Author contributions

LN, HR, and TN set up the model simulation with additional tracers. LN, with the help of TN, performed the budget analysis. LN, with the help of HR, performed the statistical analysis of the model data. LN validated the model data against observations and reanalysis dataset and wrote the manuscript with the help of all co-authors. HM and LN designed the research. HM supervised the work. All authors contributed to the article and approved the submitted version.

Acknowledgments

The research presented in this study is part of the Baltic Earth program (Earth System Science for the Baltic Sea region, see <http://www.baltic.earth>). The model simulations were performed on the computers of the North German Supercomputing Alliance (HLRN).

The long-term observation program of the IOW is partly financed by the Bundesministerium für Verkehr und digitale Infrastruktur (BMVI) and is a part of the Baltic Monitoring Program (COMBINE) of HELCOM. Some observational data were taken from ICES database. Additionally, we would like to thank the two reviewers for their constructive and helpful comments, which facilitated the improvement of the manuscript.

Conflict of interest

The authors declare that the research was conducted in the absence of any commercial or financial relationships that could be construed as a potential conflict of interest.

References

- Almroth-Rosell, E., Eilola, K., Kuznetsov, I., Hall, P., and Meier, M. (2014). A new approach to model oxygen dependent benthic phosphate fluxes in the Baltic Sea. *J. Mar. Syst.* 144, 127–141. doi: 10.1016/j.jmarsys.2014.11.007
- Almroth-Rosell, E., Wählström, I., Hansson, M., Väli, G., Eilola, K., Andersson, P., et al. (2021). A regime shift toward a more anoxic environment in a eutrophic Sea in northern Europe. *Front. Mar. Sci.* 8. doi: 10.3389/fmars.2021.799936
- Anderson, R., Winter, C., and Jürgens, K. (2012). Protist grazing and viral lysis as prokaryotic mortality factors at Baltic Sea oxic–anoxic interfaces. *Mar. Ecol. Prog. Ser.* 467, 1–14. doi: 10.3354/meps10001
- Belkin, I. M. (2009). Rapid warming of Large marine ecosystems. *Prog. Oceanogr.* 81, 207–213. doi: 10.1016/j.pocan.2009.04.011
- Breitbart, D., Levin, L. A., Oshlies, A., Grégoire, M., Chavez, F. P., Conley, D. J., et al. (2018). Declining oxygen in the global ocean and coastal waters. *Science* 359, eaam7240. doi: 10.1126/science.aam7240
- Capell, R., Bartosova, A., Tonderski, K., Arheimer, B., Pedersen, S. M., and Zilans, A. (2021). From local measures to regional impacts: modelling changes in nutrient loads to the Baltic Sea. *J. Hydrol.: Regional Stud.* 36, 100867. doi: 10.1016/j.ejrh.2021.100867
- Carstensen, J., and Conley, D. J. (2019). Baltic Sea Hypoxia takes many shapes and sizes. *Limnol. Oceanogr. Bull.* 28, 125–129. doi: 10.1002/lob.10350
- Carstensen, J., Conley, D. J., Bonsdorff, E., Gustafsson, B. G., Hietanen, S., Janas, U., et al. (2014). Hypoxia in the Baltic Sea: biogeochemical cycles, benthic fauna, and management. *AMBIO* 43, 26–36. doi: 10.1007/s13280-013-0474-7
- Conley, D. J., Björck, S., Bonsdorff, E., Carstensen, J., Destouni, G., Gustafsson, B. G., et al. (2009). Hypoxia-related processes in the Baltic Sea. *Environ. Sci. Technol.* 43, 3412–3420. doi: 10.1021/es802762a
- Conley, D. J., Humborg, C., Rahm, L., Savchuk, O. P., and Wulff, F. (2002). Hypoxia in the Baltic Sea and basin-scale changes in phosphorus biogeochemistry. *Environ. Sci. Technol.* 36, 5315–5320. doi: 10.1021/es025763w
- Copernicus (2023a) *Baltic Sea Biogeochemistry reanalysis*. Available at: https://data.marine.copernicus.eu/product/BALTICSEA_REANALYSIS_BIO_003_012 (Accessed February 16, 2023).
- Copernicus (2023b) *Baltic Sea Physics reanalysis*. Available at: https://data.marine.copernicus.eu/product/BALTICSEA_REANALYSIS_PHY_003_011 (Accessed February 16, 2023).
- Diaz, R. J., and Rosenberg, R. (2008). Spreading dead zones and consequences for marine ecosystems. *Science* 321, 926–929. doi: 10.1126/science.1156401
- Dokmanic, I., Parhizkar, R., Ranieri, J., and Vetterli, M. (2015). Euclidean distance matrices: essential theory, algorithms and applications. *IEEE Signal Process. Mag.* 32, 12–30. doi: 10.1109/MSP.2015.2398954
- Eilola, K., Gustafsson, B. G., Kuznetsov, I., Meier, H. E. M., Neumann, T., and Savchuk, O. P. (2011). Evaluation of biogeochemical cycles in an ensemble of three state-of-the-art numerical models of the Baltic Sea. *J. Mar. Syst.* 88, 267–284. doi: 10.1016/j.jmarsys.2011.05.004
- Ekau, W., Auel, H., Pörtner, H.-O., and Gilbert, D. (2010). Impacts of hypoxia on the structure and processes in pelagic communities (zooplankton, macro-invertebrates and fish). *Biogeosciences* 7, 1669–1699. doi: 10.5194/bg-7-1669-2010
- Elken, J., and Matthäus, W. (2008). “Baltic Sea Oceanography,” in *Assessment of climate change for the Baltic Sea basin* (Berlin: Springer-Verlag), 379–386.
- Elken, J., Pentti, M., Alenius, P., and Stipa, T. (2006). Large Halocline variations in the northern Baltic proper and associated meso- and basin-scale processes. *Oceanologia* 48, 91–117.
- Fennel, K., and Testa, J. M. (2019). Biogeochemical controls on coastal hypoxia. *Ann. Rev. Mar. Sci.* 11, 105–130. doi: 10.1146/annurev-marine-010318-095138
- Funkey, C. P., Conley, D. J., Reuss, N. S., Humborg, C., Jilbert, T., and Slomp, C. P. (2014). Hypoxia sustains cyanobacteria blooms in the Baltic Sea. *Environ. Sci. Technol.* 48, 2598–2602. doi: 10.1021/es404395a
- Geyer, B. (2014). High-resolution atmospheric reconstruction for Europe 1948–2012: coastDat2. *Earth System Sci. Data* 6, 147–164. doi: 10.5194/essd-6-147-2014
- Griffies, S. M. (2004). *Fundamentals of ocean climate models* (Princeton, NJ: Princeton University Press).
- Gustafsson, B. G., Schenk, F., Blenckner, T., Eilola, K., Meier, H. E. M., Müller-Karulis, B., et al. (2012). Reconstructing the development of Baltic Sea eutrophication 1850–2006. *AMBIO* 41, 534–548. doi: 10.1007/s13280-012-0318-x
- Gustafsson, B. G., and Stigebrandt, A. (2007). Dynamics of nutrients and oxygen/hydrogen sulfide in the Baltic Sea deep water. *J. Geophysical Research: Biogeosciences* 112. doi: 10.1029/2006JG000304
- Hale, S. S., Cicchetti, G., and Deacutis, C. F. (2016). Eutrophication and hypoxia diminish ecosystem functions of benthic communities in a new England estuary. In: *Frontiers in marine science* (Accessed February 15, 2023).
- Hannachi, A., Jolliffe, I. T., and Stephenson, D. B. (2007). Empirical orthogonal functions and related techniques in atmospheric science: a review. *Int. J. Climatol.* 27, 1119–1152. doi: 10.1002/joc.1499
- Hannig, M., Braker, G., Dippner, J., and Jürgens, K. (2006). Linking denitrifier community structure and prevalent biogeochemical parameters in the pelagial of the central Baltic proper (Baltic Sea). *FEMS Microbiol. Ecol.* 57, 260–271. doi: 10.1111/j.1574-6941.2006.00116.x
- Hansson, M., and Andersson, L. (2015). *Oxygen survey in the Baltic Sea 2015 extent of anoxia and hypoxia 1960–2015 - the major inflow in December 2014* (Göteborg: Swedish Meteorological and Hydrological Institute).
- Hansson, M., and Viktorsson, L. (2020). *Oxygen survey in the Baltic Sea 2020 - extent of anoxia and hypoxia 1960–2020. report oceanography no. 70* (Göteborg: Swedish Meteorological and Hydrological Institute).
- HELCOM (2021). *HELCOM Baltic Sea action plan – 2021 update* (Helsinki: HELCOM).
- Henkel, J. V., Dellwig, O., Pollehn, F., Herlemann, D. P. R., Leipe, T., and Schulz-Vogt, H. N. (2019). A bacterial isolate from the black Sea oxidizes sulfide with manganese(IV) oxide. *Proc. Natl. Acad. Sci. U.S.A.* 116, 12153–12155. doi: 10.1073/pnas.1906000116
- Hieronymus, J., Eilola, K., Hieronymus, M., Meier, M., Saraiva, S., and Karlson, B. (2018). Causes of simulated long-term changes in phytoplankton biomass in the Baltic proper: a wavelet analysis. *Biogeosciences* 15, 5113–5129. doi: 10.5194/bg-15-5113-2018
- Hietanen, S., Jäntti, H., Buizert, C., Jürgens, K., Labrenz, M., Voss, M., et al. (2012). Hypoxia and nitrogen processing in the Baltic Sea water column. *Limnol. Oceanogr.* 57, 325–337. doi: 10.4319/lo.2012.57.1.0325
- Holtermann, P., Pinner, O., Schwefel, R., and Umlauf, L. (2022). The role of boundary mixing for diapycnal oxygen fluxes in a stratified marine system. *Geophysical Res. Lett.* 49, e2022GL098917. doi: 10.1029/2022GL098917

Publisher’s note

All claims expressed in this article are solely those of the authors and do not necessarily represent those of their affiliated organizations, or those of the publisher, the editors and the reviewers. Any product that may be evaluated in this article, or claim that may be made by its manufacturer, is not guaranteed or endorsed by the publisher.

Supplementary material

The Supplementary Material for this article can be found online at: <https://www.frontiersin.org/articles/10.3389/fmars.2023.1175643/full#supplementary-material>

- Hoppe, H.-G., Giesenhausen, H. C., Koppe, R., Hansen, H.-P., and Gocke, K. (2013). Impact of change in climate and policy from 1988 to 2007 on environmental and microbial variables at the time series station boknis eck, Baltic Sea. *Biogeosciences* 10, 4529–4546. doi: 10.5194/bg-10-4529-2013
- Hordoir, R., Axell, L., Höglund, A., Dieterich, C., Fransner, F., Gröger, M., et al. (2019). Nemo-Nordic 1.0: a NEMO-based ocean model for the Baltic and north seas – research and operational applications. *Geoscientific Model. Dev.* 12, 363–386. doi: 10.5194/gmd-12-363-2019
- Huang, L., Smith, M. D., and Craig, J. K. (2010). Quantifying the economic effects of hypoxia on a fishery for brown shrimp *farfantepenaeus aztecus*. *fishm* 2010, 232–248. doi: 10.1577/C09-048.1
- ICES (2023) *Dataset collections*. Available at: <https://www.ices.dk/data/dataset-collections> (Accessed February 16, 2023).
- IOW (2023) *ODIN 2*. Available at: <https://odin2.io-warnemuende.de> (Accessed February 16, 2023).
- Jetoo, S. (2019). An assessment of the Baltic Sea action plan (BSAP) using the OECD principles on water governance. *Sustainability* 11, 3405. doi: 10.3390/su11123405
- Köuts, M., Maljutenko, I., Elken, J., Liu, Y., Hansson, M., Viktorsson, L., et al. (2021). Recent regime of persistent hypoxia in the Baltic Sea. *Environ. Res. Commun.* 3, 075004. doi: 10.1088/2515-7620/ac0cc4
- Krapf, K., Naumann, M., Duthel, C., and Meier, M. (2022). Investigating hypoxic and eutrophic area changes based on various datasets from the Baltic Sea. *Front. Mar. Sci.* 9. doi: 10.3389/fmars.2022.823476
- Kuzmina, N. P., Zhurbas, V. M., Rudels, B., Stipa, T., Paka, V. T., and Muraviev, S. S. (2008). Role of eddies and intrusions in the exchange processes in the Baltic halocline. *Oceanology* 48, 149–158. doi: 10.1134/S000143700802001X
- Large, W. G., McWilliams, J. C., and Doney, S. C. (1994). Oceanic vertical mixing: a review and a model with a nonlocal boundary layer parameterization. *Rev. Geophys.* 32, 363–403. doi: 10.1029/94RG01872
- Lehmann, A., Myrberg, K., Post, P., Chubarenko, I., Dailidienė, I., Hinrichsen, H.-H., et al. (2022). Salinity dynamics of the Baltic Sea. *Earth Syst. Dynam.* 13, 373–392. doi: 10.5194/esd-13-373-2022
- Lehmann, A., and Post, P. (2015). Variability of atmospheric circulation patterns associated with large volume changes of the Baltic Sea. *Adv. Sci. Res.* 12, 219–225. doi: 10.5194/asr-12-219-2015
- Leppäranta, M., and Myrberg, K. (2009). *Physical oceanography of the Baltic Sea* (Berlin, Heidelberg: Springer). doi: 10.1007/978-3-540-79703-6
- Liblik, T., Naumann, M., Alenius, P., Hansson, M., Lips, U., Nausch, G., et al. (2018). Propagation of impact of the recent major Baltic inflows from the Eastern gotland basin to the gulf of Finland. In: *Frontiers in marine science* (Accessed February 15, 2023).
- Limburg, K. E., and Casini, M. (2018). Effect of marine hypoxia on Baltic Sea cod *gadus morhua*: evidence from otolith chemical proxies. In: *Frontiers in marine science* (Accessed February 15, 2023).
- Matthäus, W., and Franck, H. (1992). Characteristics of major Baltic inflows—a statistical analysis. *Continental Shelf Res.* 12, 1375–1400. doi: 10.1016/0278-4343(92)90060-W
- Matthäus, W., Nehring, D., Feistel, R., Nausch, G., Mohrholz, V., and Lass, H.-U. (2008). “The inflow of highly saline water into the Baltic Sea,” in *State and evolution of the Baltic Sea 1952–2005: a detailed 50-year survey of meteorology and climate, physics, chemistry, biology, and marine environment*, edited by Feistel, R., Nausch, G., and Wasmund, N., (Hoboken, New Jersey: John Wiley & Sons, Inc.) 265–309. doi: 10.1002/9780470283134.ch10
- Meier, H. E. M., Andersson, H. C., Eilola, K., Gustafsson, B. G., Kuznetsov, I., Müller-Karulis, B., et al. (2011). Hypoxia in future climates: a model ensemble study for the Baltic sea. *geophys. Res. Lett.* 38. doi: 10.1029/2011GL049929
- Meier, H. E. M., Edman, M. K., Eilola, K. J., Placke, M., Neumann, T., Andersson, H. C., et al. (2018a). Assessment of eutrophication abatement scenarios for the Baltic Sea by multi-model ensemble simulations. In: *Frontiers in marine science* (Accessed February 15, 2023).
- Meier, H. E. M., Eilola, K., Almqvist-Rosell, E., Schimanke, S., Kniebusch, M., Höglund, A., et al. (2019). Disentangling the impact of nutrient load and climate changes on Baltic Sea hypoxia and eutrophication since 1850. *Clim. Dyn.* 53, 1145–1166. doi: 10.1007/s00382-018-4296-y
- Meier, H. E. M., Väli, G., Naumann, M., Eilola, K., and Frauen, C. (2018b). Recently accelerated oxygen consumption rates amplify deoxygenation in the Baltic Sea. *J. Geophysical Research: Oceans* 123, 3227–3240. doi: 10.1029/2017JC013686
- Ménesguen, A., Cugier, P., and Leblond, I. (2006). A new numerical technique for tracking chemical species in a multi-source, coastal ecosystem, applied to nitrogen causing ulva blooms in the bay of Brest (France). *Limnol. Oceanogr.* 51, 591–601. doi: 10.4319/lo.2006.51.1_part_2.0591
- Mohrholz, V. (2018). Major Baltic inflow statistics – revised. *Front. Mar. Sci.* 5. doi: 10.3389/fmars.2018.00384
- Murtagh, F., and Legendre, P. (2014). Ward’s hierarchical agglomerative clustering method: which algorithms implement ward’s criterion? *J. Classif.* 31, 274–295. doi: 10.1007/s00357-014-9161-z
- Neumann, T. (2007). The fate of river-borne nitrogen in the Baltic Sea – an example for the river oder. *Estuarine Coast. Shelf Sci.* 73, 1–7. doi: 10.1016/j.ecss.2006.12.005
- Neumann, T., Fennel, W., and Kremp, C. (2002). Experimental simulations with an ecosystem model of the Baltic Sea: a nutrient load reduction experiment: NUTRIENT LOAD REDUCTION EXPERIMENT. *global biogeochem. Cycles* 16, 7-1-7-7-119. doi: 10.1029/2001GB001450
- Neumann, T., Koponen, S., Attila, J., Brockmann, C., Kallio, K., Kervinen, M., et al. (2021). Optical model for the Baltic Sea with an explicit CDOM state variable: a case study with model ERGOM (version 1.2). *Geoscientific Model. Dev.* 14, 5049–5062. doi: 10.5194/gmd-14-5049-2021
- Neumann, T., Radtke, H., Cahill, B., Schmidt, M., and Rehder, G. (2022). Non-redfieldian carbon model for the Baltic Sea (ERGOM version 1.2) – implementation and budget estimates. *Geoscientific Model. Dev.* 15, 8473–8540. doi: 10.5194/gmd-15-8473-2022
- Neumann, T., Radtke, H., and Seifert, T. (2017). On the importance of major Baltic inflows for oxygenation of the central Baltic Sea: IMPORTANCE OF MAJOR BALTIC INFLOWS. *J. Geophys. Res. Oceans* 122, 1090–1101. doi: 10.1002/2016JC012525
- Olli, K., Klais, R., Tamminen, T., Ptacnik, R., and Andersen, T. (2011). Long term changes in the Baltic Sea phytoplankton community. *Boreal Environ. Res.* 16 (SUPPL A), 3–14.
- Pacanowski, R. C., and Griffies, S. M. (2000). *MOM 3.0 manual. technical report, geophysical fluid dynamics laboratory*. Princeton, USA 08542. p. 680.
- Pollock, M. S., Clarke, L. M. J., and Dubé, M. G. (2007). The effects of hypoxia on fishes: from ecological relevance to physiological effects. *Environ. Rev.* 15, 1–14. doi: 10.1139/a06-006
- Rabalais, N. N., Turner, R. E., Sen Gupta, B. K., Boesch, D. F., Chapman, P., and Murrell, M. C. (2007). Hypoxia in the northern gulf of Mexico: do the science support the plan to reduce, mitigate, and control hypoxia? *Estuaries Coasts* 30, 753–772. doi: 10.1007/BF02841332
- Radtke, H., Lipka, M., Bunke, D., Morys, C., Woelfel, J., Cahill, B., et al. (2019). Ecological regional ocean model with vertically resolved sediments (ERGOM SED 1.0): coupling benthic and pelagic biogeochemistry of the south-western Baltic Sea. *Geoscientific Model. Dev.* 12, 275–320. doi: 10.5194/gmd-12-275-2019
- Radtke, H., Neumann, T., Voss, M., and Fennel, W. (2012). Modeling pathways of riverine nitrogen and phosphorus in the Baltic Sea. *J. Geophysical Research: Oceans* 117. doi: 10.1029/2012JC008119
- Rolf, C., Walve, J., Larsson, U., and Elmgren, R. (2022). How oxygen deficiency in the Baltic Sea proper has spread and worsened: the role of ammonium and hydrogen sulphide. *Ambio* 51, 2308–2324. doi: 10.1007/s13280-022-01738-8
- Roman, M. R., Brandt, S. B., Houde, E. D., and Pierson, J. J. (2019). Interactive effects of hypoxia and temperature on coastal pelagic zooplankton and fish. In: *Frontiers in marine science* (Accessed February 15, 2023).
- Sanz-Lázaro, C., Valdemarsen, T., and Holmer, M. (2015). Effects of temperature and organic pollution on nutrient cycling in marine sediments. *Biogeosciences* 12, 4565–4575. doi: 10.5194/bg-12-4565-2015
- Savchuk, O. P. (2018). Large-Scale nutrient dynamics in the Baltic Sea 1970–2016. In: *Frontiers in marine science* (Accessed February 15, 2023).
- Schneider, B., Nausch, G., Kubsch, H., and Petersohn, I. (2002). Accumulation of total CO₂ during stagnation in the Baltic Sea deep water and its relationship to nutrient and oxygen concentrations. *Mar. Chem.* 77, 277–291. doi: 10.1016/S0304-4203(02)00008-7
- Schneider, B., Nausch, G., and Pohl, C. (2010). Mineralization of organic matter and nitrogen transformations in the gotland Sea deep water. *Mar. Chem.* 119, 153–161. doi: 10.1016/j.marchem.2010.02.004
- Schneider, B., and Otto, S. (2019). Organic matter mineralization in the deep water of the gotland basin (Baltic sea): rates and oxidant demand. *J. Mar. Syst.* 195, 20–29. doi: 10.1016/j.jmarsys.2019.03.006
- Schulz-Vogt, H. N., Pollehne, F., Jürgens, K., Arz, H. W., Beier, S., Bahlo, R., et al. (2019). Effect of large magnetotactic bacteria with polyphosphate inclusions on the phosphate profile of the suboxic zone in the black Sea. *ISME J.* 13, 1198–1208. doi: 10.1038/s41396-018-0315-6
- Su, J., Dai, M., He, B., Wang, L., Gan, J., Guo, X., et al. (2017). Tracing the origin of the oxygen-consuming organic matter in the hypoxic zone in a large eutrophic estuary: the lower reach of the pearl river estuary, China. *Biogeosciences* 14, 4085–4099. doi: 10.5194/bg-14-4085-2017
- Suikkanen, S., Laamanen, M., and Huttunen, M. (2007). Long-term changes in summer phytoplankton communities of the open northern Baltic Sea. *Estuarine Coast. Shelf Sci.* 71, 580–592. doi: 10.1016/j.ecss.2006.09.004
- Vahtera, E., Conley, D. J., Gustafsson, B. G., Kuosa, H., Pitkänen, H., Savchuk, O. P., et al. (2007). Internal ecosystem feedbacks enhance nitrogen-fixing cyanobacteria blooms and complicate management in the Baltic Sea. *AMBIO* 36, 186–194. doi: 10.1579/00447447
- Väli, G., Meier, H. E. M., and Elken, J. (2013). Simulated halocline variability in the Baltic Sea and its impact on hypoxia during 1961–2007: SIMULATED HALOCLINE VARIABILITY IN THE BALTIC SEA. *J. Geophys. Res. Oceans* 118, 6982–7000. doi: 10.1002/2013JC009192
- Vaquero-Sunyer, R., and Duarte, C. M. (2008). Thresholds of hypoxia for marine biodiversity. *Proc. Natl. Acad. Sci.* 105, 15452–15457. doi: 10.1073/pnas.0803833105

- Voss, M., Bange, H. W., Dippner, J. W., Middelburg, J. J., Montoya, J. P., and Ward, B. (2013). The marine nitrogen cycle: recent discoveries, uncertainties and the potential relevance of climate change. *Philos. Trans. R. Soc. B: Biol. Sci.* 368, 20130121. doi: 10.1098/rstb.2013.0121
- Wald, A. (1943). Tests of statistical hypotheses concerning several parameters when the number of observations is Large. *Trans. Am. Math. Soc.* 54, 426–482. doi: 10.1090/S0002-9947-1943-0012401-3
- Ward, J. H. (1963). Hierarchical grouping to optimize an objective function. *J. Am. Stat. Assoc.* 58, 236–244. doi: 10.2307/2282967
- Wasmund, N., Tuimala, J., Suikkanen, S., Vandepitte, L., and Kraberg, A. (2011). Long-term trends in phytoplankton composition in the western and central Baltic Sea. *J. Mar. Syst.* 87, 145–159. doi: 10.1016/j.jmarsys.2011.03.010
- Whitney, M. M. (2022). Observed and projected global warming pressure on coastal hypoxia. *Biogeosciences* 19, 4479–4497. doi: 10.5194/bg-19-4479-2022
- Yindong, T., Xiwen, X., Miao, Q., Jingjing, S., Yiyang, Z., Wei, Z., et al. (2021). Lake warming intensifies the seasonal pattern of internal nutrient cycling in the eutrophic lake and potential impacts on algal blooms. *Water Res.* 188, 116570. doi: 10.1016/j.watres.2020.116570

Supplementary Material

Limited ventilation of the central Baltic Sea due to elevated oxygen consumption

Lev Naumov*, Thomas Neumann, Hagen Radtke, H.E. Markus Meier

* **Correspondence:** Lev Naumov: lev.naumov@io-warnemuende.de

Supplementary Data

This supplementary material consists of figures and tables that were not included in the paper but still retranslate some important information. Supplementary material has the same structure as the main paper. Within each section, figures and tables relevant to that section are shown. The following abbreviations are used in some figures: BB – the Bornholm Basin, eGB – the eastern Gotland Basin, nGB – the northern Gotland Basin, wGB – the western Gotland Basin.

2 Materials and methods

Supplementary Table 1. Clarification for O₂ processes' names used in the paper. The same name for different processes means the linear combination of those processes.

Process	Group of processes in Figures 4, 5	Name in Supplementary Figure 22	Name in Figures 8, 9
Nitrification of NH ₄ to NO ₃	Water column processes	water_column nitrification	w_nit
Mineralization of detritus	Water column processes	water_column_mineralization	w_min_det
Mineralization of particulate organic carbon (POC)	Water column processes	water_column_mineralization	w_min_om
Mineralization of phosphorus in particulate organic carbon (POCP)	Water column processes	water_column_mineralization	w_min_om
Mineralization of nitrogen in particulate organic carbon (POCN)	Water column processes	water_column_mineralization	w_min_om
Mineralization of dissolved organic carbon (DOC)	Water column processes	water_column_mineralization	w_min_om
Mineralization of dissolved organic nitrogen (DON)	Water column processes	water_column_mineralization	w_min_om
Mineralization of dissolved organic phosphorus (DOP)	Water column processes	water_column_mineralization	w_min_om

Supplementary Material

Respiration of living organisms (lpp, spp, cya, and zoo)	Water column processes	water_column_respiration	Excluded from analysis
Photosynthesis by phytoplankton	Water column processes	Photosynthesis	Excluded from analysis
Oxidation of elemental sulfur	Water column processes	water_column_mineralization	w_min_sul
Oxidation of H ₂ S	Water column processes	water_column_mineralization	w_min_sul
Mineralization of sedimentary detritus	Sedimentary processes	sediments_mineralization	s_min_det
Coupled nitrification/denitrification after mineralization of detritus in oxic sediments	Sedimentary processes	sediments_nitdenit	s_nit
Mineralization of sedimentary particulate organic carbon (POC)	Sedimentary processes	sediments_mineralization	s_min_om
Mineralization of sedimentary phosphorus in particulate organic carbon (POCP)	Sedimentary processes	sediments_mineralization	s_min_om
Mineralization of sedimentary nitrogen in particulate organic carbon (POCN)	Sedimentary processes	sediments_mineralization	s_min_om
Coupled nitrification/denitrification after mineralization of POCN in oxic sediments	Sedimentary processes	sediments_nitdenit	s_nit
Advection	Physical fluxes	advection_<border name> (up, west, south, east, north)	Excluded from analysis
Vertical diffusion	Physical fluxes	diffusion	Excluded from analysis
Downslope mixing	Physical fluxes	other	Excluded from analysis
Convection	Physical fluxes	other	Excluded from analysis

Supplementary Table 2. Clarification for H₂S processes' names used in the paper. The same name for different processes means the linear combination of those processes.

Process	Group of processes in Figures 4, 6	Name in Supplementary Figure 23	Name in Figure 8 and Supplementary Figure 27
Mineralization of particulate organic carbon (POC). Sulfate reduction	Water column processes	mineralization_particular_om	w_min_om
Mineralization of phosphorus in particulate organic carbon (POCP). Sulfate reduction	Water column processes	mineralization_particular_om	w_min_om
Mineralization of nitrogen in particulate organic carbon (POCN). Sulfate reduction	Water column processes	mineralization_particular_om	w_min_om
Mineralization of detritus. Sulfate reduction	Water column processes	detritus_water_column	w_min_det
Mineralization of dissolved organic carbon (DOC). Sulfate reduction	Water column processes	mineralization_dissolved_om	w_min_om
Mineralization of dissolved organic phosphorus (DOP). Sulfate reduction	Water column processes	mineralization_dissolved_om	w_min_om
Mineralization of dissolved organic nitrogen (DON). Sulfate reduction	Water column processes	mineralization_dissolved_om	w_min_om
Oxidation of H ₂ S via O ₂	Water column processes	o2_oxidation	o_ox
Oxidation of H ₂ S via NO ₃	Water column processes	no3_oxidation	n_ox
Mineralization of sedimentary detritus. Sulfate reduction	Sedimentary processes	detritus_sediments	s_min_det
Mineralization of sedimentary particulate organic carbon (POC). Sulfate reduction	Sedimentary processes	mineralization_sediments	s_min_om
Mineralization of sedimentary phosphorus in particulate organic carbon (POCP). Sulfate reduction	Sedimentary processes	mineralization_sediments	s_min_om
Mineralization of sedimentary nitrogen in particulate organic carbon (POCN). Sulfate reduction	Sedimentary processes	mineralization_sediments	s_min_om

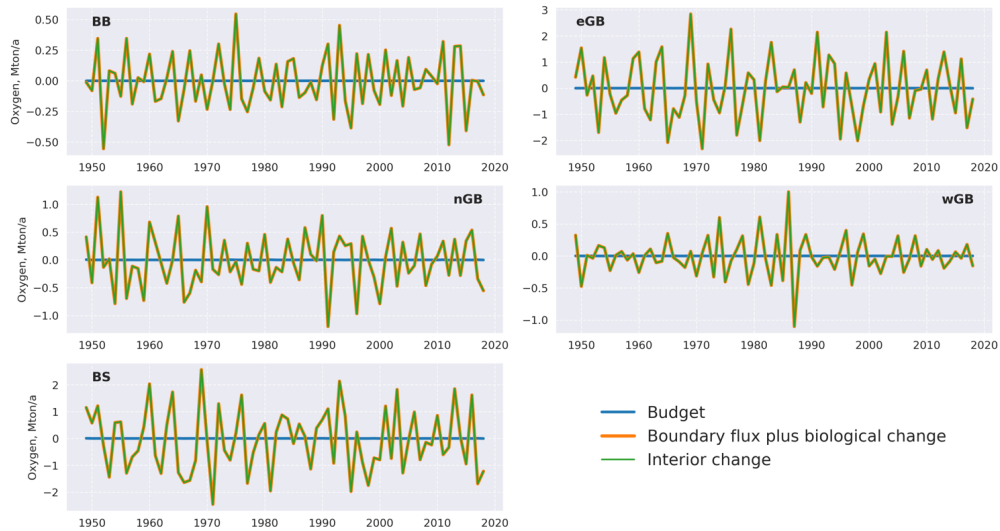
Advection	Physical fluxes	advection_<border name> (up, west, south, east, north)	Excluded from analysis
Vertical diffusion	Physical fluxes	diffusion	Excluded from analysis
Downslope mixing	Physical fluxes	other	Excluded from analysis
Convection	Physical fluxes	other	Excluded from analysis

2.2 Budget analysis

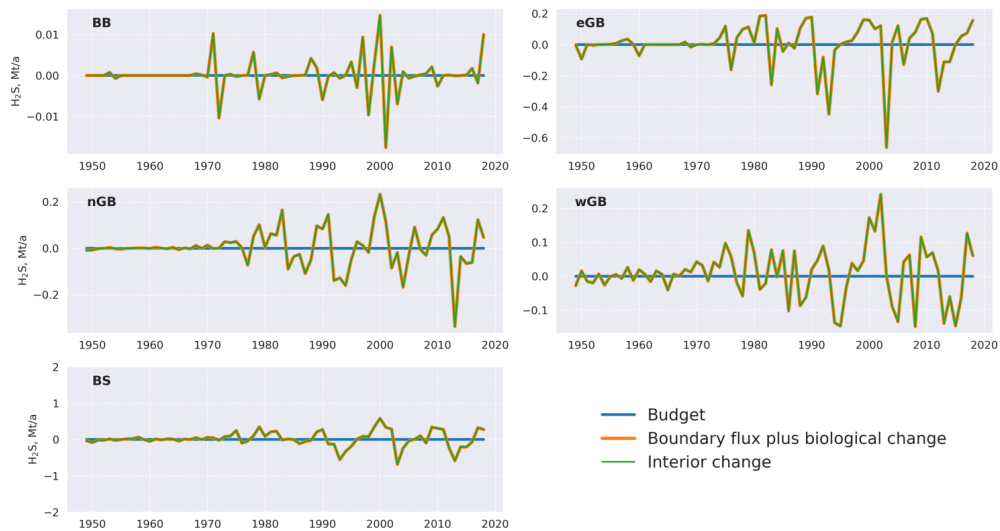
Supplementary Figures 1 and 2 show the budget closure for O₂ (Supplementary Figure 1) and H₂S (Supplementary Figure 2). The budget equation for any tracer is written as follows:

$$\frac{d}{dt} \iiint_V \text{Tr} \, dx \, dy \, dz - \iint_S \vec{v}\vec{n} \, \text{Tr} \, dx \, dy - \iiint_V \frac{\partial \text{Tr}}{\partial t} \, dx \, dy \, dz = 0$$

Where Tr stands for any tracer (O₂ and H₂S in this case), the first term represents the total change of the tracer content within the box (called “interior change” in Supplementary Figures 1 and 2), the second term describes the total transport of the tracer across all boundaries of the box, and the third term depicts the total change of the tracer concentration within the box (for oxygen it represents the change due to biochemical activity within the box). The last two terms are added and shown as the curve named “boundary flux plus biological change” in Supplementary Figures 1 and 2. The curve named “budget” represents the difference between “interior change” and “boundary flux plus biological change”. This difference should be equal to zero according to the equation listed above. It’s visible, that the “budget” curve is close to zero in both Supplementary Figures 1 and 2. This proves that EROM obeys the mass conservation law.



Supplementary Figure 1. Illustration of mass conservation law for oxygen. Interior change (green curve) represents the total change of oxygen content within the box. It equals the boundary flux plus biological change (orange curve), which represents the net oxygen input output within the volume. The orange curve was intentionally made thicker to point out its equality with the green curve.



Supplementary Figure 2. The same as Supplementary Figure 1 but for hydrogen sulfide.

2.3 Validation against the observations

Although also split into 4 boxes, the study area for the validation differs to some extent from the original study area described in the paper (Section 2) and the area shown in Supplementary Figure 3. The differences are explained by the limited number of observations (see Supplementary Figure 4). The validation timeframe is also shorter compared to the main study. It encompasses the period from 1993 to 2018 (26 years). The two main constraints for the period are observations' availability (not shown) and the time limits of the reanalysis dataset.

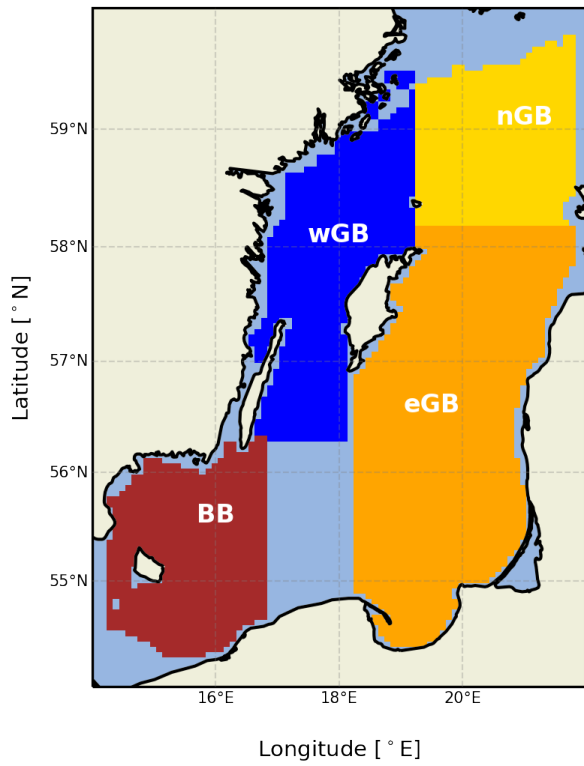
Observations were downloaded as instantaneous point measurements from 1993 to 2018 and post-processed by the following approach. Firstly, they were attributed to a specific region in the central Baltic Sea (BB, wGB, eGB, or nGB). Secondly, observations were interpolated to the model depth levels via the Nearest Neighbor (NN) method. Thirdly, observations were spatially averaged within each region. Finally, interpolated and spatially averaged observations were averaged monthly.

One notable difference between the ERGOM and SCOBIM models is the calculation of hydrogen sulfide (H_2S). In the SCOBIM model, H_2S is not separated from the O_2 state variable and is represented as a negative oxygen concentration, while in ERGOM, the H_2S dynamics is described as a separate tracer equation. To compare model results with reanalysis data, negative oxygen from reanalysis was represented as H_2S using the following equivalent rule: 1 unit of H_2S = -2 units of O_2 (Fonselius 1981).

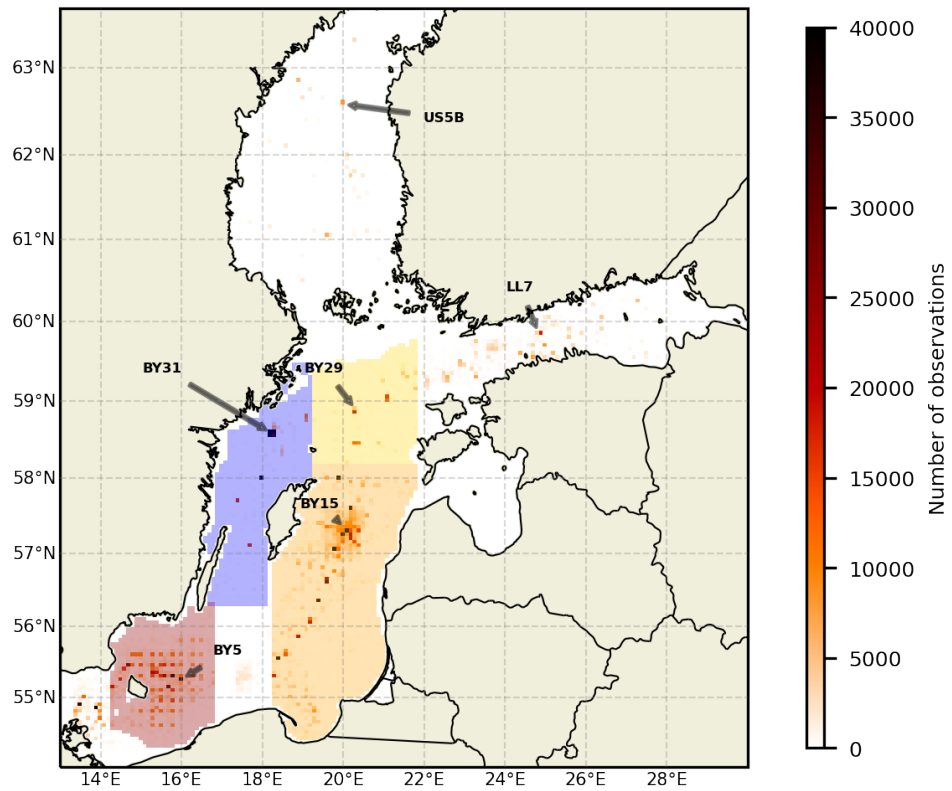
The reanalysis data from Copernicus (see Section 2 in the paper) were acquired as the monthly mean fields from 1993 to 2018. The certain steps were taken to post-process the reanalysis data. In the first step, they were interpolated to the MOM/ERGOM model grid using combined 3-dimensional linear and NN interpolation techniques and attributed to the regions of the central Baltic Sea. In the next step, they were spatially averaged within each region. The MOM/ERGOM data were only spatially averaged within each region.

To consider undersampling and seasonal cycle in the observations, months without samples were excluded from the model and reanalysis data when producing the climatological average. The variability within a month was considered to be small and was neglected.

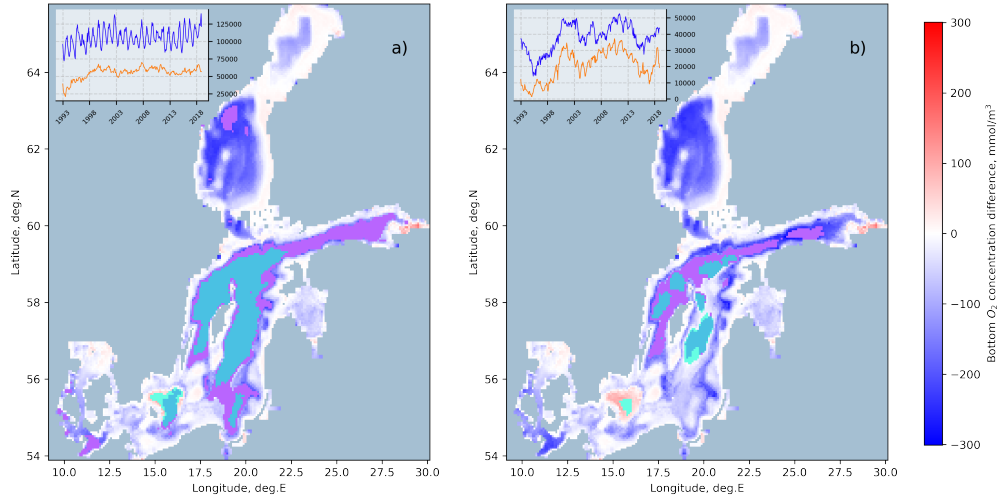
The results of the validation are presented in Supplementary Figures 3-17. Supplementary Figure 3 shows the regions used for validation. Supplementary Figure 4 depicts the spatial distribution of the observations. Note that the number of measurements is shown. One oceanographical profile usually has a few dozen of measurements. Supplementary Figure 5 shows the validation of the hypoxic area (and therefore the bottom O_2) across the whole Baltic Sea. Supplementary Figures 6-11 demonstrate climatological profiles of different variables according to the model, reanalysis, and observations. Supplementary Figures 12 and 13 describe the timeseries of surface and bottom O_2 (Supplementary Figure 12) and bottom H_2S (Supplementary Figure 13) according to the model, reanalysis, and observations. Supplementary Figures 14 and 15 show Taylor Diagrams for O_2 and H_2S data. Supplementary Figures 16 and 17 deal with halocline strength and depth calculation.



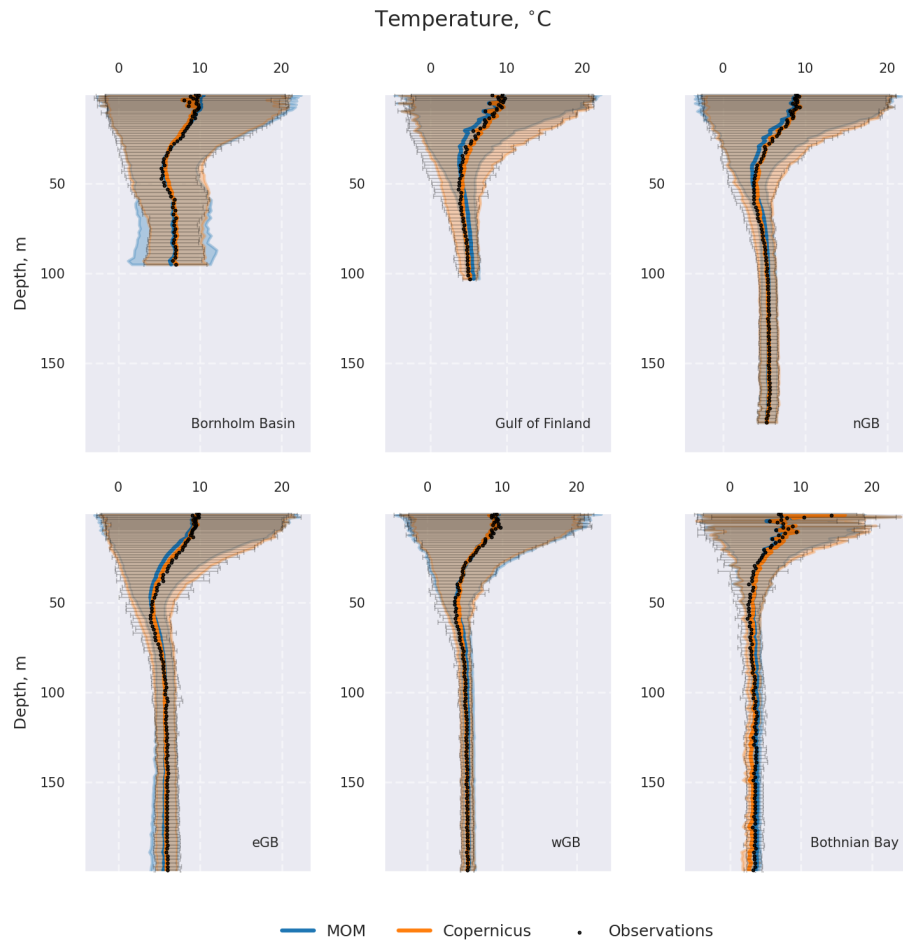
Supplementary Figure 3. The boxes used in validation. The following abbreviations are used: BB – Bornholm Basin, eGB – eastern Gotland Basin, nGB – northern Gotland Basin, wGB – western Gotland Basin.



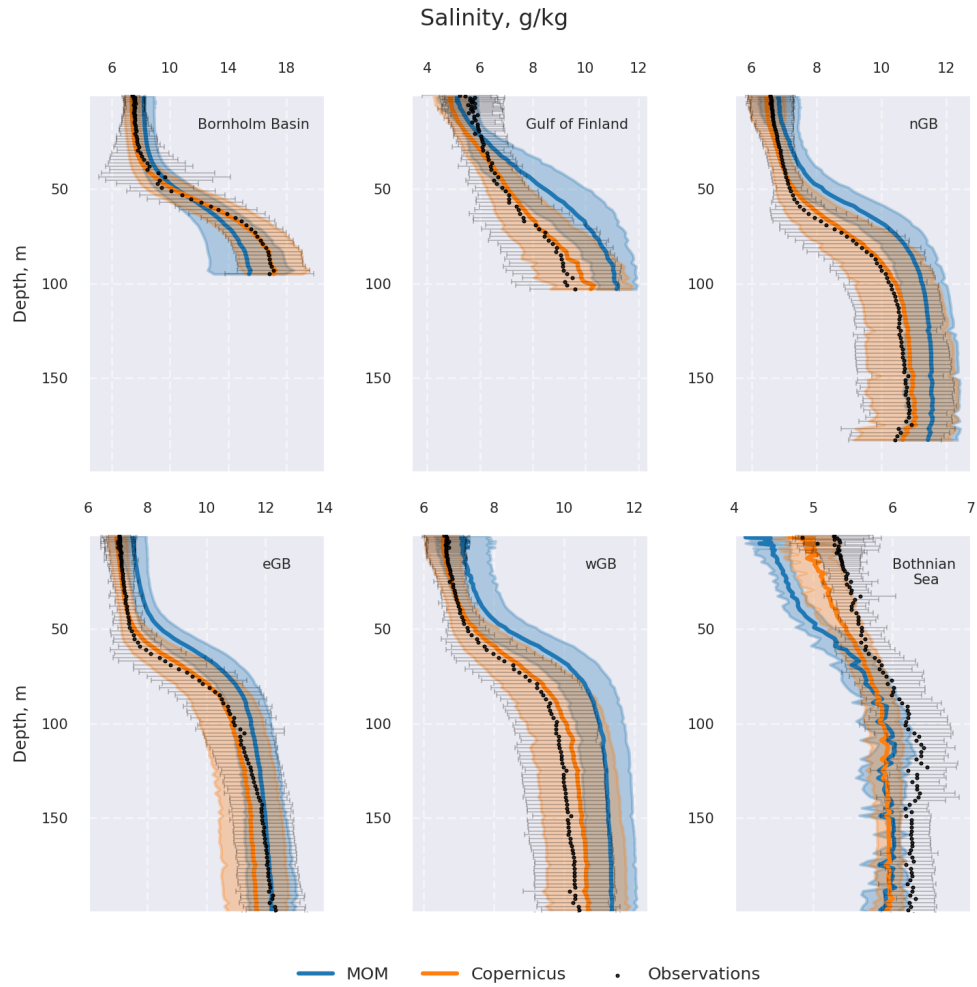
Supplementary Figure 4. Spatial distribution of the observations taken from ICES and IOW databases (both bottle T, S, O₂, and nutrients data and CTD T, S, and O₂ measurements) from 1993 to 2018. Here, one observation means a single measurement. Typical oceanographic profile has few dozens of measurements.



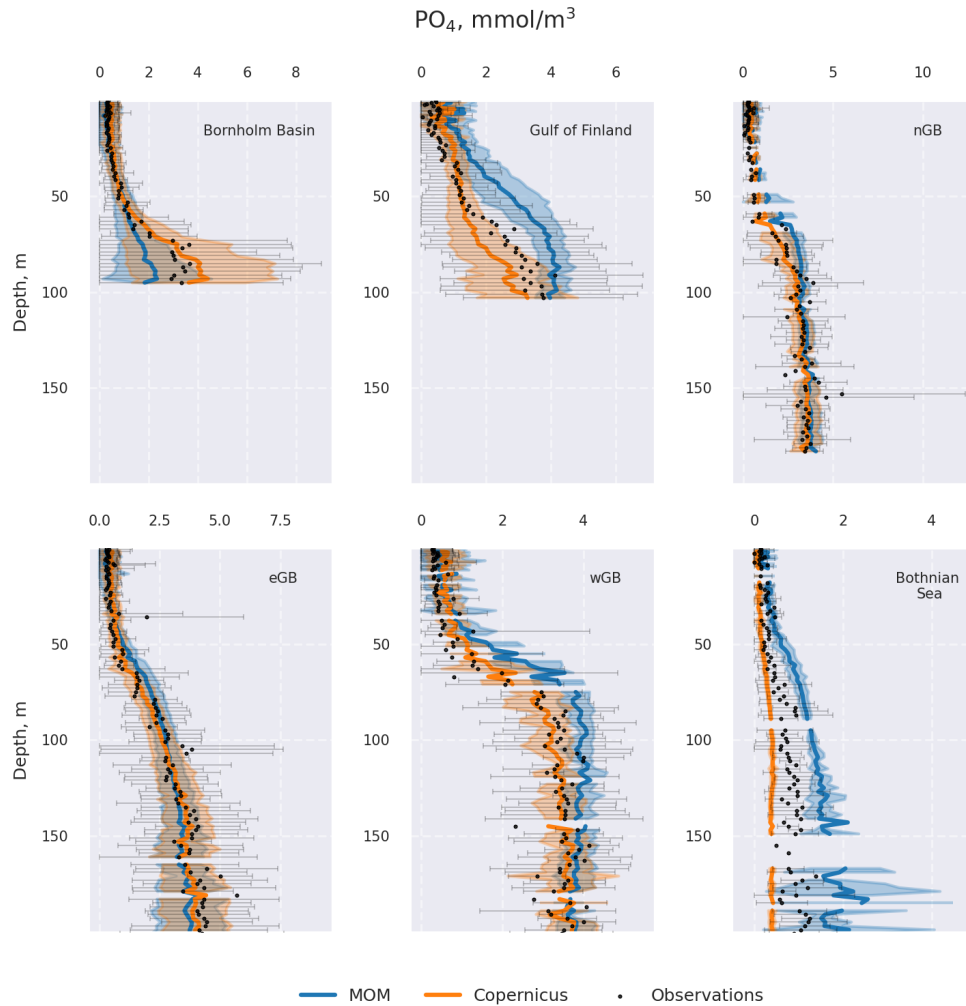
Supplementary Figure 5. Comparison of hypoxic (A) and anoxic (B) zones. Filling shows the differences between model and reanalysis data (model-reanalysis). Upper left plots demonstrate total hypoxic (A) and anoxic (B) areas in km². Orange curve represents reanalysis data, blue – model data. Violet filling highlights regions, where more than half of the study period (1993-2018) hypoxic (A) or anoxic (B) conditions were observed according to the model, but not to the reanalysis. Light turquoise filling – same as violet, but according to the reanalysis. Dark turquoise filling shows where both in the model and reanalysis data hypoxia (A) and anoxia (B) occurred more than half of the study period.



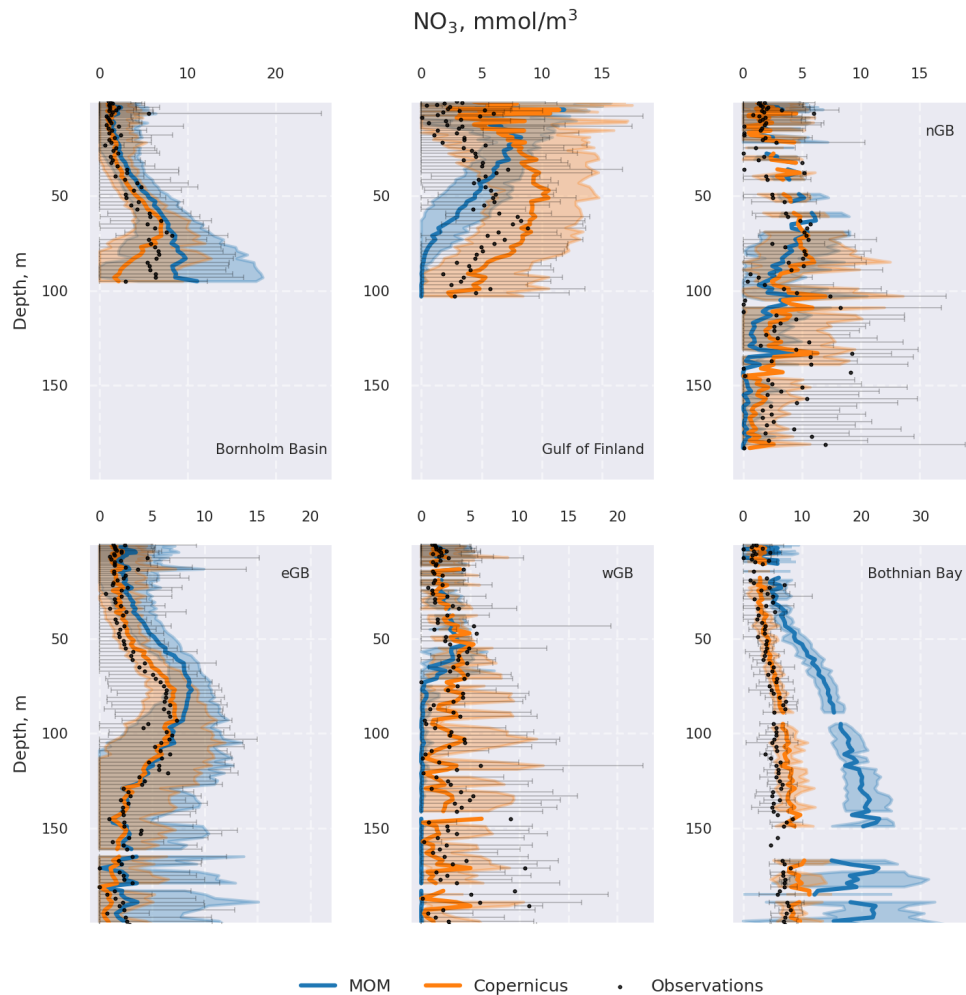
Supplementary Figure 6. Average climatology (1993-2018) profiles of temperature. Translucent areas and error bars represent 2σ deviation for mean for model/reanalysis and observational data respectively. To account for the sparseness of observations, the model and reanalysis data were undersampled.



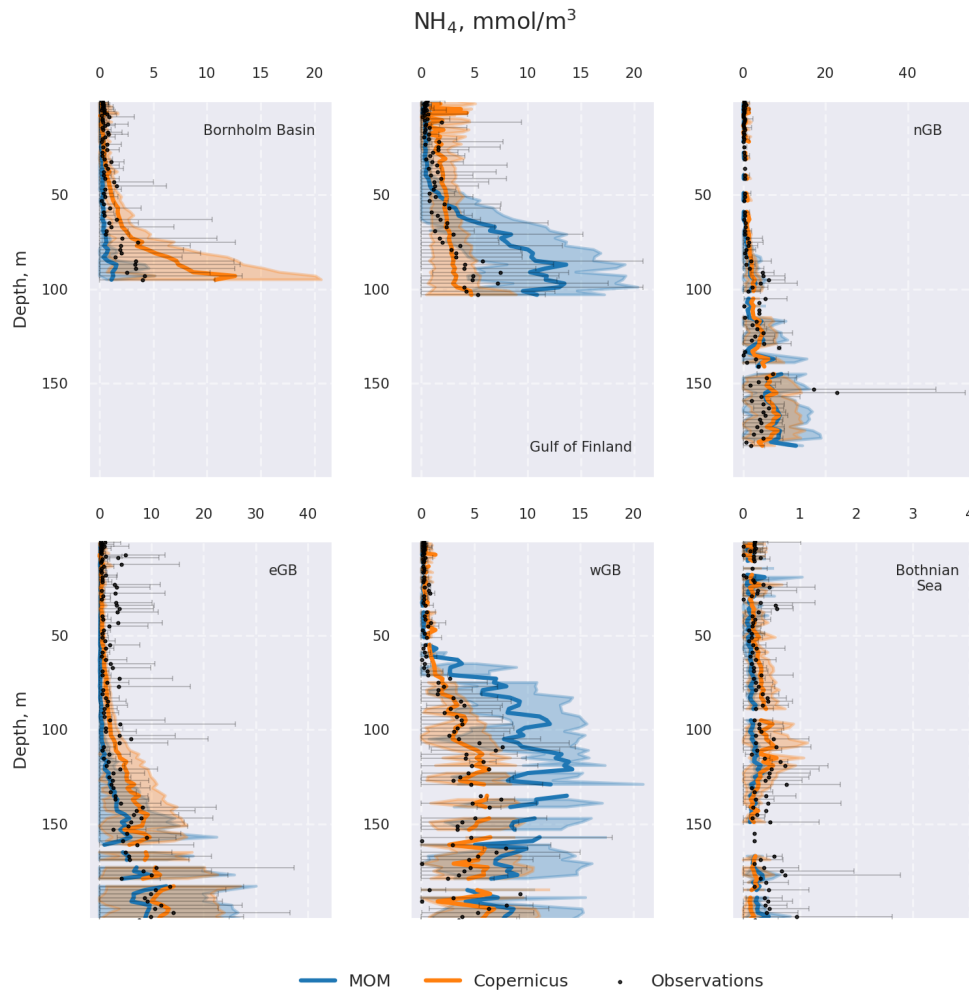
Supplementary Figure 7. Average climatology (1993-2018) profiles of salinity. Translucent areas and error bars represent 2σ deviation for mean for model/reanalysis and observational data respectively. To account for the sparseness of observations, the model and reanalysis data were undersampled.



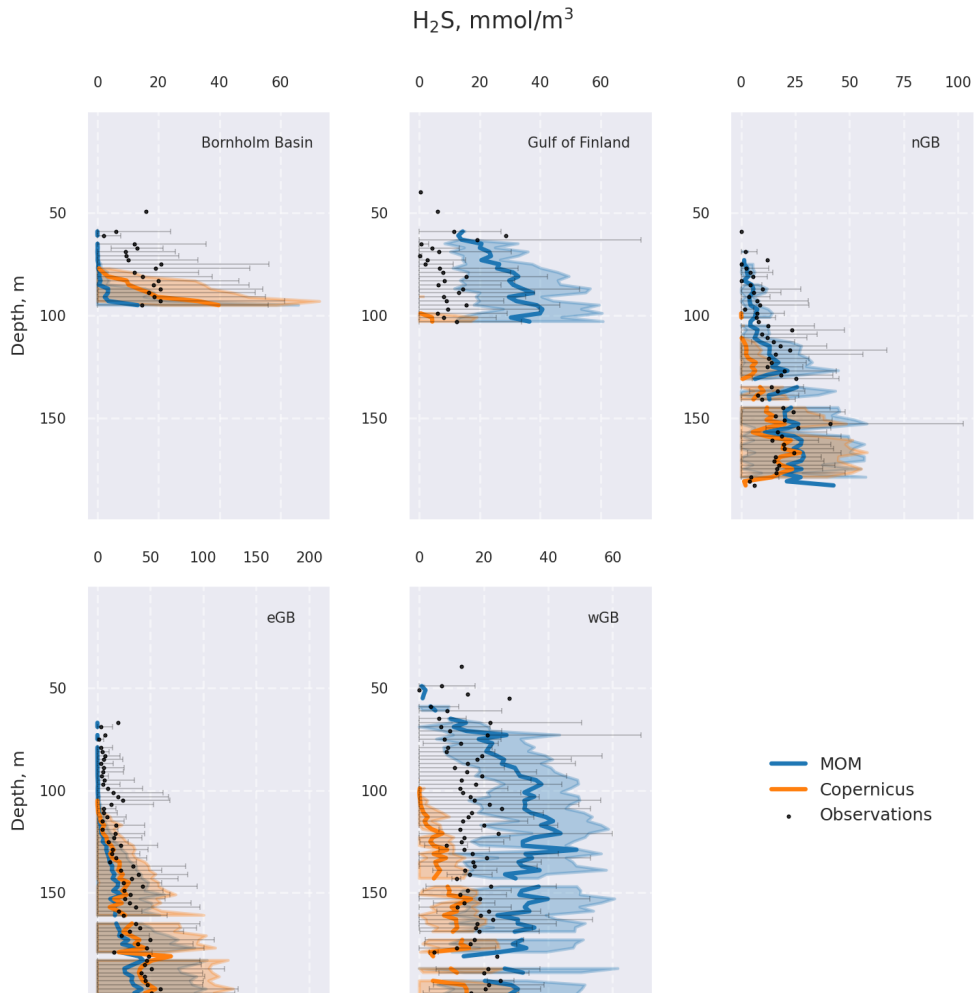
Supplementary Figure 8. Average climatology (1993-2018) profiles of phosphate. Translucent areas and error bars represent 2σ deviation for mean for model/reanalysis and observational data respectively. To account for the sparseness of observations, the model and reanalysis data were undersampled.



Supplementary Figure 9. Average climatology (1993-2018) profiles of nitrate. Translucent areas and error bars represent 2σ deviation for mean for model/reanalysis and observational data respectively. To account for the sparseness of observations, the model and reanalysis data were undersampled.

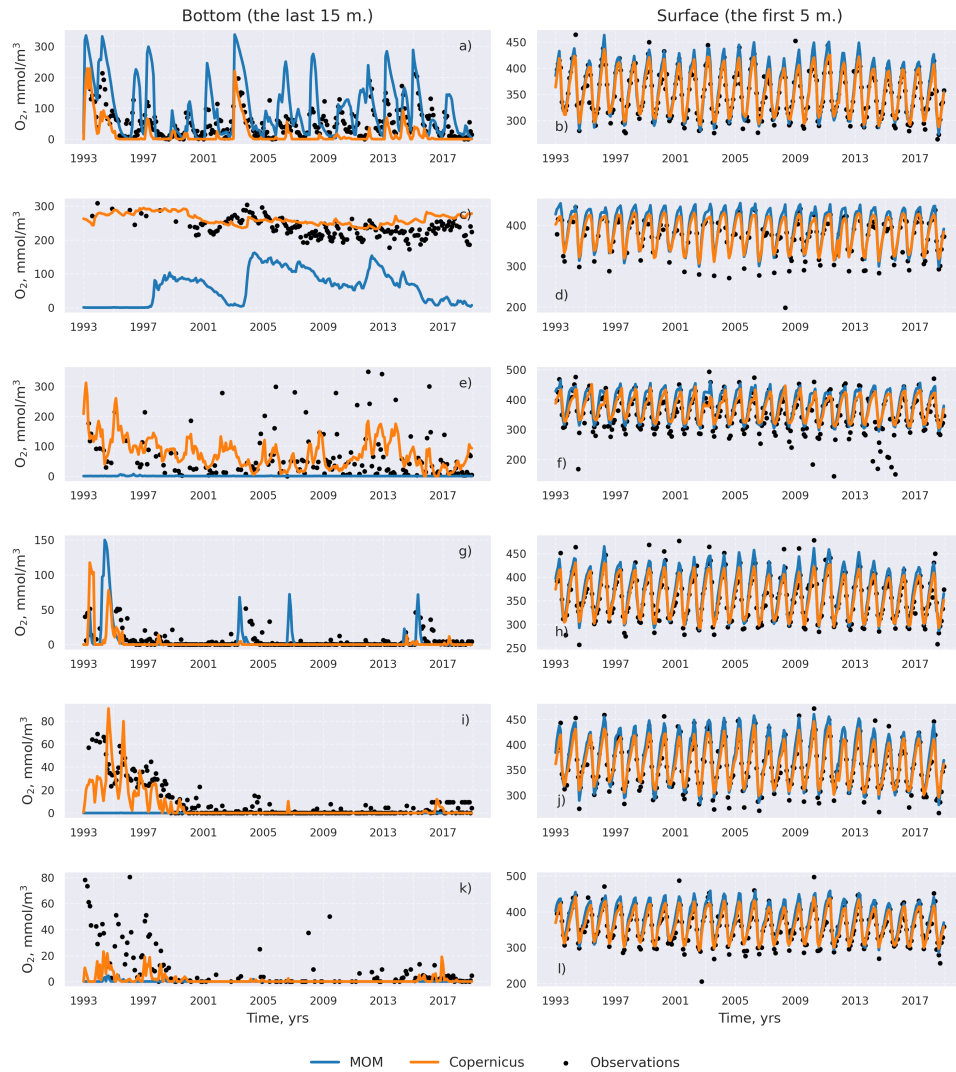


Supplementary Figure 10. Average climatology (1993-2018) profiles of ammonium. Translucent areas and error bars represent 2σ deviation for mean for model/reanalysis and observational data respectively. To account for the sparseness of observations, the model and reanalysis data were undersampled.

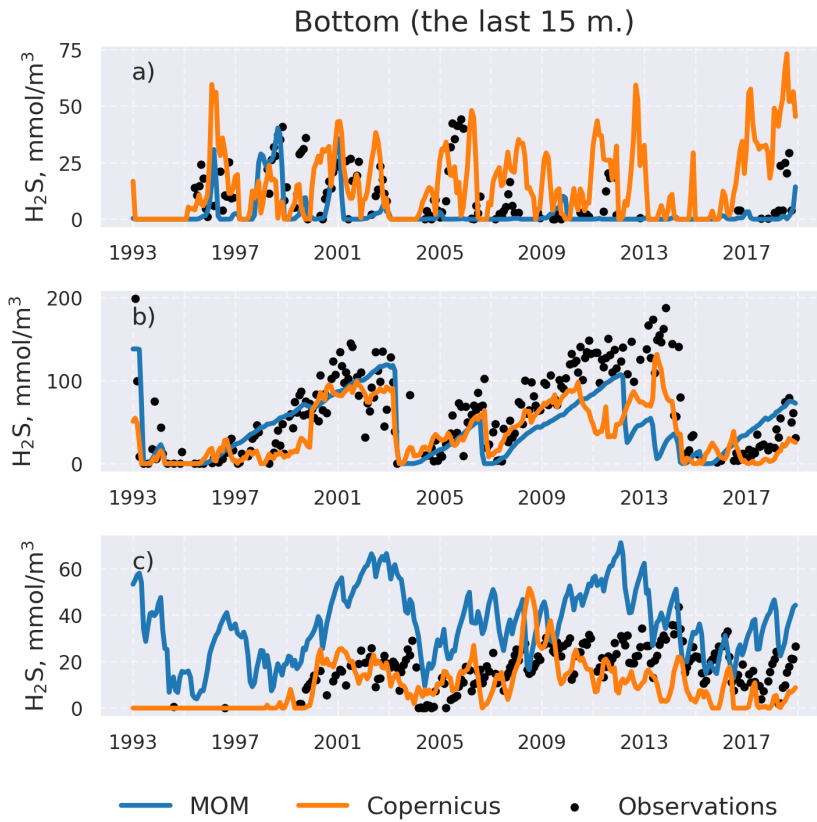


Supplementary Figure 11. Average climatology (1993-2018) profiles of hydrogen sulfite. Translucent areas and error bars represent 2σ deviation for mean for model/reanalysis and observational data respectively. To account for the sparseness of observations, the model and reanalysis data were undersampled.

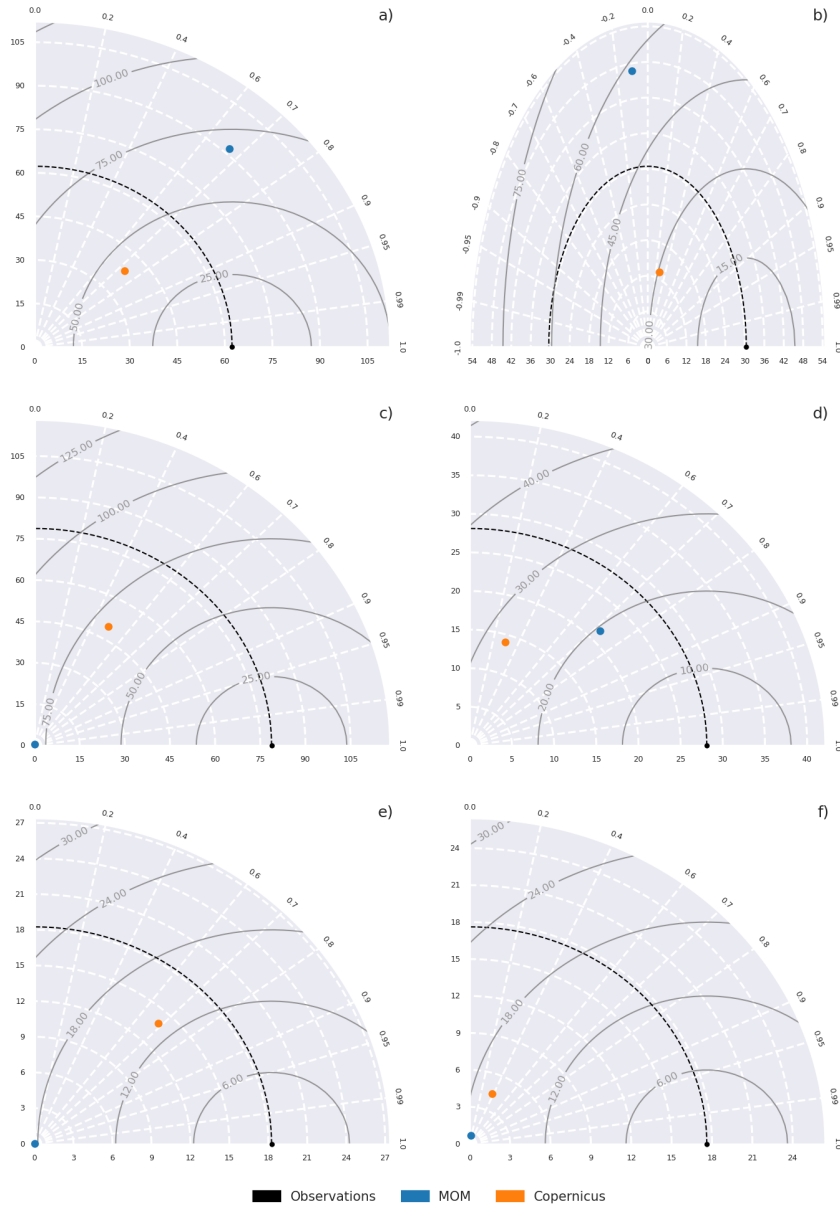
Timeseries validation and Taylor diagrams will be presented only for oxygen and hydrogen sulfite.



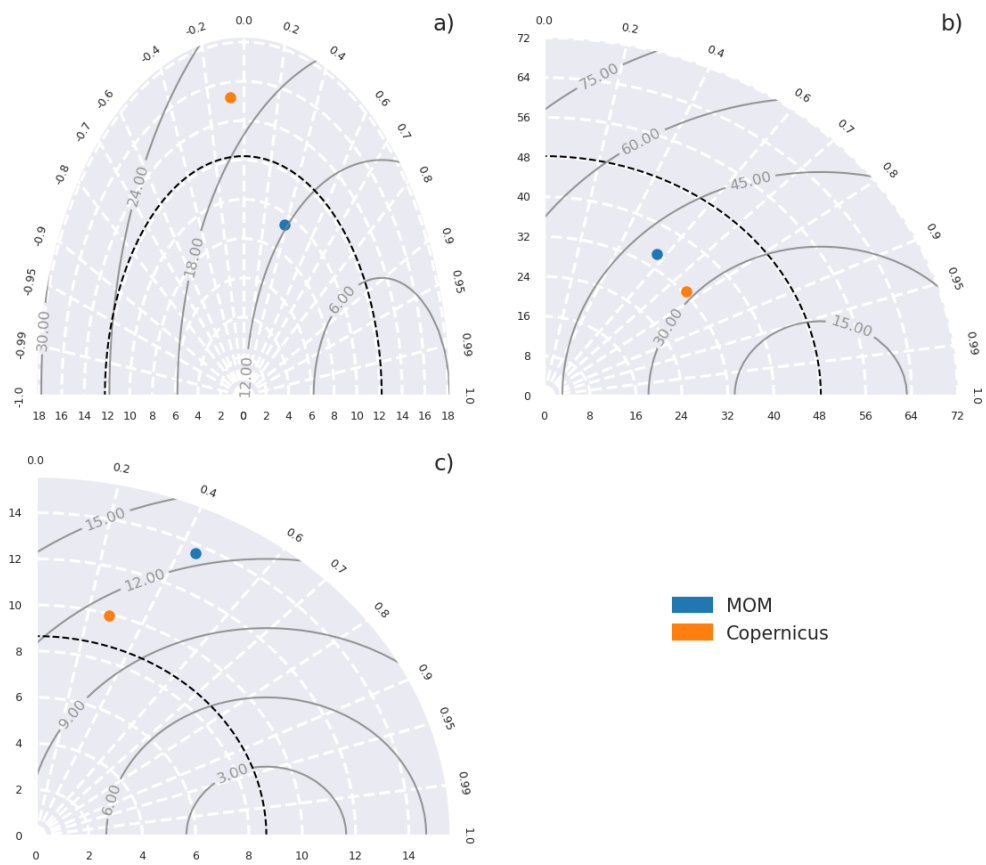
Supplementary Figure 12. Comparison of timeseries of surface (right panel) and bottom (left panel) oxygen concentrations for the Bornholm Basin (a,b), the Bothnian Sea (c,d), the Gulf of Finland (e,f), the eastern Gotland Basin (g,h), the western Gotland Basin(i,j), and the northern Gotland Basin (k,l).



Supplementary Figure 13. Comparison of timeseries of bottom hydrogen sulfite concentrations for the Bornholm Basin (a), the eastern Gotland Basin (b), and the western Gotland Basin (c).



Supplementary Figure 14. Taylor diagrams of bottom oxygen concentrations for BB (a), BS (b), GF (c), eGB (d), wGB(e), and nGB(f).



Supplementary Figure 15. Taylor diagrams of bottom hydrogen sulfide concentrations for BB (a), eGB (b), and wGB(c).

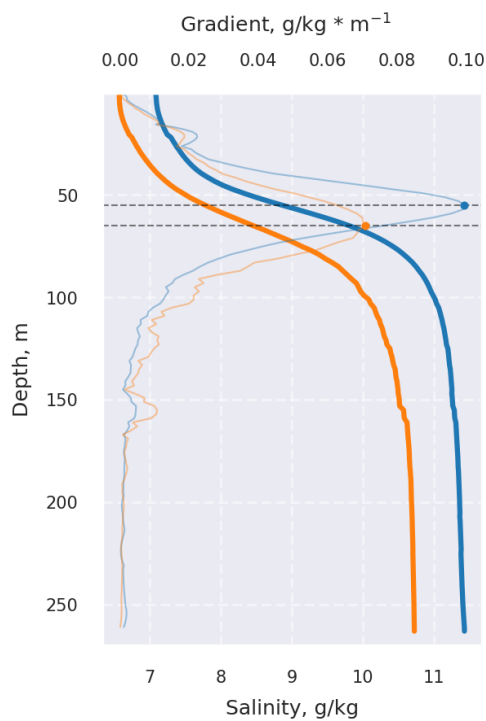
To calculate halocline depth and strength, the approach from Väli et al. (2013) was adopted. Halocline depth was defined as the depth where the maximum of the first derivative of the salinity with respect to depth is observed:

$$h_{hal} = z(\max(\frac{\partial S}{\partial z}))$$

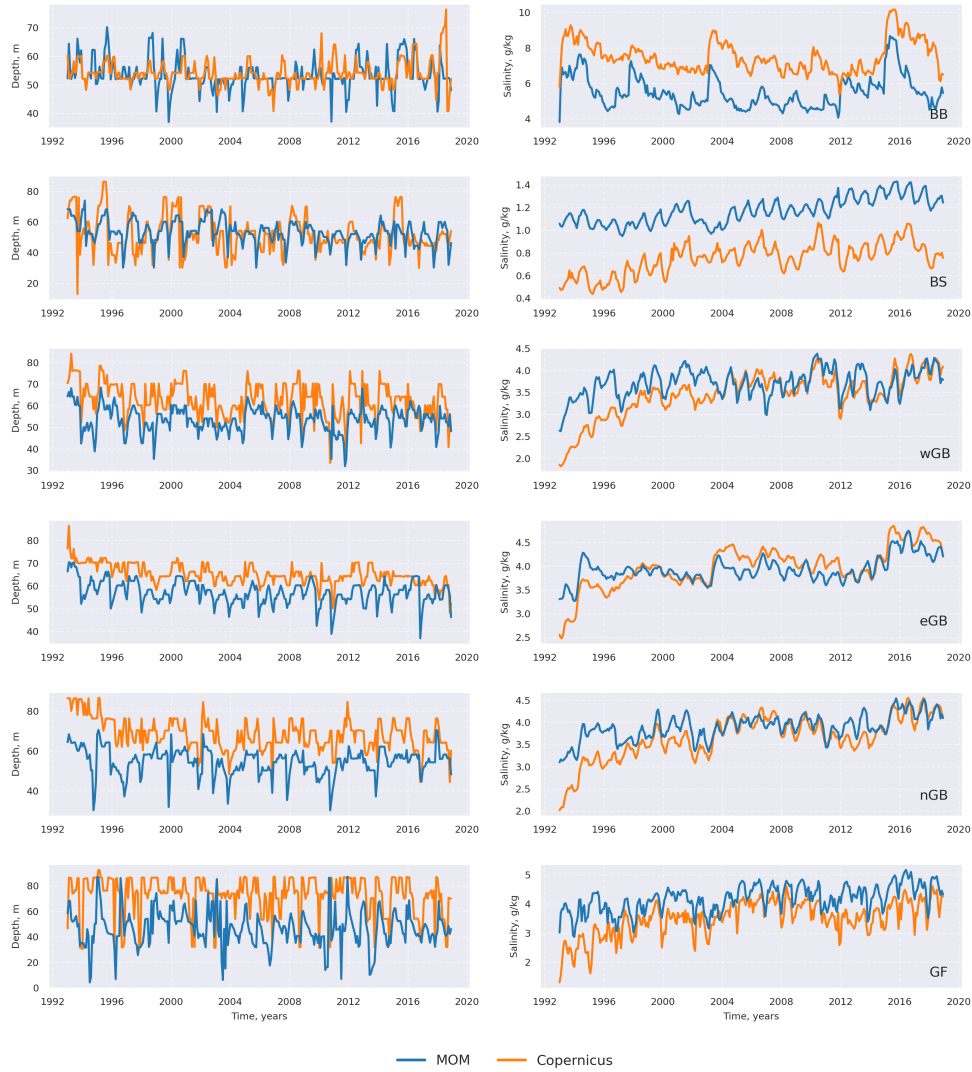
Halocline strength was calculated as the difference between the average salinity in bottom and top layers (separated by the halocline depth):

$$P_{hal} = \bar{s}_{lower} - \bar{s}_{upper}$$

The only modification to Väli et al. (2013) approach was applying the Savitzky-Golay filter (Savitzky and Golay, 1964) to the analyzed salinity profiles to make them smoother. The approach is illustrated in Supplementary Figure 16.



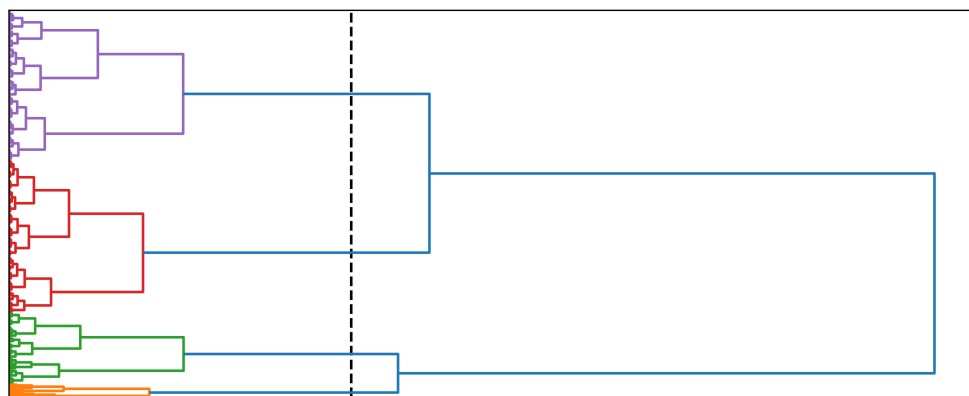
Supplementary Figure 16. Halocline depth identification example. Vivid lines represent salinity profiles, translucent lines – their derivatives. Dotted lines show estimated halocline depth with points highlighting derivative maximum. The blue color denotes MOM model data, orange – Copernicus reanalysis data.



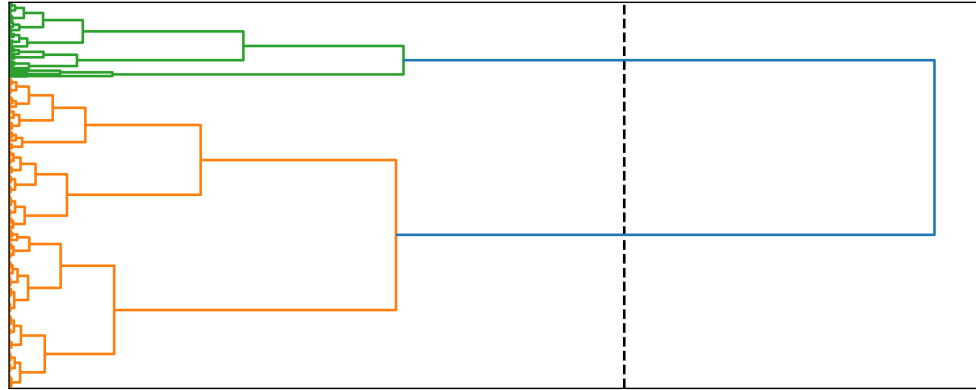
Supplementary Figure 17. Estimated halocline depth (left panel) and halocline strength (right panel). The following abbreviations are used: BB – Bornholm Basin, BS – Bothnian Sea, wGB – western Gotland Basin, eGB – eastern Gotland Basin, nGB – northern Gotland Basin, GF – Gulf of Finland. The notable differences are observed between halocline strength in the Bornholm Basin (MOM demonstrates less strength), Bothnian Sea (MOM demonstrates more strength), and Gulf of Finland (MOM demonstrates more strength).

2.4 Statistical methods used for sources and sink processing

This section shows the figures and tables related to the inflows' identification. Supplementary Figures 18 and 19 show dendrogram plots for oxygen (Supplementary Figure 18) and salt (Supplementary Figure 19) inflows. Supplementary Figure 20 demonstrates an example of detected inflows for the year 1948. Supplementary Tables 3 and 4 show the ten most significant oxygen (Supplementary Table 3) and salt (Supplementary Table 4) inflows. Supplementary Figure 21 shows the temporal distribution of salt inflows as well as the distribution of their strength.

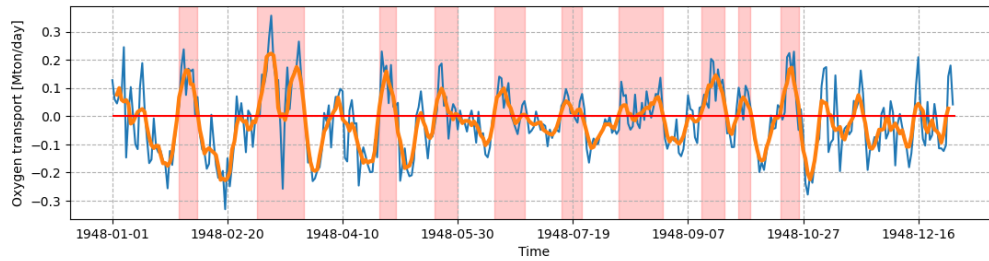


Supplementary Figure 18. Dendrogram plot for oxygen inflows clusterization. The horizontal axis depicts the distance between classes (labels are not shown). The vertical axis represents the classes. In the beginning, all datapoints form distinct clusters. In the end, all datapoints are merged into one cluster. The black dashed line shows the cutoff distance at which certain distinct clusters are formed (they are denoted by different colors). Four clusters are selected in this diagram.



Supplementary Figure 19. Dendrogram plot for salt inflows clusterization. The structure is the same as for Supplementary Figure 18. Two clusters are selected in this diagram.

2.5 Inflows detection algorithm



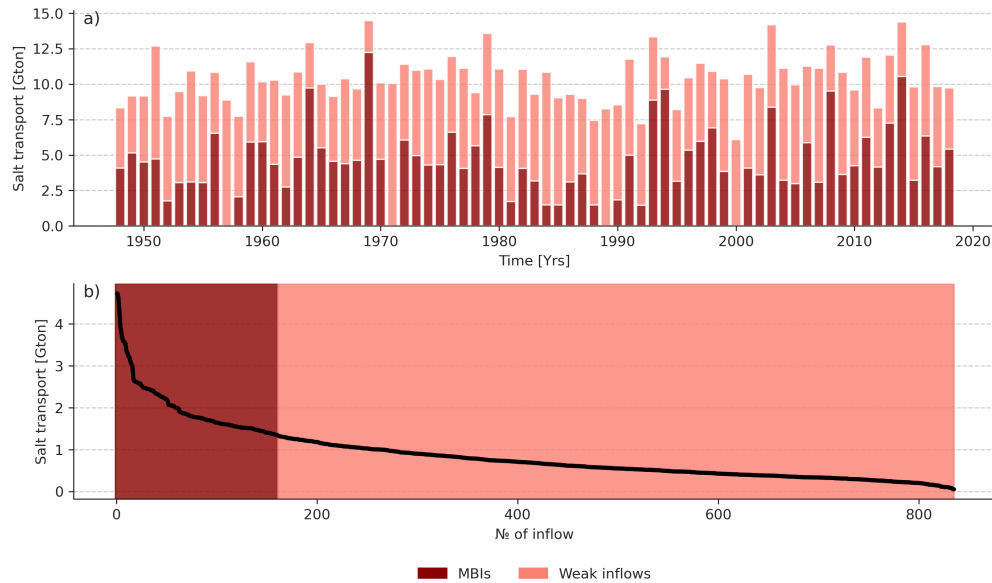
Supplementary Figure 20. Oxygen zonal transport across the Arkona transect (see Figure 1 in the paper). The orange curve denotes filtered data (5-day rolling mean filter), and the red curve indicates zero. Identified inflows are denoted by transparent red areas. The only year 1948 is shown.

Supplementary Table 3. Ten biggest oxygen inflows.

Inflow [№]	Starting date	Duration [days]	Total transport [Mt O ₂]
1	1994-03-03	20	3.23
2	1993-01-05	21	3.12
3	2014-12-03	21	2.92
4	1993-12-01	20	2.84
5	1975-11-16	39	2.82
6	1951-11-17	23	2.74
7	1998-10-08	24	2.71
8	1972-03-13	26	2.62
9	1950-02-04	21	2.57
10	2012-02-11	17	2.56

Supplementary Table 4. Ten biggest salt inflows.

Inflow [№]	Starting date	Duration [days]	Total transport [Gt Salt]
1	1951-11-10	34	4.73
2	2014-12-03	23	4.63
3	1975-11-16	44	4.31
4	1994-03-03	24	3.94
5	1993-12-01	24	3.78
6	1972-03-12	28	3.65
7	1998-10-08	24	3.59
8	1993-01-05	21	3.57
9	1964-04-02	44	3.53
10	2011-11-17	29	3.37



Supplementary Figure 21. Yearly total salt transport by inflows across Arkona transect (A). Coral color represents transport by the weak salt inflows, scarlet color represents transport by the strong salt inflows. (B) shows the distribution of salt transport per inflow. Here, the transport of the strong inflows is framed by the scarlet color. The transport of the weak inflows is framed by the coral color. It is shown that the weakest strong inflow transported around 1.5 Gt of salt into the study domain.

3 Results

3.2 Processes governing the O₂ and H₂S dynamics in the central Baltic Sea

This section shows tables and figures related to Section 3.1 in the paper. Supplementary Tables 3-8 show the climatological mean values (1948-2018) of the most significant processes contributing to the O₂ and H₂S budgets. Mt stands for 10⁹ kg; Kt stands for 10⁶ kg. Supplementary Figures 22 and 23 demonstrate the results of linear regression analysis with different processes contributing to the O₂ and H₂S budgets. Supplementary Tables 9 and 10 demonstrate the results of the linear trend analysis for the significant processes contributing to O₂ and H₂S budgets.

3.2.1 The biggest O₂ and H₂S sources and sinks

Supplementary Table 5. The biggest physical processes in different sub-basins.

Bornholm Basin	
Advection, upper boundary	0.81 Mt O ₂
Diffusion, upper boundary	0.08 Mt O ₂
Eastern Gotland Basin	
Advection, upper boundary	3.06 Mt O ₂
Advection, western boundary	2.14 Mt O ₂
Advection, northern boundary	-1.91 Mt O ₂
Diffusion, upper boundary	0.32 Mt O ₂
Northern Gotland Basin	
Advection, southern boundary	1.91 Mt O ₂
Advection, western boundary	-0.32 Mt O ₂
Diffusion, upper boundary	0.24 Mt O ₂
Advection, upper boundary	0.2 Mt O ₂
Western Gotland Basin	
Advection, upper boundary	0.46 Mt O ₂
Advection, eastern boundary	0.32 Mt O ₂
Vertical diffusion	0.15 Mt O ₂

Supplementary Table 6. Water column processes consuming most of the oxygen in different basins.

Bornholm Basin	
Nitrification of NH ₄ to NO ₃	-0.11 Mt O ₂
Mineralization of POC	-0.08 Mt O ₂
Mineralization of DOP	-0.03 Mt O ₂
Oxidation of sulfur to SO ₄	-0.02 Mt O ₂
Mineralization of detritus	-0.02 Mt O ₂
Eastern Gotland Basin	
Nitrification of NH ₄ to NO ₃	-0.57 Mt O ₂
Mineralization of POC	-0.29 Mt O ₂
Oxidation of sulfur to SO ₄	-0.2 Mt O ₂
Mineralization of detritus	-0.15 Mt O ₂
Mineralization of DOP	-0.09 Mt O ₂
Northern Gotland Basin	
Nitrification of NH ₄ to NO ₃	-0.41 Mt O ₂
Oxidation of sulfur to SO ₄	-0.35 Mt O ₂
Mineralization of POC	-0.13 Mt O ₂
Oxidation of H ₂ S to sulfur	-0.08 Mt O ₂
Mineralization of detritus	-0.08 Mt O ₂
Western Gotland Basin	
Oxidation of sulfur to SO ₄	-0.3 Mt O ₂
Nitrification of NH ₄ to NO ₃	-0.21 Mt O ₂
Oxidation of H ₂ S to sulfur	-0.08 Mt O ₂
Mineralization of POC	-0.05 Mt O ₂
Mineralization of detritus	-0.02 Mt O ₂

Supplementary Table 7. Processes in the sediments consuming most of the oxygen in different basins. Here, POCN means nitrogen in particulate organic carbon. This type of organic matter forms when there is a lack of phosphorus, so living organisms cannot produce classic organic matter.

Bornholm Basin	
Mineralization of detritus	-0.46 Mt O ₂
Mineralization of POC	-0.07 Mt O ₂
Mineralization of POCN	-0.05 Mt O ₂
Nitrification/denitrification	-0.03 Mt O ₂
Eastern Gotland Basin	
Mineralization of detritus	-1.75 Mt O ₂
Mineralization of POCN	-0.17 Mt O ₂
Mineralization of POC	-0.15 Mt O ₂
Nitrification/denitrification	-0.08 Mt O ₂
Northern Gotland Basin	
Mineralization of detritus	-0.74 Mt O ₂
Mineralization of POC	-0.06 Mt O ₂
Mineralization of POCN	-0.06 Mt O ₂
Nitrification/denitrification	-0.03 Mt O ₂
Western Gotland Basin	
Mineralization of detritus	-0.19 Mt O ₂
Mineralization of POC	-0.02 Mt O ₂
Mineralization of POCN	-0.01 Mt O ₂
Nitrification/denitrification	-0.01 Mt O ₂

Supplementary Table 8. Physical processes supplying/consuming most of the hydrogen sulfide in different basins. Bornholm Basin is omitted because all processes contributing to the H₂S physical fluxes are negligible there.

Eastern Gotland Basin	
Advection, northern boundary	-13.1 Kt H ₂ S
Northern Gotland Basin	
Advection, upper boundary	-73.06 Kt H ₂ S
Advection, western boundary	-28.68 Kt H ₂ S
Advection, southern boundary	13.1 Kt H ₂ S
Diffusion, upper boundary	-8.88 Kt H ₂ S
Downslope mixing	6.33 Kt H ₂ S
Western Gotland Basin	
Advection, upper boundary	-132 Kt H ₂ S
Advection, eastern boundary	28.68 Kt H ₂ S
Diffusion, upper boundary	-19.36 Kt H ₂ S

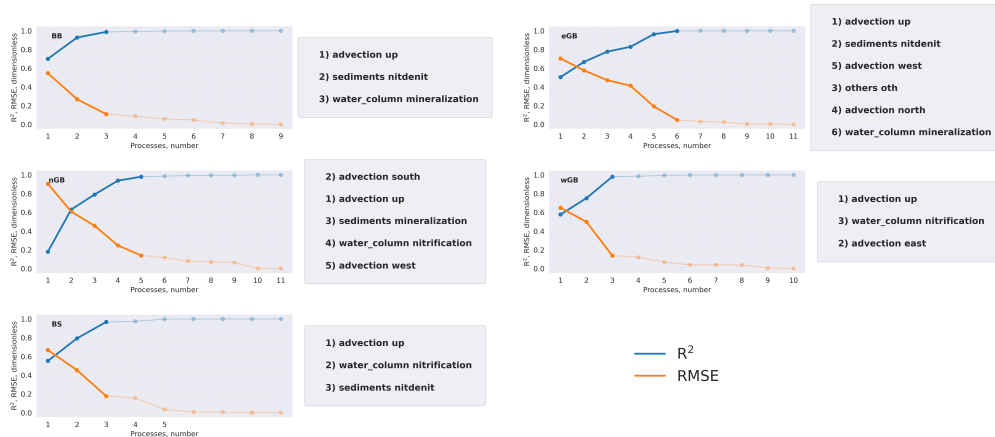
Supplementary Table 9. Water column processes producing/consuming most of the hydrogen sulfide in different basins.

Bornholm Basin	
Oxidation by O ₂	-9.5 Kt H ₂ S
Oxidation by NO ₃	-8.57 Kt H ₂ S
Mineralization of POC	2.627 Kt H ₂ S
Mineralization of detritus	0.29 Kt H ₂ S
Eastern Gotland Basin	
Oxidation by NO ₃	-113.26 Kt H ₂ S
Oxidation by O ₂	-93.5 Kt H ₂ S
Mineralization of POC	9.243 Kt H ₂ S
Mineralization of detritus	8.9 Kt H ₂ S
Northern Gotland Basin	
Oxidation by NO ₃	-196 Kt H ₂ S
Oxidation by O ₂	-175 Kt H ₂ S
Mineralization of POC	23.05 Kt H ₂ S
Mineralization of detritus	18 Kt H ₂ S
Western Gotland Basin	
Oxidation by O ₂	-175 Kt H ₂ S
Oxidation by NO ₃	-139 Kt H ₂ S
Mineralization of POC	32 Kt H ₂ S
Mineralization of detritus	26 Kt H ₂ S

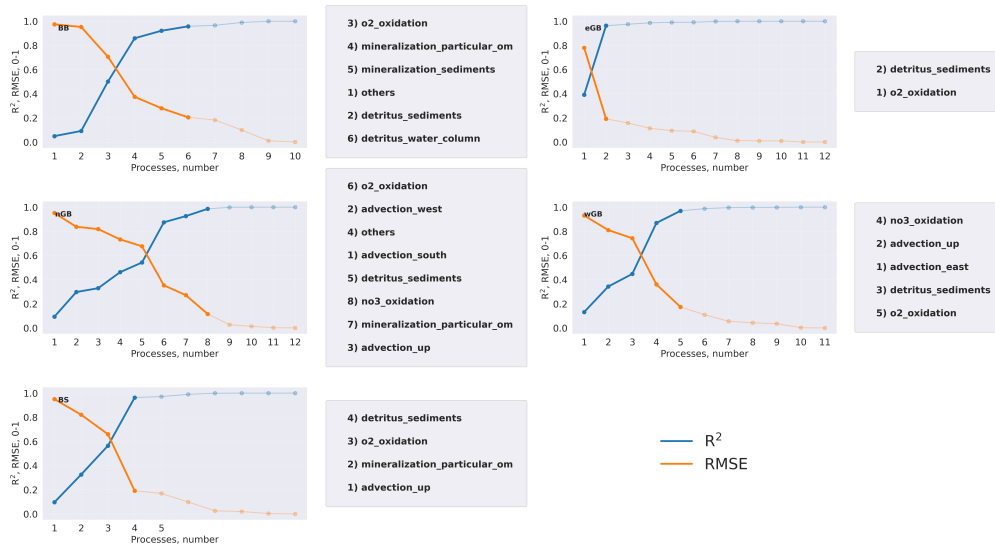
Supplementary Table 10. Processes in the sediments producing most of the hydrogen sulfide in different basins.

Bornholm Basin	
Mineralization of detritus	13.4 Kt H ₂ S
Mineralization of POC	1.52 Kt H ₂ S
Mineralization of POCN	0.88 Kt H ₂ S
Eastern Gotland Basin	
Mineralization of detritus	181 Kt H ₂ S
Mineralization of POCN	11 Kt H ₂ S
Mineralization of POC	8 Kt H ₂ S
Northern Gotland Basin	
Mineralization of detritus	387 Kt H ₂ S
Mineralization of POCN	20 Kt H ₂ S
Mineralization of POC	11 Kt H ₂ S
Western Gotland Basin	
Mineralization of detritus	345 Kt H ₂ S
Mineralization of POCN	15.2 Kt H ₂ S
Mineralization of POC	12.5 Kt H ₂ S

3.2.2 Contribution of the different processes to the O₂ and H₂S variability



Supplementary Figure 22. Results of linear regression analysis (see methods section in the paper). Blue curve shows the determination coefficient (R^2) after inclusion of a certain parameter in the model. Since the linear combination of all budget terms and their linear combinations (dependent variables) equals the total change of oxygen content within the box (independent variable), R^2 curve ultimately reaches 1 (linear model explains all variance). The same logic applies to orange curve – Root Mean Squared Error (RMSE). It ultimately reaches 0. Vivid lines highlight the processes together explaining more than 90% of the variance. Processes are shown as numbers on the horizontal axis. A description of the processes is shown in the legend boxes. The processes are sorted in accordance with their contribution to the explained variance and only processes from the vivid part of the curves are written.



Supplementary Figure 23. Same as Supplementary Figure 22, but for H₂S budget.

3.2.3 Temporal variability of O₂ and H₂S sources and sinks

Supplementary table 11. Statistics of the linear trends of the biggest processes from the oxygen budget. All processes in the table except advection can act only as oxygen sinks. Therefore, the minus sign indicates that more oxygen is being consumed, so consumption is increasing with time.

Processes	Slope [Kt O ₂ /a]	R ²	p-level
Bornholm Basin			
Mineralization of detritus (water column)	-0.15	0.63	2.90E-16
Mineralization of detritus (sediments)	-3.39	0.53	8.64E-13
Nitrification of NH ₄ to NO ₃	-1.01	0.52	1.42E-12
Mineralization of POCN (sediments)	0.68	0.41	1.94E-09
Mineralization of DOP	-0.25	0.24	1.42E-05
Nitrification/denitrification of NH ₄ in the oxic sediments	-0.084	0.18	2.81E-04
Advection, upper boundary	4.5	0.15	8.80E-04
Oxidation of sulfur to SO ₄	-0.44	0.09	1.00E-02
Eastern Gotland Basin			
Nitrification of NH ₄ to NO ₃	-5.66	0.62	4.69E-16
Mineralization of detritus (water column)	-1.25	0.54	4.53E-13
Mineralization of POCN (sediments)	3.01	0.52	1.55E-12
Mineralization of POC (sediments)	1.84	0.44	4.63E-10
Oxidation of sulfur to SO ₄	-5.69	0.32	3.44E-07
Mineralization of DOP	-0.78	0.24	1.46E-05
Mineralization of detritus (sediments)	-8.47	0.23	2.45E-05
Northern Gotland Basin			
Mineralization of POCN (sediments)	1.83	0.71	7.26E-20
Oxidation of H ₂ S to sulfur	-2.39	0.69	6.12E-19
Oxidation of sulfur to SO ₄	-9.54	0.68	2.30E-18
Mineralization of POC (sediments)	2.11	0.67	5.15E-18
Mineralization of POC (water column)	1.45	0.57	5.12E-14

Supplementary Material

Nitrification/denitrification of NH ₄ in the oxic sediments	0.46	0.51	4.20E-12
Nitrification of NH ₄ to NO ₃	-2.7	0.38	1.66E-08
Mineralization of detritus (sediments)	8.41	0.37	2.62E-08
Western Gotland Basin			
Mineralization of POC (water column)	1.17	0.77	3.56E-23
Mineralization of detritus (water column)	0.54	0.65	3.70E-17
Mineralization of POCN (sediments)	0.4	0.61	1.82E-15
Mineralization of POC (sediments)	0.68	0.6	2.54E-15
Mineralization of detritus (sediments)	3.95	0.57	5.60E-14
Nitrification/denitrification of NH ₄ in the oxic sediments	0.11	0.45	2.14E-10
Oxidation of H ₂ S to sulfur	-1.33	0.45	2.33E-10
Oxidation of sulfur to SO ₄	-3.53	0.27	4.18E-06

Supplementary table 12. Same as supplementary table 9, but for processes from the H₂S budget. Note that oxidation by O₂/NO₃ are the only processes that contribute to the H₂S sink. For them, a negative sign means that the process accelerates through time. Other processes (except advection) represent H₂S sources. For them, a negative sign means that the process decreases through time.

Processes	Slope [Kt H ₂ S/a]	R ²	p-level
Eastern Gotland Basin			
Mineralization of detritus (sediments)	5.13	0.5	7.90E-12
Oxidation by NO ₃	-2.94	0.49	1.68E-11
Mineralization of POC (sediments)	0.19	0.44	5.06E-10
Mineralization of detritus (water column)	0.24	0.29	1.54E-06
Oxidation by O ₂	-2.68	0.27	3.84E-06
Mineralization of POC (water column)	0.22	0.17	4.00E-04
Northern Gotland Basin			
Mineralization of detritus (sediments)	11.17	0.82	2.48E-27
Oxidation by NO ₃	-4.71	0.76	4.96E-23

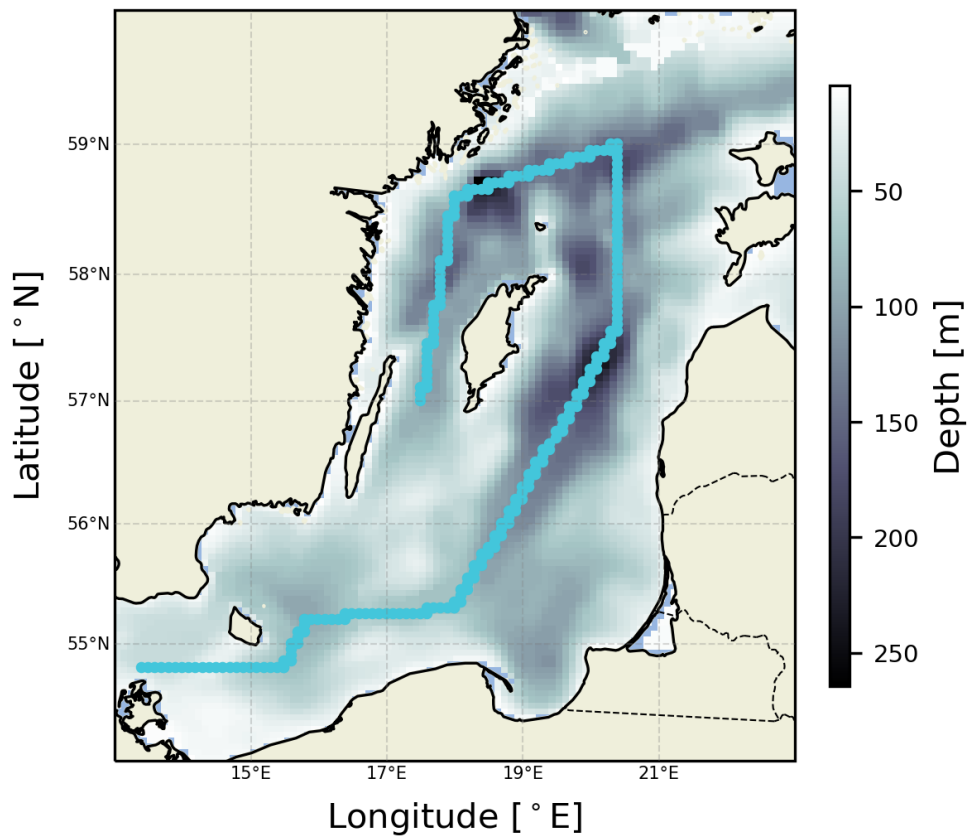
Mineralization of detritus (water column)	0.61	0.71	5.69E-20
Mineralization of POC (sediments)	0.27	0.69	2.57E-19
Oxidation by O ₂	-5.11	0.69	6.12E-19
Advection, upper boundary	-2.74	0.64	8.59E-17
Mineralization of POC (water column)	0.74	0.62	5.64E-16
Mineralization of POCN (sediments)	0.23	0.11	4.00E-03
Western Gotland Basin			
Mineralization of detritus (sediments)	6.65	0.87	5.97E-32
Mineralization of detritus (water column)	0.76	0.85	2.82E-30
Mineralization of POC (water column)	0.8	0.77	3.18E-23
Advection, upper boundary	-5.25	0.55	1.48E-13
Mineralization of POC (sediments)	0.1	0.47	5.69E-11
Oxidation by O ₂	-2.83	0.45	2.33E-10
Oxidation by NO ₃	-0.87	0.24	1.55E-05
Advection, eastern boundary	0.96	0.11	5.00E-03

3.3 Ventilation by inflows

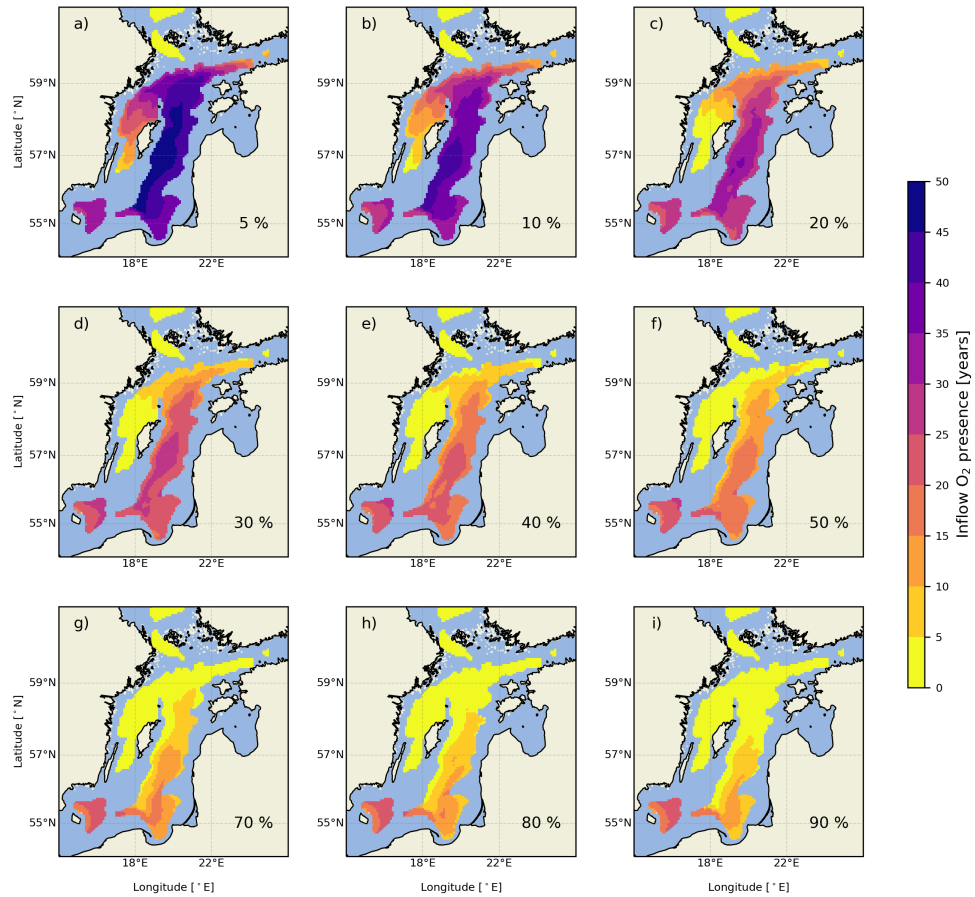
This section demonstrates the figures related to the analysis of the central Baltic Sea's ventilation by the 29 most significant O₂ inflows. Supplementary Figure 24 shows the transect used later in Supplementary Figure 26. Supplementary Figures 25 and 26 show the inflowed O₂ presence across the study area. The inflowed O₂ presence was calculated as the time when in a certain grid cell inflowed O₂ concentration was a certain fraction of O₂ that was delivered here by other sources. 5%, 10%, 20%, 30%, 40%, 50%, 70%, 80%, 90% were chosen as fractions. Therefore, both figures are made up of 9 panels. Supplementary Figure 27 shows the results of the EOF analysis of H₂S consumption/production terms during the inflow events.

3.3.1 Temporal trends in inflow's ventilation

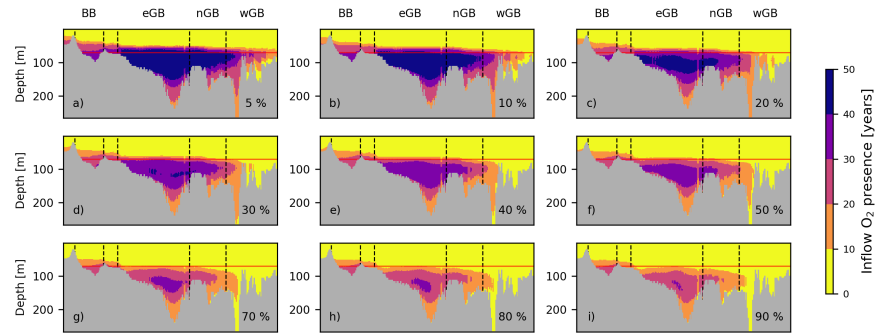
Supplementary Figure 26 shows the distribution of inflows' O₂ presence along the transect encompassing all studied sub-basins (for transect description, see Supplementary Figure 24). Supplementary Figure 26 provides a glimpse at the overall rate of oxygenation of the Baltic Sea by inflows and some regional features. Overall, it is visible that there is a substantial fraction of oxygen transported by the largest inflows into the Baltic Sea's deep waters. There are even situations when 90% of the oxygen concentration in the bottom water is the oxygen brought by the inflows, which lasted for several decades in BB, eGB, and wGB. The regional patterns, visible in Supplementary Figure 26, suggest that BB exhibits a lower inflow-oxygen ratio despite being closest to the Arkona transect, telling the oxygen mixed with other oxygen, from the atmospheric exchange or primary production. Most inflowed oxygen is concentrated within the eGB approximately at 100 meters depth. The deepest point of the eGB (Gotland Deep) is less frequently reached by the inflowing O₂, presumably due to the high salinity of water stored in the Gotland Deep. The remaining sub-basins are less well ventilated by the inflows, which is visible exceptionally well in Supplementary Figure 26 (panels F-I). A spatial pattern in the nGB follows the eGB, with some negative offset of the inflow oxygen's presence time. The deepest place in the Baltic Sea - Landsort Deep, along with other shallower basins within wGB, are the most difficult places to oxygenate. Even 5% of the oxygen being brought by inflows lasts less than 20 years out of a 70-year simulation in the deep part of the Landsort Deep. However, it should be considered that in deep areas where O₂ is limited, even a small addition of oxygen would result in a high ratio between the added oxygen and the oxygen already observed within the sub-basin. Also, Supplementary Figure 26 represents a 2-dimensional sketch that does not represent the total variability. Supplementary Figure 25 shows the same quantity as Supplementary Figure 26, but in the lat/lon plain at 70-meter depth, highlighting the inflowing oxygen's pathway. It is visible that at 70-meter depth, inflowing oxygen mostly stays within southern eGB and BB. It also points out enhanced oxygenation in the Gdansk Basin while the inflowing water propagates further to the eGB.



Supplementary Figure 24. Transect (blue line), which is used in Supplementary Figure 26 in the paper. Transect starts in the Bornholm Basin and ends in the western Gotland Basin encompassing the deepest points of the Baltic Sea.

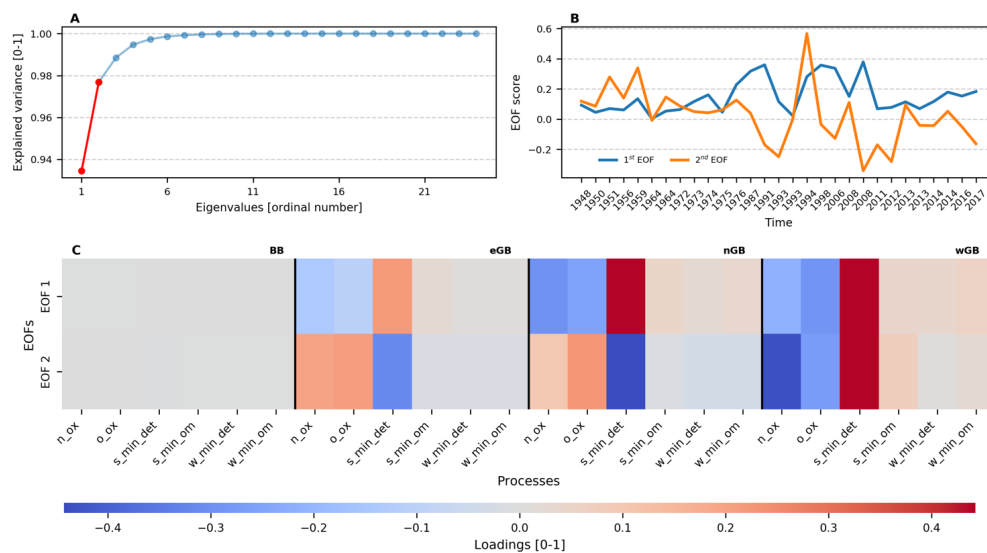


Supplementary Figure 25. Inflow presence duration (in years) for each grid cell in the longitude-latitude plane at the 70 meters depth. The metric is calculated for each grid cell as the total time when inflows O₂ concentration was a certain fraction of the total O₂ concentration in a cell. Fractions are shown in the lower right corner of each panel. They range from 5% (Panel A) to 95% (Panel I).



Supplementary Figure 26. Inflow presence duration (in years) for each grid cell along the transect from Supplementary Figure 24. The metric is calculated for each grid cell as the total time when inflows O_2 concentration was a certain fraction of the total O_2 concentration in a cell. Fractions are shown in the lower right corner of each panel. They range from 5% (Panel A) to 95% (Panel I). The black dashed lines denote different sub-basins. The solid red line marks 70 meters depth.

3.3.2 Changes in ventilation pattern



Supplementary Figure 27. Results of the EOF analysis for the integrated H₂S production/consumption during the inflow events. The structure is similar to Figure 9 in the paper. Panel A shows the fraction of the variance described by each EOF. Two EOFs selected for analysis are denoted by the red color. First EOF explains around 95% of the variance, and second – around 5%. Panel B demonstrates the temporal variability of the two significant EOFs. The first EOF demonstrates stationarity, whereas the second EOF is non-stationary. Panel C describes the loadings for the two EOFs. It is visible, that the first EOF is spatially independent, but the second one exhibits different signals in the wGB compared to the nGB and eGB. This suggests the same patterns behind the EOFs as for O₂ (see Section 3.2.2 in the paper). See Supplementary Table 2 for processes' names definition.

4 References

Fonselius, S. (1981). Oxygen and hydrogen sulphide conditions in the Baltic Sea. *Marine Pollution Bulletin* 12, 187–194. doi: 10.1016/0025-326X(81)90169-7.

Savitzky, Abraham., and Golay, M. J. E. (1964). Smoothing and Differentiation of Data by Simplified Least Squares Procedures. *Anal. Chem.* 36, 1627–1639. doi: 10.1021/ac60214a047.

Väli, G., Meier, H. E. M., and Elken, J. (2013). Simulated halocline variability in the Baltic Sea and its impact on hypoxia during 1961–2007: SIMULATED HALOCLINE VARIABILITY IN THE BALTIC SEA. *J. Geophys. Res. Oceans* 118, 6982–7000. doi: 10.1002/2013JC009192.

ARTICLE OPEN



Multidecadal climate variability dominated past trends in the water balance of the Baltic Sea watershed

H. E. Markus Meier^{1,2✉}, Leonie Barghorn¹, Florian Börgel¹, Matthias Gröger¹, Lev Naumov¹ and Hagen Radtke¹

The Baltic Sea watershed includes the territories of 14 countries in Northern, Central, and Eastern Europe. Long-term observations have shown that the climate in this area is characterised by a pronounced multidecadal variability, with a period of about 30 years, but its origin is thus far unknown. We propose that the observed ~30-year fluctuations in Baltic Sea salinity are caused by the Atlantic Multidecadal Variability and the North Atlantic Oscillation, which together modulate precipitation over the watershed and hence the river discharge into the Baltic Sea. The return of a large portion of the outflowing brackish Baltic Sea water with the inflowing salt water, due to mixing at the entrance area results in a positive feedback mechanism that amplifies the multidecadal variations in salinity. The strength of this self-amplification is considerable since atmospheric forcing has nearly the same periodicity as the response time of the freshwater content to external freshwater inputs.

npj Climate and Atmospheric Science (2023)6:58; <https://doi.org/10.1038/s41612-023-00380-9>

INTRODUCTION

The footprint of anthropogenic warming has been detected in many variables of the energy cycle, even at a regional scale¹. In Northern Europe, the warming associated with climate change significantly affects the cryosphere (snow, sea ice, lake ice, river ice and glaciers), whereas systematic changes in water cycle variables (precipitation, evaporation, river discharge, ocean salinity) are less obvious¹. In the early 1990s, the global water and energy exchanges (GEWEX) project, as part of the World Climate Research Programme, recognised the Baltic Sea catchment area as one of the regions on Earth where changes in the water cycle could be quantified². This region was singled out because the salinity of the semi-enclosed Baltic Sea depends on the freshwater supply (Supplementary Fig. 1a) from a catchment area that is about four times as large as the Baltic Sea surface (Fig. 1). As the salinity of the Baltic Sea and water exchange between the Baltic Sea and the adjacent North Sea (the latter estimated from sea level records within and outside the Baltic Sea) have been monitored since the 19th century (Supplementary Fig. 2), the Baltic Sea region is well-suited to studies of the regional water cycle, using salinity as a proxy for changes in precipitation and evaporation in the entire catchment area^{2–4}.

Rather than a systematic trend, the mean salinity of the Baltic Sea is characterised by a pronounced low-frequency variability with a period of about 30 years, at least since 1920 (Supplementary Fig. 3). This variability has been documented in long-term observations^{5–8} and historical, model-based reconstructions^{8–11}. A similar multidecadal variability describes the total river discharge from the Baltic Sea catchment area⁹ (see also Supplementary Fig. 4), individual river flows¹², barotropic saltwater inflows across the sills located in the Baltic Sea entrance area¹³ (see also Supplementary Fig. 5), water temperature¹⁴, sea level¹⁵, and atmospheric variables such as precipitation and the winds over the Baltic Sea region⁹. Centennial changes have been determined as well, including a positive trend along the north-south gradient of sea surface salinity (SSS) for the period 1900–2008⁸. However,

neither the trends in mean salinity^{6–9} nor those at selected monitoring stations¹⁶ were statistically significant.

Recent studies suggest that the Atlantic Multidecadal Variability (AMV) contributes to the observed low-frequency variability of the Baltic Sea basin^{17,18} and other regions in the Northern Hemisphere, such as the Arctic Ocean¹⁹. The AMV is defined as the low-frequency variability, with alternating anomalous warm and cold states, that characterises the annual mean, spatially averaged sea surface temperature (SST) in the North Atlantic²⁰. For the period 950–1800, Börgel et al.¹⁸ traced the AMV signal determined in a regionalised paleoclimate simulation of the last millennium²¹ to the Baltic Sea region. The AMV, with a currently observed period of 60–90 years^{22–24}, likely affected the water temperature in the Baltic Sea and partly explained the stronger increase in the mean SST of the Baltic Sea¹⁴ than of other coastal seas worldwide²⁵ as determined since the 1980s.

In mid and high northern latitudes, the most prominent pattern of climate variability is the North Atlantic Oscillation (NAO), which strongly influences the weather over northeastern North America, Greenland, and Europe during winter at time scales of about 4–10 years²⁶ and controls the strength and direction of westerly winds across the North Atlantic region. The NAO index is defined as the difference in atmospheric pressure at sea level between the Icelandic Low and the Azores High. Several studies have shown a mutual causal influence of the AMV and NAO^{27–32}. For example, Börgel et al.¹⁷ found that the AMV causes changes in the zonal position of the NAO's centres of action over time. During a positive AMV, the Icelandic Low moves further towards North America, and the Azores High further toward Europe, with the opposite occurring during a negative AMV¹⁷. As a consequence of the shifting centres of action, the correlations between the NAO and variables characterising the Northern European climate, such as water temperature, sea ice, and river discharge, vary in time¹⁷.

In this study, with the aid of historical, model-based ocean reconstructions and sensitivity experiments, we provide an explanation for the origin and mechanisms of the low-frequency variability in Baltic Sea salinity and in other variables that show a

¹Department of Physical Oceanography and Instrumentation, Leibniz Institute for Baltic Sea Research Warnemünde, 18119 Rostock, Germany. ²Department of Research and Development, Swedish Meteorological and Hydrological Institute, 60176 Norrköping, Sweden. ✉email: markus.meier@io-warnemuende.de

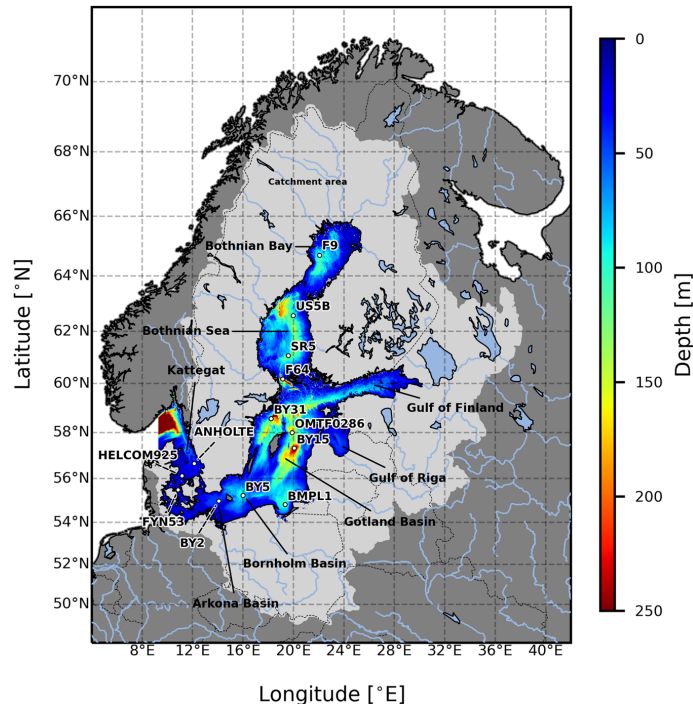


Fig. 1 Baltic Sea bathymetry. Water depth (in m)⁶⁰ and the locations of the long-term monitoring stations are shown. The domain of the Baltic Sea model is limited, with open boundaries in the northern Kattegat. The main sub-basin of the central Baltic Sea is the Gotland Basin.

Experiment	Description	Relative sea level rise	Average salinity 1900–2005
1 REF+	Reference run with a sea level rise	1 mm year ⁻¹ ⁴⁰	7.72 g kg ⁻¹
2 REF	Reference	0	7.60 g kg ⁻¹
3 RUNOFF+	Climatological mean river discharge and constant net precipitation of 2364 m ³ s ⁻¹ ⁶² , sea level rise is considered	1 mm year ⁻¹ ⁴⁰	7.61 g kg ⁻¹
4 RUNOFF	As RUNOFF+ but without sea level rise	0	7.49 g kg ⁻¹
5 WIND	As RUNOFF but with the repeated wind of the year 1904	0	5.82 g kg ⁻¹ (7.49 g kg ⁻¹ with drift correction)

period of about 30 years. For the period 1850–2008, five numerical simulations were performed, including a reference run (REF+), a sensitivity experiment that included the climatological mean freshwater supply (RUNOFF+), and both runs in which the global sea level rise (SLR) was excluded (REF and RUNOFF). Finally, a sensitivity experiment (WIND) was carried out that was identical to RUNOFF but with repeated wind fields for the year 1904 (Table 1).

We argue that the AMV is the pacemaker of the variability of the moisture transport from the North Atlantic to Northern Europe, as it periodically shifts the centres of action of the NAO with a current period of about 60 years. Hence, Northern Europe is alternately under the stronger and weaker influence of the milder, wetter North Atlantic climate. As the NAO and AMV influence Northern Europe, the combination of their respective patterns affects the annual mean precipitation over the Baltic Sea catchment area, river discharge, and the sea level in the Baltic Sea for a period of about 30 years. Consequently, salinity in the Baltic Sea oscillates

with the same periodicity due to direct dilution. However, the latter oscillation is considerably amplified because, in addition to dilution, saltwater inflows are less (more) saline during decades with increasing (decreasing) accumulated freshwater input. Due to this self-amplification, by monitoring Baltic Sea salinity, large-scale changes in the Northern Hemisphere water cycle can be detected, thereby furthering the aims of the global GEWEX project.

Our findings are also significant with respect to ecosystem functions and structure. Changes in salinity significantly affect the marine ecosystem because many species are adapted to specific salinity ranges, including the freshwater to marine conditions of the Baltic Sea^{33–35}. This study traces the origin of natural variations in salinity on multidecadal time scales. With our results, the trends caused by climate change could be separated from natural variations. Although this goal has not yet been fully achieved, decadal climate predictions for salinity may soon become possible. Such predictions could aid sustainable ecosystem

management, including the planning of fishing quotas. For instance, the reduction in weight of 3-year-old central Baltic Sea herring (*Clupea harengus*) from the late 1970s until today has been attributed to the declining salinity resulting from the multidecadal variability, which has also led to a reduction of fish catches and thus an estimated economic loss of roughly €100 million³⁶. If the decline in salinity in this or other cases had been known in time, fisheries management could have reacted to the changed environmental conditions for the fish and adjusted catch quotas, and possibly an economic loss could have been avoided.

RESULTS

The origin of the low-frequency variability in the Baltic Sea

During periods with a positive winter NAO index, the winter climate over Northern Europe is warmer and wetter, and the volume of river flow from the Baltic Sea catchment area is larger compared to the long-term mean (Fig. 2). Due to the lateral displacement of the centres of action of the NAO, in particular the Icelandic Low, the AMV affects both the location of the storm track over Northern Europe and the winter NAO index in the period band of >60 years (Fig. 3). Although this power band lies just outside the cone of influence of the wavelet power spectrum of the NAO, due to the relatively short time series since 1825³⁷ (not shown), we argue that the combination of the zonal displacement of the NAO centres and the AMV is largely responsible for the multidecadal variability of the atmospheric flow over Northern Europe. Moreover, as the temperature fluctuations related to AMV variability and the movement of the NAO centres of action have the same periodicity, the resulting signal contains the square of the AMV harmonic with a period of about 30 years. Otherwise, the impact of the interference on the NAO is relatively small (Fig. 3). Thus, the dominating wavelet power of the NAO is situated within a period band of 4–10 years and within an AMV period band of >60 years, as expected (Fig. 3). Our hypothesis, that the AMV accounts for the 30-year climate variability over Northern Europe, is supported by the relatively high wavelet coherence of the squared AMV and the winter mean zonal wind over the central Baltic Sea in that period band (not shown). However, a confirmation of our hypothesis is difficult as the observed and reconstructed time series are relatively short compared to the dominating long-time scales of the AMV. A more detailed analysis of regional climate variability, for instance, in paleoclimate simulations and their dependencies on the AMV remains for future research.

Winter precipitation over Northern Europe, mainly explained by the advection of humid air masses from the Atlantic, therefore has a pronounced low-frequency variability of about 30 years, the phase of which corresponds well with the atmospheric flow field

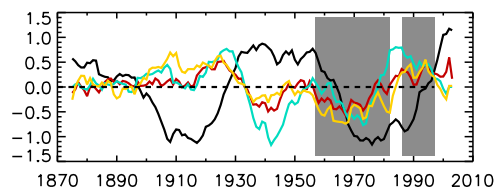


Fig. 2 Atlantic Multidecadal Variability (AMV) index, North Atlantic Oscillation (NAO) index, precipitation averaged over the Baltic Sea catchment area, and total river discharge. Low-pass filtered AMV (black)⁵⁹, precipitation⁵², river discharge¹⁰ (cyan), and the winter (December through February) NAO index³⁷ (orange), with a cut-off frequency of 12 years. All records were normalised by their standard deviations. Selected recent periods with predominantly low (1957–1982) and high (1986–1997) NAO indices are shown as grey-shaded areas.

over the region (Fig. 2). A calculation of the Pearson correlation coefficients between the low-pass filtered precipitation or river discharge and the winter NAO index with a cut-off period of 12 years (shown in Fig. 3) yielded a value of 0.76 or 0.58. Moreover, the correlation between precipitation and river discharge was similarly high (0.79), in accordance with an earlier study³⁸. Hence, river discharge is subject to multidecadal variations within the same period of about 30 years and with an amplitude of about 7% of the total mean river discharge of about $14,000 \text{ m}^3 \text{ s}^{-1}$ (Supplementary Figs. 1 and 4).

In the following, we analyse a set of sensitivity studies aimed at disentangling the contributions of the different physical drivers to the low-frequency variability of the Baltic Sea's salinity. In general, salinity in estuaries is controlled by the freshwater supply from rivers of the catchment area and precipitation minus evaporation over the sea, saltwater inflows from the open ocean, and mixing by tides and wind fields.

In the Baltic Sea, the large annual freshwater supply, comprising about 2.3% of the sea's total volume, causes a large horizontal gradient in salinity of about 20 g kg^{-1} between the entrance area and the eastern- and northern-most parts of the Baltic Sea. To examine the impact of multidecadal freshwater input variations on salinity, we performed a sensitivity experiment (RUNOFF+) based on the climatological mean freshwater input (Table 1). As the Baltic Sea is semi-enclosed, with limited water exchange with the world ocean through narrow and shallow straits (Fig. 1), wind-driven large saltwater inflows, so-called major Baltic inflows (MBIs), occur only sporadically, but they are essential for the ventilation of Baltic Sea's deep water¹³. The intensity of saltwater inflows will probably increase as the global sea level rises because, in a first approximation, the transport is proportional to the cross-section at the sills³⁹. Using the sensitivity experiments REF and RUNOFF without the global SLR, we investigated whether the SLR is responsible for the observed trends in the recent evolution of salinity. As the zonal west wind may hamper the outflow of brackish water from the Baltic Sea and thus limit the inflow of saltwater, an additional experiment with a constant wind was performed (WIND). Unlike in many other estuaries, in the Baltic Sea, the tides are small and low-frequency wind-induced mixing does not affect the temporal evolution of the mean salinity¹¹.

Impact of the freshwater supply on salinity

In the two model simulations with and without SLR (REF+ and REF), the mean salinity during 1900–2005 was 7.72 and 7.60 g kg^{-1} , respectively (Table 1). The analysis was limited to the period 1900–2005 because the reconstructed river discharge before 1900 is less reliable. The difference in mean salinity reflects the effect of the SLR relative to the sea bottom on the overall salinity in the Baltic Sea. Similar values were obtained in the two sensitivity experiments focusing on climatological freshwater input with and without SLR (RUNOFF+ and RUNOFF). The applied SLR of 1 mm year^{-1} or 10.6 cm during 1900–2005 relative to the sea bottom at the sills in the Baltic Sea entrance area⁴⁰ corresponded to a salinity increase of 0.12 g kg^{-1} or $+1.13 \text{ g kg}^{-1} \text{ m}^{-1}$, which was somewhat smaller than the value obtained in a study by Meier et al.³⁹, in which the average salinity change per SLR was $+1.41 \text{ g kg}^{-1} \text{ m}^{-1}$. The difference can be explained by the temporal evolution of the SLR, i.e., a linear vs. step-function-like increase, as in Meier et al.³⁹, and the different study periods.

The results of the sensitivity experiment RUNOFF+ suggested that the interannual variations in the total freshwater supply alone explained about 52% of the Baltic Sea's interannual mean salinity variations determined in REF+ for periods >12 years (Fig. 4). The standard deviations in RUNOFF+ amounted to 0.1 g kg^{-1} , compared with 0.2 g kg^{-1} in REF+.

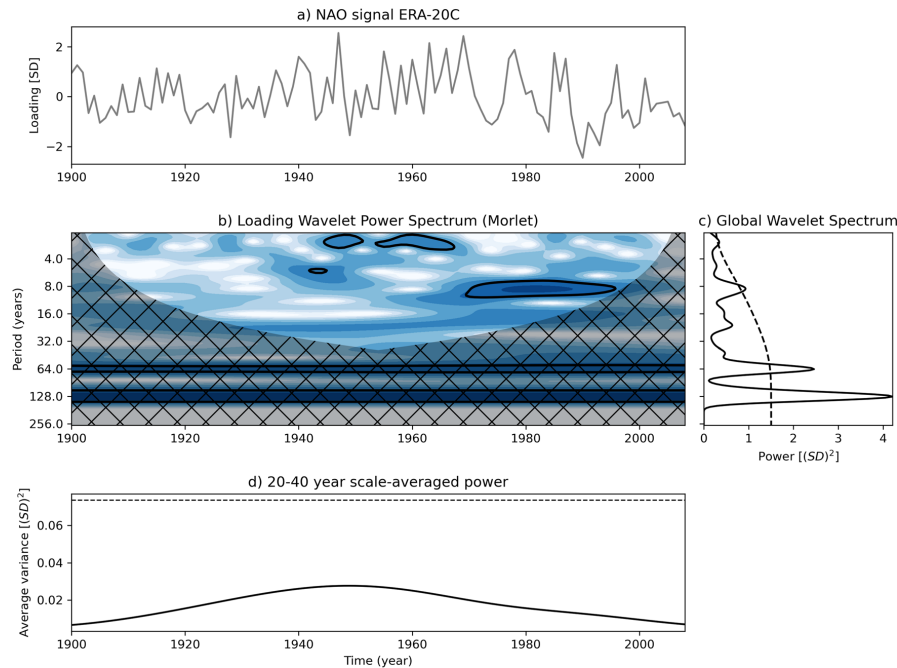


Fig. 3 Spectrum of the winter North Atlantic Oscillation (NAO) index 1900–2010. **a** Time series of the principal component of the first orthogonal function, **b** wavelet power, **c** power averaged over time and **d** wavelet power averaged for a period band of 20–40 years as a function of time. The black contour lines in the wavelet power spectrum show a 95% significance level⁶¹. The winter (December to February) NAO index was calculated from the reanalysis data ERA20C⁵⁸.

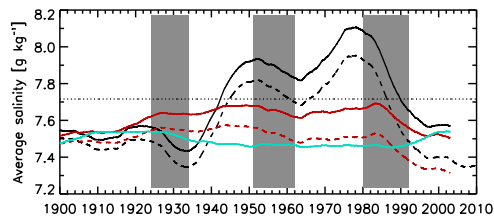


Fig. 4 Mean salinity of the Baltic Sea. Low-pass filtered, spatially averaged salinity with a cut-off period of 12 years in five numerical experiments: the reference simulation (REF+, black line), the reference simulation without a sea level rise (REF, black dashed line), and the sensitivity experiments with a climatological mean river discharge and constant net precipitation with (RUNOFF+, red line) and without (RUNOFF, red dashed line) a sea level rise and with constant wind from 1904 (WIND, cyan line). As the salinity of the WIND simulation drifted during the simulation because the wind during 1904 was not representative of the mixing input during the entire period, a drift following an e-function with an e-folding time scale of 25 years was subtracted, and the curve was shifted by a constant offset to the start value of RUNOFF in 1900. Periods with a decreasing mean salinity and a preceding local maximum in the freshwater supply (1924–1934, 1951–1962, 1980–1992) are shown as grey-shaded areas. The periods in between (1935–1950 and 1963–1979) are characterised by an increasing mean salinity and a preceding local minimum in the freshwater supply.

Impact of the freshwater supply on saltwater inflows

As data on MBIs¹³ and river discharge show a significant wavelet coherence at the period of about 30 years, with river discharge preceding saltwater inflows by about 20 years (Supplementary Fig. 6), we examined whether the freshwater supply to the Baltic Sea has a causal influence on MBIs and found that the intensity of MBIs is modulated by the accumulated freshwater supply (Fig. 5). During periods with anomalously high (low) freshwater content in the Baltic Sea, the salinity of the MBIs decreases (increases), as indicated by the difference in the inflow volume with a salinity $> 17 \text{ g kg}^{-1}$ (V_{17}) between REF+ and RUNOFF+. Although changes in V_{17} are $< 3 \text{ km}^3$, or about 20% (Fig. 5), the accumulated salt transport on a decadal time scale has a significant impact on the Baltic Sea's salt content. As in the reconstructed MBIs¹³ shown in Supplementary Fig. 5, a period of about 30 years is discernible (Fig. 5).

Our model results thus indicate a positive feedback mechanism amplifying the multidecadal oscillations in the mean salinity of the Baltic Sea. As described in the study by Mohrholz¹³, barotropic salt transports can be approximated by the product of the inflow volume and the vertically averaged salinity in the Baltic Sea entrance area (S_B) after the so-called Kattegat–Skagerrak salinity front, separating saline North Sea and brackish Baltic Sea outflow waters⁴¹, has reached the sills (Fig. 1). S_B depends on the surface layer salinity, which at a multidecadal time scale is a function of the mean salinity of the Baltic Sea. As volume transports during saltwater inflows only show small differences in their intensities

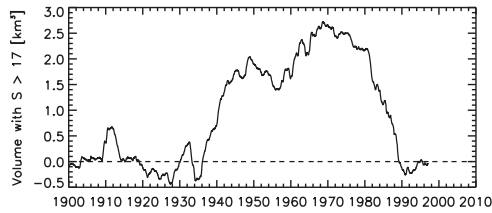


Fig. 5 Changes in saltwater inflow volume caused by low-frequency freshwater inputs. The differences in the low-pass filtered inflowing volume, with salinity $> 17 \text{ g kg}^{-1}$ and a cut-off period of 12 years, between the sensitivity experiments REF+ and RUNOFF+ are shown. The dashed line indicates zero.

with a negligible effect on mean salinity (see next sub-section), the multidecadal variations in MBIs can be explained by S_B alone. During periods characterised by an anomalously high freshwater content in the Baltic Sea, the S_B in the MBIs is, on average, smaller than during periods with an anomalously low freshwater content. Hence, the net salt import is reduced. As proof of this relationship, we calculated the surface and bottom salinity differences between REF+ and RUNOFF+ averaged during periods of decreasing mean salinity preceded by a local maximum in the freshwater supply for the years 1924–1934, 1951–1962, and 1980–1992 (Fig. 4). During these periods, the SSS in the Kattegat and the inflowing bottom salinity in the entrance area (Belt Sea) and Arkona Basin (for the location, see Fig. 1) were smaller in REF+ than in RUNOFF+ (Fig. 6a, b). Conversely, during periods with increasing mean salinity with a preceding, local minimum in freshwater supply, i.e., in 1935–1950 and 1963–1979, the SSS in the Kattegat and the inflowing bottom salinity in the entrance area (Belt Sea) and Arkona Basin were higher in REF+ than in RUNOFF+ (Fig. 6c, d). The results for V_{17} confirmed that saltwater transports related to MBIs increase (decrease) during periods of increasing (decreasing) mean salinity (Fig. 5).

Impact of wind anomalies on salinity

The results of our sensitivity experiment (WIND) suggested that the effects of the low-frequency variations of the wind on the mean salinity of the Baltic Sea (Fig. 4, blue curve) and the saltwater inflow volume V_{17} (not shown) are small. In the WIND, in addition to the constant freshwater supply, the wind fields of the year 1904 were repeated annually.

The period 1983–1992, during which there was no MBI, was an exception to the overall conclusion that wind plays only a minor role in the multidecadal salinity fluctuations¹³. During this so-called stagnation period, both the anomalously large freshwater surplus and the absence of wind patterns causing saltwater inflows resulted in a decline in the mean salinity (Fig. 4). Such stagnation periods are not unusual²¹. An analysis of paleoclimate simulations showed that periods of decreasing salinity over 10 years occur approximately once per century as part of the natural variability.

The winter mean SSS and the bottom salinity differences in RUNOFF+ between 1986–1997 and 1957–1982 are shown in Fig. 6e, f. These two periods were characterised by predominantly positive (1986–1997) and negative (1957–1982) NAO indices (Fig. 2). The SSS in the Kattegat and entrance area (Belt Sea) during 1986–1997 was higher than during 1957–1982 because of the higher sea level in the Kattegat. As a west wind hampers the outflow of surface layer water and consequently the saltwater inflow in the bottom layer at any north-south section within the Baltic Sea, the bottom salinity in the central Baltic Sea (Gotland Basin) was lower during 1986–1997 than during 1957–1982. An important role in the bottom salinity in the Gotland Basin is played

by the Słupsk Channel, which connects the western (Bornholm Basin) and central Baltic Sea. In the sensitivity experiment WIND, the bottom salinity difference in the central Baltic Sea between 1986–1997 and 1957–1982 was positive because of the absence of the hampering effect of the west wind (not shown).

Impact of the sea level in the Kattegat on salinity

The sea level in the Kattegat at the open boundary of the model domain correlated well with the daily variations of the meridional sea level pressure difference over the North Sea^{42,43}, which may suggest an effect on saltwater inflow at multidecadal time scales. However, the results of the sensitivity experiment WIND, with constant external forcing except for the varying sea level at the open boundary in the Kattegat, indicated only a small impact of low-frequency variations in the sea level of the Kattegat on the mean salinity.

DISCUSSION

Our model simulations for the past >100 years suggest that multidecadal variations in the freshwater supply roughly explain 52% of the multidecadal variations in the mean salinity of the Baltic Sea, in agreement with previous studies^{9,11}. According to Radtke et al.'s analytical approach¹¹, only about 27% of the variations can be explained by a 'direct dilution' effect. Hence, we conclude that most of the remainder of the 52% can be accounted for by a positive feedback mechanism operating between the accumulated freshwater supply and saltwater inflows into the Baltic Sea. During periods of enhanced freshwater supply, (1) the salinity in the surface layer decreases, (2) the location of the Kattegat–Skagerrak front moves northward, and (3) the salinity at the sills decreases. Consequently, inflow events are less saline and thereby amplify the freshening of the water body during phases of enhanced freshwater supply. As the turnover period of the freshwater content, i.e., the time scale of the internal response to external freshwater variations, roughly matches the period of external forcing in the multidecadal power band⁴⁴, this coincidence results in a considerable amplification of the salinity oscillations with a periodicity of about 30 years.

Based on Fig. 6, we estimate a peak-to-peak salinity difference—both at the sea surface and bottom and due to the moving Kattegat–Skagerrak front—of about 0.5 g kg^{-1} between selected decades with anomalous high and low freshwater input. This salinity difference would be roughly 2.5% of the salinity of 20 g kg^{-1} in the Baltic Sea entrance area. As the mean salinity varies by ~7–8% peak-to-peak (Fig. 4), at least about one-third of these variations can be roughly explained by the self-amplification effect, over and above the direct dilution effect¹¹. Hence, these two processes, dilution and amplification, explain most of the signal.

Due to the self-amplification mechanism and the unique setting of the Baltic Sea, systematic changes in its water balance, e.g., those resulting from an intensified hydrological cycle of Northern Europe or the changes in large-scale atmospheric circulation patterns caused by global warming⁴⁵, might be detected earlier in the Baltic Sea than elsewhere in the Northern Hemisphere.

Our sensitivity experiments allowed us to distinguish between the influences of the low-frequency oscillations in the freshwater supply, wind forcing, and the water level in the Kattegat on the salinity of the Baltic Sea. The results suggest a dominant effect of freshwater variations via direct dilution and the above-described feedback mechanism. The remaining low-frequency variability can be explained by the timing of saltwater inflows and, in particular, the absence of these events during stagnation periods. The direct impact of the multidecadal wind variability on transport in the sea redistributes the salinity within the Baltic Sea via Ekman dynamics⁴⁶, but the impact on the mean salinity variations is only minor.

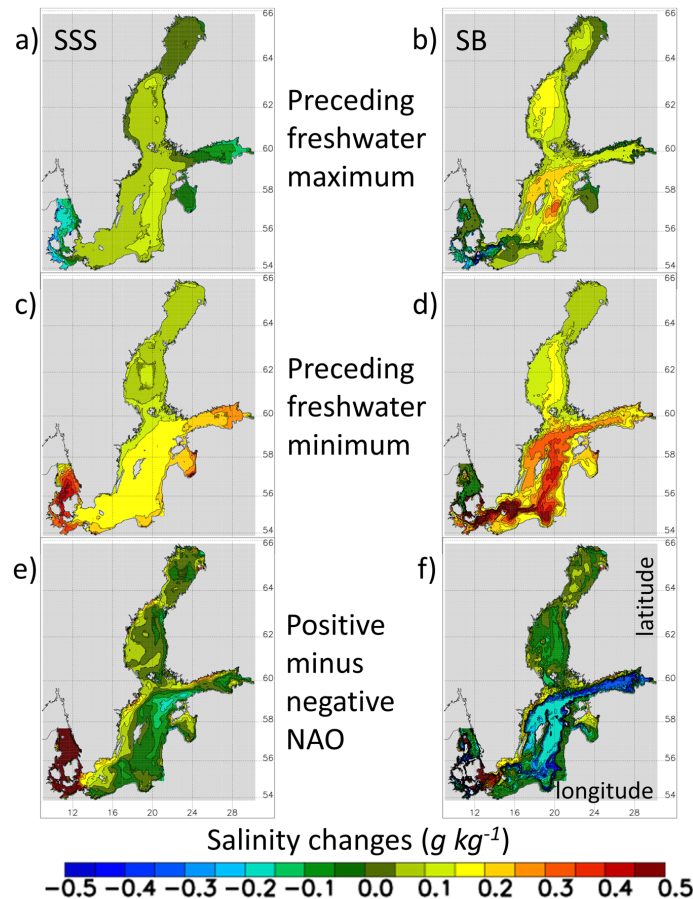


Fig. 6 Differences in sea surface and bottom salinities (in g kg^{-1}) caused by river discharge and west wind anomalies. **a, b** Differences in the autumn and winter mean (September to February), sea surface salinity (SSS) (**a**), and bottom salinity (SB) (**b**) between RUNOFF+ averaged during 1924–1934, 1951–1962 and 1980–1992, i.e., periods with a decreasing mean salinity (Fig. 4) and with a preceding, local maximum in the freshwater supply (Fig. 2). **c, d** Same as (**a**) and (**b**) but showing the averaged salinity difference during 1935–1950 and 1963–1979 with increasing mean salinity (Fig. 4) and a preceding local minimum in the freshwater supply (Fig. 2). **e, f** Differences in the winter SSS (**e**) and bottom salinity (**f**) according to RUNOFF+ between 1986–1997 (a period with predominantly positive NAO indices, i.e., wet and with a low salinity) and 1957–1982 (a period with predominantly negative NAO indices, i.e., dry and with a high salinity).

The in situ observations of the national monitoring programme in the Baltic Sea for the period 1982–2016 showed a decrease in upper layer salinity of -0.005 , to $-0.014 \text{ g kg}^{-1} \text{ year}^{-1}$, and an increase in the sub-halocline deep layer salinity of $+0.02$ to $+0.04 \text{ g kg}^{-1} \text{ year}^{-1}$, thereby strengthening the stratification⁴⁷. Vertical stratification is controlled by saltwater inflows and vertical diffusion across the halocline. Hence, saltwater intrusions into the central Baltic Sea result in a sawtooth-like temporal progression of the unfiltered stratification record (not shown). In the absence of large saltwater inflows and the presence of an anomalously high freshwater supply, stratification decreased during the stagnation period 1980–1992. In 1993, it dramatically increased again. Hence, the temporal sequence of saltwater inflows, rather than the freshwater supply, mainly explains the trends since 1980 observed by Liblik and Lips⁴⁷. Although the freshwater supply largely controls multidecadal variations in mean salinity (Supplementary Fig. 3), which is mainly controlled by the SSS, the effect of

multidecadal freshwater input variations on the changes in stratification is smaller than the effect of MBLs over time scales >4 years (Supplementary Fig. 7). An accumulation of power within the 20- to the 40-year period band was not statistically significant (Supplementary Fig. 8).

METHODS

A detailed description of the Baltic Sea model setup was presented in a previous study¹⁰. Here we provide a summary of the physical module.

Model description

The Rossby Centre Ocean model, a three-dimensional ocean circulation model coupled to a Hibler-type, multi-category sea-ice model, was used^{48–51}. Subgrid-scale mixing in the ocean was

parameterised using a state-of-the-art $k-\epsilon$ turbulence closure scheme with flux boundary conditions. A flux-corrected, monotonicity-preserving transport scheme, without explicit horizontal diffusion, was embedded in the model. The model domain comprised the Baltic Sea and the Kattegat, with lateral open boundaries in the northern Kattegat (Fig. 1). The horizontal resolution was 3.7 km, and the vertical resolution was 3 m.

Atmospheric forcing

Regionalised reanalysis data for 1958–2007, historical station data of daily sea level pressure, and monthly air temperature observations were used in the reconstruction of multivariate 3-h, high-resolution atmospheric forcing fields (HiResAFF) for the period 1850–2008, based on the analogue method⁵². The latter searches for the atmospheric surface fields that are most similar to the historical observations in a library of predictands from the calibration period 1958–2007. The predictands or analogues are multivariate atmospheric forcing fields of 2 m air temperature, 2 m specific humidity, 10 m wind, precipitation, total cloud cover, and mean sea level pressure recorded in the Rossby Centre Atmosphere Ocean model⁵³, with a horizontal resolution of $0.25^\circ \times 0.25^\circ$ (~25 km) interpolated onto a regular geographical grid.

River discharge

Monthly mean river flows were calculated from several merged data sets (Supplementary Fig. 1). Since the inter-annual variability of the reconstructed river discharge was significantly underestimated before but not after 1900 (Supplementary Fig. 1), the analysis was limited to the period 1900–2008.

Lateral boundary data

Daily mean sea level elevations at the lateral boundary were calculated from the reconstructed meridional sea level pressure gradient across the North Sea⁴², Gustafsson et al.⁴³ calculated the correlations of the various frequency bands using empirical orthogonal functions (EOFs) to avoid underestimating extremes. The mean value of the time series was subtracted and replaced at the lateral boundary by the mean sea level in the Nordic Height System 1960⁵⁴. A linearly rising mean sea level of 1 mm year^{-1} relative to the sea bottom at the sills in the entrance area was implemented by continuously deepening the water depth at all grid points^{40,55}. A spatially differing land uplift with greater rates in the north than in the south was not considered. In the case of inflow, temperature and salinity were nudged towards the observed climatological seasonal mean profiles for 1980–2005 located north of the lateral boundary in Kattegat.

Initial conditions

After a spin-up simulation for 1850–1902 utilising the reconstructed forcing described above, the physical variables calculated for the end of the spin-up simulation on January 1, 1903, were used as the initial conditions for January 1, 1850.

Experimental strategy

A 159-year reference simulation for 1850–2008 was performed using the forcing data described above (henceforth referred to as REF+). In addition to REF+, four sensitivity experiments were carried out with the same experimental setup as in REF+ but with modified forcing data to identify the main drivers of the multidecadal variability (Table 1). The sensitivity experiments REF, RUNOFF and WIND have previously been analysed^{8,10}. In REF+ and RUNOFF+, the global eustatic sea level rise was considered.

The RUNOFF+ and RUNOFF sensitivity experiments with climatological mean freshwater input were conducted to investigate the effects of interannual to multiannual variations in river

discharge on the salinity of the Baltic Sea. In the WIND experiment, in addition to the freshwater input, interannual variations in atmospheric forcing were also neglected by repeating the 1904 atmospheric forcing for all years. The results of this sensitivity experiment show the effect of the low-frequency variations of the wind field on salinity. As 1904 does not contain an MBI event, the salinity decreases with an e-folding time scale of 25 years. Conversely, the atmospheric forcing with a year with MBI would result in a drift to higher salinity. However, regardless of the chosen sensitivity experiment, the influence of the multidecadal variations in the wind field on the salinity can be studied after subtracting the drift.

Previous studies concluded that ice cover in the Baltic Sea in the 20th century had no influence on salinity⁹. Therefore, this effect was not analysed here.

Evaluation of saltwater inflows

Sporadic events of large saltwater inflows, so-called MBIs, are essential for the ventilation of the Baltic Sea's deep water¹³. Simulated MBIs, calculated from the inflowing volume with salinity $> 17 \text{ g kg}^{-1}$ (V_{17}), were close to the MBIs calculated from the observations of Mohrholz¹³. The largest inflow on record was in 1951. Three out of the four largest MBIs, i.e. those in 1921, 1951, and 2014, were also identified as record events in the simulation when the reference run was prolonged⁵⁶. Only the MBI in 1898 was not reproduced, probably due to the inaccurate data used as forcing in our simulation or in the reconstruction of the MBIs¹³. Furthermore, a distinct stagnation period from 1983 to 1992 was identified in our simulation, as was also observed. This analysis demonstrated that our modelled MBIs sufficiently well reproduced the observed MBIs.

Evaluation of salinity at selected stations

Supplementary Fig. 2 shows the simulated and observed sea surface and bottom salinities at selected monitoring stations with relatively long records of observations (Fig. 1). At stations located within the Baltic Sea, the model accurately reproduced the pronounced multidecadal variability of about 30 years, both at the sea surface and the sea bottom (Supplementary Fig. 2, see also Fig. 4 and Supplementary Fig. 3). However, there was less agreement between the model's results and observations at the three available stations located in the entrance area, i.e., the Kattegat and the Great Belt. This was in part due to the sparse measurements in this area and to the difficulty of adequately evaluating the model in this highly dynamic transition area between the North Sea and the Baltic Sea. Furthermore, at some stations located in the central Baltic Sea (e.g., BY15, OMTF0286, BY31), there was also less agreement between the model's results for bottom salinity and observations during about 1950–1970. Probably the simulated intensity of the large MBI in 1951 is underestimated. Please note that long-term reconstructed atmospheric fields have been used as forcing data whose quality is less good than that of reanalysis data or observations. If high-quality atmospheric forcing data are used, the RCO model can reproduce saltwater inflows well⁵⁷.

For further results of the model evaluation, the reader is referred to Meier et al.¹⁰.

Observational datasets

The winter (December to February) NAO index was derived from long-term observations of the difference in sea level pressure between Reykjavik, Iceland, and Gibraltar, Spain (available from the Climatic Research Unit, University of East Anglia; <https://crudata.uea.ac.uk/cru/data/nao/nao.dat>)³⁷ and from an EOF analysis of the reanalysis data ERA20C⁵⁸. Despite differences in the resulting records, the conclusions of this study do not depend on

the method used to calculate the NAO index. The annual mean AMV index was calculated from SST anomalies recorded in the HadISST dataset⁵⁹ averaged over the North Atlantic between 0 and 70°N latitude. Precipitation data from the HiResAFF dataset⁵² were averaged over the Baltic Sea catchment area between 9.6°E and 32°E and between 52.4°N and 67.4°N. The simulated salinity was evaluated using observations from the International Council for the Exploration of the Sea (ICES) at <https://www.ices.dk/data-ports/Pages/ocean.aspx>. These measurements were post-processed to fill gaps, following the method of Radtke et al.¹¹.

DATA AVAILABILITY

The observational and model data analysed in this study and displayed in the figures are publicly available from the Leibniz Institute for Baltic Sea Research Warnemünde (IOW) at the doi server <https://doi.io-warnemuende.de/10.12754/data-2023-0001>. Water depth data compiled by Seifert and Kayser⁶⁰ and saltwater inflow data D55 calculated by Mohrholz¹³ are publicly available from <https://www.io-warnemuende.de/topography-of-the-baltic-sea.html> and <https://www.io-warnemuende.de/major-baltic-inflow-statistics-7274.html> (<http://doi.io-warnemuende.de/10.12754/data-2018-0004>), respectively. These datasets are provided through the Creative Commons (CC) data license of type CC BY 4.0 (<https://creativecommons.org/licenses/by/4.0/>).

CODE AVAILABILITY

The model code of the ocean model used for the historical simulations is publicly available from the Swedish Meteorological and Hydrological Institute, Norrköping, Sweden (<https://www.smhi.se>, E-mail: smhi@smhi.se).

Received: 4 November 2022; Accepted: 16 May 2023;

Published online: 05 June 2023

REFERENCES

- Meier, H. E. M. et al. Climate change in the Baltic Sea region: a summary. *Earth Syst. Dynam.* **13**, 457–593 (2022).
- Reckermann, M. et al. BALTEX—an interdisciplinary research network for the Baltic Sea region. *Environ. Res. Lett.* **6**, 045205 (2011).
- Meier, H. E. M., Rutgersson, A. & Reckermann, M. An Earth System Science Program for the Baltic Sea region. *Eos* <https://doi.org/10.1002/2014EO130001> (2014).
- Lehmann, A. et al. Salinity dynamics of the Baltic Sea. *Earth Syst. Dynam.* **13**, 373–392 (2022).
- Samuelsson, M. Interannual salinity variations in the Baltic Sea during the period 1954–1990. *Cont. Shelf Res.* **16**, 1463–1477 (1996).
- Winsor, P., Rodhe, J. & Omstedt, A. Erratum: Baltic Sea ocean climate: an analysis of 100 yr of hydrographical data with focus on the freshwater budget. *Clim. Res.* **25**, 183 (2003).
- Winsor, P., Rodhe, J. & Omstedt, A. Baltic Sea ocean climate: an analysis of 100 yr of hydrographical data with focus on the freshwater budget. *Clim. Res.* **18**, 5–15 (2001).
- Kniesbusch, M., Meier, H. E. M. & Radtke, H. Changing salinity gradients in the Baltic Sea as a consequence of altered freshwater budgets. *Geophys. Res. Lett.* **46**, 9739–9747 (2019).
- Meier, H. E. M. & Kauker, F. Modeling decadal variability of the Baltic Sea: 2. Role of freshwater inflow and large-scale atmospheric circulation for salinity. *J. Geophys. Res.* **108**, 3368 (2003).
- Meier, H. E. M. et al. Disentangling the impact of nutrient load and climate changes on Baltic Sea hypoxia and eutrophication since 1850. *Clim. Dyn.* **53**, 1145–1166 (2019).
- Radtke, H., Brunnabend, S. E., Gräwe, U. & Meier, H. E. M. Investigating interdecadal salinity changes in the Baltic Sea in a 1850–2008 hindcast simulation. *Climate* **16**, 1617–1642 (2020).
- Gailiūšis, B., Kriaučiūniene, J., Jakimavičius, D. & Sarauskienė, D. The variability of long-term runoff series in the Baltic Sea drainage basin. *Baltica* **24**, 45–54 (2011).
- Mohrholz, V. Major Baltic inflow statistics—revised. *Front. Mar. Sci.* **5**, 384 (2018).
- Kniesbusch, M., Meier, H. E. M., Neumann, T. & Börgel, F. Temperature Variability of the Baltic Sea Since 1850 and Attribution to Atmospheric Forcing Variables. *J. Geophys. Res.* **124**, 4168–4187 (2019).
- Medvedev, I. & Kulikov, E. Low-frequency Baltic Sea level spectrum. *Front. Earth Sci.* **7**, 284 (2019).
- Fonselius, S. & Valderrama, J. One hundred years of hydrographic measurements in the Baltic Sea. *J. Sea Res.* **49**, 229–241 (2003).
- Börgel, F., Frauen, C., Neumann, T. & Meier, H. E. M. The Atlantic Multidecadal Oscillation controls the impact of the North Atlantic Oscillation on North European climate. *Environ. Res. Lett.* **15**, 104025 (2020).
- Börgel, F., Frauen, C., Neumann, T., Schimanke, S. & Meier, H. E. M. Impact of the Atlantic Multidecadal Oscillation on Baltic Sea Variability. *Geophys. Res. Lett.* **45**, 9880–9888 (2018).
- Cai, Q., Beletsky, D., Wang, J. & Lei, R. Interannual and decadal variability of Arctic Summer Sea Ice associated with atmospheric teleconnection patterns during 1850–2017. *J. Clim.* **34**, 9931–9955 (2021).
- Enfield, D. B., Mestas-Núñez, A. M. & Trimble, P. J. The Atlantic Multidecadal Oscillation and its relation to rainfall and river flows in the continental U.S. *Geophys. Res. Lett.* **28**, 2077–2080 (2001).
- Schimanke, S. & Meier, H. E. M. Decadal-to-centennial variability of salinity in the Baltic Sea. *J. Clim.* **29**, 7173–7188 (2016).
- Knight, J. R., Folland, C. K. & Scaife, A. A. Climate impacts of the Atlantic Multidecadal Oscillation. *Geophys. Res. Lett.* **33**, L17706 (2006).
- Schlesinger, M. E. & Ramankutty, N. An oscillation in the global climate system of period 65–70 years. *Nature* **367**, 723–726 (1994).
- Sutton, R. T. & Hodson, D. L. R. Atlantic ocean forcing of North American and European summer climate. *Science* **309**, 115–118 (2005).
- Belkin, I. M. Rapid warming of large marine ecosystems. *Prog. Oceanogr.* **81**, 207–213 (2009).
- Hurrell, J. W. Decadal trends in the North Atlantic Oscillation: regional temperatures and precipitation. *Science* **269**, 676–679 (1995).
- Peings, Y. & Magnusdottir, G. Forcing of the wintertime atmospheric circulation by the multidecadal fluctuations of the North Atlantic Ocean. *Environ. Res. Lett.* **9**, 034018 (2014).
- Gastineau, G. & Frankignoul, C. Influence of the North Atlantic SST variability on the atmospheric circulation during the twentieth century. *J. Clim.* **28**, 1396–1416 (2015).
- Delworth, T. L. et al. The central role of ocean dynamics in connecting the North Atlantic oscillation to the extratropical component of the Atlantic multidecadal oscillation. *J. Clim.* **30**, 3789–3805 (2017).
- Delworth, T. L. & Zeng, F. The impact of the North Atlantic oscillation on climate through its influence on the Atlantic Meridional overturning circulation. *J. Clim.* **29**, 941–962 (2016).
- Wills, R. C. J., White, R. H. & Levine, X. J. Northern hemisphere stationary waves in a changing climate. *Curr. Clim. Chang. Rep.* **5**, 372–389 (2019).
- Sun, C., Li, J. & Jin, F.-F. A delayed oscillator model for the quasi-periodic multidecadal variability of the NAO. *Clim. Dyn.* **45**, 2083–2099 (2015).
- Remane, A. Die Brackwasserfauna: mit besonderer Berücksichtigung der Ostsee. *Zool. Anz. Suppl.* **7**, 34–74 (1934).
- Vuorinen, I. et al. Scenario simulations of future salinity and ecological consequences in the Baltic Sea and adjacent North Sea areas—implications for environmental monitoring. *Ecol. Indic.* **50**, 196–205 (2015).
- Holopainen, R. et al. Impacts of changing climate on the non-indigenous invertebrates in the northern Baltic Sea by end of the twenty-first century. *Biol. Invasions* **18**, 3015–3032 (2016).
- Dippner, J. W., Fründt, B. & Hammer, C. Lake or Sea? The Unknown Future of Central Baltic Sea Herring. *Front. Ecol. Evol.* **7**, 143 (2019).
- Jones, P. D., Jonsson, T. & Wheeler, D. Extension to the North Atlantic oscillation using early instrumental pressure observations from Gibraltar and south-west Iceland. *Int. J. Climatol.* **17**, 1433–1450 (1997).
- Kauker, F. & Meier, H. E. M. Modeling decadal variability of the Baltic Sea: 1. Reconstructing atmospheric surface data for the period 1902–1998. *J. Geophys. Res.* **108**, 3268 (2003).
- Meier, H. E. M., Höglund, A., Eilola, K. & Almroth-Rosell, E. Impact of accelerated future global mean sea level rise on hypoxia in the Baltic Sea. *Clim. Dyn.* **49**, 163–172 (2017).
- Madsen, K. S., Hoyer, J. L., Suursaar, Ü., She, J. & Knudsen, P. Sea level trends and variability of the Baltic Sea From 2D statistical reconstruction and altimetry. *Front. Earth Sci.* **7**, 243 (2019).
- Rodhe, J. & Winsor, P. On the influence of the freshwater supply on the Baltic Sea mean salinity. *Tellus A* **54**, 175–186 (2002).
- Gustafsson, B. G. & Andersson, H. C. Modeling the exchange of the Baltic Sea from the meridional atmospheric pressure difference across the North Sea. *J. Geophys. Res.* **106**, 19731–19744 (2001).
- Gustafsson, B. G. et al. Reconstructing the development of Baltic Sea eutrophication 1850–2006. *Ambio* **41**, 534–548 (2012).
- Döös, K., Meier, H. E. M. & Döscher, R. The Baltic haline conveyor belt or the overturning circulation and mixing in the Baltic. *Ambio* **33**, 261–266 (2004).

45. Busuioc, A., Chen, D. & Hellström, C. Temporal and spatial variability of precipitation in Sweden and its link with the large-scale atmospheric circulation. *Tellus A* **53**, 348–367 (2001).
46. Krauss, W. & Brüggge, B. Wind-produced water exchange between the Deep Basins of the Baltic Sea. *J. Phys. Oceanogr.* **21**, 373–384 (1991).
47. Liblik, T. & Lips, U. Stratification has strengthened in the Baltic Sea—an analysis of 35 years of observational data. *Front. Earth Sci.* **7**, 174 (2019).
48. Meier, H. E. M., Döscher, R. & Faxén, T. A multiprocessor coupled ice-ocean model for the Baltic Sea: application to salt inflow. *J. Geophys. Res.* **108**, 3273 (2003).
49. Meier, H. E. M. Modeling the pathways and ages of inflowing salt-and freshwater in the Baltic Sea. *Estuar. Coast. Shelf Sci.* **74**, 610–627 (2007).
50. Meier, H. E. M. On the parameterization of mixing in three-dimensional Baltic Sea models. *J. Geophys. Res.* **106**, 30997–31016 (2001).
51. Mårtensson, S., Meier, H. E. M., Pemberton, P. & Haapala, J. Ridged sea ice characteristics in the Arctic from a coupled multicategory sea ice model. *J. Geophys. Res.* **117**, C00D15 (2012).
52. Schenk, F. & Zorita, E. Reconstruction of high resolution atmospheric fields for Northern Europe using analog-upscaling. *Climate* **8**, 1681–1703 (2012).
53. Döscher, R. et al. The development of the regional coupled ocean-atmosphere model RCAO. *Boreal Environ. Res.* **7**, 183–192 (2002).
54. Ekman, M. & Mäkinen, J. Mean sea surface topography in the Baltic Sea and its transition area to the North Sea: a geodetic solution and comparisons with oceanographic models. *J. Geophys. Res.* **101**, 11993–11999 (1996).
55. Meier, H. E. M., Dieterich, C. & Gröger, M. Natural variability is a large source of uncertainty in future projections of hypoxia in the Baltic Sea. *Commun. Earth Environ.* **2**, 50 (2021).
56. Meier, H. E. M., Väli, G., Naumann, M., Eilola, K. & Frauen, C. Recently accelerated oxygen consumption rates amplify deoxygenation in the Baltic Sea. *J. Geophys. Res.* **123**, 3227–3240 (2018).
57. Meier, H. E. M., Döscher, R., Broman, B. & Piechura, J. The major Baltic inflow in January 2003 and preconditioning by smaller inflows in summer-autumn 2002: a model study. *Oceanologia* **46**, 557–579 (2004).
58. Poli, P. et al. ERA-20C: an atmospheric reanalysis of the twentieth century. *J. Clim.* **29**, 4083–4097 (2016).
59. Rayner, N. A. et al. Global analyses of sea surface temperature, sea ice, and night marine air temperature since the late nineteenth century. *J. Geophys. Res.* **108**, 4407 (2003).
60. Seifert, T. & Kayser, B. A high resolution spherical grid topography of the Baltic Sea. *Issue 9 of Meereswissenschaftliche Berichte* (Institut für Ostseeforschung, Warnemünde 77–88 (Marine Science Report, Baltic Sea Research Institute, 1995).
61. Grinsted, A., Moore, J. C. & Jevrejeva, S. Application of the cross wavelet transform and wavelet coherence to geophysical time series. *Nonlinear Proc. Geophys.* **11**, 561–566 (2004).
62. Meier, H. E. M. & Döscher, R. Simulated water and heat cycles of the Baltic Sea using a 3D coupled atmosphere-ice-ocean model. *Boreal Environ. Res.* **7**, 327–334 (2002).

ACKNOWLEDGEMENTS

The research presented in this study is part of the Baltic Earth programme (Earth System Science for the Baltic Sea region, see <http://www.baltic.earth>) and was funded

by the Swedish Research Council for Environment, Agricultural Sciences and Spatial Planning (Formas) through the ClimeMarine project within the framework of the National Research Programme for Climate (grant No. 2017-01949). Data from the IOW's long-term monitoring programme were used.

AUTHOR CONTRIBUTIONS

H.E.M.M. designed the research, performed the sensitivity simulations, analysed the model results and wrote the paper with the help of all co-authors: L.B., F.B., M.G., L.N. and H.R. L.B. and F.B. performed the wavelet analyses and L.N. analysed the model results vs. observations. H.R. prepared the salinity observations and analysis tools.

FUNDING

Open Access funding enabled and organized by Projekt DEAL.

COMPETING INTERESTS

The authors declare no competing interests.

ADDITIONAL INFORMATION

Supplementary information The online version contains supplementary material available at <https://doi.org/10.1038/s41612-023-00380-9>.

Correspondence and requests for materials should be addressed to H. E. Markus Meier.

Reprints and permission information is available at <http://www.nature.com/reprints>

Publisher's note Springer Nature remains neutral with regard to jurisdictional claims in published maps and institutional affiliations.



Open Access This article is licensed under a Creative Commons Attribution 4.0 International License, which permits use, sharing, adaptation, distribution and reproduction in any medium or format, as long as you give appropriate credit to the original author(s) and the source, provide a link to the Creative Commons license, and indicate if changes were made. The images or other third party material in this article are included in the article's Creative Commons license, unless indicated otherwise in a credit line to the material. If material is not included in the article's Creative Commons license and your intended use is not permitted by statutory regulation or exceeds the permitted use, you will need to obtain permission directly from the copyright holder. To view a copy of this license, visit <http://creativecommons.org/licenses/by/4.0/>.

© The Author(s) 2023

Multidecadal climate variability dominated past trends in the water balance of the Baltic Sea catchment area

H. E. Markus Meier^{1,2,*}, Leonie Barghorn¹, Florian Börgel¹, Matthias Gröger¹, Lev Naumov¹, and Hagen Radtke¹

¹Department of Physical Oceanography and Instrumentation, Leibniz Institute for Baltic Sea Research Warnemünde, 18119 Rostock, Germany.

²Department of Research and Development, Swedish Meteorological and Hydrological Institute, 60176 Norrköping, Sweden.

*e-mail: markus.meier@io-warnemuende.de

Corresponding author:

H. E. Markus Meier

Department of Physical Oceanography and Instrumentation

Leibniz Institute for Baltic Sea Research Warnemünde

Seestrasse 15

18119 Rostock

Germany

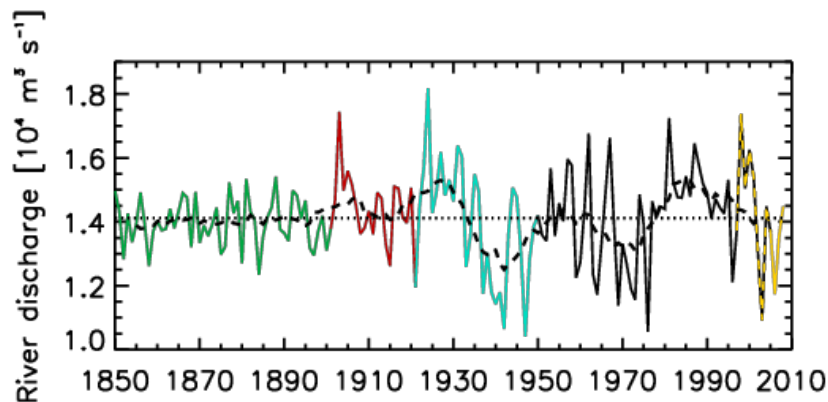
Tel.: +49 381 5197 150

E-mail: markus.meier@io-warnemuende.de

Supplementary Information

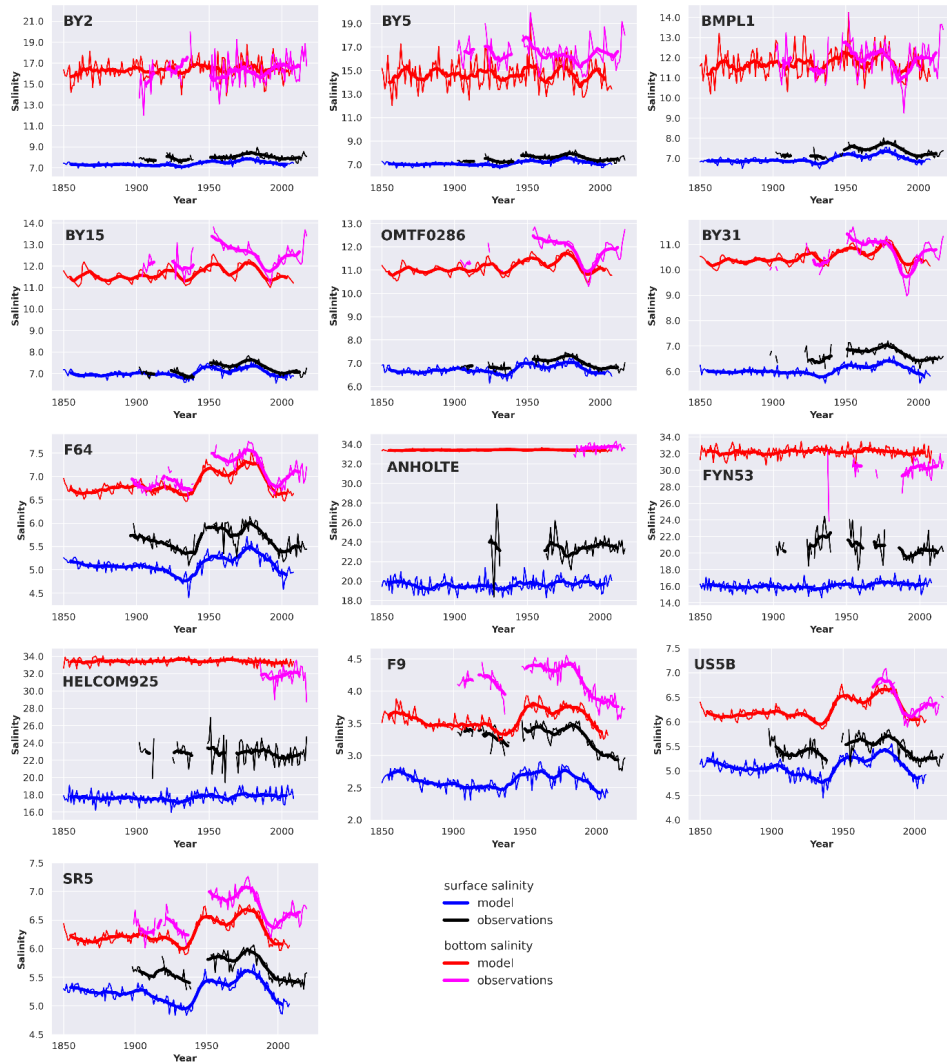
This Supplementary Information consists of Supplementary Figures 1–8.

Supplementary Figures

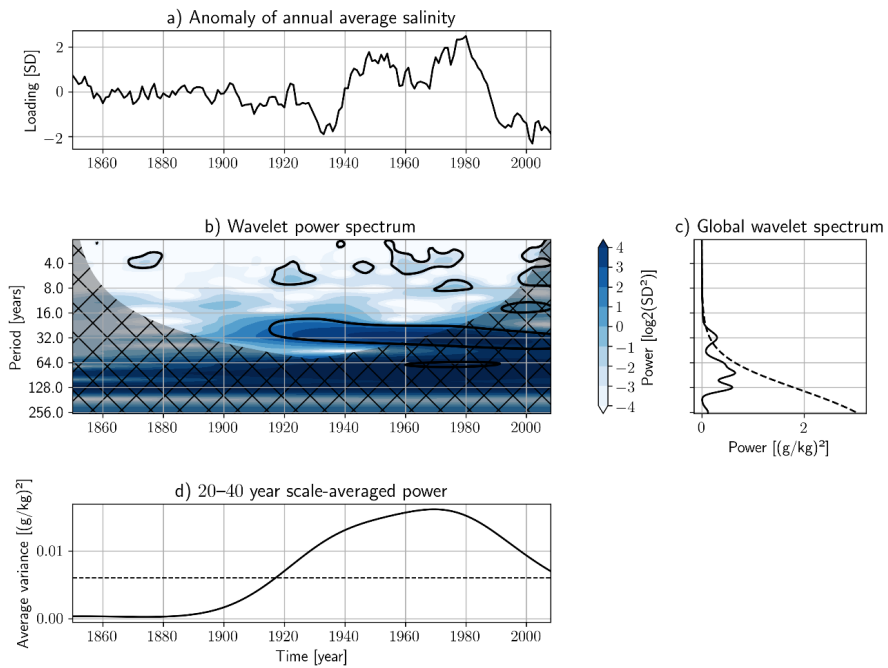


Supplementary Fig. 1 Reconstructed total river discharge to the Baltic Sea 1850-2008.

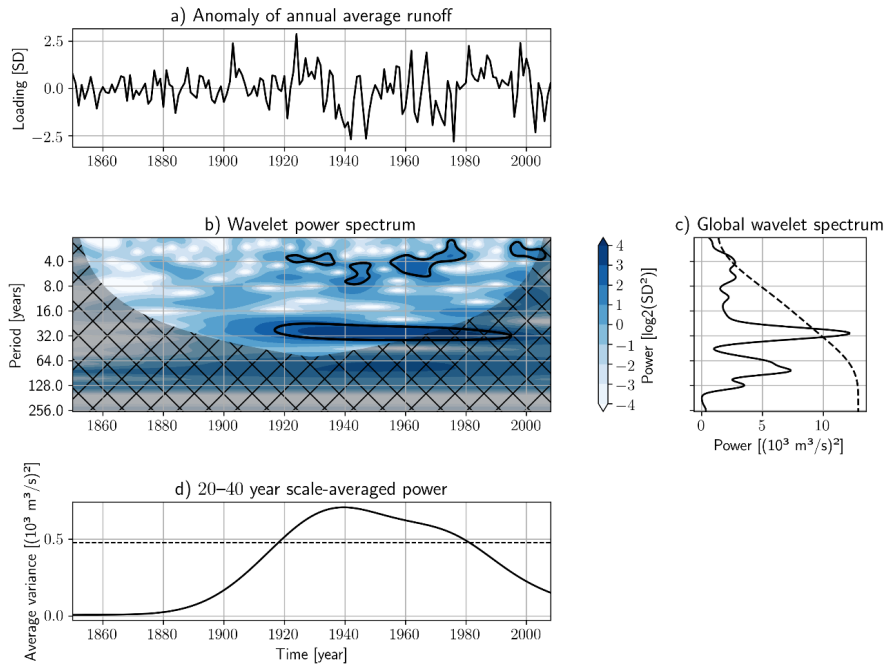
Annual (solid line) and low-pass filtered (dashed line) river discharge reconstructed from various datasets (indicated by different colors) with a cut-off period of 12 years by Meier et al. (2019). The long-term mean (1850-2008) river runoff to the Baltic Sea (dotted line) amounts to $14,100 \text{ m}^3 \text{ s}^{-1}$. (Source: Meier et al., 2019; their Fig. 3 published open access under the terms of the Creative Commons Attribution 4.0 International licence)



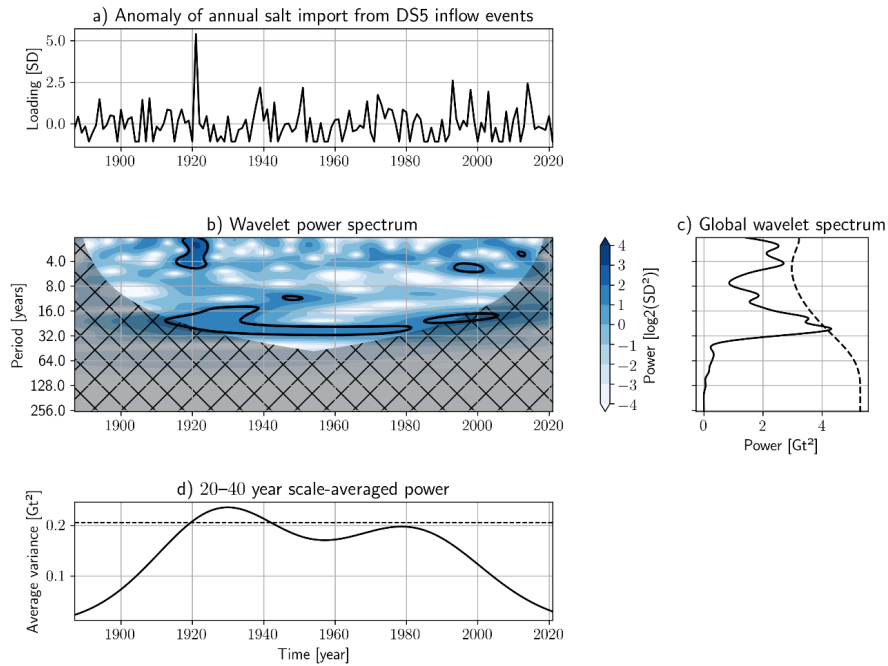
Supplementary Fig. 2 Simulated and observed sea surface and bottom salinities at various monitoring stations. Salinities in g kg^{-1} . Following Radtke et al. (2020), measurements are post-processed to fill gaps. Thin lines: annual averages. Thick lines: 11-year running mean. In Fig. 1, the locations of the long-term monitoring stations are shown.



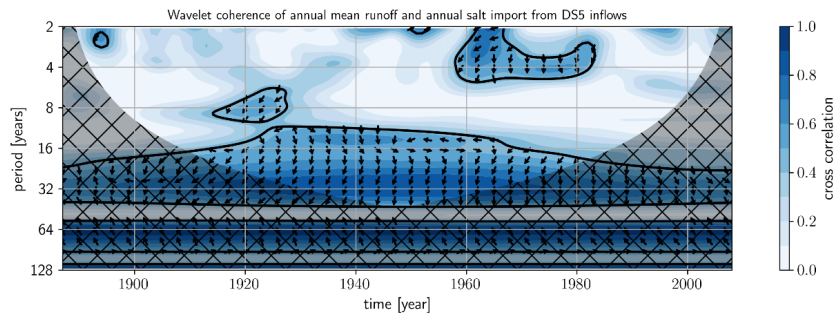
Supplementary Fig. 3 Spectrum of annual mean salinity averaged over the Baltic Sea 1850-2008. Shown are results of the reference simulation REF+. a) Time series, b) wavelet power, c) power averaged over time and d) wavelet power averaged for the period band between 20 and 40 years as a function of time. The black contour lines in the wavelet power spectrum show the 95% significance level (Grinsted et al., 2004).



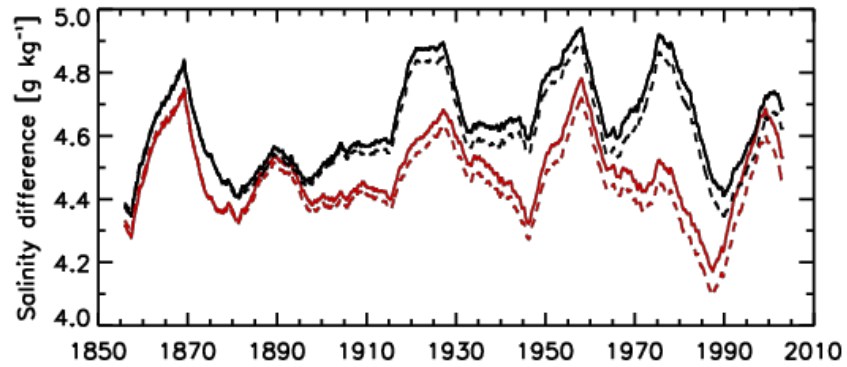
Supplementary Fig. 4 Spectrum of the annual river discharge to the Baltic Sea 1850-2008. a) Time series, b) wavelet power, c) power averaged over time and d) wavelet power averaged for the period band between 20 and 40 years as a function of time. The black contour lines in the wavelet power spectrum show the 95% significance level (Grinsted et al., 2004). (Data source: Meier et al., 2019)



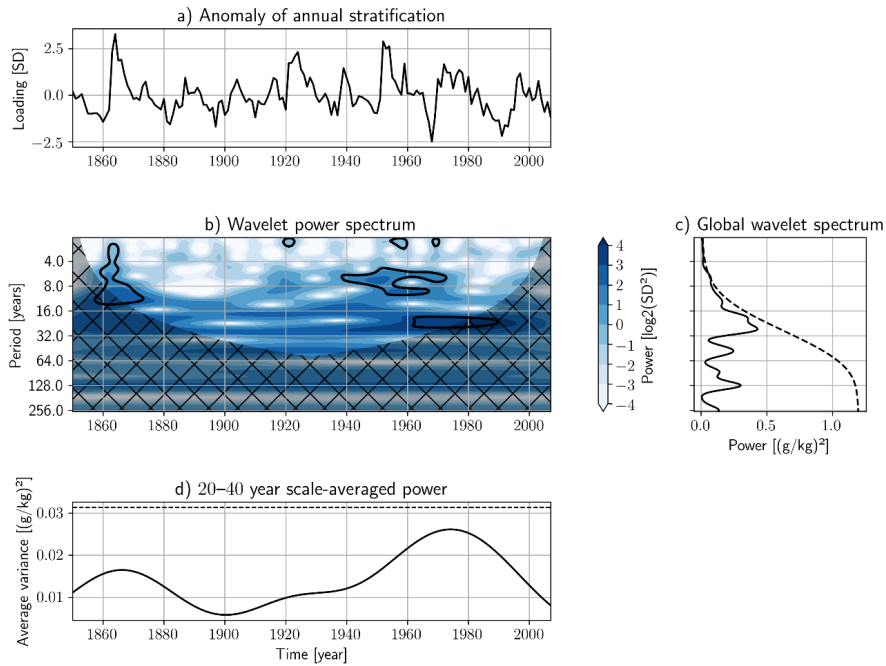
Supplementary Fig. 5 Spectrum of the annual mean salt import from reconstructed Major Baltic Inflows (so-called DS5 events) 1887-2021. a) Time series, b) wavelet power, c) power averaged over time and d) wavelet power averaged for the period band between 20 and 40 years as a function of time. The black contour lines in the wavelet power spectrum show the 95% significance level (Grinsted et al., 2004). (Data source: Mohrholz, 2018)



Supplementary Fig. 6 Wavelet coherence between the annual mean river discharge and the annual mean salt import from DS5 inflow events 1887-2008. The black contour lines show the 95% significance level (Grinsted et al., 2004). The arrows in the significant regions indicate the phase relationship between the signals: pointing right (left) in phase (antiphase), and river discharge leading (lagging) the salt import straight down (up). (Data source: Mohrholz, 2018; Meier et al., 2019)



Supplementary Fig. 7 Stratification in the central Baltic Sea. Low-pass filtered salinity difference (in g kg^{-1}) between sea surface and bottom salinity at Gotland Deep (BY15) with a cut-off period of 12 years. For the location of the monitoring station BY15 see Fig. 1. The curves show the numerical experiments REF+ (black solid line), REF (black dashed line), RUNOFF+ (red solid line) and RUNOFF (red dashed line).



Supplementary Fig. 8 Spectrum of annual mean stratification in the central Baltic Sea

1850-2008. Shown is the salinity difference (in g kg^{-1}) between sea surface and bottom salinity at Gotland Deep (BY15) in the numerical experiment REF+. a) Time series, b) wavelet power, c) power averaged over time and d) wavelet power averaged for the period band between 20 and 40 years as a function of time. The black contour lines in the wavelet power spectrum show the 95% significance level (Grinsted et al., 2004).

References

Grinsted, A., Moore, J. C., & Jevrejeva, S. Application of the cross wavelet transform and wavelet coherence to geophysical time series. *Nonlinear Proc. Geoph.*, **11**(5/6), 561-566 (2004).

Meier, H. E. M., et al. Disentangling the impact of nutrient load and climate changes on Baltic Sea hypoxia and eutrophication since 1850. *Clim. Dyn.*, **53**(1), 1145-1166 (2019).

Mohrholz, V. Major Baltic inflow statistics—revised. *Front. Mar. Sci.*, **5**, 384 (2018).

Radtke, H., Brunnabend, S. E., Gräwe, U., & Meier, H. E. M. Investigating interdecadal salinity changes in the Baltic Sea in a 1850–2008 hindcast simulation. *Clim. Past*, **16**(4), 1617-1642 (2020).



OPEN ACCESS

EDITED BY
Elinor Andrén,
Södertörn University, Sweden

REVIEWED BY
Tarang Khangaonkar,
Pacific Northwest National Laboratory
(DOE), United States
Adolf Konrad Stips,
European Commission, Italy

*CORRESPONDENCE
Lev Naumov
✉ lev.naumov@io-warnemuende.de

RECEIVED 01 June 2023
ACCEPTED 21 July 2023
PUBLISHED 11 August 2023

CITATION
Naumov L, Meier HEM and Neumann T
(2023) Dynamics of oxygen sources and
sinks in the Baltic Sea under different
nutrient inputs.
Front. Mar. Sci. 10:1233324.
doi: 10.3389/fmars.2023.1233324

COPYRIGHT
© 2023 Naumov, Meier and Neumann. This
is an open-access article distributed under
the terms of the [Creative Commons
Attribution License \(CC BY\)](#). The use,
distribution or reproduction in other
forums is permitted, provided the original
author(s) and the copyright owner(s) are
credited and that the original publication in
this journal is cited, in accordance with
accepted academic practice. No use,
distribution or reproduction is permitted
which does not comply with these terms.

Dynamics of oxygen sources and sinks in the Baltic Sea under different nutrient inputs

Lev Naumov*, H. E. Markus Meier and Thomas Neumann

Department of Physical Oceanography and Instrumentation, Leibniz Institute for Baltic Sea Research Warnemünde, Rostock, Germany

The Baltic Sea is one of the marine systems suffering from pronounced man-made hypoxia due to the elevated nutrient loads from land. To mitigate hypoxia expansion and to return the Baltic Sea to a good environmental state, the Baltic Sea Action Plan (BSAP), regulating the waterborne and airborne nutrient input, was adopted by all states surrounding the Baltic Sea. However, at the moment, no significant shrinking of the hypoxic area is observed. In this study, two scenario simulations of the future state of the deep parts of the central Baltic Sea (deeper than 70 meters) were carried out, utilizing a 3-dimensional numerical model. Climate change effects on meteorology, hydrology, and oceanic state were not included. We focused on O₂ and H₂S sources and sinks under different nutrient input scenarios. We found that under the BSAP scenario, all subbasins in the central Baltic Sea, especially the northern and western Gotland Basin, show significant improvement, namely, oxygenation and oxidation of the deposited reduced material, ceasing its advection to the upper layers and neighboring basins. We found that the nutrient loads are responsible for more than 60% and 80% of the O₂ and H₂S sources and sinks variability, respectively, at the interannual time scale. We showed that the Baltic Sea could return to the initial state in 1948, but under the more rigorous 0.5 BSAP scenario (nutrient input is halved compared to the BSAP). However, since we observed no hysteresis effect, the system would probably reach the initial state but over a timeframe longer than the 71-year future simulation period.

KEYWORDS

Baltic Sea, O₂ and H₂S sources and sinks, Baltic Sea Action Plan, nutrient reduction, modeling

1 Introduction

Hypoxia, or dissolved oxygen concentrations in the water column below a certain threshold (usually 2 ml O₂/l) (Conley et al., 2009; Savchuk, 2018; Stoicescu et al., 2019), is a pronounced problem in numerous marine systems worldwide, which is currently deteriorating (Diaz and Rosenberg, 2008; Breitburg et al., 2018). The main factor favoring the low oxygen concentrations is elevated anthropogenic nutrient loads from

land promoting eutrophication (Heathwaite et al., 1996; Knuuttila et al., 2017; Ator et al., 2020). However, climate change also affects global deoxygenation (Whitney, 2022). One example of a marine system suffering from elevated hypoxia is the Baltic Sea - a semi-enclosed sea in Northern Europe. Due to some natural properties, such as limited water exchange with the North Sea, which lead to a long residence time (Leppäranta and Myrberg, 2009) and a pronounced permanent halocline, located around 60 meters depth (Väli et al., 2013; Uurasjärvi et al., 2021), which limits the exchange between the upper and lower layers, the Baltic Sea is naturally prone to hypoxia (Gustafsson et al., 2012). Lenz et al. (2015) studied the sediment cores from the Baltic Sea and concluded that hypoxic conditions occurred in the Baltic Sea after the establishment of the halocline. However, hypoxic area in the Baltic Sea has been dramatically increasing since the 1960s (Almroth-Rosell et al., 2021; Kouts et al., 2021; Krapf et al., 2022). It was attributed to the elevated nutrient (P and N) loads from land (Larsson et al., 1985). To mitigate the ongoing eutrophication, the Baltic Sea Action Plan (BSAP) was developed by the Helsinki Commission (HELCOM) in 2007 (HELCOM, 2007; Backer et al., 2010). Later, the BSAP was updated a few times, with the last version applied in 2021 (HELCOM, 2021). One function of the BSAP is to provide information about the maximum allowable nutrient input (MAI) to the Baltic Sea. Adherence to the MAI should guarantee hypoxic area reduction and transition to a better state of the Baltic Sea. However, despite the nutrient loads reduction policy, no significant improvement has been observed yet (Hansson and Viktorsson, 2020). Vahtera et al. (2007) coined the term “vicious circle” for the Baltic Sea, which describes the possible damping mechanism for oxygenation. A model study (Neumann et al., 2002) supported the “vicious circle” mechanism, namely, the stable cyanobacteria biomass supported by the release of the sedimentary phosphorus under anoxic conditions. The “vicious circle” mechanism was further discussed and developed in several studies, for example (Rydin et al., 2017; Meier et al., 2018; Savchuk, 2018). Despite the overall awareness of the oxygen dynamics in the Baltic Sea, only a few studies disentangled the oxygen sources and sinks in the Baltic Sea (Gustafsson and Stigebrandt, 2007; Schneider et al., 2010; Naumov et al., 2023). Sources and sinks of oxygen and hydrogen sulfide in the central Baltic Sea demonstrated substantial changes during the last 70 years. Meier et al. (2018) highlighted the switch between oxygen consumption in sediments to more water column consumption. Naumov et al. (2023) conducted a trend analysis of oxygen and hydrogen sulfide sources and sinks and came to similar conclusions for oxygen. As for hydrogen sulfide, they found an increasing spread between its production in the sediments and consumption in the water column leading to elevated advection to the upper layers. There are also studies projecting oxygen concentrations in the future (e.g., Meier et al., 2011; Friedland et al., 2012; Neumann et al., 2012; Meier et al., 2022). Those projections include both climate and nutrient forcings. Our aim is to study only the nutrient forcing, focusing on the oxygen and hydrogen sulfide sources and sinks under changing nutrient input. It will help to disentangle the two forcing factors and to understand the possible future state of the Baltic Sea and might be useful in future adjustments of the BSAP.

2 Materials and methods

2.1 Model description

To investigate oxygen and hydrogen sulfide dynamics in the central Baltic Sea, we used the 3-dimensional coupled regional MOM-ERGOM model. Modular Ocean Model (MOM) version 5 (Griffies, 2012) served as a hydrodynamical model reproducing ocean motion and dynamics of the two principal tracers (temperature and salinity) by solving the set of primitive equations. K-profile parametrization (KPP, Large et al., 1994) was used as the turbulence closure scheme. Our MOM setup utilizes regular orthogonal Arakawa B grid with z^* coordinate vertical scheme and a predictor-corrector scheme (Griffies, 2012). Ecological Regional Ocean Model (ERGOM) (Radtke et al., 2019; Neumann et al., 2021; Neumann et al., 2022) was used as a biogeochemical model. ERGOM reproduces cycles of the main nutrients (C, N, P) as well as oxygen (O_2) and hydrogen sulfide (H_2S), which is represented by the separate active tracer in the model. The complete model description can be found in (Neumann et al., 2022). An open boundary was placed in Skagerrak permitting exchange with the North Sea. Our model setup has three nautical miles horizontal resolution, while the vertical resolution varies from 0.5 to 2 meters. This setup has been used multiple times to model the Baltic Sea dynamics. It includes a recent study by Naumov et al. (2023) and a few others (e.g., Neumann, 2010; Voss et al., 2011; Kuznetsov and Neumann, 2013). Recently the model was thoroughly validated (see Naumov et al., 2023). As a short validation summary, the model reasonably reproduced the central Baltic Sea dynamics. However, possibly due to the overestimated exchange with the North Sea and, therefore, too strong halocline, hypoxic and anoxic areas were larger in the model compared to the reanalysis data.

2.2 Formulation of O_2 and H_2S budgets

A budget concept implies the balance between sources and sinks of a given substance in a certain box. If the sources exceed the sinks, the total amount of an arbitrary substance within the box increases, and vice versa (Yurkovskis et al., 1993; Fennel and Testa, 2019). Mathematically it could be summarized by the following equation:

$$\frac{d}{dt} \iiint_V Tr \, dx \, dy \, dz - \iint_S \bar{v} Tr \, dx \, dy - \iiint_V \frac{\partial Tr}{\partial t} \, dx \, dy \, dz = 0$$

Where Tr stands for any tracer. The first term in the equation represents the total change of the amount of tracer in time, which, by definition, equals the internal change of the tracer within the box, for instance, due to the biochemical processes (the third term) plus the total flux across all boundaries of the box (the second term). For oxygen, the budget consists of advective and diffusive supply across the box's boundaries, as well as the supply due to the photosynthesis, which is situated in the photic level during the vegetation period, and biochemical consumption in the water column and sediments expressed as higher trophic level organisms' respiration, mineralization of organic matter, nitrification, and oxidation of H_2S . For hydrogen sulfide, the

budget is formulated as advection and diffusion fluxes across the boundaries and mineralization of organic matter (sulfide reduction) in the sediments and water column. Hydrogen sulfide is consumed via the oxidation by O_2 or NO_3^- . For the description of all processes contributing to the O_2 and H_2S budgets in ERGOM and their aggregations, see [Supplementary Table 1](#). Four boxes situated in the central Baltic Sea, each representing a specific subbasin, were investigated: the Bornholm Basin (BB), the eastern Gotland Basin (eGB), the northern Gotland Basin (nGB), and the western Gotland Basin (wGB). The upper boundary for each box was set to a 70-meter depth, excluding the upper oxygen-reach layer. The boxes spanned the water column down to the bottom. Their locations can be found in [Figure 1](#).

2.3 Nutrient input scenarios

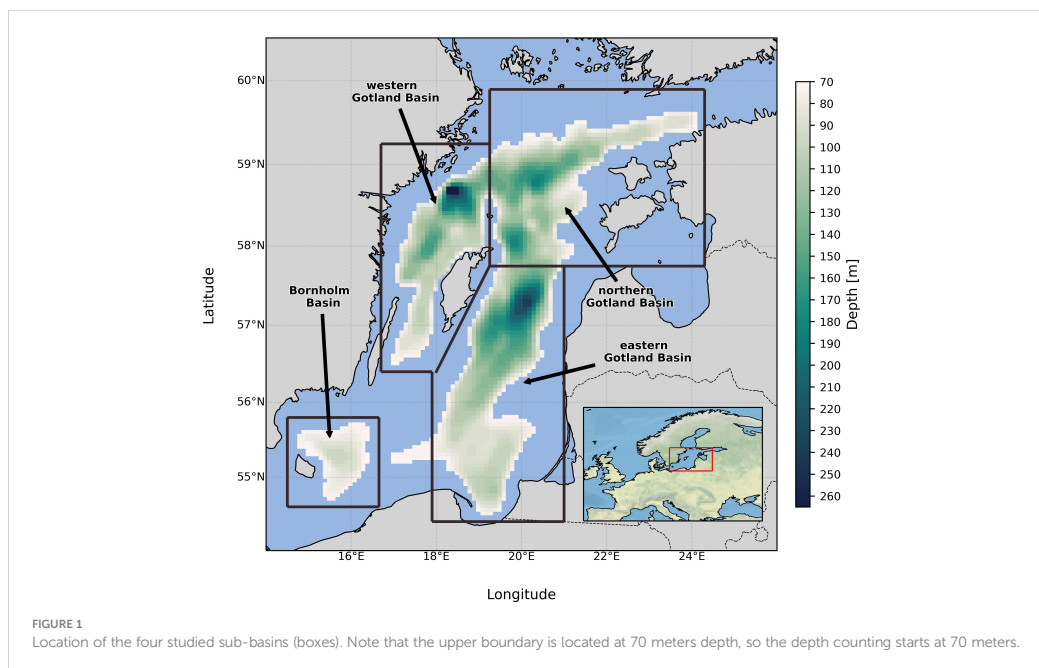
This study features three different nutrient input scenarios. The reference scenario is based on the simulation analyzed in [Naumov et al. \(2023\)](#). It employs HELCOM's actual nutrient loads from 1948 to 2018 ([Svendsen and Gustafsson, 2020](#)). Data gaps were filled with linear interpolation. The BSAP scenario imposes constant nutrient loads based on the level of the Maximum Allowable Input (MAI) ([HELCOM, 2021](#)). The total input of P and N into the Baltic Sea at levels no more than the BSAP MAI should guarantee the Baltic Sea's transition into a "good environmental status" ([Borja et al., 2015](#)). Since BSAP specifies only total loads without separating airborne and waterborne loads, the climatology seasonal cycle of the atmospheric nutrient input was applied. The halved BSAP MAI scenario (0.5 BSAP) assumes that the loads would be constant on the level of the half from the BSAP MAI (both waterborne and airborne input). The two reduction scenarios span the timeframe from 2019 to 2089 (71 years) and start from initial conditions taken from the last year of the reference scenario. Total nitrogen loads to the Baltic Sea under the BSAP scenario are set to 792.2 Kton/a (97% of the actual nitrogen loads averaged for the last ten years – 815.4 Kton/a). Under the 0.5 BSAP scenario, the total nitrogen loads equal 396.1 Kton/a (48% of the average actual loads for the last ten years). Total phosphorus loads under the BSAP and 0.5 BSAP scenarios equal 21.72 and 10.86 Kton/a, respectively. This constitutes 82 and 41% of the current total phosphorus loads – 26.33 Kton/a, respectively. So the BSAP goals have not been fully achieved yet, but the actual loads are very close to them. For more information, see [Supplementary Figures 1, 2](#). In reference and nutrient reduction scenarios, we applied identical atmospheric forcing, namely CoastDat2 atmospheric fields from 1948 to 2018 ([Geyer, 2014](#)). Therefore, we neglect the impact of future climate change and natural variability, focusing only on the nutrient loads effect on the Baltic Sea's eutrophication.

3 Results and discussion

3.1 Trends in O_2 and H_2S sources and sinks

Following the approach of [Naumov et al. \(2023\)](#), we aggregated all O_2 and H_2S budget terms into three categories based on their origin

(physical or biological) and domain (water column or sediments): physical processes encompassing all oxygen fluxes with physical origin, mainly lateral and vertical advection (phy), oxygen fluxes with biological origin situated in the water column, e.g., remineralization of OM and zooplankton respiration (bio), and oxygen fluxes located in the sediments, e.g., remineralization of the sedimentary detritus (sed). Results are shown in [Figure 2](#) (oxygen) and [Supplementary Figure 3](#) (hydrogen sulfide). [Figure 2](#) shows significant changes in the oxygen consumption pattern under both BSAP and 0.5 BSAP scenarios. Especially significant changes happened in the nGB, where oxygen consumption shifted back to the sediments at the end of the study period in both scenarios (with 0.5 BSAP amplifying the reported changes). The wGB demonstrates a similar pattern. However, it achieved sediment dominance in the consumption only under the 0.5 BSAP scenario. Under the BSAP scenario, a significant negative trend was only observed in sedimentary consumption. Elevated oxygen consumption in the sediments under BSAP and 0.5 BSAP scenarios, most visible in the nGB, can be interpreted as a positive sign indicating reoxygenation of the sediments. As was concluded by [Naumov et al. \(2023\)](#), less oxygen consumption in the sediments indicates the absence of oxygen, which means no electron acceptor available for the reactions. As sediments contact with oxygen again, the reduced material is getting oxidized promoting oxygen consumption in the sediments. This mechanism is more pronounced under the more rigorous 0.5 BSAP scenario. Noticeably, a significant positive trend in physical fluxes was observed under the 0.5 BSAP scenario, which is related to better ventilation due to the improved oxygen conditions in the neighboring nGB. Unlike nGB and wGB, BB and eGB are closer to the Baltic Sea's entrance and therefore receive more oxygen via advection ([Liblik et al., 2018](#); [Naumov et al., 2023](#)), do not demonstrate striking trends in consumption terms. The only significant trend in the BB is the positive trend in sedimentary consumption under the 0.5 BSAP scenario, indicating the best oxygen conditions among the studied subbasins. In the eGB, significant positive trends in the water column oxygen consumption were observed under both BSAP and 0.5 BSAP scenarios. It also points out the improvement because less consumption in the water column indicates less reduced material stored there. H_2S sources and sinks ([Supplementary Figure 3](#)) also demonstrated substantial changes. By the end of the study period, the eGB came to the dynamic balance between H_2S sources and sinks, indicating that H_2S is not deposited. The same changes by the end of the period are observed even in the nGB under the 0.5 BSAP scenario. Under the BSAP scenario, a significant reduction in H_2S production and consumption is observed in the nGB. However, it stabilizes in the 2070s. Despite that, advection to the upper layers in the nGB stops by the end of the study period in both scenarios. The wGB demonstrated the most noticeable difference between the BSAP and 0.5 BSAP scenarios. Under the BSAP scenario, wGB is still exporting H_2S to the upper layer by the end of the study period, although to a much lower extent than in the beginning. Sedimentary production exhibits a significant negative trend but stabilizes in the 2070s, and water column consumption shows no trend under the BSAP scenario. Under the 0.5 BSAP scenario, both consumption and production of H_2S converge to zero in the wGB, removing any export to the upper layers via advection.



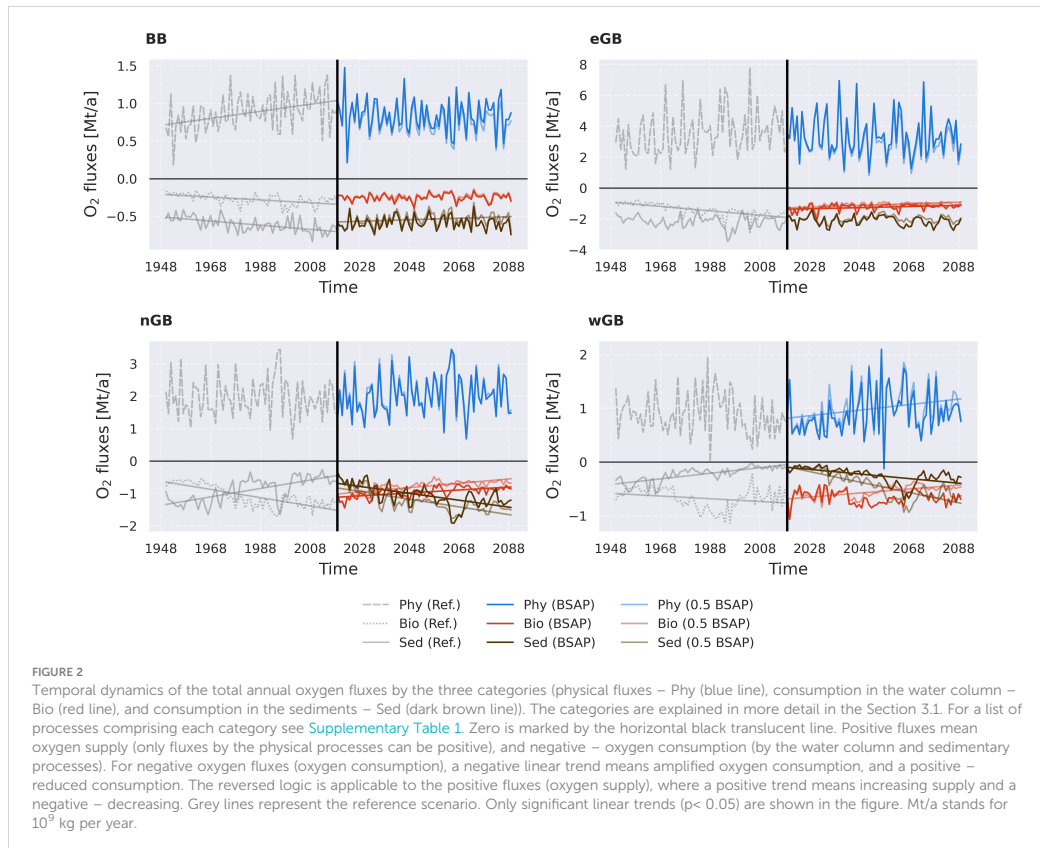
3.2 Budgets' composition

To evaluate different sources and sinks' contribution to the oxygen and hydrogen sulfide variability, we employed a linear regression framework proposed by Naumov et al. (2023). This linear model allows us to estimate the explained interannual variability by each group of processes. We used the same groups (phy, bio, and sed) as in the previous section. The results are shown in Figure 3. It can be seen that the general pattern is similar compared to the one by Naumov et al. (2023), which is advection dominance for oxygen in both considered scenarios. Another pattern for oxygen is less explained variability by the water column processes (especially in the BB and eGB) moving from the reference scenario to the 0.5 BSAP. This pattern complements the conclusions from the previous section, namely, the elevated variability of the sedimentary processes towards the end of the simulation. The composition of the processes contributing to the H₂S budget is generally more complex (both regionally and in different scenarios). It points to the strong connection between H₂S dynamics and nutrient forcing (see Supplementary Figure 4 for additional information). Overall, it can be stated that H₂S dynamics is more affected by the nutrient loads reduction than oxygen dynamics, with some regional differences existing in both cases.

3.3 O₂ and H₂S dynamics induced by the nutrient forcing

Nutrient loads dynamics determine a significant fraction of oxygen variability in the Baltic Sea (Meier et al., 2019). Here, we

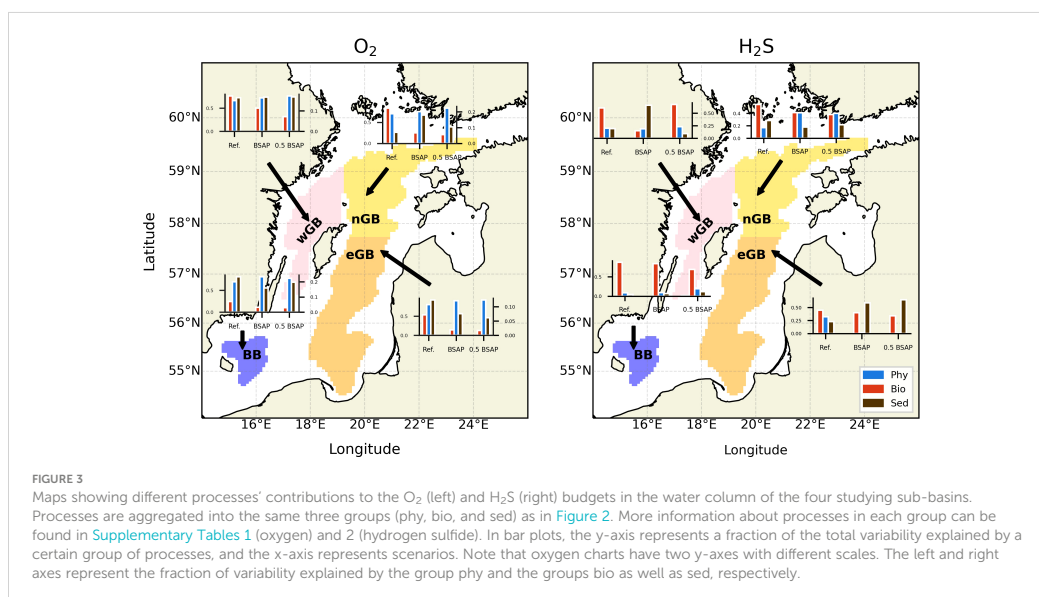
quantify its contribution to the oxygen and hydrogen sulfide sources and sinks variability under the considered scenarios. We employed Empirical Orthogonal Functions (EOFs), based on eigenvectors and eigenvalues (Hannachi et al., 2007). It allows a decomposition of the complex multidimensional data into a set of orthogonal functions with a reduced number of dimensions by calculating eigenvalues and eigenvectors of the data's correlation/covariance matrix and multiplying the latter with the original matrix. We applied such an EOF analysis to the matrices of oxygen and hydrogen sulfide budget terms' annual consumption/production anomalies during the reference period (1948-2018). Then we projected the resulting EOFs into future projections. Resulting EOFs are guaranteed to represent the same process during the reference period and future scenarios. The results are presented in Figure 4 (for oxygen) and Supplementary Figure 4 (for hydrogen sulfide). Based on the eigenvalues, the first three EOFs were considered significant for both elements (Panel A in Figure 4; Supplementary Figure 4). For O₂, the first EOF explains around 60% of the total variability, the second EOF about 20%, and the third about 10%. For H₂S, the eigenvalues converge quicker, with the first EOF already explaining 85% of the total variability and the last two EOFs around 5% each. The leading EOF in both O₂ and H₂S data can be attributed to the same process based on its loadings (Panel E in both figures). Both for O₂ and H₂S data, the leading EOF demonstrates a strong positive connection with anomalies of sedimentary detritus' oxidation (either by oxygen or sulfate reduction). This means that when the score of the first EOF is positive (from the 1970s to the 2030s, according to Panel B in both figures), there is an intensified H₂S production due to the



mineralization of sedimentary detritus in the nGB. The same is true (but to a lesser extent) for the other regions of the Gotland Basin. At the same time, detritus is less mineralized by oxygen in the nGB and wGB but more in the eGB, indicating reduced material deposition in the nGB and wGB. The negative score of the first EOF, which is observed at the beginning of the reference period and after the 2030s, indicates the overall improvement of the oxygen conditions in the central Baltic Sea (no long-term deposition of the reduced material and oxidation of existing H₂S, especially in the remote basins). This allowed us to attribute the leading EOF to the nutrient forcing. The last two EOFs were attributed to the inflow activity and natural variability. They do not exhibit any significant difference between the reference period and the future projections (for both BSAP and 0.5 BSAP scenarios). The first EOFs for BSAP and 0.5 BSAP are highly correlated (>0.9), which suggests that there are no significant differences in how the nutrient load reduction affects the marine system for the BSAP and more rigorous 0.5 BSAP scenarios; however, the first EOF for 0.5 BSAP scenario shows a more negative score compared to the first EOF of the BSAP scenario, which means the more resilient state and more improvement.

3.4 Discussion

Our results suggest that oxygen conditions in the central Baltic Sea will substantially improve both under BSAP and 0.5 BSAP scenarios, especially in the remote nGB and wGB, which, however, did not significantly diminish the hypoxic area, only the anoxic area significantly shrank at the end of the study period (see [Supplementary Figure 5](#)), which is related to the significant oxygen debt in the deep central Baltic Sea ([Rolf et al., 2022](#)). However, our study uses atmospheric forcing from 1948–2018, which completely ignores possible changes, such as changes in stratification and internal nutrient cycle ([Meier et al., 2011](#); [Hordoir and Meier, 2012](#)), that could worsen the results to some extent, but, based on the results by [Saraiva et al. \(2019\)](#); [Meier et al. \(2021\)](#) and [Bartosova et al. \(2019\)](#), the effect of nutrient load reduction policy should dominate climate change impacts, at least in the near future. Elevated halocline strength observed in the model ([Naumov et al., 2023](#)) also worsens oxygen conditions in the deep sea, which could mimic the negative effects in the real system related to climate change. Still, the dynamics of cyanobacteria blooms might be underestimated in the model since



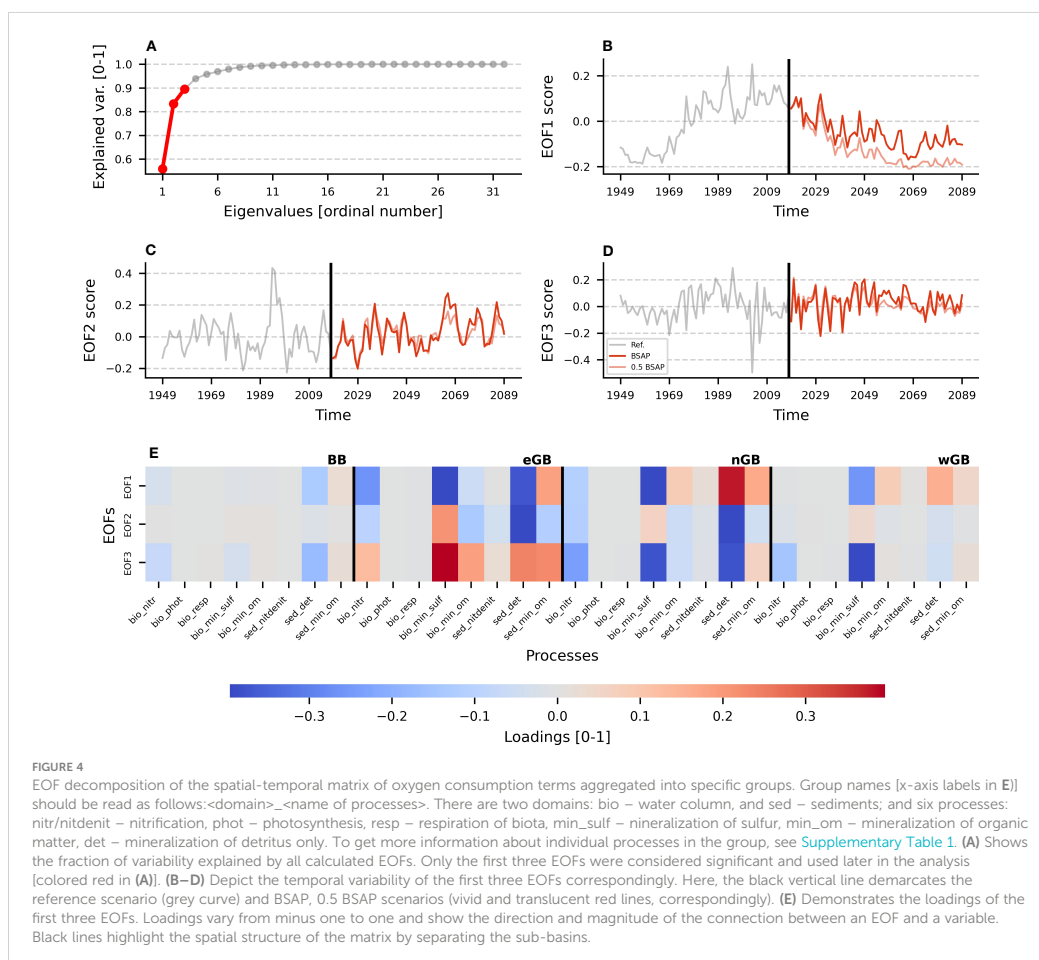
their blooms may get amplified by climate change. Since significant positive trends in nitrates were observed everywhere across the Gotland Basin (see Supplementary Figures 6–9), it could potentially lead to a serious deterioration in case of a sudden short-time anoxia and release of the sedimentary phosphorus (Mort et al., 2010). Another possible shortcoming of the study is related to the difficulties in validating the sources and sinks of O₂ and H₂S due to the lack of proper observational data (long-term monitoring at the specific station in the deep Baltic Sea). Only studies by Schneider et al. (2010) and Gustafsson and Stigebrandt (2007) reconstructed the oxygen sources and sinks based on observational data. Unfortunately, their results cannot be qualitatively compared to our model findings due to the different spatiotemporal scales and different formulations of processes in the model. Still, they exhibit similar patterns (elevated oxygen consumption by nitrification after more oxygen enters the system, for example).

4 Conclusions

1. The central Baltic Sea under the MAIs of the BSAP and the halved BSAP showed an improvement and transition to a more oxic state after 2018 within the simulated 71 years. However, the hypoxic area did not reduce dramatically in both scenarios, pointing out the high oxygen debt in the deep central Baltic Sea.
2. Positive changes were observed in all regions of the Gotland Basin, especially in the remote northern and western Gotland basins. In the nGB, a shift from consumption in the water column to consumption in the sediments was observed in both BSAP and 0.5 BSAP. In the wGB, the same changes were observed under 0.5 BSAP. Positive trends in

the water column oxygen consumption are mostly explained by the reduced oxidation of hydrogen sulfide and nitrification towards the end of the simulation (the year 2089). In the sediments, the increased consumption is mostly attributed to the elevated oxidation of organic matter towards the end of the simulation. Faster improvement in the remote basins was attributed to the positive feedback related to the reduction of H₂S concentration in eGB and, therefore, its less advection to the nGB and wGB. Elevated oxygen concentrations in the eGB could also lead to more effective ventilation of the remote basins by inflowing oxygen due to reduced consumption on the way to the remote basins.

3. The general trend to the less explained variance by water column oxygen consumption and more by the sedimentary oxygen consumption was found across all studied subbasins. Physical fluxes (mainly advection) explain most oxygen variability in all scenarios. Hydrogen sulfide dynamics was found to be more region dependent and influenced by the different nutrient input scenarios.
4. Three EOFs were identified as patterns governing the dynamics of oxygen and hydrogen sulfide in the reference scenario. For oxygen budget terms, the first EOF explained approx. 60% of the variability, the second – approx. 20%, and the third – approx. 10%. For the hydrogen sulfide dynamics, the first EOF explained more than 80% of the variability, and all three EOFs together explained more than 95%. The last two EOFs were attributed to the inflows' activity and the natural variability, and the first EOF – to the change in the nutrient forcing with positive (deposition of reduced material and organic matter, deoxygenation) and negative (oxidation of the reduced material, oxygenation) phases. The first EOF



went into the constant negative phase (no deposition of reduced material and oxidation of already existing one) in the 2050s (O_2 , BSAP), the 2030s (O_2 , 0.5 BSAP), and the 2030s (H_2S , both BSAP and 0.5 BSAP), indicating resilient transformation to the oxic regime.

5. According to our model study, it is possible for the Baltic Sea to return to its initial state (the year 1948) within 71 years under the 0.5 BSAP scenario (see [Figures 2, 4](#)). Under the BSAP scenario, the Baltic Sea state comes close to the initial state but did not reach it within the simulation time.

[2021-update.pdf](#). The generated model data needed for reproducing the analysis can be found on the IOW server (<http://doi.io-warnemuende.de/10.12754/data-2023-0009>).

Author contributions

LN prepared the nutrient input datasets with the help of TN. LN performed the simulations and analyzed the data. LN and HEMM designed the research. HEMM supervised the work. All authors contributed to the article and approved the submitted version.

Data availability statement

Baltic Sea Action Plan Maximum allowable input nutrient loads (2021 update) can be found within the following document: <https://helcom.fi/wp-content/uploads/2021/10/Baltic-Sea-Action-Plan->

Funding

We thank the Open Access Fund of Leibniz Association for funding the publication of this article.

Acknowledgments

The research presented in this study is part of the Baltic Earth program (Earth System Science for the Baltic Sea region, see <http://www.baltic.earth>). The model simulations were performed on the North German Supercomputing Alliance (HLRN) computers. In addition, we thank two reviewers for their helpful comments that improved the manuscript's quality.

Conflict of interest

The authors declare that the research was conducted in the absence of any commercial or financial relationships that could be construed as a potential conflict of interest.

References

- Almroth-Rosell, E., Wählström, I., Hansson, M., Väli, G., Eilola, K., Andersson, P., et al. (2021). A regime shift toward a more anoxic environment in a Eutrophic sea in Northern Europe. *Front. Mar. Sci.* 8. doi: 10.3389/fmars.2021.799936
- Astor, S. W., Blomquist, J. D., Webber, J. S., and Chanut, J. G. (2020). Factors driving nutrient trends in streams of the Chesapeake Bay watershed. *J. Environ. Qual.* 49, 812–834. doi: 10.1002/jeq2.20101
- Backer, H., Leppänen, J.-M., Brusendorff, A. C., Forsius, K., Stankiewicz, M., Mehtonen, J., et al. (2010). HELCOM Baltic Sea Action Plan – A regional programme of measures for the marine environment based on the Ecosystem Approach. *Mar. Pollut. Bull.* 60, 642–649. doi: 10.1016/j.marpolbul.2009.11.016
- Bartosova, A., Capell, R., Olesen, J. E., Jabloun, M., Refsgaard, J. C., Donnelly, C., et al. (2019). Future socioeconomic conditions may have a larger impact than climate change on nutrient loads to the Baltic Sea. *Ambio* 48, 1325–1336. doi: 10.1007/s13280-019-01243-5
- Borja, A., Elliott, M., Andersen, J. H., Cardoso, A. C., Carstensen, J., Ferreira, J. G., et al. (2015). *Report on potential Definition of Good Environmental Status. Deliverable 6.2. (DEVOTES Project)*. 62pp. Available at: <https://mcc.jrc.ec.europa.eu/documents/201502120842.pdf>
- Breitburg, D., Levin, L., Oschlies, A., Grégoire, M., Chavez, F., Conley, D., et al. (2018). Declining oxygen in the global ocean and coastal waters. *Sci. (New York N.Y.)* 359, 7240. doi: 10.1126/science.aam7240
- Conley, D. J., Björck, S., Bonsdorff, E., Carstensen, J., Destouni, G., Gustafsson, B. G., et al. (2009). Hypoxia-related processes in the Baltic Sea. *Environ. Sci. Technol.* 43, 3412–3420. doi: 10.1021/es082762a
- Diaz, R. J., and Rosenberg, R. (2008). Spreading dead zones and consequences for marine ecosystems. *Science* 321, 926–929. doi: 10.1126/science.1156401
- Fennel, K., and Testa, J. M. (2019). Biogeochemical controls on coastal hypoxia. *Annu. Rev. Mar. Sci.* 11, 105–130. doi: 10.1146/annurev-marine-010318-095138
- Friedland, R., Neumann, T., and Schernewski, G. (2012). Climate change and the Baltic Sea action plan: Model simulations on the future of the western Baltic Sea. *J. Mar. Syst.* 105–108, 175–186. doi: 10.1016/j.jmarsys.2012.08.002
- Geyer, B. (2014). High-resolution atmospheric reconstruction for Europe 1948–2012: coastDat2. *Earth Sys. Sci. Data* 6, 147–164. doi: 10.5194/essd-6-147-2014
- Griffies, S. M. (2012). *Elements of the modular ocean model. GFDL ocean group technical report no. 7* (Princeton, NJ, USA: NOAA/Geophysical Fluid Dynamics Laboratory), 632.
- Gustafsson, B. G., Schenk, F., Blenckner, T., Eilola, K., Meier, H. E. M., Müller-Karulis, B., et al. (2012). Reconstructing the development of Baltic Sea eutrophication 1850–2006. *AMBIO* 41, 534–548. doi: 10.1007/s13280-012-0318-x
- Gustafsson, B. G., and Stigebrandt, A. (2007). Dynamics of nutrients and oxygen/hydrogen sulfide in the Baltic Sea deep water. *J. Geophys. Res.: Biogeosci.* 112, G02023. doi: 10.1029/2006JG000304
- Hannachi, A., Jolliffe, I. T., and Stephenson, D. B. (2007). Empirical orthogonal functions and related techniques in atmospheric science: A review. *Int. J. Climatol.* 27, 1119–1152. doi: 10.1002/joc.1499
- Hansson, M., and Viktorsson, L. (2020). *Oxygen Survey in the Baltic Sea 2020 - Extent of Anoxia and Hypoxia 1960-2020. Report Oceanography no. 70* (Göteborg: Swedish Meteorological and Hydrological Institute).
- Heathwaite, A. L., Johnes, P. J., and Peters, N. E. (1996). Trends in nutrients. *Hydrological Processes* 10, 263–293. doi: 10.1002/(SICI)1099-1085(199602)10:2<263::AID-HYP441>3.0.CO;2-K
- HELCOM (2007). *The HELCOM Baltic Sea Action Plan* (Helsinki: Helsinki Commission). Available at: www.helcom.fi
- HELCOM (2021). *HELCOM Baltic Sea Action Plan – 2021 update* (Helsinki: HELCOM).
- Hordoir, R., and Meier, H. E. M. (2012). Effect of climate change on the thermal stratification of the Baltic sea: a sensitivity experiment. *Clim Dyn* 38, 1703–1713. doi: 10.1007/s00382-011-1036-y
- Knuutila, S., Räike, A., Ekholm, P., and Kondratyev, S. (2017). Nutrient inputs into the Gulf of Finland: Trends and water protection targets. *J. Mar. Syst.* 171, 54–64. doi: 10.1016/j.jmarsys.2016.09.008
- Köuts, M., Maljutenko, I., Elken, J., Liu, Y., Hansson, M., Viktorsson, L., et al. (2021). Recent regime of persistent hypoxia in the Baltic Sea. *Environ. Res. Commun.* 3, 075004. doi: 10.1088/2515-7620/ac0cc4
- Krapf, K., Naumann, M., Duthel, C., and Meier, H. E. M. (2022). Investigating hypoxic and euxinic area changes based on various datasets from the Baltic Sea. *Front. Mar. Sci.* 9, 823476. doi: 10.3389/fmars.2022.823476
- Kuznetsov, I., and Neumann, T. (2013). Simulation of carbon dynamics in the Baltic Sea with a 3D model. *J. Mar. Syst.* 111–112, 167–174. doi: 10.1016/j.jmarsys.2012.10.011
- Large, W. G., McWilliams, J. C., and Doney, S. C. (1994). Oceanic vertical mixing: a review and a model with a nonlocal boundary layer parameterization. *Rev. Geophys.* 32, 363–403. doi: 10.1029/94RG01872
- Larsson, U., Elmgren, R., and Wulff, F. (1985). Eutrophication and the Baltic Sea: causes and consequences. *Ambio* 14, 1–6.
- Lenz, C., Jilbert, T., Conley, D. J., and Slomp, C. P. (2015). Hypoxia-driven variations in iron and manganese shuttling in the Baltic Sea over the past 8 kyr. *Geochem. Geophys. Geosys.* 16, 3754–3766. doi: 10.1002/2015GC005960
- Leppäranta, M., and Myrberg, K. (2009). *Physical Oceanography of the Baltic Sea* (Berlin, Heidelberg: Springer). doi: 10.1007/978-3-540-79703-6
- Liblik, T., Naumann, M., Alenius, P., Hansson, M., Lips, U., Nausch, G., et al. (2018). Propagation of impact of the recent major Baltic inflows from the Eastern Gotland basin to the gulf of Finland (Accessed February 15, 2023).
- Meier, H. E. M., Andersson, H. C., Eilola, K., Gustafsson, B. G., Kuznetsov, I., Müller-Karulis, B., et al. (2011). Hypoxia in future climates: A model ensemble study for the Baltic Sea. *Geophys. Res. Lett.* 38. doi: 10.1029/2011GL049929
- Meier, H. E. M., Dieterich, C., and Gröger, M. (2021). Natural variability is a large source of uncertainty in future projections of hypoxia in the Baltic Sea. *Commun. Earth Environ.* 2, 1–13. doi: 10.1038/s43247-021-00115-9
- Meier, H. E. M., Dieterich, C., Gröger, M., Duthel, C., Börgel, F., Safonova, K., et al. (2022). Oceanographic regional climate projections for the Baltic Sea until 2100. *Earth Sys. Dynamics* 13, 159–199. doi: 10.5194/esd-13-159-2022
- Meier, H. E. M., Eilola, K., Almroth-Rosell, E., Schimanke, S., Kniesbusch, M., Höglund, A., et al. (2019). Disentangling the impact of nutrient load and climate changes on Baltic Sea hypoxia and eutrophication since 1850. *Clim Dyn* 53, 1145–1166. doi: 10.1007/s00382-018-4296-y
- Meier, H. E. M., Väli, G., Naumann, M., Eilola, K., and Frauen, C. (2018). Recently accelerated oxygen consumption rates amplify deoxygenation in the Baltic Sea. *J. Geophys. Res.: Oceans* 123, 3227–3240. doi: 10.1029/2017JCO13686

Publisher's note

All claims expressed in this article are solely those of the authors and do not necessarily represent those of their affiliated organizations, or those of the publisher, the editors and the reviewers. Any product that may be evaluated in this article, or claim that may be made by its manufacturer, is not guaranteed or endorsed by the publisher.

Supplementary material

The Supplementary Material for this article can be found online at: <https://www.frontiersin.org/articles/10.3389/fmars.2023.1233324/full#supplementary-material>

- Mort, H. P., Slomp, C. P., Gustafsson, B. G., and Andersen, T. J. (2010). Phosphorus recycling and burial in Baltic Sea sediments with contrasting redox conditions. *Geochimica Cosmochimica Acta* 74, 1350–1362. doi: 10.1016/j.gca.2009.11.016
- Naumov, L., Neumann, T., Radtke, H., and Meier, H. E. M. (2023). Limited ventilation of the central Baltic Sea due to elevated oxygen consumption. *Front. Mar. Sci.* doi: 3389/fmars.2023.1175643
- Neumann, T. (2010). Climate-change effects on the Baltic Sea ecosystem: A model study. *J. Mar. Syst.* 81, 213–224. doi: 10.1016/j.jmarsys.2009.12.001
- Neumann, T., Eilola, K., Gustafsson, B., Müller-Karulis, B., Kuznetsov, I., Meier, H. E. M., et al. (2012). Extremes of temperature, oxygen and blooms in the Baltic Sea in a changing climate. *AMBIO* 41, 574–585. doi: 10.1007/s13280-012-0321-2
- Neumann, T., Fennel, W., and Kremp, C. (2002). Experimental simulations with an ecosystem model of the Baltic Sea: A nutrient load reduction experiment: NUTRIENT LOAD REDUCTION EXPERIMENT. *Global Biogeochem. Cycles* 16, 7-1-7-7-119. doi: 10.1029/2001GB001450
- Neumann, T., Koponen, S., Attila, J., Brockmann, C., Kallio, K., Kervinen, M., et al. (2021). Optical model for the Baltic Sea with an explicit CDOM state variable: a case study with Model ERGOM (version 1.2). *Geosci. Model. Dev.* 14, 5049–5062. doi: 10.5194/gmd-14-5049-2021
- Neumann, T., Radtke, H., Cahill, B., Schmidt, M., and Rehder, G. (2022). Non-Redfieldian carbon model for the Baltic Sea (ERGOM version 1.2) – implementation and budget estimates. *Geosci. Model. Dev.* 15, 8473–8540. doi: 10.5194/gmd-15-8473-2022
- Radtke, H., Lipka, M., Bunke, D., Morys, C., Woelfel, J., Cahill, B., et al. (2019). Ecological Regional Ocean Model with vertically resolved sediments (ERGOM SED 1.0): coupling benthic and pelagic biogeochemistry of the south-western Baltic Sea. *Geosci. Model. Dev.* 12, 275–320. doi: 10.5194/gmd-12-275-2019
- Rolf, C., Walve, J., Larsson, U., and Elmgren, R. (2022). How oxygen deficiency in the Baltic Sea proper has spread and worsened: The role of ammonium and hydrogen sulphide. *Ambio* 51, 2308–2324. doi: 10.1007/s13280-022-01738-8
- Rydin, E., Kumblad, L., Wulff, F., and Larsson, J. P. (2017). Remediation of a Eutrophic Bay in the Baltic Sea. *Environ. Sci. Technol.* 51, 4559–4566. doi: 10.1021/acs.est.6b06187
- Saraiva, S., Meier, H. E. M., Andersson, H., Höglund, A., Dieterich, C., Gröger, M., et al. (2019). Uncertainties in projections of the Baltic Sea ecosystem driven by an ensemble of global climate models. *Front. Earth Sci.* 6. doi: 10.3389/feart.2018.00244
- Savchuk, O. P. (2018). Large-scale nutrient dynamics in the Baltic Sea 1970–2016 (Accessed February 15, 2023).
- Schneider, B., Nausch, G., and Pohl, C. (2010). Mineralization of organic matter and nitrogen transformations in the Gotland Sea deep water. *Mar. Chem.* 119, 153–161. doi: 10.1016/j.marchem.2010.02.004
- Stoicescu, S.-T., Lips, U., and Liblik, T. (2019). Assessment of eutrophication status based on sub-surface oxygen conditions in the gulf of Finland (Baltic Sea) (Accessed May 22, 2023).
- Svendsen, L. M., and Gustafsson, B. (2020). *Waterborne nitrogen and phosphorus inputs and water flow to the Baltic Sea 1995–2018*. Available at: <https://helcom.fi/baltic-sea-trends/environment-fact-sheets/eutrophication/> (Accessed May 22, 2023).
- Uurasjärvi, E., Pääkkönen, M., Setälä, O., Koistinen, A., and Lehtiniemi, M. (2021). Microplastics accumulate to thin layers in the stratified Baltic Sea. *Environ. pollut.* 268, 115700. doi: 10.1016/j.envpol.2020.115700
- Vahtera, E., Conley, D. J., Gustafsson, B. G., Kuosa, H., Pitkänen, H., Savchuk, O. P., et al. (2007). Internal ecosystem feedbacks enhance nitrogen-fixing cyanobacteria blooms and complicate management in the Baltic Sea. *AMBIO* 36, 186–194. doi: 10.1579/00447447
- Väli, G., Meier, H. E. M., and Elken, J. (2013). Simulated halocline variability in the Baltic Sea and its impact on hypoxia during 1961–2007: SIMULATED HALOCLINE VARIABILITY IN THE BALTIC SEA. *J. Geophys. Res. Oceans* 118, 6982–7000. doi: 10.1002/2013JC009192
- Voss, M., Dippner, J. W., Humborg, C., Hürdler, J., Korth, F., Neumann, T., et al. (2011). History and scenarios of future development of Baltic Sea eutrophication. *Estuarine Coast. Shelf Sci.* 92, 307–322. doi: 10.1016/j.jecss.2010.12.037
- Whitney, M. M. (2022). Observed and projected global warming pressure on coastal hypoxia. *Biogeosciences* 19, 4479–4497. doi: 10.5194/bg-19-4479-2022
- Yurkovskis, A., Wulff, F., Rahm, L., Andruzaitis, A., and Rodriguez-Medina, M. (1993). A nutrient budget of the gulf of Riga; Baltic Sea. *Estuarine Coast. Shelf Sci.* 37, 113–127. doi: 10.1006/jecss.1993.1046

Supplementary Material

Dynamics of oxygen sources and sinks in the Baltic Sea under different nutrient inputs

Lev Naumov*, H.E. Markus Meier, Thomas Neumann

* **Correspondence:** Lev Naumov: lev.naumov@io-warnemuende.de

1 Supplementary Data

This supplementary material consists of figures and tables that are not included in the paper but still contain important information. Supplementary material has the same structure as the main paper. Within each section, figures and tables relevant to that section are shown. The following abbreviations are used in some figures: BB – the Bornholm Basin, eGB – the eastern Gotland Basin, nGB – the northern Gotland Basin, and wGB – the western Gotland Basin.

2 Materials and methods

Supplementary Table 1. Clarification for O₂ processes' names used in the paper. The same name for different processes means the sum of those processes.

Process	Name in Figures 2, 3, and Supplementary Figure 3	Name in Figure 4 and Supplementary Figure 4
Nitrification of NH ₄ ⁺ to NO ₃ ⁻	Bio	Bio_nitr
Mineralization of detritus	Bio	Bio_min_om
Mineralization of particulate organic carbon (POC)	Bio	Bio_min_om
Mineralization of phosphorus in particulate organic carbon (POCP)	Bio	Bio_min_om
Mineralization of nitrogen in particulate organic carbon (POCN)	Bio	Bio_min_om
Mineralization of dissolved organic carbon (DOC)	Bio	Bio_min_om
Mineralization of dissolved organic nitrogen (DON)	Bio	Bio_min_om
Mineralization of dissolved organic phosphorus (DOP)	Bio	Bio_min_om
Respiration of living organisms (lpp, spp, cya, and zoo)	Bio	Bio_resp
Photosynthesis by phytoplankton	Bio	Bio_phot

Supplementary Material

Oxidation of elemental sulfur	Bio	Bio_min_sulf
Oxidation of H ₂ S	Bio	Bio_min_sulf
Mineralization of sedimentary detritus	Sed	Sed_det
Coupled nitrification/denitrification after mineralization of detritus in oxic sediments	Sed	Sed_nitdenit
Mineralization of sedimentary particulate organic carbon (POC)	Sed	Sed_min_om
Mineralization of sedimentary phosphorus in particulate organic carbon (POCP)	Sed	Sed_min_om
Mineralization of sedimentary nitrogen in particulate organic carbon (POCN)	Sed	Sed_min_om
Coupled nitrification/denitrification after mineralization of POCN in oxic sediments	Sed	Sed_nitdenit
Advection	Phy	Excluded from analysis
Vertical diffusion	Phy	Excluded from analysis
Downslope mixing	Phy	Excluded from analysis
Convection	Phy	Excluded from analysis

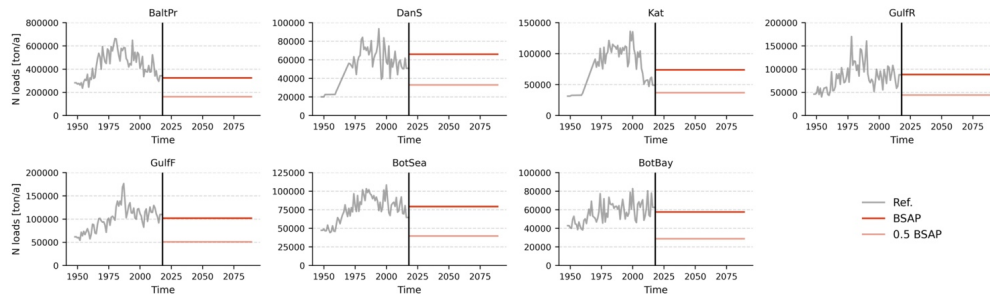
Supplementary Table 2. Clarification for H₂S processes' names used in the paper. The same name for different processes means the sum of those processes.

Process	Name in Figures 2, 3, and Supplementary Figure 3	Name in Figure 4 and Supplementary Figure 4
Mineralization of particulate organic carbon (POC). Sulfate reduction	Bio	mineralization_particular_om
Mineralization of phosphorus in particulate organic carbon (POCP). Sulfate reduction	Bio	mineralization_particular_om
Mineralization of nitrogen in particulate organic carbon (POCN). Sulfate reduction	Bio	mineralization_particular_om
Mineralization of detritus. Sulfate reduction	Bio	detritus_water_column
Mineralization of dissolved organic carbon (DOC). Sulfate reduction	Bio	mineralization_dissolved_om
Mineralization of dissolved organic phosphorus (DOP). Sulfate reduction	Bio	mineralization_dissolved_om

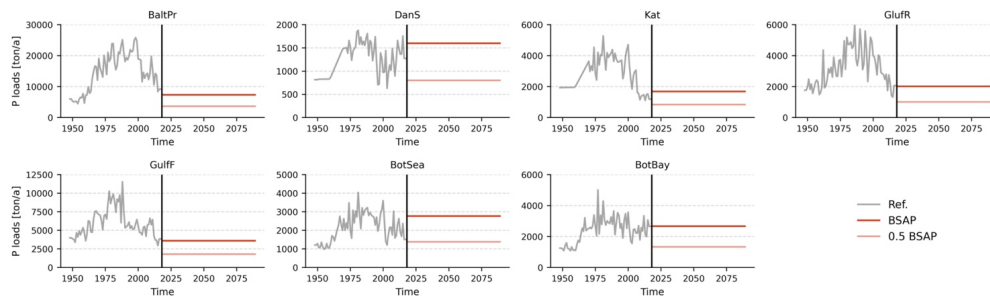
Mineralization of dissolved organic nitrogen (DON). Sulfate reduction	Bio	mineralization_dissolved_om
Oxidation of H ₂ S via O ₂	Bio	o2_oxidation
Oxidation of H ₂ S via NO ₃ ⁻	Bio	no3_oxidation
Mineralization of sedimentary detritus. Sulfate reduction	Sed	detritus_sediments
Mineralization of sedimentary particulate organic carbon (POC). Sulfate reduction	Sed	mineralization_sediments
Mineralization of sedimentary phosphorus in particulate organic carbon (POCP). Sulfate reduction	Sed	mineralization_sediments
Mineralization of sedimentary nitrogen in particulate organic carbon (POCN). Sulfate reduction	Sed	mineralization_sediments
Advection	Phy	advection_<border name> (up, west, south, east, north)
Vertical diffusion	Phy	diffusion
Downslope mixing	Phy	other
Convection	Phy	other

2.3 Nutrient input scenarios

The figures related to Section 2.3 of the main text are presented here. Those include Supplementary Figures 1 and 2, depicting total nitrogen and phosphorus loads into the Baltic Sea HELCOM subbasins, respectively. They show all three considered scenarios.



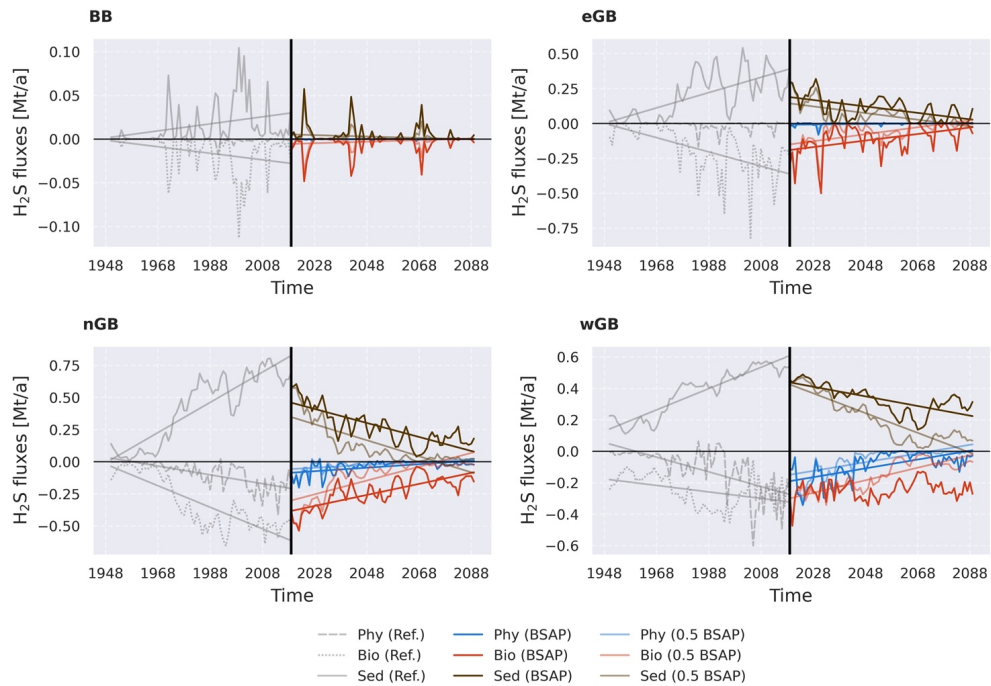
Supplementary Figure 1. Total (airborne and waterborne) nitrogen loads to the HELCOM basins of the Baltic Sea. Reference data are HELCOM data and BSAP and 0.5 BSAP loads are constants at the Maximum Allowable Input (MAI) and half of MAI levels, respectively. The following abbreviations are used: BaltPr – Baltic Proper, DanS – Danish straits, Kat – Kattegat, GulfR – Gulf of Riga, GulfF – Gulf of Finland, BotSea – Bothnian Sea, and BotBay – Bothnian Bay.



Supplementary Figure 2. The same as Supplementary Figure 1, but for phosphorus.

3.1 Trends in O₂ and H₂S sources and sinks

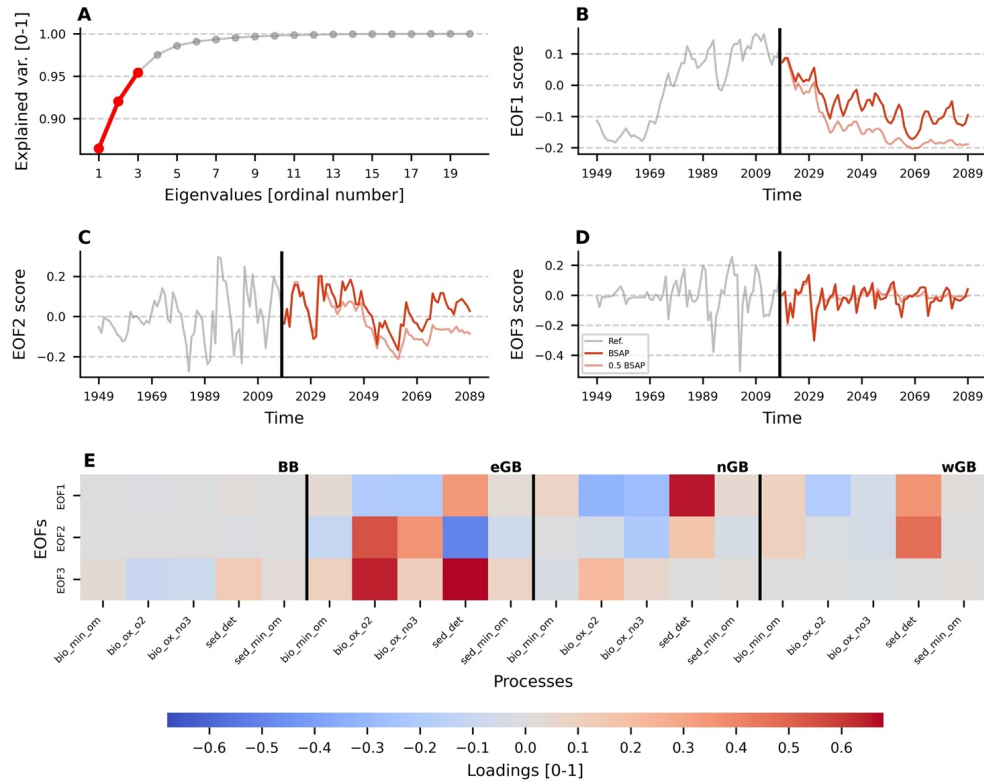
The figure related to Section 3.1 of the main text is presented here. Supplementary Figure 3 shows a trend analysis for the H₂S sources and sinks split into three groups: bio (water column processes – the sink of H₂S), sed (sedimentary processes – the source of H₂S), and phy (physical processes, mainly advection – mainly the sink of H₂S). See Supplementary Table 2 for more information about the processes in each group.



Supplementary Figure 3. Trend analysis of H₂S sources and sinks. Processes were aggregated into three groups: phy, bio, and sed. To learn more about processes within each group, see Supplementary Table 2. Each panel represents a specific subbasin indicated above the upper left corner of the plot. Only significant trends (p -value < 0.05) are shown in the figure. Mt/a stands for 10^9 kg per year.

3.3 O₂ and H₂S dynamics induced by the nutrient forcing

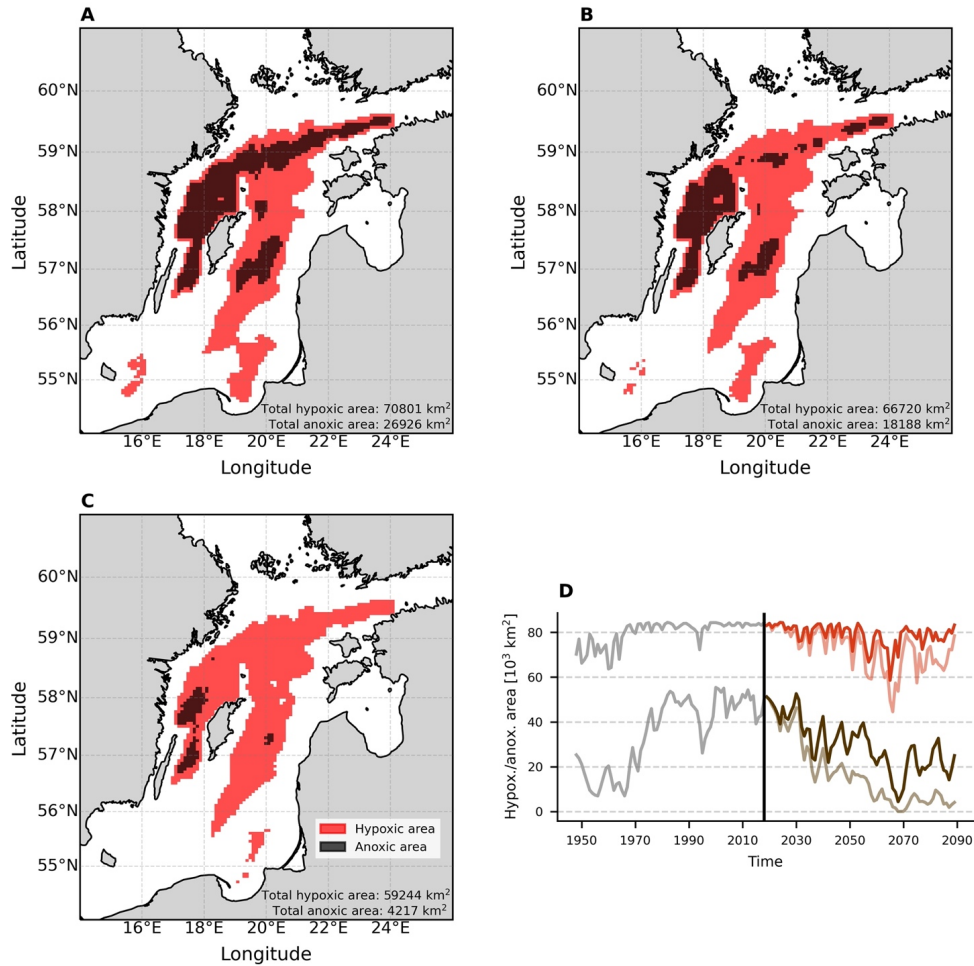
The figure related to Section 3.3 of the main text is presented here. Supplementary Figure 4 shows an EOF analysis for the H₂S sources and sinks. See Supplementary Table 2 for more information about the processes behind each name.



Supplementary Figure 4. EOF decomposition of the spatial-temporal matrix of H₂S consumption terms aggregated into specific groups (to get more information about individual processes in the group, see Supplementary Table 2). Panel A shows the fraction of variability explained by all calculated EOFs. Only the first three EOFs were considered significant and used later in the analysis (colored red in panel A). Panels B-D depict temporal variability of the first three EOFs correspondingly. Here, the black vertical line demarcates the reference scenario (grey curve) and BSAP, 0.5 BSAP scenarios (vivid and translucent red lines, correspondingly). Panel E demonstrates the loadings of the first three EOFs. Loadings vary from minus one to one and show the direction and magnitude of the connection between an EOF and a variable. Black lines highlight the spatial structure of the matrix by separating the subbasins.

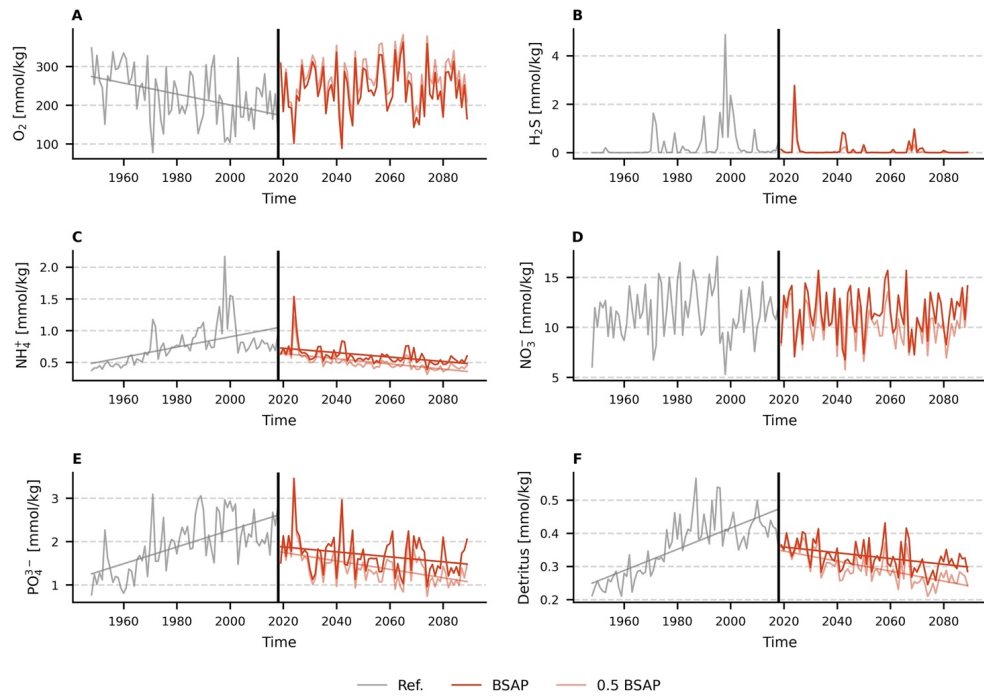
3.4 Discussion

The figures related to Section 3.4 of the main text are presented here. Supplementary Figure 5 shows the mean hypoxic and anoxic areas in the central Baltic Sea and their temporal variability for each scenario. Supplementary Figures 6-9 depict the temporal dynamics of the different variables in each subbasin for all considered scenarios.



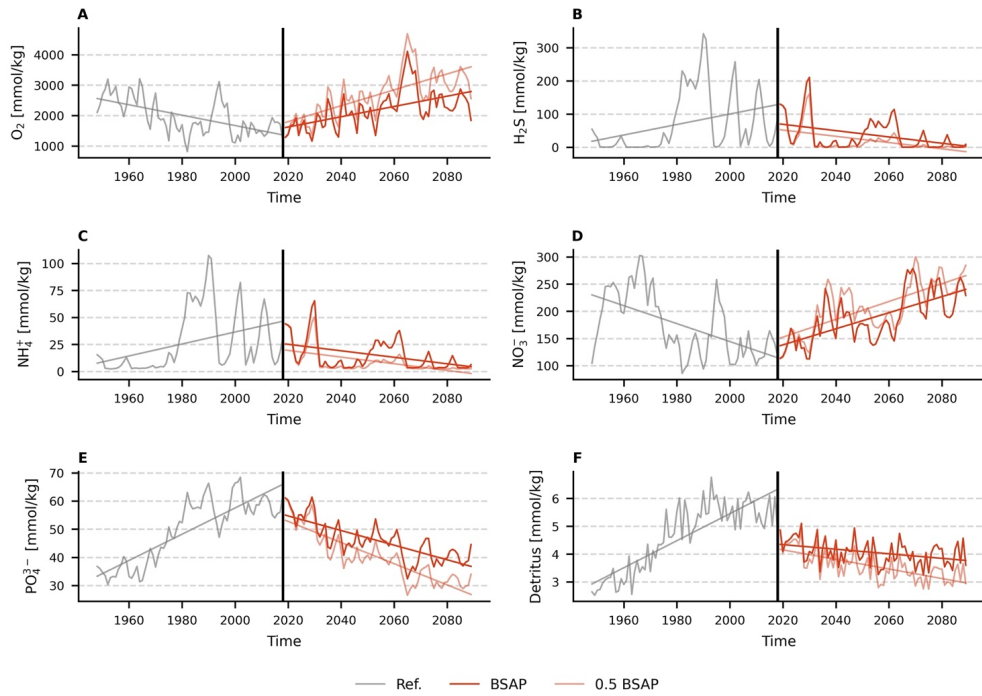
Supplementary Figure 5. Mean hypoxic (red) and anoxic (black) areas locations for the reference scenario (A), the BSAP scenario (B), and the 0.5 BSAP scenario (C). The grid cell is considered hypoxic or anoxic if more than half of the study period hypoxia or anoxia was observed there. Panel D shows the temporal variability of hypoxic (red) and anoxic (black) areas for the BSAP scenario (vivid lines) and for the 0.5 BSAP scenario (translucent lines). A grey color marks the reference period.

BB

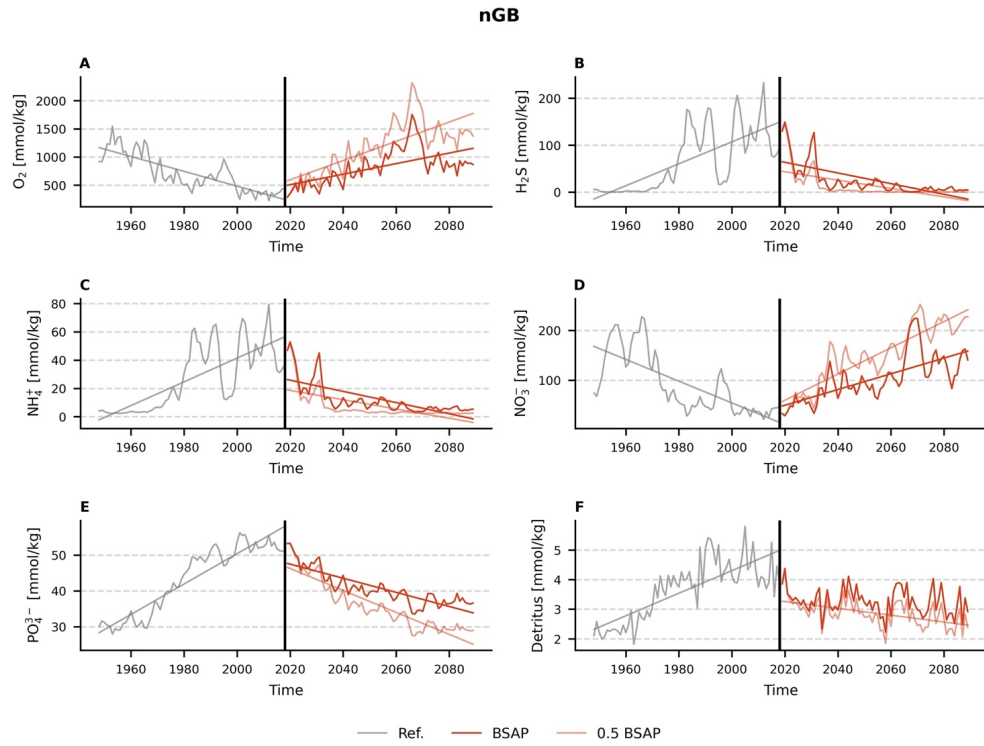


Supplementary Figure 6. Temporal variability of the integrated oxygen content (A), hydrogen sulfide content (B), ammonium content (C), nitrate content (D), phosphate content (E), and detritus content (F) under the BSAP scenario (vivid lines) and 0.5 BSAP scenario (translucent lines) in the Bornholm Basin (BB). Integration was limited in the vertical plane by a depth of 70 meters. Reference period is marked by the grey color. Only significant ($p < 0.05$) linear trends are shown.

eGB

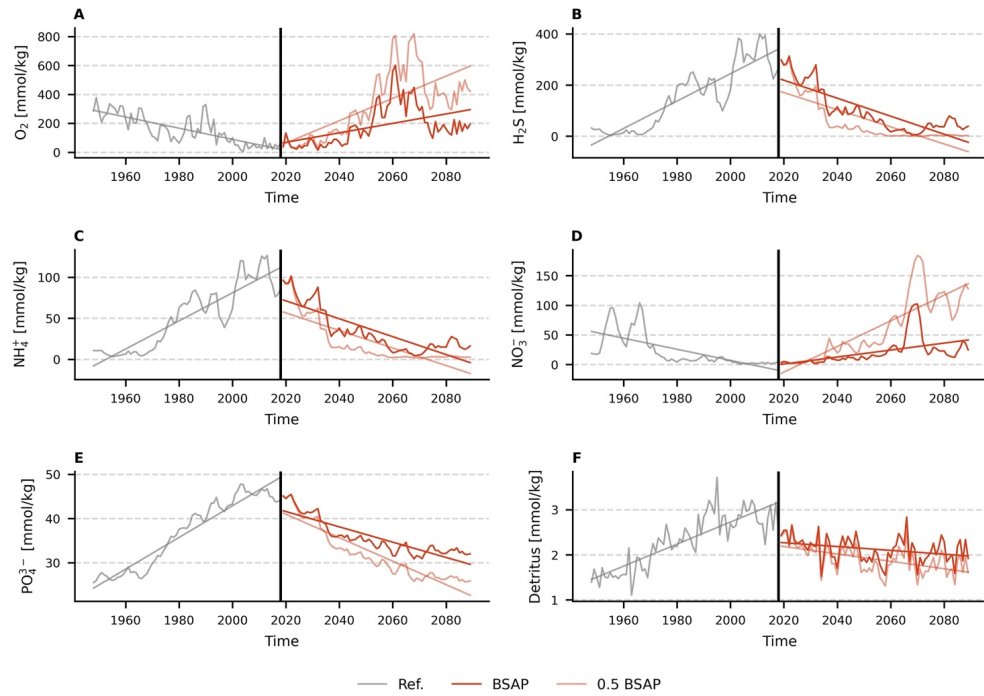


Supplementary Figure 7. Same as Supplementary Figure 6, but in the eastern Gotland Basin (eGB).



Supplementary Figure 8. Same as Supplementary Figure 6, but in the northern Gotland Basin (nGB).

wGB



Supplementary Figure 9. Same as Supplementary Figure 6, but in the western Gotland Basin (wGB).